

SYNTHESIS, DEVELOPMENT AND BIOCHEMICAL CHARACTERIZATION OF
SMALL MOLECULE, ISOFORM-SELECTIVE PHOSPHOLIPASE D INHIBITORS
AND PHOTOACTIVATABLE PROBES

By

Robert Raymond Lavieri

Dissertation

Submitted to the Faculty of the
Graduate School of Vanderbilt University
in partial fulfillment of the requirements

for the degree of

DOCTOR OF PHILOSOPHY

in

Pharmacology

December, 2014

Nashville, Tennessee

Approved:

Tina M. Iverson, Ph.D.

H. Alex Brown, Ph.D.

Craig W. Lindsley, Ph.D.

David Cortez, Ph.D.

Lawrence J. Marnett, Ph.D.

For my family

ACKNOWLEDGEMENTS

Many people and organizations have provided both tremendous support to me and essential contributions to the work described herein. I owe a debt of gratitude to both of my undergraduate advisors, Chester S. Fornari Ph.D. and Erik J. Wielenberg, Ph.D. Professor Fornari was my biochemistry academic advisor and first PI. He encouraged me to continue studying biochemistry. Although the connection to pursuing a Ph.D. in pharmacology may not be obvious I also owe a huge debt of gratitude to Professor Erik J. Wielenberg, my philosophy major academic advisor. In his courses I learned how to form arguments based on data and how to effectively present such arguments in written and oral forms of communication. What skills could be more fundamental to earning a Ph.D. in any discipline?

I would like to thank the Vanderbilt University community. I can't even count the number of times I was able to find someone on campus who had a chemical, instrument or skill that I needed and said person was more than willing to provide some help to me. These kinds of interactions can save thousands of dollars and days or weeks of time. I would also like to thank the entire Department of Pharmacology at Vanderbilt. Many of the faculty who take the time to teach portions of the first-year IGP course, and especially the core pharmacology curriculum, were able to distill and convey fundamental concepts that one simply has to know to understand pharmacology and physiology. Specifically, I would like to thank Professor Tina Iverson who, during the scientific communications course, "strongly encouraged" me to approach public speaking in a much more serious and methodical way.

The VICB has been very good to me in many ways and I hope that in the future I am somehow able to help students involved with the VICB. I was fortunate enough to be a trainee on Professor Marnett's Integrative Training in Therapeutic Discovery (ITTD) training grant which involved (with about 2 days notice) a trip to Pfizer's research and development site in St. Louis, Missouri for an inside look at everything (including incredible seats at a Cardinal's baseball game) guided by the site director herself. In addition to all of the funding sources for both of the labs I worked in I would also like to thank The Pharmaceutical Research and Manufacturers of America Foundation (PhRMA) for awarding me a predoctoral fellowship.

I owe an absolutely enormous debt of gratitude that I am almost certain I will never be able to repay to both of my advisors. Alex agreed not only to let me work for him, but also to let me be co-advised by he and Craig. I thank both Alex and Craig for their scientific expertise and guidance, their ability to keep vibrant labs up and running, their patience with me as I made many mistakes, and their continued support as I continue my career.

I thank my dissertation committee for overseeing my training and providing honest, candid feedback. I had the good fortune of being able to interact with all of my committee members in some capacity beyond their role as committee members and for that I am also thankful.

I thank everyone in both research groups for all of their expertise, knowledge and time. Specifically, I thank Ron Bruntz with whom I enjoyed many nights searching through the west end area of Nashville anytime from 11 pm to 1 am when we left the lab and wanted to locate a restaurant other than Wendys or TGI Fridays that was actually

open. Ron also taught me some useful things to know about recombinant protein expression and purification. I also thank my friends for their encouragement and patience as I struggled at times through the experience that is graduate education.

I thank my Family. My parents have always provided me with everything I ever needed to thrive and any shortcomings I take as my own responsibility. My sister and extended family have also always been completely supportive of me in any way that they have been able to be. I also thank Missy for everything she has done to keep our house and lives functioning while I was finishing my degree. Finally, I would like to thank my son Bobby for helping me to keep some perspective on life and for reminding me (about every 5 seconds) of the power of the human smile.

Finally, while I draw inspiration from many great motorcycle racers and racecar drivers I would like to thank Mario Andretti for his words, which have always served me well: “If everything seems under control, you’re just not going fast enough.”

TABLE OF CONTENTS

	Page
DEDICATION.....	ii
ACKNOWLEDGEMENTS.....	iii
LIST OF FIGURES	x
LIST OF ABBREVIATIONS	xvii
Chapter	
I. INTRODUCTION.....	1
Enzymes with phospholipase D activity	1
Overview	1
Non-HKD enzymes	4
HKD enzymes.....	11
Primary sequence.....	11
Structure.....	12
Catalytic mechanism: hydrolysis versus transphosphatidylation	13
Interfacial kinetics	15
<i>In vitro</i> enzyme activity assays.....	16
Cellular enzyme activity assays.....	18
PLD enzymes from microorganisms and model organisms	18
Plant	18
Fungal	20
Budding yeast	20
Fission yeast	20
<i>C. elegans</i>	21
<i>Drosophila melanogaster</i>	21
Zebrafish.....	22
Mammalian PLD	23
Isoforms	23
Tissue expression and subcellular localization.....	25
Tissue expression.....	25
PLD1 subcellular localization	25
PLD2 subcellular localization	26
Regulation.....	26
Divalent cations	26
Post-translational modifications	27
Lipid cofactors	29

Regulatory proteins.....	30
Signaling pathways.....	32
Receptor tyrosine kinases	32
G protein coupled receptors.....	33
The mammalian target of rapamycin.....	34
Functional consequences of PLD inhibition or overexpression	36
Respiratory burst.....	36
Transport and endocytosis	37
Platelet aggregation	39
Neuronal physiology.....	40
Cell invasion and metastasis.....	42
Cell proliferation and apoptosis.....	43
PLD as a potential therapeutic target.....	50
Druggability.....	51
Cancer	52
Alzheimer's disease.....	54
Thrombotic disease.....	55

II. SYNTHESIS AND BIOCHEMICAL CHARACTERIZATION OF POTENT, ISOFORM-SELECTIVE PLD INHIBITORS

Introduction	57
History	57
Indirect inhibitors of PLD activity.....	59
Direct inhibitors of PLD activity	61
First generation.....	61
Second generation: The identification of halopemide as a PLD inhibitor	65
Initial SAR studies based on the halopemide scaffold	67
Optimization of Halopemide for PLD1 specificity	70
The impact of various halogenated privileged structures on PLD1 potency and selectivity	70
Incorporation of a key (<i>S</i>)-methyl group that allows for the 1,700-fold PLD1 selective inhibitor VU0359595	77
Summary of the SAR leading to VU0359595	80
Synthesis and characterization of VU0359595	82
Chemical synthesis of VU0359595	82
Chiral resolution of VU0359595 diastereomers and PLD inhibitory activities thereof	84
Optimization of an alternative scaffold that confers PLD2 selectivity	87
Initial SAR containing the 1,3,8-triazaspiro[4,5]decan-4-one privileged structure	87
Synthesis of various 3 and/or 4 halogenated 1,3,8-triazaspiro[4,5]decan-4-ones	94

Preliminary evaluation of N-(2-(1-(3-Fluorophenyl)-4-oxo-1,3,8-triazaspiro[4.5]decan-8-yl)ethyl)-2-naphthamide (VU0364739) and VU0359595	99
Biological activity.....	99
Pharmacokinetics.....	102
A (<i>S</i>)-methyl group dramatically increases PLD1 potency within a PLD2-preferring chemotype	104
Materials and methods.....	106
Cell culture	106
Endogenous PLD enzyme activity assay.....	107
Assessment of cell proliferation via WST-1 assay.....	108
Assessment of caspase 3/7 activity.....	108
<i>In vitro</i> pharmacokinetic studies.....	109
<i>In vivo</i> pharmacokinetic studies	110
Plasma protein binding	111
Liquid chromatography/mass spectrometry analysis for pharmacokinetic experiments.....	112
<i>In vivo</i> experiments.....	112
<i>In vitro</i> experiments.....	113
Medicinal chemistry	113
General synthetic methods.....	113
Chemical experimentals	115

III. DEVELOPMENT OF AZIDE AND DIAZIRINE-CONTAINING PLD PHOTOPROBES AND A STRATEGY TO VERIFY COVALENT LABELING OF THE ENZYME	138
Introduction	138
Photoaffinity labeling of proteins	138
Overview	138
Commonly utilized photoactivatable functional groups.....	140
Diazirine-based photoaffinity labeling.....	140
Azide-containing PLD photoaffinity probes	142
Cellular and <i>in vitro</i> potency	142
Verification of the photolysis reaction in a model system	144
Verification of protein stability during UV irradiation	146
Development of a strategy to confirm covalent labeling of PLD.....	147
Enzyme activity assay following dialysis of a known noncovalent inhibitor	147
Enzyme activity assay following dialysis of an azide-containing photoprobe	150
Proteolysis and CID MS/MS analysis of arylazide-labeled, truncated PLD1 and PLD2 constructs	151
Analysis of arylazide photoprobe fragments under CID conditions	151
In-gel trypsin digestion.....	154

Trifluoromethylaryldiazirine-containing PLD photoaffinity probes	155
Rationale for the use of a carbene	155
Truncated PLD1c <i>in vitro</i> potency and specificity	156
Confirmation of photolysis via LC-MS	156
Verification of protein stability during UV irradiation	157
Verification of covalent labeling via dialysis and enzyme activity assay	158
Fragmentation of the diazirine-containing probe with CID and HCD to identify fragments	160
CID fragments	160
HCD fragments	162
In-solution proteolysis with trypsin to increase data quality and sequence coverage (compared to in-gel digests)	163
Proteomic analysis of diazirine-labeled, truncated PLD1c	164
HCD MS/MS analysis	164
Data analysis	168
Materials and methods	170
HFMT.PLD2.d308 expression and purification	170
Modifications to PLD1c.d311 chromatography	172
Dialysis assay procedure	172
Photolabeling procedure	173
UV irradiation	173
In-gel trypsin digestion	173
In-solution trypsin digestion	175
Proteomics methods and data analysis	175
 IV. SUMMARY AND FUTURE DIRECTIONS	 177
 COPYRIGHT PERMISSIONS	 189
 REFERENCES	 194

LIST OF FIGURES

Figure		Page
CHAPTER I		
1.	PLD-catalyzed hydrolysis and transphosphatidylation	2
2.	Various enzyme-catalyzed reactions that produce PtdOH and some of the cellular functions regulated by PtdOH	4
3.	Hopping versus scooting modes of catalysis occurring at a lipid bilayer	6
4.	Comparison of the domain architectures of PLD enzymes from various organisms	12
5.	Proposed PLD reaction mechanism.....	14
6.	Mammalian PLD domain architecture	24
7.	Causes of mortality in the United States of America: 1950 versus 2006	54

CHAPTER II

1.	Reported indirect PLD inhibitors 1-10	59
2.	Reported direct PLD inhibitors 11-20	62
3.	Structure of halopemide (21) and an optimized analog called FIPI (22)	66
4.	An iterative analog synthesis workflow diagram for the development of isoform selective PLD inhibitors.....	68
5.	Initial SAR studies on halopemide	70
6.	Focused lead optimization strategy to improve PLD1 potency and selectivity within scaffold 25 , and parallel strategy to improve PLD2 potency and selectivity within scaffold 26	71
7.	Synthetic scheme for various halogenated benzimidazolones	72
8.	Chemical structures of plain, 4-F, 5-F, 5-Cl, 5-Br, and 6-F benzimidazolone scaffolds used in an attempt to improve PLD1 potency and selectivity.....	73
9.	Chemical structures and activities of various unsubstituted 1-(piperidin-4-yl)-1 <i>H</i> -benzo[<i>d</i>]imidazol-2(3 <i>H</i>)-ones.....	74
10.	Chemical structures and activities of various halogenated 1-(piperidin-4-yl)-1 <i>H</i> -benzo[<i>d</i>]imidazol-2(3 <i>H</i>)-ones.....	76
11.	Chemical structures and activities of various halogenated 1-(piperidin-4-yl)-1 <i>H</i> -benzo[<i>d</i>]imidazol-2(3 <i>H</i>)-ones coupled to an ethylenediamine linker containing a chiral (<i>S</i>)-methyl group	78
12.	Concentration response curves for 41p (VU0359595) in the cellular PLD1 and PLD2 enzyme activity assays	80
13.	Key structure activity relationships that led to the development of 41p (VU0359595).....	81
14.	Key structural modifications (shown in red) that led to the development of 41p (VU0359595)	82
15.	Chemical synthesis of 41p (VU0359595) from commercially available starting materials.....	83

16.	Chemical structures of the two diastereomers of 41p (VU0359595).....	84
17.	UV absorbance trace showing the separation of the two diastereomers of 41p (VU0359595).....	85
18.	UV absorbance trace showing the purity of each diastereomer of 41p (VU0359595).....	86
19.	Concentration response curves for each diastereomer of 41p (VU0359595) in the cellular PLD1 and PLD2 enzyme activity assays.....	87
20.	Chemical structures of various scaffolds tested for their ability to confer PLD2 selectivity	88
21.	Synthetic scheme for various 1,3,8-triazaspiro[4,5]decan-4-one-containing PLD inhibitors	89
22.	Chemical structures and activities of various 1,3,8-triazaspiro[4,5]decan-4-ones	91
23.	Chemical structures and activities of various 1,3,8-triazaspiro[4,5]decan-4-ones	93
24.	Chemical synthesis of various halogen substituted 1,3,8-triazaspiro[4,5]decan-4-ones	95
25.	Chemical synthesis of various halogen substituted 1,3,8-triazaspiro[4,5]decan-4-one-containing PLD2 inhibitors	96
26.	Chemical structures and activities of various 1,3,8-triazaspiro[4,5]decan-4-one-containing PLD2 inhibitors	97
27.	Concentration response curves for 71a (VU0364739)	98
28.	Inhibition of PLD2 with 71a (VU0364739) leads to decreased proliferation of MDA-MB-231 cells.....	100
29.	Inhibition of PLD2 leads to a time-dependent decrease in proliferation of MDA-MB-231 cells	101
30.	Inhibition of PLD2 leads to increased apoptosis in MDA-MB-231 cells compared with minimal effect of PLD1 inhibition	102
31.	Pharmacokinetic profile of 41p (VU0359595) and 71a (VU0364739) in rat	103
32.	Chemical structures and activities of PLD2 preferring inhibitor 63a	104

33.	Chemical structures and activities of PLD2 preferring inhibitor 71a (VU0364739).....	105
34.	Key structural modifications (shown in blue) that led to the development of 71a (VU0364739)	106

CHAPTER III

1.	Idealized workflow for a photoaffinity labeling experiment.....	139
2.	The three most commonly used photoactivatable groups: (1) benzophenones, (2) azides and (3) diazirines.	140
3.	First generation PLD photoaffinity probes containing arylazides.....	143
4.	Photolysis reaction of compound 4 and subsequent insertion of a nitrene into compound 8	145
5.	LC-MS characterization of the photolysis reaction of compound 4 and subsequent insertion of a nitrene into compound 8	146
6.	PLD enzyme activity in response to UV irradiation at 310 nm.....	147
7.	SDS-PAGE gel comparing the mobility of untreated and treated HFMT.PLD2.d308.....	148
8.	Dialysis based strategy to determine if PLD has been covalently labeled by a photoprobe.....	148
9.	VU0364739 binding to HFMT.PLD2.d308 is reversible	150
10.	Arylazide compound 4 covalently labels HFMT.PLD2.d308 in a UV light exposure-dependent manner	151
11.	Compound 4 reacts with water to form a hydroxylamine after being activated by UV light.....	152
12.	MS2 fragments formed from the <i>m/z</i> 474 peak corresponding to compound 11	153
13.	MS2 fragments formed from the <i>m/z</i> 476 peak corresponding to compound 11	153
14.	Chemical structure of compound 15 (VU0487289)	155
15.	<i>In vitro</i> enzyme activity assays of recombinant PLD1 and PLD2 constructs in response to compound 15 (VU0487289) treatment.....	156
16.	LC-MS characterization of the photolysis reaction of compound 15 and subsequent reaction of the carbene with methanol	157

17.	<i>In vitro</i> enzyme activity assay of recombinant PLD1c.d311 in response to UV treatment at 365 nm and various concentrations of 15 plus/minus UV light	158
18.	Trifluoromethylaryldiazirine compound 15 covalently labels HFMT.PLD2.d308 in a UV light exposure-independent manner	159
19.	Trifluoromethylaryldiazirine compound 15 covalently labels HFMT.PLD2.d308 in a UV light exposure-independent manner	160
20.	MS1 spectrum (zoomed) of 15	161
21.	MS2 spectrum of <i>m/z</i> 537 from 15 under CID conditions	162
22.	MS2 spectrum of <i>m/z</i> 537 from 15 under HCD conditions	163
23.	Base peak chromatogram of trypsin digested PLD1c.d311	164
24.	The carbene formed from the photoactivation of trifluoromethylaryldiazirine 15 reacts with water to form an alcohol	165
25.	Base peak chromatogram of trypsin digested PLD1c.d311 plus a large molar excess of 15 (treated with UV light)	166
26.	Zoomed view of <i>m/z</i> 565 peak from Figure 25	167
27.	Zoomed view of <i>m/z</i> 555/557 peak from Figure 25	167

Figure	Page
CHAPTER IV	
1. Structure of halopemide (1) and an optimized analog called FIPI (2)	178
2. Initial SAR studies on halopemide	180
3. Key structural modifications (shown in red) that led to the development of 6 (VU0359595).....	181
4. Key structural modifications (shown in blue) that led to the development of 8 (VU0364739)	182
5. Pharmacokinetic profile of VU0359595 and VU0364739 in rat.....	183
6. HFMT.PLD2.d308 displays substrate inhibition kinetics	185
7. Chemical structures of azide 9 and diazirine 10 -containing photoprobes.....	186
8. Chemical structure of alkyne-containing photoprobe 11	187

LIST OF ABBREVIATIONS

AEBSF	4-(2-aminoethyl)benzene sulfonyl fluoride
Arf	ADP ribosylation factor
ATX	Autotaxin
CID	Collision-induced dissociation
clogP	Calculated octanol-water partition coefficient
cLPtdOH	Cyclic lyso-phosphatidic acid
DAG	Diacylglycerol
DAGK	Diacylglycerol kinase
DMPK	Drug metabolism and pharmacokinetics
DMSO	Dimethyl sulfoxide
DNA	Deoxyribonucleic acid
EGFR	Epidermal growth factor receptor
ESI-MS	Electrospray ionization mass spectrometry
FDA	Food and Drug Administration
fMLP	Formyl-Met-Leu-Phe
GPCR	G protein-coupled receptor
GPI	Glycosylphosphatidylinositol
GPI-PLD	Glycosylphosphatidylinositol phospholipase D
GTP	Guanosine-5'-triphosphate
HCD	Higher-energy collisional dissociation
HFMT	6x His-Flag-MBP-TEV
HPLC	High-performance liquid chromatography

IgE	Immunoglobulin E
IP3	Inositol trisphosphate
IV	Intravenous
LPE	Lysophosphatidylethanolamine
LPS	Lysophosphatidylserine
LC-MS	Liquid chromatography, mass spectrometry
LPAAT	Lysophosphatidic acid acyltransferase
LPtdCho	Lysophosphatidylcholine
LPtdOH	Lysophosphatidic acid
MALDI-TOF	Matrix-assisted laser desorption/ionization-time of flight
MS/MS	Tandem mass spectrometry
mTOR	The mammalian target of rapamycin
m/z	Mass to charge ratio
NADPH	Nicotinamide adenine dinucleotide phosphate
NAE	N-acylethanolamine
NAPE	N-acylphosphatidylethanolamine
NAPE-PLD	N-acyl phosphatidylethanolamine phospholipase D
NCBI	National Center for Biotechnology Information
NMR	Nuclear magnetic resonance
PAP	Purple-acid phosphatase
PH	Pleckstrin homology domain
PIP	Phosphatidylinositol 4-phosphate
PI(4,5)P ₂	Phosphatidylinositol 4,5-bisphosphate

PIP ₃	Phosphatidylinositol (3,4,5)-trisphosphate
PI3K	Phosphatidylinositol-4,5-bisphosphate 3-kinase
PKC	Protein kinase C
PLC	Phospholipase C
PLD	Phospholipase D
PMA	Phorbol 12-myristate 13-acetate
PO	<i>Peroral</i> , by mouth
PtdCho	Phosphatidylcholine
PtdOH	Phosphatidic acid
PX	Phox homology domain
RNA	Ribonucleic acid
RNAi	RNA interference
RTK	Receptor tyrosine kinase
SAR	Structure activity relationship
scPLD	<i>Streptomyces chromofuscus</i> phospholipase D
SDS-PAGE	Sodium dodecyl sulfate-polyacrylamide gel electrophoresis
shRNA	Short hairpin RNA
SH2	Src homology 2 domain
siRNA	Small interfering RNA
SM	Sphingomyelin
TLC	Thin-layer chromatography
UV	Ultraviolet
VICB	Vanderbilt Institute of Chemical Biology

Chapter I

INTRODUCTION

Enzymes with phospholipase D activity

Overview

Lipids are essential biomolecules that fulfill roles as structural building blocks, energy storage units and both inter-cellular and intra-cellular signaling molecules. The term “lipid” encompasses a structurally diverse group of molecules including (but not limited to) fat-soluble vitamins, sterols, fatty acids and glycerophospholipids. Many lipids, and the enzymes that modify them, play fundamental roles in both human physiology and various human pathologies (Vance and Vance, 2002).

Many enzymes, including phospholipases, facilitate the biochemical transformation of various lipids. Phospholipase D's (PLD) phosphodiesterase enzyme activity was first observed in various plant species (Hanahan and Chaikoff, 1947a; Hanahan and Chaikoff, 1947b; Hanahan and Chaikoff, 1948). Subsequently, enzymes from a plethora of organisms, including humans, were reported to display PLD activity. Over a timespan of about 60 years more than 4000 PLD enzyme sequences have been entered into the NCBI GenBank database (Selvy et al., 2011). Endogenously, PLD catalyzes the hydrolysis of phosphatidylcholine (PtdCho) into phosphatidic acid (PtdOH) and free choline; however, in the presence of some primary alcohols (*n*-butanol is shown in **Figure 1**) PLD catalyzes a transphosphatidylation reaction (**Figure 1**). In fact, it is possible to monitor PLD enzyme activity in intact cells and model organisms (such as

zebrafish) by monitoring the amount of phosphatidylalcohol produced by PLD in the presence of deuterated *n*-butanol (Brown, 2007; Zeng et al., 2009).

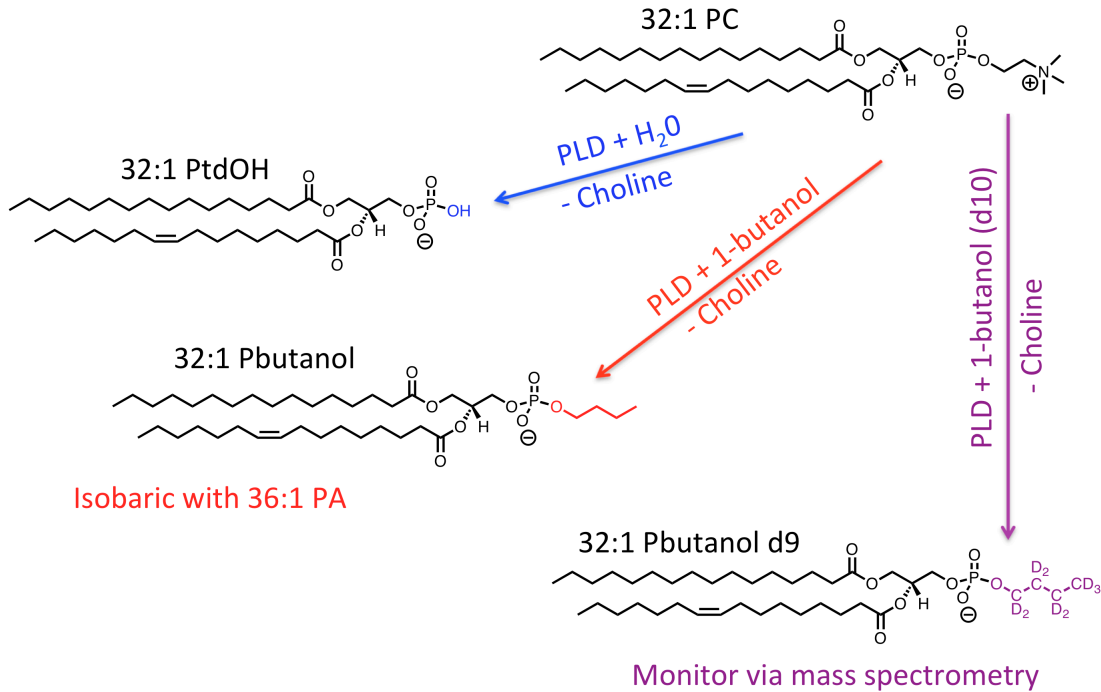


Figure 1. PLD-catalyzed hydrolysis and transphosphatidylation. The hydrolysis reaction is highlighted in blue, and the transphosphatidylation reaction is depicted in red. A transphosphatidylation reaction utilizing deuterated *n*-butanol is shown in purple.

PtdOH plays roles in both normal physiological processes and a variety of disease states. As an example, because of its relatively the small, polar head group PtdOH causes changes in membrane curvature that promote membrane fusion events, such as vesicular trafficking and endocytosis (Stace and Ktistakis, 2006). Yet, altered PtdOH signaling has been observed in multiple cancer types (Noh et al., 2000; Park et al., 2009; Yamada et al., 2003; Zhao et al., 2000), neurodegenerative diseases (Oliveira and Di Paolo, 2010), and thrombotic diseases (Elvers et al., 2010). These observations coupled with the fact that

the first reported PLD1 knockout mice (Elvers et al., 2010) were viable, fertile, developed normally and did not display morphological or behavioral abnormalities suggest that PLD and other enzymes that modulate cellular levels of PtdOH may be viable drug targets.

PtdOH can be generated by sequential enzyme-catalyzed acylations of glycerol-3-phosphate, or generated in response to changes in cell signaling pathways (Athenstaedt and Daum, 1999; Athenstaedt et al., 1999; Gibellini and Smith, 2010). All glycerophospholipids synthesized in eukaryotic membranes transition through PtdOH, a pathway characterized by Eugene Kennedy and his colleagues in the 1950s (Gibellini and Smith, 2010; Kennedy, 1958). PtdOH that is utilized for cell signaling purposes is typically generated by enzymes that modify lipids already present in a cell membrane. In addition to PLD this includes enzymes such as lysophosphatidic acid acyltransferase (LPAAT) which acylates lysophosphatidic acid (LPtdOH) and diacylglycerol kinase (DAG kinase), which phosphorylates diacylglycerol (DAG) at the *sn*-3 position (Selvy et al., 2011) (**Figure 2**). Thus, it is important to consider both that PtdOH generated from these different signaling sources may not be identical in function and that pharmacologically blocking the production of PtdOH from one source may alter the amount of PtdOH being produced by a different enzyme.

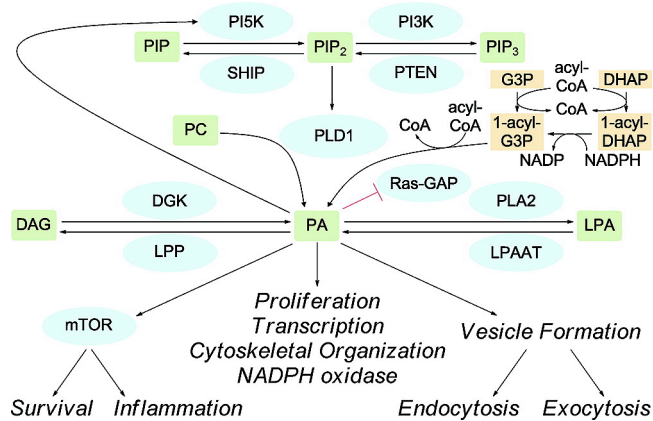


Figure 2. Various enzyme-catalyzed reactions that produce PtdOH and some of the cellular functions regulated by PtdOH. In this figure only PC=phosphatidylcholine, PA=phosphatidic acid and LPA=lysophosphatidic acid (Figure reproduced with permission from Selvy *et al.* 2011).

Many enzymes with PLD activity share a conserved HxKxxxxDx₆GSxN catalytic motif (HKD) (Ponting and Kerr, 1996). Based on sequence, these enzymes compose the PLD superfamily, and are thought to follow a similar reaction mechanism. The two human PLD isoforms discussed extensively herein both contain bilobal HKD catalytic domains (Hammond *et al.*, 1995; Lopez *et al.*, 1998). Enzymes that possess PLD catalytic activity yet do not contain even a single HKD catalytic motif display a variety of structures and possible catalytic mechanisms. While many of these non-HKD enzymes play important biological roles that are relevant to human physiology at times they are not the focus of this dissertation and are only discussed briefly below.

Non-HKD Enzymes

Enzymes that possess PLD-like catalytic activity yet do not contain a conserved HKD catalytic motif are termed non-HKD PLDs. A detailed discussion of these enzymes is not relevant to this dissertation, but a brief overview of some of them for completeness

and comparison to the conserved HKD-containing PLDs is included. A more thorough discussion of these enzymes can be found in Selvy *et al.* 2011.

The most well characterized non-HKD PLD is a 57 kDa enzyme secreted by *Streptomyces chromofuscus*, scPLD (Imamura and Horiuti, 1979; Yoshioka, 1991). Unlike the conserved HKD PLDs, scPLD can act as both a phosphodiesterase and a phosphatase (Zambonelli *et al.*, 2003). Site-directed mutagenesis studies utilizing scPLD show that catalysis occurs via a metal-dependent mechanism similar to that of the purple-acid phosphatase family (PAP); a Fe^{3+} cation is required for the one-step, acid-base catalyzed reaction mechanism, whereas substrate binding appears to occur in a Mn^{2+} cation dependent fashion (Zambonelli *et al.*, 2003). Like HKD-containing PLDs, scPLD can catalyze a transphosphatidylolation reaction, although it does so far less efficiently than HKD-containing PLD enzymes (Yang and Roberts, 2003).

A key difference in the enzymology between HKD-containing PLDs and scPLD is that HKD-containing PLD enzyme activity is dependent on the surface mole fraction of substrate within a lipid micelle or vesicle whereas scPLD activity is not dependent on the surface mole fraction of substrate within a lipid micelle or vesicle (Stieglitz *et al.*, 1999). Put another way the HKD-containing PLD enzymes are sensitive to how a substrate is presented whereas scPLD activity is not sensitive to how a substrate is presented. These different modes of catalysis are also referred to as the “hopping” versus “scooting” mode of enzyme activity (**Figure 3**).

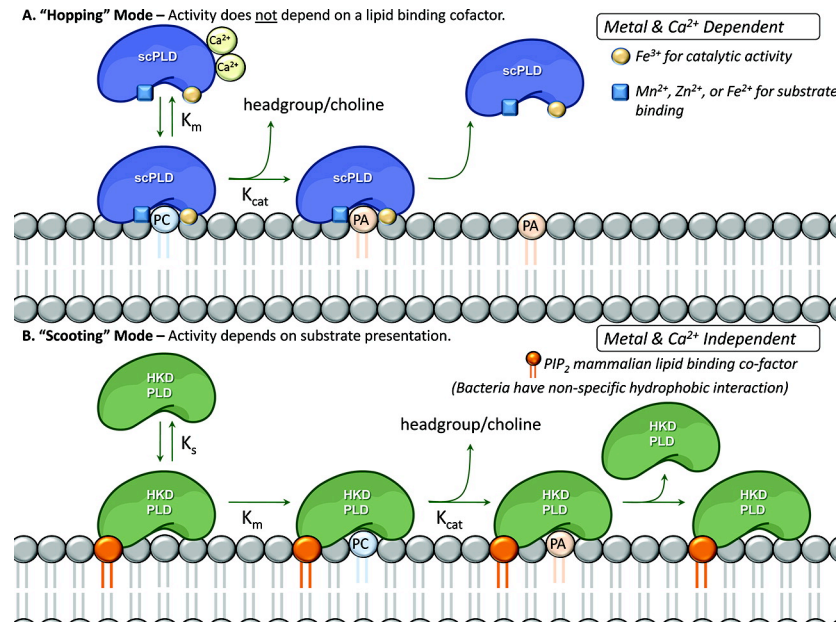


Figure 3. Hopping versus scooting modes of catalysis occurring at a lipid bilayer. **A.** A “hopping” mode enzyme does not depend on a lipid cofactor to facilitate substrate binding/turnover **B.** A “scooting” mode enzyme is sensitive to substrate presentation (Figure reproduced with permission from Selvy *et al.* 2011).

Interestingly, bacteria and poisonous spiders both utilize non-HKD-containing, PLD-like enzymes as virulence factors or toxins. The Gram-positive pathogens *Corynebacterium* and *Arcanobacterium* both secrete divalent cation dependent, non-HKD PLDs (Cuevas and Songer, 1993; McNamara *et al.*, 1995; Yabu *et al.*, 2008). These enzymes have been shown to function as virulence factors (Hodgson *et al.*, 1992; McNamara *et al.*, 1994; Soucek and Souckova, 1974). In contrast to the conserved HKD PLD enzymes that hydrolyze PtdCho these bacterial enzymes hydrolyze sphingomyelin (SM). Again in contrast to mammalian sphingomyelinases that release PtdCho and ceramide these bacterial enzymes release choline and ceramide-1-phosphate (Hodgson *et al.*, 1990; Lucas *et al.*, 2010). The PLD-like enzyme from *Corynebacterium* has been shown to possess lysophospholipase D activity, that is to say this enzyme can hydrolyze lysophosphatidylcholine (LPtdCho) to generate lysophosphatidic acid (LPtdOH) (van

Meeteren et al., 2004). LPTdOH is a ligand for various G protein-coupled receptors (GPCR) and this activity of the PLD-like enzyme from *Corynebacterium* may initiate a variety of inflammatory signaling events concomitant with bacterial infection.

The non-HKD-containing, PLD-like enzymes from *Corynebacterium* and *Arcanobacterium* both function as virulence factors *in vivo*. They cause a range of clinical symptoms including thrombosis, hemolysis and vascular leakage (Lucas et al., 2010). Additionally, the LPTdOH from *Corynebacterium* likely causes platelet aggregation, endothelial cell permeability and a generalized pro-inflammatory response to infection (van Meeteren et al., 2004).

The non-HKD-containing, PLD-like enzyme from the brown recluse spider, *Loxosceles reclusa*, shares significant sequence homology with the *Corynebacterium* and *Arcanobacterium* non-HKD-containing, PLD-like enzyme that catalyzes the hydrolysis of SM to ceramide-1-phosphate (Murakami et al., 2005). Other spiders of the genus *Loxosceles* also express this enzyme as it a critical component of various spider venoms. Much the same as the bacterial enzymes discussed above these enzymes cause clinical symptoms such as dermonecrosis, thrombosis, vascular leakage, hemolysis and generalized inflammation (Futrell, 1992; Tambourgi et al., 1998; van Meeteren et al., 2004). The crystal structures of the two subtypes of this enzyme, both from *Loxosceles laeta*, have been determined and the active site structural differences lead to a likely explanation for their differences in catalytic activity (de Giuseppe et al., 2011; Murakami et al., 2005).

Prior to a more in-depth discussion of the classical HKD-containing PLD enzymes there are several human enzymes with PLD-like activity that will be briefly

addressed: (1) Glycosylphosphatidylinositol phospholipase D (GPI-PLD), (2) N-acyl phosphatidylethanolamine phospholipase D (NAPE-PLD) and (3) autotaxin (ATX). Although these enzymes differ from the HKD-containing PLD superfamily enzymes significantly in sequence, structure and enzymology they perform PLD-like reactions and play important roles in human biology.

GPI-PLD catalyzes the hydrolysis of the phosphodiester bond of glycosylphosphatidylinositol (GPI) thereby releasing inositolphosphoglycan (a non-N-acylated hexosamine coupled to inositol phosphate, IPG) and PtdOH (Jones et al., 1997; Jones and Varela-Nieto, 1998). GPI-PLD catalysis occurs at its N-terminus via a Zn^{2+} binding site coordinated by five histidine residues (Raikwar et al., 2005). Notably, GPI-PLD shares distant homology with PI-PLC (Li et al., 1994). GPI-PLD is a secreted enzyme and perturbations in serum levels of this enzyme have been identified in several diseases including acute hepatitis (Raymond et al., 1994), nonalcoholic fatty liver disease (Chalasani et al., 2006), and type 1 diabetes (Deeg et al., 2001; Schofield et al., 2002). Pharmacological modulation of GPI-PLD activity has been suggested as a possible therapeutic modality for some of these diseases (Brunner et al., 1996; Chalasani et al., 2006; Deeg et al., 2007; Tang et al., 2009).

NAPE-PLD catalyzes the hydrolysis of various *N*-acyl phosphatidylethanolamine species to generate the endocannabinoid *N*-acylethanolamine (NAE) and PtdOH (Okamoto et al., 2004; Schmid et al., 1983). Like GPI-PLD, NAPE-PLD utilizes Zn^{2+} to catalyze hydrolysis (Wang et al., 2006). NAPE-PLD displays substrate specificity for NAPE and does not appear to hydrolyze PtdCho or other potential lipid substrates (Wang et al., 2006). Additionally, this enzyme does not catalyze a transphosphatidylation

reaction (Okamoto et al., 2004). When the *N*-acyl chain of NAPE is arachidonate, the NAE generated by NAPE-PLD is anandamide, a cannabinoid receptor (CB1 and CB2) antagonist. These receptors are expressed in the central nervous system or immune system, respectively (Wang and Ueda, 2009). Endocannabinoid signaling is implicated in a diverse range of physiological processes such as appetite, pain sensation, mood, memory, and fertility (Pertwee, 2008). Endocannabinoid signaling is proving to be a highly complex network that is currently under intense investigation and has generated significant interest from the pharmaceutical industry.

The NAPE-PLD knockout mice generated by Leung and colleagues were viable, healthy and showed no overt differences in behavior compared to wild-type controls (Leung et al., 2006). In these mice, levels of NAPE increased in the brain, while total NAE decreased, as one might reasonably expect with a NAPE-PLD knockout animal. However, levels of polyunsaturated NAE (including anandamide) were not significantly altered indicating that some NAPE-PLD independent pathway is likely to be generating certain NAE species (Leung et al., 2006). Potent, small molecule inhibitors of NAPE-PLD are not present in the literature at this time, but may have clinical utility. The perturbation of various endocannabinoid signaling pathways is an active area of drug development as a variety of disease states appear to display altered endocannabinoid signaling (Burch et al., 2009; Pacher et al., 2006; Zajicek et al., 2003; Zhang et al., 2011).

Technically, Autotaxin (ATX) is a Lysophospholipase D. ATX possesses a variety of enzyme activities including phospholipase activity (Aoki et al., 2002; Clair et al., 2003; Umezu-Goto et al., 2002) and nucleotide pyrophosphate hydrolytic activity (Clair et al., 1997). Lysophospholipids, including lysophosphatidylcholine (LPtdCho),

lysophosphatidylethanolamine (LPE), and lysophosphatidylserine (LPS) are all ATX substrates (van Meeteren et al., 2005). Like both previously discussed non-HKD PLDs ATX catalysis is dependent on Zn^{2+} ions. However, unlike the other human non-HKD enzymes previously discussed, ATX can catalyze both hydrolysis and transphosphatidylation (Tania et al., 2010). ATX is expressed as a preproenzyme and subsequently secreted via an N-terminal secretion signal. ATX is present in human blood and its lysoPLD activity is the main source of LPtdOH in human blood (Tokumura et al., 2002; Tsuda et al., 2006). Depending on its immediate microenvironment, ATX will either hydrolyze LPtdCho to form LPtdOH, or transphosphatidylate LPtdCho, and use the free hydroxyl group in the *sn*-2 position to generate cyclic LPtdOH (cLPtdOH) (Tsuda et al., 2006). These different products appear to exert different physiological effects. LPtdOH (Ren et al., 2006) is important in chemotactic cell migration and platelet aggregation, whereas cLPtdOH (Murakami-Murofushi et al., 1993) inhibits cell proliferation, cell invasion and metastasis.

ATX knockout mice die at approximately embryonic day 10 (Tanaka et al., 2006). While normally this would not be evidence in favor of pursuing ATX as a drug target this case is somewhat unique. Further research into which product of ATX is necessary for life (or if both are) may yet allow for highly specific pharmacological modulation of ATX in various disease states.

HKD Enzymes

Primary sequence

Whereas the so termed “non-HKD” PLDs display a wide range of primary sequence/structure variability and catalytic mechanisms the HKD enzymes all (by definition) share a conserved catalytic domain. Hence, the HKD enzymes share a mechanism for the hydrolysis of phosphodiester bonds. As with any attempt to neatly (and artificially) categorize biological entities no one system can be considered perfect; we have argued for the inclusion of all phosphodiesterases with a conserved HKD (or HKD-like) motif in the PLD superfamily (Selvy et al., 2011). The rationale for this nomenclature is one based on function: these enzymes share a S_N2 ping-pong reaction mechanism that proceeds through a covalent phospho-histidine intermediate (Liscovitch et al., 2000; Stanacev and Stuhne-Sekalec, 1970).

PLD enzymes have been identified in nearly all forms of life. After a significant number of PLD genes from different organisms were sequenced a common set of conserved motifs (I-IV) were observed including the conserved catalytic sequence HxKxxxxDx₆G(G/S)xN (HKD) (Ponting and Kerr, 1996). It appears likely that a gene duplication event occurred during evolution as a variety of viruses and prokaryotes contain a single HKD catalytic domain, whereas many PLDs (including the human enzyme) contain two HKD motifs comprising a bilobal catalytic domain (Koonin, 1996) (**Figure 4**).

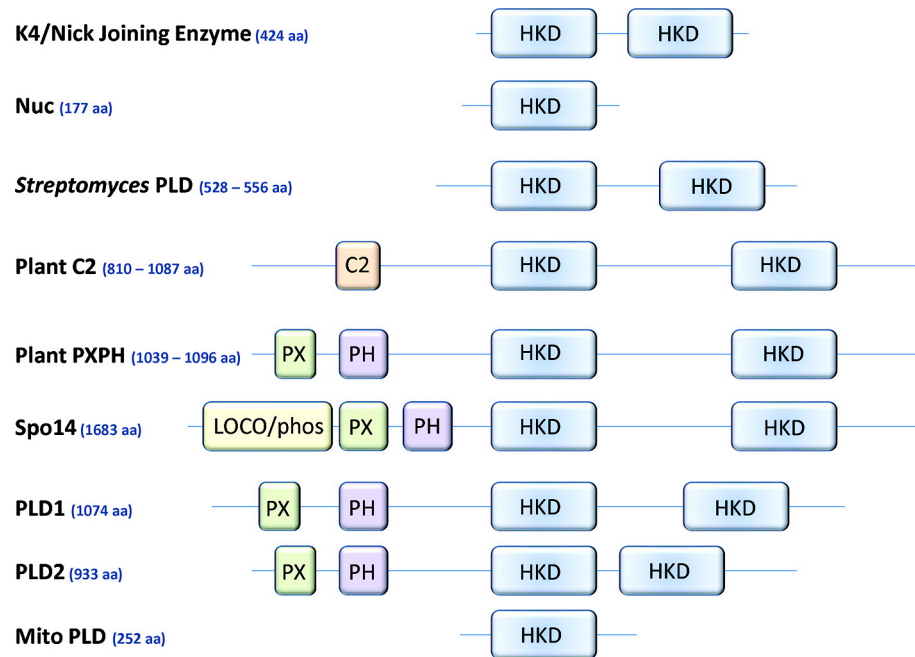


Figure 4. Comparison of the domain architectures of PLD enzymes from various organisms (Figure reproduced with permission from Selvy *et al.* 2011).

Structure

Most of the structure-function relationships inferred about eukaryotic PLDs are necessarily based on the structures of bacterial PLDs, because the eukaryotic enzymes have proven exceptionally challenging to express, purify, stabilize and crystallize. From the limited number of crystal structures that have been reported from bacterial enzymes it does appear that a conserved tertiary structure about the HKD catalytic motif(s) exists (Abergel *et al.*, 2001; Davies *et al.*, 2002a; Davies *et al.*, 2002b; Leiros *et al.*, 2000a; Leiros *et al.*, 2000b; Rudolph *et al.*, 1999; Stuckey and Dixon, 1999).

In 2000 the first bilobal catalytic domain-containing PLD enzyme structure was reported (Leiros *et al.*, 2000b). Biochemical experiments performed on this *Streptomyces sp.* PMF PLD have provided some evidence about the function(s) of certain domains (Uesugi and Hatanaka, 2009). In terms of the HxKxxxxDx₆G(G/S)xN catalytic motif the

histidine and lysine residues, which interact directly with a substrate, are on β -strands whereas the GG/GS residues sit in the base of the active site and appear to have an effect on substrate specificity and overall thermostability of the enzyme (Ogino et al., 2007).

Catalytic mechanism: hydrolysis versus transphosphatidylation

In the 1960s and 1970s Yang *et al.* (Yang et al., 1967) and Stanacev and Stuhne-Sekalec *et al.* (Stanacev and Stuhne-Sekalec, 1970) proposed that PLD catalysis proceeds through a two-step “ping-pong” reaction mechanism including the formation of a covalent phospho-protein intermediate. Understandably so, the tools available to these groups at the time limited their ability to precisely examine the specific residues required for catalysis. In the 1990s with developments in fields such as DNA sequencing and phylogenetics it became ever more practical to ask biochemical questions based on evidence from molecular evolution. Based on the observations of Ponting and Kerr (Ponting and Kerr, 1996) and Koonin (Koonin, 1996) which showed conserved, duplicate HxKxxxxDx₆G(G/S)xN motifs in the PLD superfamily members, it was suggested that the key residue(s) for PLD catalysis reside within this stretch of amino acids.

Studies performed in the 1990s using a 1-HKD bacterial enzyme, Nuc endonuclease (Gottlin et al., 1998), and a 2-HKD bacterial PLD, *Yersinia pestis* murine toxin (YMT) (Rudolph et al., 1999), showed that histidine residues are the key residues in the PLD catalytic mechanism. These studies both support the reaction mechanism that is currently favored within the field (**Figure 5**) and are in agreement with additional, independent evidence discussed below.

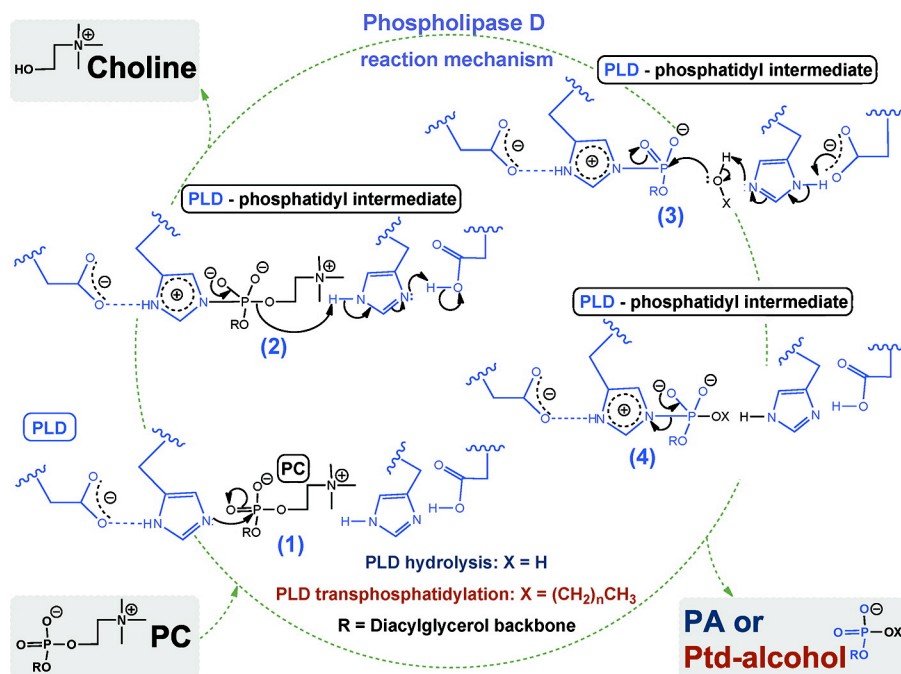


Figure 5. Proposed PLD reaction mechanism. In this figure only PC=phosphatidylcholine and PA=phosphatidic acid (Figure reproduced with permission from Selvy *et al.* 2011).

In this enzyme-catalyzed reaction mechanism the N-terminal histidine residue within the HKD motif acts as a nucleophile and attacks the phosphate group of the substrate, (step 1, **Figure 5**) and forms a covalent phospho-histidine intermediate. The histidine residue of the C-terminal HKD motif behaves as a general acid, and donates a proton to the choline leaving group (step 2, **Figure 5**). Formation of the phospho-histidine intermediate has been proposed to be the rate-limiting step. Subsequent nucleophilic attack by a hydroxyl group from either a water molecule or a primary alcohol (steps 3 and 4, **Figure 5**) followed by PtdOH or phosphatidylalcohol product release rapidly occurs in parallel (Yang and Roberts, 2003). For human PLD, and most HKD PLDs, short chain primary alcohols are actually preferred as a nucleophile over water. Thus, transphosphatidylation can occur even at very low concentrations of alcohol (Stanacev and Stuhne-Sekalec, 1970).

Independent evidence from structural studies and biophysics work supports the validity of the reaction mechanism described above. Whether present as a homodimer or in a bilobal catalytic domain the two HKD catalytic motifs appear in close proximity to each other (Leiros et al., 2000b; Stuckey and Dixon, 1999). Even more provocatively, Leiros *et al.* were able to soak a short chain PtdCho (dibutyrylphosphatidylcholine) substrate into PMF PLD crystals and capture crystal structures of reaction intermediates, including the phospho-histidine intermediate (Leiros et al., 2004). Additionally, Orth *et al.* were able to capture the covalent phospho-histidine intermediate using electrospray ionization mass spectrometry (ESI-MS) (Orth et al., 2010). Thus, a consilience of evidence from the fields of phylogenetics, biochemistry and structural biology appears to indicate that the reaction mechanism discussed above (**Figure 5**) is correct.

Interfacial kinetics

In vivo, lipids are often present as parts of a complex mixture of components in a biological membrane. Therefore, the substrates of many lipid-modifying enzymes are neither freely soluble nor are they in great excess compared to relevant enzyme concentrations (Deems, 2000). These two conditions mean that many lipid-modifying enzymes violate some of the basic assumptions of Michaelis-Menten kinetics. PLD fits into this category of lipid-modifying enzymes and actually demonstrates interfacial kinetics (Henage et al., 2006).

One important, practical consequence of studying interfacial enzymes is that in addition to what are commonly termed K_m and k_{cat} an additional variable, K_s , must also be taken into account. This additional variable describes the membrane association step of a

lipid-modifying enzyme during catalysis. Much like other steps in catalysis, membrane association can be affected by a multitude of variables including charge, local pH, membrane fluidity, substrate presentation etc. (Deems, 2000).

In order to study kinetic parameters for “scooting” (**Figure 3**) enzymes, such as human PLD, interfacial binding, K_s , must be measured separately from K_m and k_{cat} . There are a variety of ways to study protein-lipid binding (and in turn K_s) ranging from classic methods such as the sedimentation of sucrose loaded vesicles (Buser and McLaughlin, 1998) to a rather interesting, new liposome microarray technology (Saliba et al., 2014). Following determination of K_s , Michaelis-Menten kinetic assumptions can be applied for “scooting” mode enzymes if the bulk lipid concentration is much, much greater than K_s , and interfacial binding is saturated. The mole fraction of substrate is varied while bulk lipid concentration is held constant by compensating for variation in the mole fraction of substrate with a neutral lipid, called a neutral diluent. This format for studying kinetic parameters of an interfacial enzyme is referred to as surface dilution kinetics (Carman et al., 1995). A thorough kinetic analysis of mammalian PLD (Henage et al., 2006) has been reported.

***In vitro* enzyme activity assays**

The first biochemical assays of PLD activity were performed using radioactivity to monitor the amount of substrate depleted or product formed over time via thin layer chromatography (TLC). In these experiments the migration of lipid species (substrate and product) on a TLC plate was compared to the migration of known standards (Yang et al., 1967). Following these initial experiments a variety of assay types have been

described. Commercial kits are available for measuring PLD activity *in vitro*; however, these kits indirectly measure choline release via a color change caused by two subsequent enzyme-catalyzed reactions (Amplex® Red PLD assay kit, Life Technologies <http://www.lifetechnologies.com/order/catalog/product/A12219>). This method of assaying PLD activity can be useful because it can be utilized with a monomeric (short chain) PtdCho substrate thus removing the lipid association step from the reaction mechanism. However, the correct controls must be performed in order to ensure that nothing in the assay conditions interferes with either of the two enzymes responsible for using choline to catalyze a color change via the formation of resorufin (emission at 585 nm) from the amplex® red reagent.

Enzyme activity assays in which the substrate is presented as part of a liposome are more laborious and complex, but are unequivocally more physiologically relevant (Brown et al., 1993; Brown et al., 2007). In these assays a tritium-containing choline headgroup remains in the soluble portion of a reaction mixture while the insoluble lipids are precipitated and subsequently pelleted via centrifugation. In this fashion, the amount of substrate turned over can be directly measured and quantified via scintillation counting. Sonication can be used to prepare liposomes; however, sonication causes the formation of multilamellar vesicles. These vesicles do allow for the measurement of enzyme activity, and the comparison of different reaction conditions within the same assay. However, the inter-assay variability in surface concentration of substrate can be significant, making multilamellar vesicles less than ideal for precise measurements. Extrusion is the gold-standard method for generating nearly uniform, unilamellar vesicles.

Cellular enzyme activity assays

As far back as the 1960s it was known that, in addition to hydrolysis, PLD enzymes could also catalyze a transphosphatidylation reaction (Yang et al., 1967). Importantly, Stanacev and Stuhne-Sekalec showed that a significant amount of transphosphatidylation occurs even with very small amount of alcohol present (Stanacev and Stuhne-Sekalec, 1970). As with *in vitro* PLD enzyme activity assays, TLC was used to visualize phosphatidylalcohols by monitoring the co-migration of radioisotopically labeled lipids with phosphatidylalcohol standards. More recently, a robust, non-radioisotope-based cellular enzyme activity assay was developed (Brown et al., 2007). In this assay ESI-MS is utilized to monitor the formation of deuterated phosphatidylbutanol following incubation of cells with low concentrations of deuterated *n*-butanol. The use of deuterated *n*-butanol facilitates measurement of the resultant deuterated phosphatidylbutanol species because the mass to charge ratio of the species formed using non-deuterated *n*-butanol is located in a noisy area of the mass spectrum observed when examining a cellular lipid extract.

PLD enzymes from microorganisms and model organisms

Plant PLD

As is the case with many important human genes and proteins the basis for much (if not most) of what we know about human PLD was originally discovered in model organisms. Plants in particular have played a central role in the history of PLD. While an extremely comprehensive review of plant PLD enzymes can be found in Selvy *et al.*

2011, a brief overview of the PLD enzymes from several model/eukaryotic organisms, including plants, is included below.

The first report of PLD enzyme activity was from a carrot extract in 1947 (Hanahan and Chaikoff, 1947b) and about 20 years later the hydrolytic and transphosphatidylolation activities of PLD were measured in cabbage extracts (Yang et al., 1967). In 1994 the first PLD was cloned from a castor bean (Wang et al., 1994). Most of the plant PLD literature has made use of the model organism *Arabidopsis thaliana*. Given that the entire genome of this organism has been sequenced the identification and genetic manipulation of plant PLDs in this organism was quite feasible.

Plant PLD enzymes contain two-conserved HKD motifs and can be divided into essentially two groups, C2-PLDs and PXP-PLDs, based on the type of amino-terminal regulatory domains present upstream of the catalytic domain (Elias et al., 2002; Wang, 2000). C2-PLDs have an N-terminal C2 calcium-binding domain that is not found in mammalian PLDs (Hong et al., 2010). The PXP-PLDs from plants are more closely related to mammalian PLDs, and have amino-terminal phox homology (PX) and pleckstrin homology (PH) domains important for mediating specific lipid interactions (Hong et al., 2010; Qin and Wang, 2002). At least 12 *Arabidopsis* PLD genes have been identified, of which ten are classified as C2-PLD genes and two are classified as PXP-PLD genes (Li et al., 2009).

Members of the Plant C2-PLD subdomain have been divided into 5 groups: PLD α , PLD β , PLD γ , PLD δ , PLD ϵ . The defining characteristic of all C2-PLDs is the C2 domain at the amino terminus that is important in calcium sensing and phospholipid binding (Wang, 1999; Wang, 2000). Two plant PLDs, PLD ζ 1 and PLD ζ 2, have been

identified that contain N-terminal phox homology (PX) and pleckstrin homology (PH) lipid binding domains (Qin and Wang, 2002; Taniguchi et al., 2010). These PXPX-containing PLDs do not require calcium for catalysis, rather these enzymes catalyze PtdCho hydrolysis in a PI(4,5)P₂ dependent manner (Qin and Wang, 2002). These enzymes are more similar to the mammalian PLD enzymes than their C2 domain-containing counterparts.

Fungal PLD

Budding yeast

PLD enzyme activity was observed in yeast long before any specific PLD genes were identified in yeast. In the 1970s PLD activity was observed in *Saccharomyces cerevisiae* following glucose stimulation (Dharmalingam and Jayaraman, 1971; Grossman et al., 1973). It wasn't until about 20 years later that a variety of studies identified PLD enzymes in various yeast species. PLD1 from yeast, called Spo14, was identified in *Saccharomyces cerevisiae* (Ella et al., 1995; Honigberg et al., 1992; Kishida and Shimoda, 1986; Rose et al., 1995). Spo14 shares sequence and biochemical similarities the other eukaryotic PLDs discussed herein. Spo14 has been shown play a role in yeast sporulation (Honigberg et al., 1992; Rose et al., 1995), vesicular trafficking (Neiman, 1998) and mating (Harkins et al., 2008).

Fission yeast

A 2-HKD-containing PLD enzyme was also cloned from *Schizosaccharomyces pombe* (Harkins et al., 2010). The PLD enzyme from *Schizosaccharomyces pombe*

shares significant sequence homology with Spo14, but does display some clear biochemical differences from Spo14. Unlike Spo14, PI(4,5)P₂ does not have any effect on *Schizosaccharomyces pombe* PLD enzyme activity. Similar to Spo14, *S. pombe* PLD1 plays functional roles in sporulation and mating. Also similar to Spo14, this *S. pombe* PLD1 was shown to catalyze both hydrolysis and transphosphatidylation (Harkins et al., 2010).

***C. elegans* PLD**

As recently as a 2009 review article (Raghu et al., 2009b) there is very little information published about the PLD gene from *Caenorhabditis elegans* (*C. elegans*). A single, 1427 aa PLD has been cloned from *C. elegans* and although this enzyme is expressed throughout the pharyngeal muscles and neurons a clear function for this enzyme has not been shown (Nakashima, 2000). PLD knockout animals do not demonstrate a visible phenotype (Liu et al., 1999; Matthies et al., 2006). A recent study performed by Kinchen *et al.* suggests this enzyme may regulate phagosome dynamics, which would be in agreement with some work on the mammalian PLD enzymes (Kinchen et al., 2008).

***Drosophila melanogaster* PLD**

Drosophila PLD (dPLD) is quite similar to *C. elegans* PLD in many respects. The dPLD enzyme contains 2 HKD catalytic motifs as well as PX and PH domains (Raghu et al., 2009b). *Drosophila* PLD enzyme activity was first described in larvae grown on ethanol-containing food (Miller et al., 1993). LaLonde *et al.* later isolated

dPLD cDNA from *Drosophila* (LaLonde et al., 2005). *Drosophila* PLD plays roles in vesicular trafficking (LaLonde et al., 2006) and phototransduction (Raghu et al., 2009a). Much like the case of *C. elegans*, dPLD null mutants are viable; however, unlike the *C. elegans* knockouts the dPLD null mutants do display some clear abnormalities. *Drosophila* PLD deficient animals demonstrate problems with cellularization and decreased photoreceptor signal transduction rendering the animals less sensitive to light stimulus (LaLonde et al., 2006).

Zebrafish PLD

In 2003 Ghosh *et al.* cloned a portion of a PLD enzyme from zebrafish (*Danio rerio*) (Ghosh et al., 2003). Several years later Zeng *et al.* reported the complete zPLD1 sequence along with substantial *in vitro* and *in vivo* characterization of zPLD1 (Zeng et al., 2009). Zebrafish PLD is strikingly similar to human mammalian PLD1 in many ways. This enzyme possesses the two HKD motifs present in most eukaryotic PLDs and responds to many of the same regulatory factors as the mammalian PLD1 enzyme.

PLD activity can be measured in intact zebrafish simply by treating zebrafish with a solution containing deuterated *n*-butanol. Zeng *et al.* monitored zPLD1 activity via ESI-MS as was depicted in **Figure 1**. Using several independent approaches Zeng *et al.* showed that zPLD1 plays a role in vascular development. Knocking zPLD1 down with morpholinos caused impaired intersegmental blood vessel formation (Zeng et al., 2009). Further utilization of zebrafish as a model system in which to monitor PLD activity *in vivo* could facilitate a greater understanding of the functional roles of PLD with respect to both physiology and various pathologies.

Mammalian PLD

Isoforms

The focus of this dissertation is, of course, the pharmacological inhibition of human PLD enzymes and as such the rest of the text will focus almost exclusively on the mammalian PLD enzymes. PLD activity in mammalian tissues was first observed in 1973 (Saito and Kanfer, 1973). Since that observation has taken place various mammalian PLD enzymes have been cloned and studied. For many years biochemical and genetic means were used to probe the functions PLD plays in cells and whole animals, but more recently serious attempts at creating small-molecule enzyme inhibitors have been undertaken (Selvy et al., 2011).

The two PLD enzymes most relevant to this dissertation (and most well characterized) are PLD1 (Hammond et al., 1995) and PLD2 (Colley et al., 1997; Lopez et al., 1998; Steed et al., 1998). These two isoforms share about 50% sequence identity including near complete identity around the two conserved HKD catalytic motifs present in each isoform. A notable region of difference among the two isoforms is a loop region N-terminal to a conserved polybasic PI(4,5)P₂ binding domain (Sciorra et al., 1999) (**Figure 6**). PLD1 contains a thermolabile loop region that varies in size depending on the splice variant expressed (PLD1a = 116 aa versus PLD1b = 78 aa) (Hammond et al., 1997). PLD2 essentially does not have this loop region at all. Shortened, inactive splice variants with unknown functions of both PLD1 and PLD2 have been identified (Steed et al., 1998).

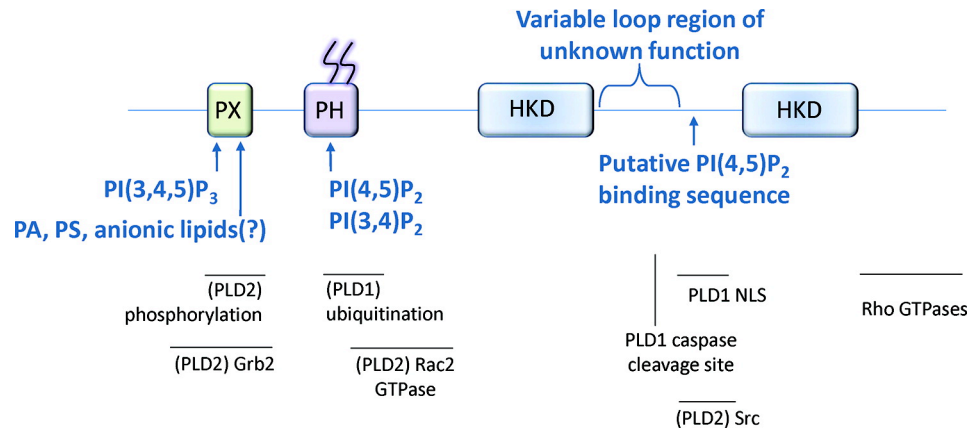


Figure 6. Mammalian PLD domain architecture (Figure reproduced with permission from Selvy *et al.* 2011).

Similar to PLD enzymes from some of the eukaryotic model organisms discussed above both PLD1 and PLD2 contain the same regulatory domains at their N-termini. The PX and PH domains are known to facilitate interactions with lipid membranes (Steed *et al.*, 1998). These N-terminal regulatory domains are not required for catalytic activity (Sung *et al.*, 1999). In the case of PLD, removing portions of the N-terminus of the protein (up to a point) actually appears to increase PLD1 activity (Henage *et al.*, 2006). Notably, removing more than about 311 amino acids from the N-terminus of PLD1 leads to catalytically inactive constructs (unpublished data, Lavieri and Brown). In contrast to the N-terminus, any perturbations at the C-terminus of either PLD1 or PLD2 seem to decrease catalytic activity (Liu *et al.*, 2001).

In addition to the relatively well characterized PLD1 and PLD2 isoforms there are two other reported human PLD enzymes that are not nearly as well characterized and differ quite substantially from PLD1/PLD2 in overall domain architecture and sequence identity. A single-HKD enzyme, called mitoPLD, was recently identified (Choi *et al.*,

2006). It appears that the physiologically relevant substrate of this PLD is cardiolipin. Cardiolipin is abundant in mitochondrial membranes and mitoPLD appears to play a role in promoting mitochondrial fusion events (Choi et al., 2006). The PLD3 enzyme contains two HxKxxxxD/E motifs (one motif contains aspartic acid, the other contains glutamic acid) (Cao et al., 1997). However, essentially no biochemical characterization of this gene or protein has taken place and the protein does not appear to possess canonical PLD enzyme activity (Osisami et al., 2012).

Tissue expression and subcellular localization

Tissue expression

PLD1 and PLD2 are both expressed in nearly all mammalian tissues. In general, it seems that PLD is regulated at the level of cell signaling as opposed to being regulated at the level of gene expression. PLD1 is expressed particularly well in the human heart, pancreas, brain, uterus and intestine. PLD2 is expressed particularly well in the brain, placenta lung, thymus, prostate and uterus (Lopez et al., 1998).

PLD1 subcellular localization

Under basal conditions PLD1 tends to localize to perinuclear membranes, lysosomes and endosomes (Brown et al., 1998; Colley et al., 1997; Du et al., 2003; Hughes and Parker, 2001). The biochemical basis for this localization has been investigated to some extent and features such as palmitoylation have been used to explain membrane association under basal conditions (Sugars et al., 1999). Notably, catalytically inactive point mutants (PLD1b K466E and K860E) localize to endosomes in a similar

fashion as wildtype enzyme, indicating that catalytic activity and membrane binding are, to some extent, independent biochemical events. Following stimulation with agents such as IgE or PMA PLD1 translocates to the plasma membrane (Brown et al., 1998; Du et al., 2003). These results seem to suggest a model wherein some extracellular stimulus must cause PLD to translocate to the cell membrane thereby activating the enzyme.

PLD2 subcellular localization

Unlike the dynamic membrane interactions observed in the case of PLD1, PLD2 is typically found at the cell membrane. This has been shown using overexpressed and native expression levels of PLD2 (Colley et al., 1997; Du et al., 2004). Under agonist stimulation PLD2 appears to co-localize with the relevant receptor(s) and participate in receptor desensitization/recycling (Du et al., 2004). Various extracellular stimuli can in fact alter PLD2 localization. As an example, EGF-stimulation causes PLD2 to localize to membrane ruffles (Honda et al., 1999)

Regulation

Divalent cations

As was the case with the PLD enzymes from various organisms discussed earlier mammalian PLD enzyme activity is influenced by divalent cation concentrations. *In vivo*, PLD activity is affected by changes in calcium concentration, which suggests calcium facilitates some kind of signaling cascade involving PLD, such as PKC signaling, and indirectly modulates PLD activity (Ohguchi et al., 1996). *In vitro* PLD activity is sensitive to both magnesium and calcium concentrations; however, about half

maximal enzyme activity can be obtained in the absence of either cation (Brown et al., 1995). Magnesium concentrations at or above 1 mM have stimulatory effects. By contrast calcium does not seem to exert a large effect *in vitro* (Brown et al., 1995).

Post-translational modification

While PLD activity *in vivo* largely appears to be regulated quite acutely at the cell signaling level PLD is subject to several classic mechanisms of post-translational modification. Both PLD1 (Sugars et al., 1999) and PLD2 (Xie et al., 2002b) are palmitoylated at two cysteine residues within their respective PH domains. In PLD1, C240 and C241 are palmitoylated (Sugars et al., 1999), and in PLD2 C223 and C224 are palmitoylated (Xie et al., 2002b). Based on studies comparing wildtype to Cys to Ala point mutants (unable to be palmitoylated), these modifications do not significantly affect *in vitro* catalytic activity; however, *in vivo* catalytic activity and proper cellular localization of the protein are both decreased (Sugars et al., 1999).

A number of papers have reported various phosphorylations of PLD1 and PLD2. The physiological consequence of these phosphorylations, if any, is not always known and can be highly dependent on a variety of other signaling events occurring in parallel. It has been known for some time that various PKC isoforms can stimulate PLD1 activity both *in vitro* and *in vivo* (Singer et al., 1995). Interestingly, several residues on PLD1 are phosphorylated by PKC (Kim et al., 1999), yet activation of PLD1 *in vitro* appears to be phosphorylation-independent (Hu and Exton, 2003).

Recently, several papers have reported some precise PLD2 phosphorylation sites and some of the relevant physiological consequences. Proteomics analyses of COS-7

cells stimulated with PMA resulted in the identification of several phosphorylated residues: S134, S146, S243, T72, T99, T252 (Chen and Exton, 2005). However, the exact functional consequences of many of these events are not known, and may depend on many dependent variables. Henkels *et al.* utilized MS-based proteomic analysis to identify phosphorylated residues on PLD2 (Henkels et al., 2010). The Epidermal growth factor receptor (EGFR) decreases PLD2 catalytic activity via phosphorylation at Tyr296. In response to JAK3 phosphorylation of Tyr415 PLD2 activity increases and Src phosphorylation Tyr511 has no effect on catalytic activity (Henkels et al., 2010). However, the Src phosphorylation likely exerts a structural/biophysical change that affects intermolecular interactions.

In 2010 Yin *et al.* showed that PLD1, but not PLD2, is multi-monoubiquitinated (Yin et al., 2010). Interestingly, inhibition of PLD1 activity either via genetic or pharmacological means decreases the amount of ubiquitination observed. Similarly, interfering with the proper localization of the PLD1 also caused a lower level of ubiquitination to occur. Thus it appears that to be targeted for degradation PLD1 must be both catalytically active and properly localized. Also, the degradation of PLD1 was blocked by proteasome inhibitors, but not by inhibitors of other proteases (Yin et al., 2010). Ubiquitination appears to be a previously unrecognized PLD1 negative regulatory mechanism.

In addition to being palmitoylated, phosphorylated and ubiquitinated PLD can be cleaved by caspases. Both PLD1 and PLD2 can be cleaved by caspases 3 and 8, and PLD1 is also a substrate of caspase 7 (Jang et al., 2008a; Jang et al., 2008b; Riebeling et al., 2008). Unlike PLD2, caspase proteolysis appears to regulate PLD1 localization and

activity in a complex fashion. *In vivo*, caspase 3 cleaves PLD1 primarily at position 545 resulting in the liberation of a 56 kDa C-terminal fragment which localizes to the nucleus via an exposed nuclear localization sequence and a 60 kDa N-terminal fragment (NF-PLD1) that remains in the cytosol (Jang et al., 2008a). Full length PLD1 acts to suppress apoptosis by decreasing p53 signaling. Once proteolyzed, the PLD1 fragment acts as a dominant negative (for the full length PLD1 enzyme) thereby causing an increase in p53 signaling (Jang et al., 2008b). Ultimately, the caspase 3 cleavage of PLD1 causes an increase in p53 dependent apoptotic signaling.

Lipid cofactors

The importance of PIP₂ as a cofactor for mammalian PLD enzymes is highlighted by the fact that during the development of the gold standard *in vitro* reconstitution enzyme activity assay it was discovered that PIP₂ was required to detect choline hydrolysis catalyzed by PLD purified from HL-60 membranes (Brown et al., 1993). Liscovitch *et al.* also showed that PIP₂ stimulates brain membrane PLD activity *in vitro* (Liscovitch et al., 1994). A few years later when PLD1 and PLD2 were recombinantly expressed and purified PIP₂ was again required to measure PLD catalytic activity *in vitro* (Colley et al., 1997; Hammond et al., 1995; Lopez et al., 1998). Other PIP species, including PIP₃, are also able to stimulate PLD activity, albeit to a lesser extent than PIP₂ (Hammond et al., 1997).

PIP₂ is known to bind to PLD at two separate sites. The polybasic PI(4,5)P₂ binding motif binds PIP₂ with high specificity and affinity. Both *in vitro* catalytic activity and PIP₂ binding decreased substantially when these residues in PLD2 were

mutated (Sciorra et al., 1999). Interestingly, these mutations did not affect PLD2 subcellular localization leading naturally to the hypothesis that the PIP₂ binding site contained within the PH domain must govern subcellular localization. Mutation of the conserved residues (compared to other PH domains) in the PLD2 PH domain yielded an enzyme that was inactive in intact cells, but was in fact catalytically active *in vitro*. Additionally, mutating Arg237 and Trp238 to alanine residues resulted in PLD2 partitioning into detergent-soluble membrane fractions instead of detergent-insoluble membrane fractions, where the wildtype enzyme is normally located (Sciorra et al., 2002).

Regulatory proteins

The ADP-ribosylation factor (Arf) proteins are small GTPases that play roles in a variety of cellular events such as vesicle formation and cytoskeletal rearrangement (Campa and Randazzo, 2008). A significant number of studies have shown that various small GTPases regulate PLD activity. Initially, it was found that adding cytosol and GTPγS (a non-hydrolysable GTP analog that activates small G proteins) to HL-60 cell membranes stimulated PLD activity. Subsequently, the specific factor responsible for stimulating PLD activity was isolated and identified as an Arf GTPase (Brown et al., 1993; Cockcroft et al., 1994). Arf1 and Arf6 were the first proteins shown to stimulate PLD activity in an *in vitro* reconstitution assay (Brown et al., 1993). Soon after these discoveries data seemed to suggest that only PLD1 (and not PLD2) is highly responsive to Arf stimulation (Colley et al., 1997). Indeed, several groups have shown PLD

activation by Arf in excess of 10-fold (Hammond et al., 1997; Henage et al., 2006; Lopez et al., 1998).

Much like Arf, the Rho family of small GTPases, including RhoA, Cdc42, Rac1 and Rac2, plays roles in regulating cytoskeletal rearrangement (Boureaux et al., 2007). Studies utilizing purified PLD1a and PLD1b have shown that RhoA, Rac1 and Cdc42 all directly activate PLD1 (Singer et al., 1995; Hammond et al., 1997; Henage et al., 2006; Walker and Brown, 2002). Much like Arf, the Rho family proteins do not cause robust changes in PLD2 activity (Colley et al., 1997). While the exact points of interaction between PLD1 and Rho are not known, various studies indicate that the interaction likely occurs near the C-terminus of PLD1 (Cai and Exton, 2001).

In addition to Arf and Rho, several other small GTPases have been shown to modulate PLD activity. Both *in vitro* and *in vivo* (mouse) work has shown that Ras can signal through PLD in a physiologically relevant manner (Buchanan et al., 2005; Carnero et al., 1994). RalA appears to be involved in PLD activation and can be co-immunoprecipitated with PLD1, but it seems that the relationship between RalA and PLD1 is not direct (Kim et al., 1998; Luo et al., 1997). Additionally, Rheb has also been reported to activate PLD1 *in vitro* (Sun et al., 2008).

The interactions between PLD and PKC are fairly complex and only a brief summary is included below. In intact cells PKC stimulates both PLD1 and PLD2 activity downstream of phospholipase C (PLC) activation. PKC phosphorylates PLD1 and PLD2 at serine and threonine residues, but it appears that PLD activation is not phosphorylation-dependent (Chen and Exton, 2004; Kim et al., 1999). PKC stimulated (via PMA) PLD activity occurs immediately, but maximal PLD phosphorylation occurs

roughly an hour later with a concomitant decrease in PLD activity, suggesting phosphorylation of PLD by PKC actually decreases PLD activity (Chen and Exton, 2004; Hu and Exton, 2003). The PKC binding domain on PLD was mapped to the N-terminus of PLD1b (Kook and Exton, 2005); however, PKC is able to activate N-terminally truncated PLD1 in a phosphorylation-independent mechanism (Henage et al., 2006) and N-terminally truncated PLD1 still co-immunoprecipitated with PKC (Sung et al., 1999). Thus, it appears that there are actually two PKC binding sites on PLD1, an N-terminal site and a C-terminal site (Park et al., 1998). *In vitro*, PKC stimulates the activity of full-length PLD1 to a greater magnitude than PKC stimulates an N-terminally truncated PLD1 construct (Henage et al., 2006). The various ways in which PKC and the various small GTPases interact with PLD likely contribute to a multifaceted regulatory network *in vivo*.

Signaling pathways

Receptor tyrosine kinases

The epidermal growth factor receptor (EGFR) is a prototypical receptor tyrosine kinase (RTK). Binding of EGFR to its ligand, epidermal growth factor, leads to RTK dimerization and autophosphorylation. The subsequent activation of various signal transduction pathways includes those that regulate cell proliferation, differentiation and survival. Both wildtype and mutant EGFR receptors are often overexpressed in cancer cells and targeting EGFR directly, or indirectly, has been an ongoing approach utilized to treat various cancers (Herbst, 2004). The autophosphorylation of several tyrosine residues located in the cytoplasmic portion of the receptor creates a high affinity binding site for

several important intracellular proteins containing Src-homology 2 (SH2) domains including Src, PLC γ 1, Grb2 and PI3K (Riese et al., 2007). It has been appreciated for some time that EGFR activation leads to an increase in PLD activity (Fisher et al., 1991).

There are several possible ways that EGFR activation can cause an increase in PLD activity. The most thoroughly characterized EGFR-PLD activation pathway starts when PLC γ 1 binds to an activated EGFR receptor. Next, PLC γ 1 hydrolyzes PI(4,5)P₂ to produce DAG and IP₃. IP₃ causes an increase in calcium levels, which in addition to DAG, activates PKC (Rana and Hokin, 1990). As was previously discussed, PKC is a well-established activator of PLD (Henage et al., 2006). In addition to the well known PLC γ 1-PKC signaling pathway EGFR can also signal to PLD through the Ras signaling pathway. RalA is a Ras effector and GTP-bound RalA appears to activate PLD (Luo et al., 1997; Voss et al., 1999). In a distinct mechanism, PLD2 is directly, physically activated by an activated EGFR complex. PLD2 binds directly to the SH2 domain of the EGFR-bound Grb2 (Di Fulvio et al., 2007).

G protein-coupled receptors

G protein-coupled receptors (GPCR) are cell surface, transmembrane receptors that mediate an enormous number of physiologically relevant cell signaling events and as such have been the focus of many drug development projects. Under basal conditions, GPCRs bind various heterotrimeric G-proteins. Ligand binding to the extracellular domain(s) of a GPCR leads to a conformational change in the receptor that causes GDP to GTP exchange in the G α subunit of a G-protein (Qin et al., 2011). The GTP-bound G α subunit then dissociates from the G $\beta\gamma$ subunit and each subunit can participate in various

downstream signaling events. The various classes of heterotrimeric G-proteins activate different cell signaling pathways. After a ligand bound GPCR triggers guanine nucleotide exchange, GTP-bound $G\alpha_q$ causes PLC β to hydrolyze PI(4,5)P₂ leading to the formation of DAG and IP₃ (Rhee, 2001). IP₃ triggers calcium release from intracellular stores which activates PKC, and DAG also activates PKC. As was previously discussed in more detail, PKC activates PLD (Plonk et al., 1998; Xie et al., 2002a). In addition to the classical $G\alpha_q$ activation pathway several GPCRs and G-proteins are capable of stimulating PLD activity, including $G\alpha_{12/13}$.

The $G\alpha_{12/13}$ class of heterotrimeric G-proteins activates PLD in a small GTPase dependent manner (Mitchell et al., 1998). In the case of $G\alpha_{12}$, PLD1 is ultimately activated by RhoA through a Pyk2-dependent mechanism. $G\alpha_{13}$ activates the γ subtype of PI3K thereby causing the production of PIP₃. Upon PIP₃ binding, ARNO and Rho GEF cause guanine nucleotide exchange to occur on Arf and RhoA, respectively (Plonk et al., 1998). These activated small GTPases can then directly activate PLD. The GPCR activation of PLD pathways described above are by no means comprehensive as there are many ways that GPCRs can activate PLD.

The mammalian target of rapamycin

While it appears likely that there is some signaling relationship between PLD and mTOR the precise mechanism of such a relationship is likely complicated and many studies to date have utilized methods which can very easily lead to incorrect conclusions. Initial reports associating the PtdOH produced by PLD with mTOR activation used primary alcohols (at very high concentrations) to cause a decrease in the amount of

PtdOH formed (instead phosphatidylalcohols were formed) (Fang et al., 2001; Toschi et al., 2009). In these studies the treatment of cells with primary alcohols caused a decrease in mTOR kinase activity, as measured by the amount of phospho p70S6K kinase. In two separate papers Chen *et al.* utilized MBA-MB-231 breast cancer cells to argue that elevated PLD activity provides an alternative survival signal (from PI3K) in mTOR-dependent cancer cells (Chen et al., 2005; Chen et al., 2003).

A more recent biophysics study utilized NMR spectroscopy to examine the PtdOH binding site on the FRB domain of mTOR (Leone et al., 2006). This work is undoubtedly significant and interesting; however, it is important to keep in mind that enzymes other than PLD can produce PtdOH. Both LPAAT (Blaskovich et al., 2013) and DAGK (Avila-Flores et al., 2005; Gorentla et al., 2011) have been shown to modulate mTOR signaling. Furthermore, recent work utilizing shRNA targeting PLD1 appears to show a decrease in phospho p70S6K compared to control shRNA (Sun et al., 2008). Somewhat puzzlingly, pharmacological inhibition of PLD with small-molecule inhibitors developed in our own lab has not yielded results consistent with some published findings concerning PLD and mTOR (unpublished data, Lavieri, Brown and Lindsley). This may simply be a case where the immediate pharmacological inhibition of PLD enzyme activity does something very different than the much longer-term knockdown of enzyme expression caused by RNA interference techniques. To make things even more confusing, mTOR signaling is one of the most complex, redundant, intertwined signaling networks known and more in depth characterization of many mTOR targets, simultaneously, will probably be necessary to better understand the relationship between PLD and mTOR.

Functional consequences of PLD inhibition or overexpression^a

Respiratory burst

Nicotinamide adenine dinucleotide phosphate-oxidase (NADPH oxidase) is a membrane bound enzyme complex that sits quiescently in neutrophils, eosinophils and mononuclear phagocytes until activated during respiratory burst. Upon activation, NADPH oxidase generates superoxide by transferring electrons from NADPH inside the cell across the cell membrane and then coupling the electrons to molecular oxygen. The superoxide radical is further transformed into hydrogen peroxide and hypohalous acids (e.g., hypochlorous acid), which are used as a form of ‘chemical warfare’ by human cells to attack human pathogens (Babior et al., 2002).

A host of experiments done in cells have indicated a role for PLD in NADPH oxidase activation. When PtdOH production in cultured human neutrophils is blocked via the use of *n*-butanol, the respiratory burst, as measured by O₂ production, was almost completely blocked (Rossi et al., 1990). There is additional evidence that PLD is involved in regulating NADPH oxidase activity both in cells and *in vitro*: when the leukotriene B₄ receptor is activated, levels of presqualene diphosphate rapidly decline thereby removing a negative regulatory element from inhibiting PLD’s capacity to stimulate NADPH oxidase activity (Levy et al., 1999).

Agwu and colleagues gathered the first evidence suggesting that didecanoyl-PtdOH activates NADPH oxidase *in vitro* by combining subcellular fractions in order to reconstitute NADPH oxidase activity and showing that didecanoyl-PtdOH activated this combination of subcellular fractions (Agwu et al., 1991). Almost a decade later McPhail

^a The text appearing on pages 36-68 is reproduced almost exactly with permission from Selvy et al. *Chemical Reviews*. **2011**. Copyright 2011 American Chemical Society.

et al. showed that, *in vitro*, PtdOH activates a protein kinase that phosphorylates and activates a component of the NADPH oxidase complex, p47-phox (McPhail et al., 1999). In 2011 Norton *et al.* utilized small molecule PLD inhibitors and PLD2 knockout mice to show that PLD1 (and not PLD2) regulates the production of reactive oxygen species in neutrophils (Norton et al., 2011). An excellent review of PLD function in respiratory physiology was provided by Cummings and colleagues (Cummings et al., 2002).

Transport and endocytosis

Vesicles are the primary means by which cells store, move and dispose of a multitude of cellular components. Eukaryotic cells are composed of various organelles that effectively share information and cargo via vesicular trafficking, which involves three steps: (1) budding from the donor compartment; (2) transport and/or targeting to a specific acceptor compartment, and (3) fusion of the vesicle with the acceptor compartment. Vesicular trafficking is a fundamental biological process and an excellent review was written by Bonifacino and Glick (Bonifacino and Glick, 2004). For a concise review of the role PLD plays in membrane trafficking the reader is referred to a review by Roth (Roth, 2008). Previous efforts to characterize the role of PLD in vesicular trafficking relied heavily on primary alcohols to block PLD-mediated PtdOH formation, but more recently drug-like, small molecules have been utilized to study the role of PLD in vesicular trafficking.

The use of primary alcohols to block PLD-mediated PtdOH formation or monitor product formation in cells by several groups yielded the first evidence supporting a role for PLD in exocytosis. Xie *et al.* measured significant increases in the amount of

phosphatidylethanol formed by HL60 granulocytes treated with ethanol during primary granule secretion. Additionally, ethanol dose-dependently decreased the release of myeloperoxidase from the HL60 granulocytes (Xie et al., 1991) and ethanol also blocked IgE-receptor-mediated mast cell degranulation (Gruchalla et al., 1990). Chen *et al.* showed that 1% *n*-butanol was sufficient to decrease the release of nascent secretory vesicles from the trans-golgi network, which they independently confirmed in parallel by treating permeabilized cells with a catalytically inactive PLD mutant (K898R). PLD also increases the release of nascent secretory vesicles in permeabilized cells (Chen et al., 1997). Additional evidence that PLD plays an important role in exocytosis was acquired via genetic manipulations in *Saccharomyces cerevisiae*. Ella *et al.* discovered a PLD gene in yeast and generated a genetic knockout, noting that diploid yeast lacking the PLD gene were unable to sporulate (Ella et al., 1996). These results suggest a broad role for PLD in regulating cell growth and division.

A role for PLD in endocytosis has been described and supported by the use of *n*-butanol, catalytically inactive mutants, and RNAi. PLD activity is required for agonist mediated-epidermal growth factor receptor internalization: (1) *n*-butanol decreases the agonist-stimulated internalization of the epidermal growth factor receptor; (2) overexpression of PLD1 or PLD2 increases the agonist-stimulated internalization of the epidermal growth factor receptor and (3) overexpression of catalytically inactive PLD1 or PLD2 decreases the agonist-stimulated internalization of the epidermal growth factor receptor (Shen et al., 2001). PLD activity is also required for μ -opioid receptor internalization: (1) *n*-butanol decreases the internalization of the μ -opioid receptor, and (2) overexpression of catalytically inactive PLD2 decreases the internalization of the μ -

opioid receptor (Koch et al., 2004; Koch et al., 2003). Recently, studies have taken advantage of RNAi as a means to examine the effects of PLD inhibition on endocytosis. Bhattacharya *et al.* showed that *n*-butanol, overexpression of a catalytically inactive PLD2, or PLD2 RNAi treatment all decrease the internalization of the mGluR1a metabotropic glutamate receptor (Bhattacharya et al., 2004). Du *et al.* also utilized RNAi to show that overexpression of a dominant-negative PLD2 (K758R) or transfection with PLD2 RNAi decreased the internalization of the angiotensin II type 1 receptor (Du et al., 2004).

A role for PLD1 in macroautophagy has been established by a rigorous set of experiments employing *n*-butanol, a pharmacological inhibitor, RNAi treatment and genetic knockout of PLD1 in a mouse. All of these treatments decreased autophagy as measured by a variety of different readouts (Dall'armi et al., 2010). Inhibition of autophagy via PLD1 inhibition may be desirable in some disease states and not others; the recent development of a 1700-fold PLD1-selective inhibitor (Lewis et al., 2009) should facilitate testing this hypothesis *in vivo*. PLD2 ablation via gene targeting in mice rescues memory deficits in a mouse model of Alzheimer's disease (Oliveira and Di Paolo, 2010). The recent development of a centrally penetrant PLD2-selective inhibitor (Lavieri et al., 2010) should facilitate rigorous *in vivo* target validation of PLD2 for Alzheimer's disease.

Platelet aggregation

A role for PLD in platelet activation has been previously suggested (Vorland and Holmsen, 2008). Due to the lack of small molecule inhibitors, previous studies had to

utilize imprecise tools that could not address how inhibiting PLD activity affected platelet aggregation (Haslam and Coorsen, 1993). However, in 2009 Disse *et al.* determined that PLD1 regulates the secretion of von Willebrand factor from endothelial cells utilizing either *n*-butanol or RNAi (Disse et al., 2009). Von Willebrand factor is one of the major procoagulant and proinflammatory proteins required for hemostasis and a deficiency of von Willebrand factor (von Willebrand disease) is the most common inherited bleeding disorder. Disse *et al.* first suggested that PLD might be involved in regulating the secretion of von Willebrand factor from vascular endothelial cells by showing that *n*-butanol decreased its histamine-induced secretion from vascular endothelial cells. Using an independent method of decreasing PLD activity, RNAi, Sadler *et al.* showed that PLD1 knockdown dramatically decreased the histamine-induced secretion of von Willebrand factor, whereas PLD2 RNAi had no effect on its histamine-induced secretion (Sadler, 1998).

Neuronal physiology

There has long been an association between PLD and neuronal physiology and pathology, but some truly provocative animal model data facilitated by gene targeting have recently emerged. A comprehensive review of the role of PLD in brain function is provided by Oliveira (Oliveira and Di Paolo, 2010). In the 1970s PLD activity was reported in mammalian brain tissue (Kobayashi and Kanfer, 1987; Saito and Kanfer, 1973). Reports have implicated PLD in the process of neurite outgrowth (Zhang et al., 2004) and functional roles for PLD in receptor trafficking, specifically the internalization

of opioid receptors and metabotropic glutamate receptors have also been reported (Bhattacharya et al., 2004; Koch et al., 2003).

A possible pathophysiological role for PLD in Alzheimer's disease has been suggested. Two groups independently reported increased PLD activity in brain tissue homogenates from Alzheimer's patients as compared to controls (Jin et al., 2007; Kanfer et al., 1996). Overexpressing amyloid precursor protein causes an increase in PLD activity in P19 mouse embryonic carcinoma cells (Lee et al., 2001). The amyloid β (1-40)-stimulated increase in PLD activity was correlated with the release of lactate dehydrogenase, which makes it reasonable to speculate that some of the neurotoxic actions of amyloid β (1-40) are mediated by PLD (Cox and Cohen, 1997).

The neurotoxic peptide α -synuclein has been implicated in the pathophysiology of both Parkinson's disease and Alzheimer's disease (Leong et al., 2009). Additionally, two point mutations in α -synuclein are genetically linked to familial Parkinson's disease (Kruger et al., 1998; Polymeropoulos et al., 1997). All three naturally occurring synuclein isoforms α , β , and γ -synuclein were reported to inhibit PLD2 *in vitro* (Jenco et al., 1998). Ahn *et al.* reported that PLD1 and PLD2 co-immunoprecipitate with α -synuclein, but also showed that PLD does not appear to impact the physiological lesions caused by α -synuclein (Ahn et al., 2002). By contrast, a collaborative investigation by the Selkoe and Brown laboratories found that under numerous experimental conditions α -synuclein does not inhibit PLD in cells or *in vitro* (Rappley et al., 2009).

Cell invasion and metastasis

Cancer cell invasion and metastasis are distinct, but not unrelated processes. Invasion refers to the ability of cancer cells to invade adjacent normal tissue, whereas metastasis refers to the ability of cancer cells to gain access to a circulatory system (blood or the lymphatic system) and colonize distinct and spatially distant physiological environments (Poste and Fidler, 1980). One of the critical early steps in metastasis is the invasion of surrounding tissue in order to gain access to either the blood or lymphatic system (Bacac and Stamenkovic, 2008). Some of the hallmarks of this invasion process include rearrangement of the actin cytoskeleton, increased cell motility and secretion of matrix metalloproteinases (Bacac and Stamenkovic, 2008). PLD has been shown to play a role in regulating all of these processes (Foster and Xu, 2003).

Experiments utilizing inactivating mutations of PLD suggest that inhibiting PLD enzymatic activity decreases cancer cell invasion (Zheng et al., 2006) and cells transfected with a dominant-negative PLD1 were unable to form actin stress fibers when stimulated with either phorbol myristate acetate (PMA) or lysophosphatidic acid (LPLtdOH), whereas wildtype cells were able to form actin stress fibers (Kam and Exton, 2001). A number of studies have shown that increased PLD activity leads to an increase in the invasion of cancer cells as measured by transwell migration assays and decreased PLD activity leads to a decrease in the invasion of cancer cells (Imamura, 1993; Knoepp et al., 2008; Park et al., 2009; Scott et al., 2009; Williger et al., 1999). PLD activity also regulates the expression of MMP-2 and MMP-9, the 72 kDa and 92 kDa gelatinases, respectively (Kato, 2005; Park et al., 2009; Reich et al., 1995; Williger et al., 1999).

The signaling pathways that connect PLD enzymatic activity to MMP expression are not entirely clear. A more complete understanding of how PLD drives MMP expression in specific cancers may lead to a better understanding of how to tailor antimetastatic therapies. To date, the vast majority of evidence implicating PLD in cell invasion comes from experiments utilizing *n*-butanol, overexpression of wildtype or dominant-negative PLD1/2 and/or RNAi. Furthermore, pharmacological inhibition of PLD1 and PLD2 with a dual-isoform inhibitor, VU0155056, decreases the invasion of several cancer cell lines in a Matrigel™ transwell invasion assay (Scott et al., 2009). Another group used the halopemide analog (FIPI), which was originally reported by Monovich *et al.* (Monovich, 2007) and showed that PLD inhibition blocked actin cytoskeleton reorganization, cell spreading and chemotaxis (Su et al., 2009).

Cell proliferation and apoptosis

Increased PLD expression and enzymatic activity have been observed in a variety of human cancers including breast (Noh et al., 2000), renal (Zhao et al., 2000), brain (Park et al., 2009), and colorectal (Yamada et al., 2003). Overexpression of PLD promotes cell growth and proliferation despite the presence of a variety of apoptotic stimuli (Joseph et al., 2002; Zhong et al., 2003). Furthermore, PLD activity is required for mutant Ras driven tumorigenesis in mice (Buchanan et al., 2005). Experiments utilizing inactivating mutations of PLD suggest that inhibiting PLD enzymatic activity increases cancer cell apoptosis (Shi et al., 2007). On a molecular level PLD has been implicated in oncogenic signaling pathways involving the epidermal growth factor receptor (Snider et al., 2010), matrix metalloproteinase (MMP) expression (Park et al.,

2009; Williger et al., 1999), p53 (Hui et al., 2004; Hui et al., 2006), the mammalian target of rapamycin (mTOR) (Chen et al., 2005) and Ras (Zhao, 2007). The signaling network interactions between PLD and the various Ras signaling pathways constitute a series of complex interactions. One such example is the observation that the recruitment of Raf-1 kinase (which is activated by Ras) to the plasma membrane is dependent upon a direct interaction with PtdOH (Rizzo, 1999; Rizzo et al., 2000). PLD activity contributes to key events in the oncogenic process including growth signaling, gatekeeper override, suppression of apoptosis and metastasis (Foster and Xu, 2003).

A wide variety of extracellular factors that stimulate cell proliferation have been shown to increase PLD activity. Platelet derived growth factor (PDGF) (Plevin et al., 1991), fibroblast growth factor (FGF) (Motoike et al., 1993) and EGF (Song et al., 1994) are able to significantly increase PLD activity in a variety of different cell lines under physiological conditions. Additionally, cells that are transformed by mutations in several robustly validated oncogenes also display increased PLD activity. Notably, cells transformed by v-Ras (Buchanan et al., 2005) or v-Raf (Frankel et al., 1999) display PLD activity that is several-fold higher than untransformed cells. PLD also facilitates the activation of the mitogen-activated protein kinase (MAPK) cascade (Foster and Xu, 2003). Treatment of cells with PtdOH (the enzymatic product of PLD) suppresses p53 expression (Jang et al., 2008b). PLD also acts to suppress the expression of p53 by stabilizing the MDM2-p53 complex (Hui et al., 2004). There are studies suggesting that PLD regulates the activity of mTOR, but the exact molecular mechanism of the PLD-mTOR interaction is being interrogated (Foster, 2009).

The laboratory of David Foster and other laboratories have reported that PLD activity regulates hypoxia inducible factor (HIF) expression. Under normoxic conditions the von Hippel-Lindau (VHL) tumor suppressor gene is expressed and encodes part of an E3 ubiquitin ligase that targets the α subunits of HIF for degradation by the proteasome (Kaelin, 2007). There are two known conditions in which overexpression of HIF occurs and provides a survival advantage to cancer cells: (1) von Hippel-Lindau disease and (2) in the hypoxic tumor microenvironment. The result is that unregulated overexpression of HIF leads to angiogenesis, increased red blood cell production, and a shift to anaerobic metabolism (Ohh, 2006). Toschi *et al.* utilized two VHL-deficient renal cancer cell lines (786-0 and RCC4) to show that HIF2 α expression is dependent on PLD. The authors provide evidence for this conclusion by using three independent approaches: (1) treating cells with *n*-butanol, (2) the expression of dominant-negative PLD constructs and (3) the use of RNAi targeted to PLD1 and/or PLD2 (Toschi et al., 2008).

It has been shown that decreasing PLD activity via genetic or biochemical approaches can increase cancer cell apoptosis (Foster and Xu, 2003; Zhong et al., 2003). There are also previous reports linking PLD to changes in caspase activity (Jang et al., 2008a; Jang et al., 2008b). However, few accounts exist of how pharmacological inhibition of PLD affects cancer cell apoptosis. In 2010, we showed that a PLD2-selective inhibitor, VU0364739, decreased the proliferation of MDA-MB-231 cells in a dose and time-dependent manner. VU0364739 also caused a several-fold increase in caspase 3/7-activity indicating that VU0364739 likely causes a decrease in cell proliferation (at least in part) by inducing apoptosis (Lavieri et al., 2010).

The Wnt signaling pathway has emerged as a central regulator of cell proliferation

and mutations in this pathway are clearly linked to oncogenesis. Briefly, there are several known Wnt signaling pathways (for reviews of the other Wnt pathways see (Katoh, 2005) and (Kohn and Moon, 2005)) and the canonical Wnt signaling pathway leads to the stabilization of β -catenin, which in turn activates T-cell factor-dependent transcription of a variety of target genes (Clevers, 2006). Kang *et al.* utilized *n*-butanol, RNAi and pharmacological inhibitors to provide good evidence of a relationship between PLD and the Wnt signaling pathway. Their principal findings were that: (1) Wnt3a increases PLD1 expression and activity in cultured cells, and β -catenin and TCF4 were required for this effect; (2) decreasing PLD activity decreases the ability of β -catenin to increase the transcription of PLD1 and other Wnt target genes; (3) PLD1 is necessary for Wnt-driven anchorage-independent growth and β -catenin/TCF4 are necessary for PLD1-driven anchorage-independent growth; and (4) the expression levels of PLD1 and PLD2 were substantially increased in the colon, liver and stomach tissues of mice after injection with LiCl (a known Wnt pathway agonist) (Kang *et al.*, 2011; Kang *et al.*, 2010; Kang and Min do, 2010).

The mitogen activated protein kinase (MAPK) pathway is a well-characterized mechanism by which cells transmit extracellular signals from the cell surface to the nucleus and ultimately alter gene transcription. Several components of the MAPK pathway are frequently mutated, overexpressed and/or hyperactivated in human cancers (McCubrey *et al.*, 2007). The three known mammalian Raf isoforms, A-Raf, B-Raf and C-Raf, are serine/threonine kinases that lie in the middle of the MAPK pathway and have normal physiological roles as well as roles as oncogenes. All three Raf isoforms have been studied extensively *in vitro* and in cells. Additionally, all three Raf isoforms have

been knocked out in mice (Leicht et al., 2007). A-Raf knockout mice die within days of birth (Pritchard et al., 1996), while both B-Raf (Wojnowski et al., 1997) and C-Raf (Wojnowski et al., 1998) knockouts are lethal *in utero*. Raf kinase signaling has also been exploited into FDA approved drugs. Sorafenib, a small molecule C-Raf inhibitor developed by Bayer and Onyx, is approved for the treatment of advanced renal cell carcinoma http://www.accessdata.fda.gov/drugsatfda_docs/applletter/2005/021923ltr.pdf and advanced hepatocellular carcinoma http://www.accessdata.fda.gov/drugsatfda_docs/applletter/2007/021923s004,s005,s006,s007.pdf. Additionally, several other companies have Raf inhibitors at various stages of development in their pipelines (Schreck and Rapp, 2006).

Recent work done by several different groups has provided evidence for a strong link between PLD and C-Raf kinase. In 1996 Ghosh *et al.* reported several findings that have been confirmed and expanded upon by other groups. They found that: (1) C-Raf binds to PtdOH; (2) The PtdOH binding site of C-Raf is between residues 389 and 423; (3) C-Raf does not bind phosphatidylalcohols and (4) treatment of Madin-darby canine kidney cells (MDCK) with 1% ethanol reduced the translocation of C-Raf from the cytosol to the plasma membrane following treatment with 12-O-tetradecanoylphorbol-13-acetate (Ghosh et al., 1996). In agreement with earlier findings, Rizzo *et al.* showed that C-Raf binds PtdOH and found that mutating arginine 398 to an alanine substantially reduced C-Raf's ability to bind PtdOH. Phosphatidic acid does not activate C-Raf kinase either *in vitro* or *in vivo* (Rizzo, 1999). Mutations that disrupt the C-Raf-PtdOH interaction prevent the recruitment of C-Raf to membranes, but disruption of the Ras-Raf interaction does not prevent the recruitment of C-Raf to membranes. Expression of a

dominant-negative Ras mutant did not prevent insulin-dependent C-Raf translocation to the plasma membrane, but did inhibit the phosphorylation of MAPK and the PtdOH binding region of C-Raf was sufficient to target green fluorescent protein to membranes. Taken together these results suggest a model whereby PtdOH is both necessary and sufficient to target C-Raf to membranes, whereas Ras is not required to target C-Raf to membranes. However, in order for C-Raf to be activated, Ras must be present. Therefore, PtdOH is required to bring C-Raf into proximity of Ras, then Ras activates C-Raf (Rizzo et al., 2000). Much of the data in support of this paradigm were gathered via dominant-negative, overexpression and mutation experiments, because RNAi and pharmacological inhibitors were not widely available at the time of the relevant studies. Two reports have also shown that overexpression of C-Raf can either stimulate or inhibit PLD activity depending on the level of C-Raf activity. Low intensity C-Raf activity stimulates PLD activity (Frankel et al., 1999), whereas high intensity C-Raf activity inhibits PLD activity (Joseph et al., 2002).

The mammalian target of rapamycin (mTOR) is a serine/threonine kinase that belongs to the phosphoinositide 3-kinase (PI3K)-related kinase family and serves as one of the master regulators of cell growth and division (Sabatini, 2006). The ability of PI3K to modulate mTOR activity is well-established (Vivanco and Sawyers, 2002), but a detailed, well-substantiated understanding of the interaction between PLD and mTOR is currently still being developed (Foster, 2009). In 2001 Fang *et al.* showed that the treatment of cells with *n*-butanol decreases mTOR downstream signaling, as measured by the activity of p70S6K. In the same studies *n*-butanol blocked a serum-induced increase in p70S6K activity suggesting that PLD might be involved in mTOR signaling. It should

be noted that the PtdOH produced by PLD appears to be necessary, but not sufficient, for mTOR signaling. In experiments where cells were deprived of amino acids, PtdOH was not able to stimulate mTOR signaling (Fang et al., 2001). This original report linking PLD to mTOR provides relatively modest evidence in favor of the conclusion that PLD regulates mTOR signaling, because *n*-butanol was the only tool used to block PLD-mediated PtdOH production.

In 2003 Chen *et al.* noted that PLD appears to confer resistance to rapamycin-induced cell death (Chen et al., 2003). They showed that the IC₅₀ value for rapamycin-induced cell death in a cell line with relatively low PLD activity was about 10 nM, whereas the IC₅₀ for rapamycin-induced cell death in a cell line with relatively high PLD activity was about 10 μM. Additionally, when a dominant-negative PLD2 construct was transfected into cells with high PLD activity, the cells showed increased sensitivity to rapamycin (Chen et al., 2005). A different group showed that PLD1 RNAi decreases the amount of phosphorylated p70S6K in B16 melanoma cells (Ohguchi et al., 2005).

Interestingly, Veverka *et al.* published a solution NMR structure of phosphatidic acid bound to the FKBP12-rapamycin binding domain of mTOR (Veverka et al., 2008). This is compelling evidence that PtdOH binds to mTOR, but in and of itself does not provide proof as to whether or not the PtdOH that binds mTOR *in vivo* is made by PLD. Data from two different reports suggest the role PLD may play in mTOR signaling. Sun *et al.* showed that the suppression of TSC2 (via the transfection of a dominant-negative TSC2) strongly activates PLD in cells. They subsequently showed that recombinant Rheb purified from bacteria activates PLD1-immunocomplexes pulled-down from CHO cells. This suggests a model where the small GTPase Rheb (known to be regulated by

TSC2 (Zhang, 2003)) either activates PLD directly or activates a protein pulled-down with PLD, which then in turn activates PLD (Sun et al., 2008). Toschi *et al.*, through the use of *n*-butanol and dominant-negative PLD constructs, showed that PtdOH produced by PLD is required for the formation of mTORC1 and mTORC2 complexes in 786-0 cells (Toschi et al., 2009). Recently, Xu *et al.* showed that when T24 cells are treated with a combination of both a PLD1 (VU0379595) inhibitor and a PLD2 inhibitor (VU0364739), there is a decrease in mTOR activation as measured by phosphorylated p70S6K (Xu et al., 2011). Interestingly, Lehman *et al.* observed that PtdOH produced by PLD can directly activate p70S6K independently of mTOR signaling (Lehman et al., 2007). In 2011 Arous *et al.* reported that oleate activated mTOR in cultured cells suggesting a possible mechanistic explanation for the increase in liver cancer seen in the obese population. Arous *et al.* claim that the oleate activation of mTOR is dependent on PLD, but provided only indirect evidence for this claim by using *n*-butanol as a “PLD inhibitor.” Furthermore, the effect of *n*-butanol on well-validated readouts of mTOR activation, such as p70S6K phosphorylation, was relatively small (Arous et al., 2011).

A preponderance of evidence collected by independent groups indicates that PLD provides a survival signal in human cancer cells. Most of this evidence is from experiments in cultured cells that utilized *n*-butanol. Some groups have used primary cells isolated from humans and more recently groups have begun using RNAi, dominant-negatives, overexpression and small molecule inhibitors. Additionally, animal model experiments have only recently been published (Buchanan et al., 2005; Zeng et al., 2009). Many of the cell signaling details about both PLD1 and PLD2 can now be more

rigorously investigated through the use of molecular genetic techniques and small molecule inhibitors in both cell culture experiments and animal models of disease.

PLD as a potential therapeutic target

Druggability

Although the biochemistry, enzymology and pharmacology of PLD have been studied for more than half a century, the systematic investigation of PLD as a therapeutic target only began in the last few years. With the advent and commercialization of RNAi technology a generally better, more direct and more specific method to inhibit PLD has become available. The report of small molecule PLD inhibitors (Monovich, 2007) and the extensive effort that resulted in the development of drug-like, isoform-selective PLD inhibitors present a new opportunity for research within the field of lipid signaling (Lavieri et al., 2009; Lavieri et al., 2010; Lewis et al., 2009; Scott et al., 2009).

While the exact mechanism of action of these small molecule PLD inhibitors is still under investigation, the traditional view of PLD signaling is that PLD signals through the production of PtdOH, but there are still protein-protein and protein-lipid interactions to be taken into account. In 2011 Doti *et al.* showed that amino acids 762-801 of PLD1 interact with phosphoprotein enriched in diabetes/phosphoprotein enriched in astrocytes (PED/PEA15) (Doti et al., 2010). The PED/PEA15 protein is overexpressed in several tissues in individuals with type 2 diabetes and its overexpression in cultured cells and transgenic animals impairs insulin regulation of glucose transport by a mechanism that is dependent on its physical interaction with PLD (Viparelli et al., 2008). It is interesting to consider the possibility of pharmacological agents that would act not to

inhibit PLD catalytic activity, but rather to block interactions between PLD and PED/PEA15.

In 2010 PLD1^{-/-} and PLD2^{-/-} mice were reported for the first time (Dall'armi et al., 2010; Elvers et al., 2010; Oliveira et al., 2010). The recent publication of viable PLD1 and PLD2 knockout mice and the report of isoform-selective, small molecule PLD inhibitors have made PLD a target of interest for several disease states.

Cancer

Buchanan *et al.* reported a provocative set of experiments utilizing xenograft tumor models in mice. In order to explore how decreasing PLD activity would affect the ability of oncogenic Ras to transform cells, Buchanan *et al.* generated rat fibroblasts that stably overexpress a dominant-negative PLD, referred to as Rat-2V25 cells (Kam and Exton, 2001). They showed that PLD activity is necessary for the H-Ras induced transformation of Rat-2 fibroblasts. Wildtype Rat-2 fibroblasts transfected with H-Ras^{V12} grow in soft agar and form tumors in nude mice, but Rat-2V25 cells (that overexpress a dominant-negative PLD) do not form colonies in soft agar and do not form tumors in nude mice when transfected with H-Ras^{V12}. Additionally, when exogenous PtdOH was added to the Rat-2V25 cells these cells were able to grow in soft agar and form tumors in nude mice (Buchanan et al., 2005). This study provided some of the first *in vivo* validation of PLD as a viable cancer target situated downstream of one of the most commonly mutated genes in all human cancer types.

Using zebrafish as a vertebrate model organism, Zeng *et al.* showed that zPld1 is required for angiogenesis (Zeng et al., 2009). Zebrafish treated with morpholino

oligonucleotides targeted to zPld1 showed impaired intersegmental blood vessel development. While clearly a less specific approach, zebrafish embryos incubated with *n*-butanol also showed impaired intersegmental blood vessel development. Although intended to investigate the role of PLD in vertebrate development, the major finding of these studies is certainly additional evidence that inhibiting PLD may be a useful therapeutic approach in the treatment of cancer. The identification of PLD as a possible cancer drug target is based on observations of increased PLD activity or expression in tissue samples obtained from cancer patients (Buchanan et al., 2005; Noh et al., 2000; Shen et al., 2010; Uchida et al., 1997; Yamada et al., 2003; Zhao et al., 2000). Furthermore, PLD1^{-/-} and PLD2^{-/-} mice are viable, develop normally, are fertile and exhibit behavior indistinguishable from wildtype littermates (Dall'armi et al., 2010; Elvers et al., 2010; Oliveira et al., 2010) suggesting that prolonged inhibition of one PLD isoform would be therapeutically viable. While many diseases cause both human pain and suffering as well as economic loss, cancer continues to be a particularly challenging disease to treat or cure. We have made great strides in treating certain, specific cancer types but there is a clearly a significant unmet medical need for new, better cancer treatments. Compared to other diseases, we have not made the same progress in helping cancer patients over the last ~50 years despite massive investments by both the public and private sectors (**Figure 7**).

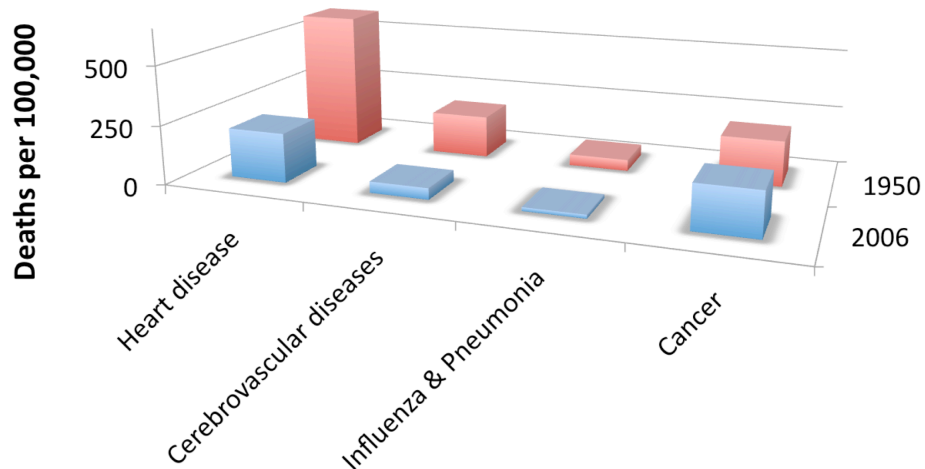


Figure 7. Causes of mortality in the United States of America: 1950 versus 2006. Sources: 1950 Mortality Data - CDC/NCHS, NVSS, Mortality Revised. U.S. Mortality Data 2006, Centers for Disease Control and Prevention, 2009. Adapted from American Cancer Society.

Alzheimer's disease

The recent reports of PLD1 and PLD2 knockout mice described viable animals with protection from various disease states (Dall'armi et al., 2010; Elvers et al., 2010; Oliveira et al., 2010). The PLD2^{-/-} mice (generated via gene targeting) facilitated research on a possible role for PLD in Alzheimer's disease (Oliveira et al., 2010). Oligomeric amyloid β stimulates PLD activity in cultured neurons and ablation of PLD2 via gene targeting blocks this effect. *In vivo* PLD activity is increased in the brain of a mouse model of Alzheimer's disease and PLD2 ablation via gene targeting rescues memory deficits and confers neuronal protection in a mouse model of Alzheimer's disease despite a significant amyloid β load. Mass spectrometry-based analysis of lipids in the brains of animals with PLD2 knocked out in the background of a wildtype or Alzheimer's mouse model shows striking acyl chain specificity and compensatory

mechanisms in PtdOH metabolism. Interestingly, the total amount of PtdOH present in either the mouse model of Alzheimer's disease or the mouse model of Alzheimer's disease crossed with a PLD2 knockout mouse (ADxPLD2KO) is essentially the same, but specific PA molecular species change by as much as 50% in the ADxPLD2KO (Oliveira et al., 2010). The preparation of a PLD2 knockout mouse and the cross between a PLD2 knockout mouse and a mouse model of Alzheimer's disease yielded excellent *in vivo* data on the role of PLD in a neurodegenerative disease. Additionally, the recent report of a centrally penetrant PLD2 inhibitor sets the stage for potential, preclinical target validation (Lavieri et al., 2010).

Thrombotic disease

In 2010 Elvers *et al.* reported the generation of PLD1 homozygous knockout mice. The PLD1^{-/-} mice display impaired $\alpha_{11b}\beta_3$ integrin activation in response to major agonists and show defective glycoprotein 1b-dependent aggregate formation under "high shear" conditions. These molecular alterations resulted in protection from thrombosis and ischemic brain injury without increasing bleeding time. Blood flow was monitored in two arterial thrombosis models triggered by chemical or mechanical perturbations and showed decreased occlusion in the PLD1^{-/-} mice compared to wildtype mice, thus showing protection against thrombosis. This highly provocative study also reported no difference in bleeding time between wildtype mice and PLD1^{-/-} mice. The implications of this work are exciting as the current pharmacological approaches used to prevent stroke and other thrombotic events (e.g., aspirin, clopidogrel and warfarin) increase bleeding times, which can be problematic. In summary, Elvers *et al.* showed that PLD1

is not required for normal hemostasis, but PLD1 is required for occlusive thrombus formation (Elvers et al., 2010). Clearly, mouse model data must be extrapolated to human physiology with caution, but this study provides exceptionally strong evidence that PLD1 should be interrogated as a therapeutic target in thrombotic disease. The development of a drug that protects against thrombosis and ischemic brain injury without affecting a patient's ability to form clots in the case of trauma would be a major clinical advancement.

Chapter II^b

SYNTHESIS AND BIOCHEMICAL CHARACTERIZATION OF POTENT, ISOFORM-SELECTIVE PLD INHIBITORS

Introduction

History

Until recently, there were few chemical tools available to probe PLD function, and no small molecules existed that would allow one to dissect the individual roles of PLD1 and PLD2. Historically, the field has relied on the overexpression of catalytically active or inactive forms of either PLD1 or PLD2, or utilized RNAi targeted to the individual isoforms in an effort to discern discrete roles for PLD1 and PLD2. In order to assess the therapeutic potential of PLD1 or PLD2 inhibition, and/or dual inhibition of both isoforms, the historical data must be verified with small molecule inhibitors. Until recently, direct, small molecule PLD inhibitors were not available, and none of the early small molecule PLD inhibitors afforded isoform selectivity.

Moreover, the most utilized class of molecules to study PLD function over the past 20 years has been primary alcohols, (e.g., *n*-butanol). Alcohols are often, incorrectly described in the literature as “PLD inhibitors.” It is important to emphasize that alcohols are not PLD inhibitors, rather *n*-butanol (as well as some other primary alcohols) blocks PLD-catalyzed PtdOH production by competing with water as a nucleophile, thereby

^b Significant portions of this chapter are adapted with permission from the following journal articles: Lavieri et al. *Journal of Medicinal Chemistry*. **2010**. Copyright 2010 American Chemical Society. Lavieri et al. *Bioorganic and Medicinal Chemistry Letters*. **2009**. Copyright 2009 Elsevier Ltd. Lewis et al. *Bioorganic and Medicinal Chemistry Letters*. **2009**. Copyright 2009 Elsevier Ltd.

causing the formation of phosphatidylbutanol in a transphosphatidylation reaction. Additionally, there are concerns that *n*-butanol may not fully block PtdOH production and that it may also be promiscuous in cell-based assays affecting multiple “targets” in addition to PLD/transphosphatidylation. Thus, conclusions reached in the literature from studies employing *n*-butanol alone should be viewed with caution. Those data require further confirmation with isoform-selective small molecule PLD inhibitors, RNA interference (RNAi) knockdowns, and genetic knockouts.

Over the past twenty years, a diverse range of chemotypes **1-20** have been reported as inhibitors of either PLD or PLD signaling (**Figures 1 and 2**) based on activity in an equally diverse array of PLD assays. Thus, quantitative, and in some instances qualitative, comparisons with regards to PLD activity are not possible. As a result, early PLD inhibitors fall into two categories, direct and indirect inhibitors. As many of these inhibitors have not been thoroughly studied, these divisions by mechanism of action must be interpreted with caution.

Indirect Inhibitors of PLD Activity

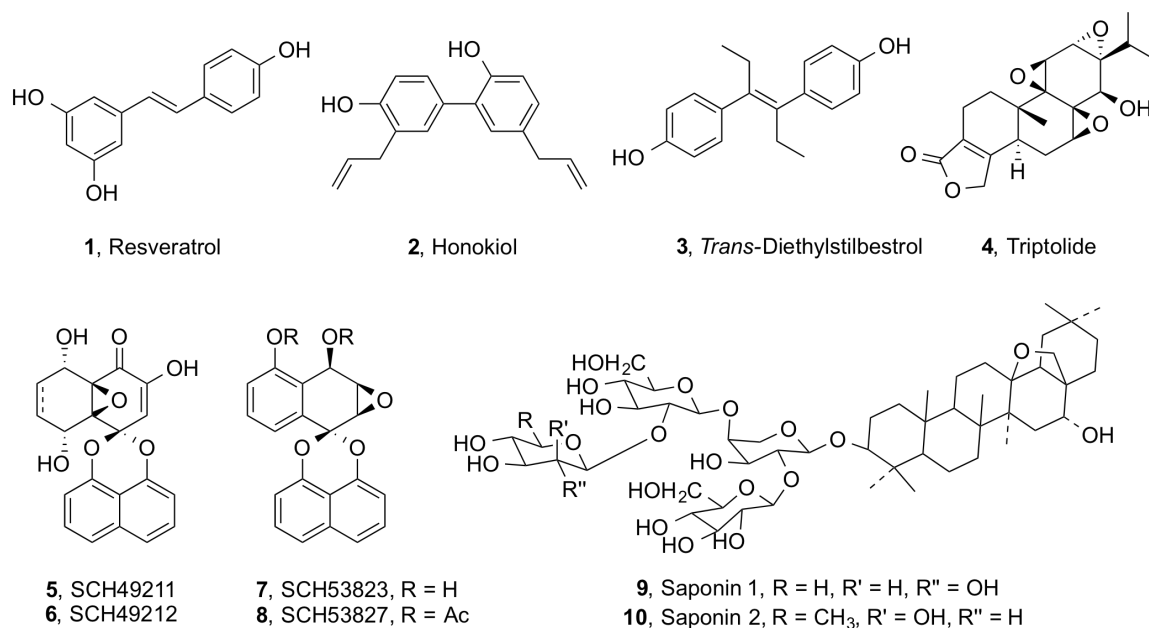


Figure 1. Reported indirect PLD inhibitors **1-10** (Figure reproduced with permission from Selvy *et al.* 2011).

Several compounds, **1-10**, have been identified that inhibit PLD enzymatic activity in cells and/or decrease PLD protein expression in cells, but do not directly inhibit PLD enzymatic activity *in vitro* (**Figure 1**). These compounds are not ideal chemical probes, because many of them are not potent and/or have a large number of known molecular targets in a variety of different signaling pathways. Resveratrol (**1**), a polyphenol found in the skin of red grapes, inhibits the production of PtdOH by human neutrophils with an IC_{50} of approximately 50 μ M. Additionally, in experiments where cells were treated with 1% ethanol, resveratrol blocked the formation of phosphatidylethanol, which suggests that resveratrol decreases PLD enzymatic activity (Tou and Urbizo, 2001). Honokiol (**2**), a natural product that was isolated from the seed cones of *Magnolia grandiflora*, has been shown to have antimicrobial (Clark *et al.*, 1981), antiangiogenic (Bai *et al.*, 2003) and proapoptotic (Shigemura *et al.*, 2007)

properties. Honokiol (20 μ M) was shown to block the formation of phosphatidylbutanol in MDA-MB-231 cells treated with 0.8% *n*-butanol indicating that honokiol decreases PLD activity in cells. However, honokiol (concentrations up to 50 μ M) had no effect on PLD enzymatic activity *in vitro* (Garcia et al., 2008). Trans-diethylstilbestrol (**3**), a synthetic compound that is structurally similar to resveratrol, inhibits the formation of both PtdOH and phosphatidylethanol (in cells treated with 1% ethanol) slightly more potently than resveratrol (Tou and Urbizo, 2008). Triptolide (**4**), a diterpene triepoxide isolated from *Tripterygium wilfordii* that has been used in traditional Chinese medicine for centuries, and recently entered clinical trials (Kitzen et al., 2009) (semisynthetic derivative). Triptolide was a hit in a screen designed to identify compounds that decrease PLD expression (Kang et al., 2009). However, triptolide was also a hit in an earlier screen designed to identify compounds that suppress the human heat shock response (Westerheide et al., 2006) and more recently Titov *et al.* identified XPB, a subunit of the transcription factor TFIIH, as a molecular target of triptolide (Titov et al., 2011). Regardless of its therapeutic potential, triptolide's indirect mechanism of action and other known molecular targets render the compound inadequate as a chemical probe for studying the cellular functions of PLD.

In the mid 1990s, Schering-Plough reported on the isolation of a series of polycyclic ketoepoxide metabolites from fungal cultures. SCH49211 (**5**) and SCH49212 (**6**), isolated from cultures of *Natrassia mangiferae*, were shown to inhibit PLD activation with IC₅₀s of 11 mM and 12 mM, respectively, in HL60 cells treated with formyl-Met-Leu-Phe (fMLP) (Chu et al., 1994). Shortly after this first report, the same group disclosed SCH53823 (**7**), isolated from the dead leaves of *Ruercus virginiana*, and

then prepared the corresponding acylated derivative, SCH53827 (**8**) to enable structure determination. Interestingly, the unnatural product **8** inhibited PLD activation, with an IC_{50} of 17 μ M in HL60 cells employing the fMLP PLD assay (Chu et al., 1996). Around the same time, Hedge and co-workers described the isolation and characterization of saponin 1 (**9**) and saponin 2 (**10**) from the extract of the leaves of *Myrsine australis* (Hegde et al., 1995). Both natural products were shown to inhibit fMLP stimulated PLD with IC_{50} s of 8 μ M and 24 μ M, respectively. It has previously been observed that certain ceramide lipids and the aminoglycoside antibiotic neomycin also inhibit PLD activity.

Direct inhibitors of PLD activity

First generation

Over the past 10 years several compounds that inhibit PLD directly have been identified. These compounds decrease PLD enzymatic activity measured by transphosphatidylolation in cells and measured by the hydrolysis of 3 H-PtdCho in an *in vitro* reconstitution assay (**Figure 2**). These direct-acting inhibitors can be categorized into three classes: (1) phosphate mimetics, (2) natural products and (3) synthetic, drug-like small molecules. The identification and subsequent optimization of some of these compounds was a major advance in the field of lipid cell signaling. Indeed, the lack of small molecule ligands to use as tools to probe both the cellular and *in vivo* roles of each PLD isoform has arguably hindered the validation of PLD as a potential therapeutic target, and studies with *n*-butanol (**11**) have clearly provided some erroneous data.

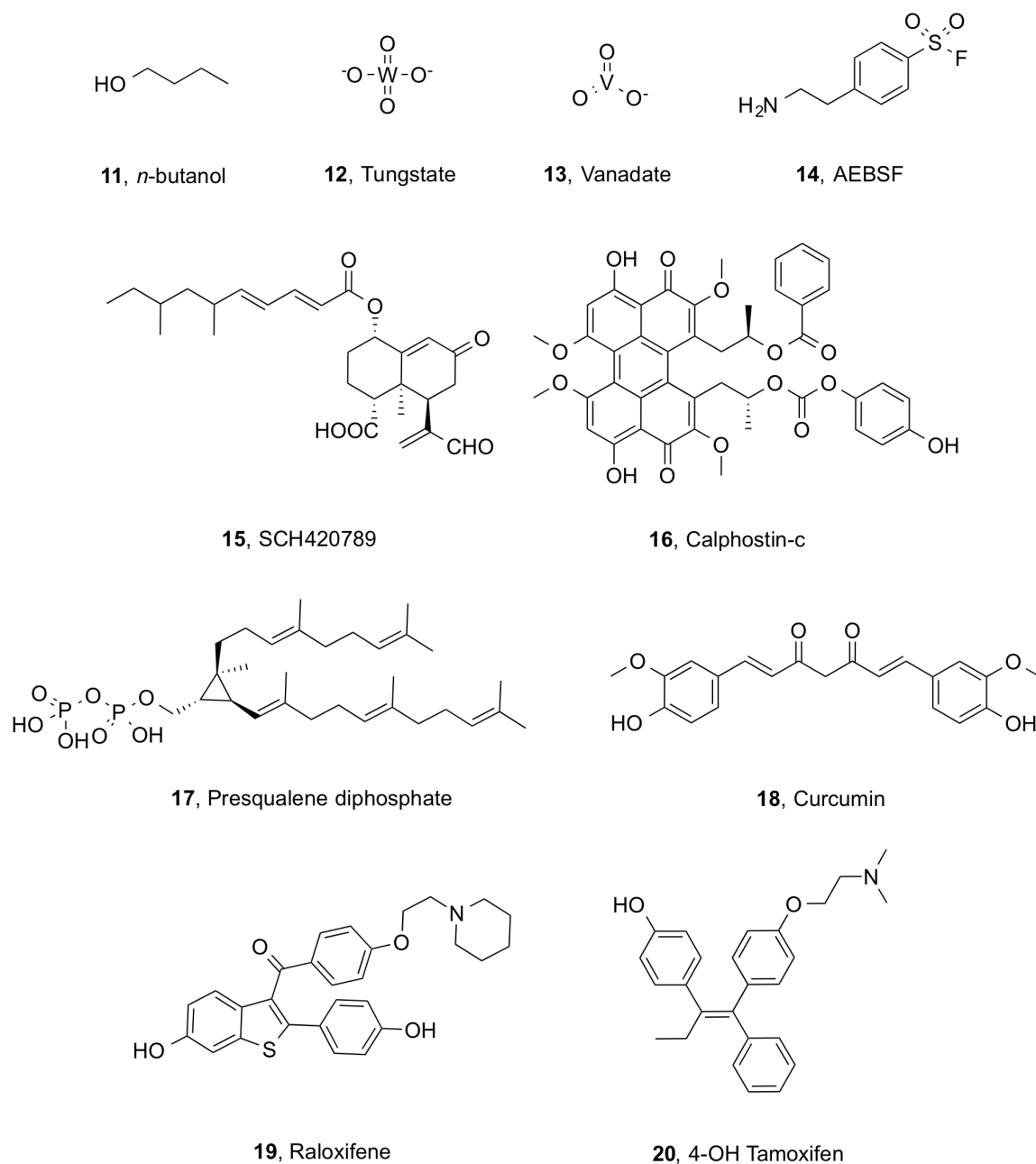


Figure 2. Reported direct PLD inhibitors **11-20** (Figure reproduced with permission from Selvy *et al.* 2011).

Crystal structures have not been determined for either human PLD1 or PLD2, but a crystal structure of a bacterial PLD, *Streptomyces* sp. strain PMF, was published in 2000 and this structure contains a phosphate molecule bound in the enzyme's active site (Leiros *et al.*, 2000b). In 2002 Davies *et al.* reported that tungstate (**12**) and vanadate

(13) inhibit a PLD superfamily member, tyrosyl-DNA phosphodiesterase, as evidenced by both an *in vitro* enzyme activity assay and multiple crystal structures (Davies et al., 2002a; Davies et al., 2003). Subsequently, tungstate and vanadate, both phosphate mimetics, were identified as PLD inhibitors via the *in vitro* reconstitution assay of PLD. Gomez-Cambronero reported that during purification of PLD from human granulocytes a standard protease cocktail inhibited PLD activity (Andrews et al., 2000). Deconvolution of the six inhibitor cocktail identified the serine protease inhibitor 4-(2-aminoethyl)benzene sulfonyl fluoride, (AEBSF) (14), as the active compound. AEBSF inhibits both basal and stimulated PLD activity with an IC_{50} of 75 μ M. Interestingly, 14 is an electrophilic compound with the capacity to covalently modify proteins, limiting its potential as a chemical probe. Moreover, the S-F bond may be hydrolyzed to the corresponding sulfonic acid by water to generate a phosphate mimetic. SCH420789 (15), a fungal metabolite, was isolated and shown to inhibit PLD *in vitro* with an IC_{50} value of approximately 10 μ M (McDonald et al., 2004). Calphostin-c (16), a perylenequinone compound from the fungus *Cladosporium caldosporoides*, was identified as a direct-acting inhibitor of PLD and previously shown to inhibit protein kinase C directly *in vitro* (Diwu et al., 1994). Protein kinase C activates PLD in cells and directly *in vitro* (Brown et al., 2007) so it could be reasonably inferred that the most plausible explanation for calphostin-c's ability to inhibit PLD activity in cells would be its ability to block PKC activation of PLD. However, calphostin-c inhibits both PLD1 and PLD2 directly with reported IC_{50} values of 100-200 nM for both isoforms (Sciorra et al., 2001). Presqualene diphosphate (17), a constituent of human leukocyte membranes, was shown to inhibit both *Streptomyces chromofuscus* PLD (IC_{50} = 100 nM) and human PLD1b (IC_{50} > 1

μM) *in vitro* (Levy, 2005). Curcumin (**18**), the predominant yellow pigment in turmeric (*Curcuma longa*), is a polyphenolic compound that has been used in Ayurvedic medicine for thousands of years and currently is the subject of a large number of basic and clinical research studies (Hatcher et al., 2008). Yamamoto *et al.* showed that curcumin inhibits the PLD activity present in a membrane preparation with an IC_{50} of $10 \mu\text{M}$ (Yamamoto et al., 1997). Furthermore, we have observed that curcumin inhibits recombinant, purified PLD1 and PLD2 *in vitro* (Scott, Armstrong, and Brown, unpublished observations).

Two selective estrogen receptor modulators (SERMs), raloxifene (**19**) and 4-OH tamoxifen (**20**), were identified as direct modulators of human PLD1 and PLD2 (Eisen and Brown, 2002). Their identification as modulators of PLD activity is consistent with an interesting, continuing trend that SERMs appear to have a myriad of estrogen receptor-independent effects. SERMs have hydroxyl groups positioned so as to mimic the structure of estradiol; this allows SERMs to bind to the estrogen receptor and block activation of the receptor by its endogenous ligand. Therefore, SERMs are typically used to treat estrogen receptor-positive breast cancer. However, an interesting observation is that tamoxifen decreases tumor growth in about 10-15% of estrogen receptor-negative tumors (Jaiyesimi et al., 1995). Additionally, tamoxifen inhibits the growth of estrogen receptor-negative cancer cell lines and induces apoptosis in these cells (Perry et al., 1995). PLD activity and/or expression are frequently increased in breast cancer (Noh et al., 2000) so it is plausible that one of the estrogen receptor-independent effects of SERMs could be PLD inhibition. Indeed, raloxifene inhibits PLD1 ($\text{IC}_{50} = 4.3 \mu\text{M}$) and PLD2 ($\text{IC}_{50} = 3.4 \mu\text{M}$) directly *in vitro* and in several different cell lines ($\text{IC}_{50} = 5\text{-}10 \mu\text{M}$) (Eisen and Brown, 2002; Scott et al., 2009).

The actions of tamoxifen on PLD both *in vitro* and in cells are more complicated. Tamoxifen is a prodrug; the actions of tamoxifen are realized primarily through its active metabolites, including 4-OH tamoxifen (Borgna and Rochefort, 1981). 4-OH tamoxifen is 100-fold more potent than tamoxifen at suppressing estrogen receptor-dependent cell proliferation and 4-OH tamoxifen binds to the estrogen receptor with 20 to 30-fold higher affinity than tamoxifen (Coezy et al., 1982; Jordan et al., 1977). Tamoxifen actually stimulates PLD1 and PLD2 activity *in vitro* and in some cell lines (during a 30 minute treatment); however, the active metabolite of tamoxifen, 4-OH tamoxifen, stimulates PLD1 *in vitro* yet inhibits PLD2 *in vitro*, albeit with poor potency ($IC_{50} > 20 \mu M$). 4-OH tamoxifen inhibits PLD1 and PLD2 in cells with an IC_{50} of about $5 \mu M$ on each isoform (Eisen and Brown, 2002). Interestingly, tamoxifen blocked phorbol ester stimulated PLD activity in an estrogen receptor-negative human breast cancer cell line (MCF-7) at concentrations of 2-5 μM only during longer (24 h) treatments and did not block phorbol ester stimulated PLD activity during a short (0.5 h) treatment (Kiss and Anderson, 1997).

Second generation: The identification of halopemide as a PLD Inhibitor

A renaissance in the PLD inhibitor field began in 2007 with a brief report from a group at Novartis on a high throughput screen to identify PLD2 inhibitors for use as inflammatory mediators. This effort identified halopemide (**21**), a psychotropic agent originally reported by Janssen in the late 1970s and early 1980s for numerous neuroscience indications (**Figure 3**) as a PLD2 inhibitor with an IC_{50} value of $1.5 \mu M$ (Monovich, 2007). This short report was limited to a succinct description of the synthesis of fourteen halopemide analogs where alternative amide moieties were surveyed,

resulting in the discovery of **22**, later coined FIPI, with an IC_{50} of 200 nM and good rat pharmacokinetics. However, there was no mention of PLD1 inhibition in this initial paper, but it was subsequently found that halopemide (**21**) potently inhibits both PLD1 (cellular IC_{50} = 21 nM, *in vitro* IC_{50} = 220 nM) and PLD2 (cellular IC_{50} = 300 nM, *in vitro* IC_{50} = 310 nM) as does **22** (PLD1 cellular IC_{50} = 1 nM, *in vitro* IC_{50} = 9.5 nM; PLD2 cellular IC_{50} = 44 nM, *in vitro* IC_{50} = 17 nM) (Scott et al., 2009). Thus, halopemide (**21**) and all the halopemide analogs presented in this initial report are more accurately described as dual PLD1/2 inhibitors, and even show a slight preference for PLD1 inhibition. Despite these issues, the halopemide (**21**) scaffold is an excellent starting point for a PLD inhibitor development campaign due to the potent PLD inhibition, favorable preclinical drug metabolism and pharmacokinetic profile, and most importantly, extensive history in multiple clinical trials (Loonen and Soudijn, 1985).

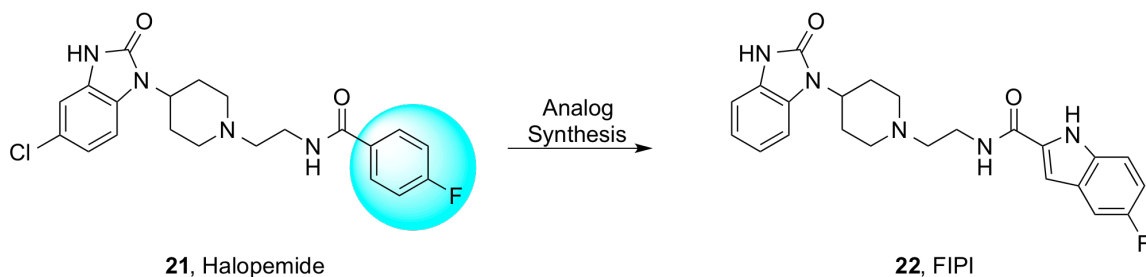


Figure 3. Structure of halopemide (**21**) and an optimized analog called FIPI (**22**) (Figure reproduced with permission from Selvy *et al.* 2011).

Halopemide (**21**), also known as R 34301, is related to the butyrophenone-based neuroleptics such as spiperone and haloperidol, and was originally developed as an anti-emetic drug, but was later found to possess unique psychotropic effects as a dopamine antagonist (Loonen and Soudijn, 1985). **21** was found to be a ‘psychic energizer’ having effects on the negative symptoms, as well as the positive symptoms of schizophrenia

without the extrapyramidal side effects common to standard atypical antipsychotic agents (Loonen et al., 1981). As was eluded to above, halopemide (**21**) was evaluated in five separate clinical trials with over 100 schizophrenic, oligophrenic and autistic patients receiving the drug (Loonen and Soudijn, 1985). Efficacy was observed in the majority of patients, and importantly, no adverse side effects or toxicities were noted, despite achieving plasma exposures of 100 ng/mL to 360 ng/mL from the 20 mg/kg and 60 mg/kg doses of 21, respectively (van Rooij et al., 1979). At these plasma concentrations, PLD1 was clearly inhibited, suggesting inhibition of PLD by this chemotype is safe in humans and a therapeutically viable mechanism.

Initial SAR studies based on the halopemide scaffold

Human PLD1 and PLD2 respond to different stimuli both *in vitro* and *in vivo* (Brown et al., 2007). Additionally, in some cancer types only one PLD isoform is upregulated at the protein expression and/or enzyme activity level (Noh et al., 2000; Yamada et al., 2003). More recently, studies in PLD knockout animals have defined clear, non-overlapping roles and therapeutic potential for both PLD1 and PLD2. For these reasons the development of isoform-selective PLD inhibitors is a desirable goal not only from a discovery science perspective, but also from the vantage point of a drug discovery effort. After the initial report on halopemide synthesis and inhibitor properties, we have synthesized and assayed numerous analogs in an effort to develop isoform-specific PLD inhibitors via an iterative analog library synthesis workflow (**Figure 4**) (Lavieri et al., 2009; Lavieri et al., 2010; Lewis et al., 2009; Scott et al., 2009).

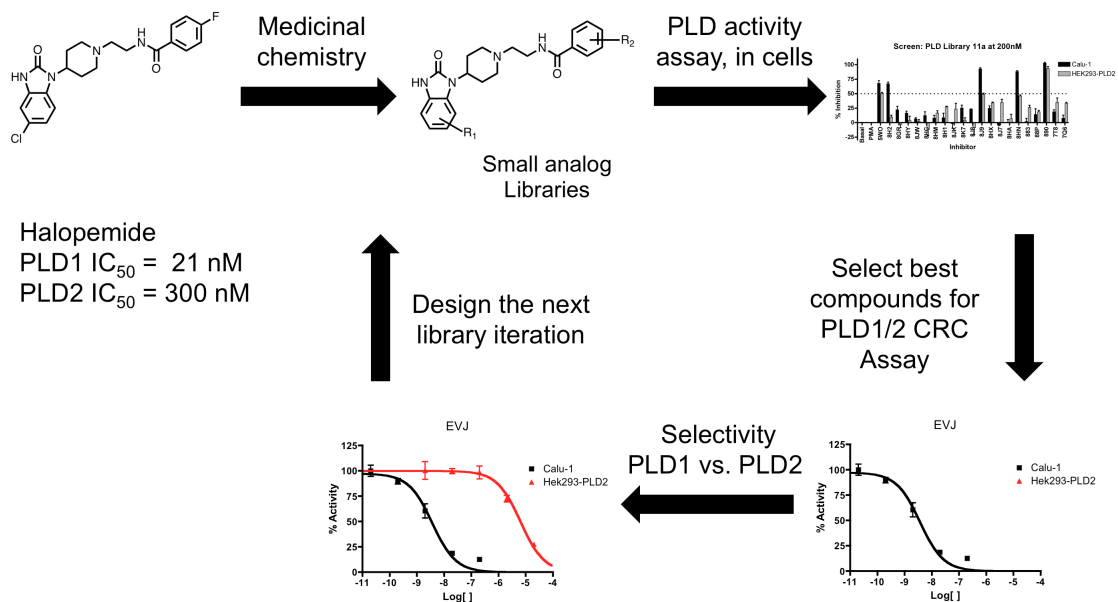


Figure 4. An iterative analog synthesis workflow diagram for the development of isoform selective PLD inhibitors.

The first phase of isoform-specific PLD inhibitor development was reported in early 2009 (Scott et al., 2009). As shown in **Figure 5**, a matrix library approach was employed to survey three regions of **21** simultaneously to afford a 3 x 3 x 30 library of ~270 halopemide analogs employing standard solution phase parallel synthesis techniques combined with mass-directed preparative LC-MS. Rigorous pharmacological characterization of a representative subset of the ~270 compounds was performed; IC_{50} values were reported in cell systems engineered to give only a PLD1 or a PLD2 response as well as IC_{50} values that were determined on recombinant PLD1 and PLD2 enzymes purified from insect cells. Data from both an *in vitro* enzyme activity assay and a cellular activity assay show that the compounds inhibit PLD1/2 directly and that the compounds effectively permeate the cell membrane. Many of the compounds display low nanomolar potency values, and this library produced a number of dual PLD1/2 inhibitors and a

number of moderately preferring PLD1 analogs. This first generation effort did afford the first PLD1-selective inhibitor, VU0155069 (**23**), where the chiral (*S*)-methyl group significantly enhanced PLD1 preference to ~163-fold over PLD2 in a cell-based assay. Subsequent iterations of lead optimization found the chiral (*S*)-methyl group as a general moiety that increased PLD1 inhibition. While the piperidinyl benzimidazolone-containing analogs failed to display any preference for PLD2 inhibition, a triazaspirone congener uniformly increased PLD2 inhibition to provide the first PLD2 (10-fold PLD2 preferring) selective inhibitor, VU0155072 (**24**). Additionally, some of the compounds decreased the ability of several breast cancer cell lines to invade through a Matrigel™ membrane in a transwell migration assay, which is consistent with earlier studies showing this enzyme's role in regulating cell migration (Park et al., 2009; Scott et al., 2009; Williger et al., 1999; Zheng et al., 2006).

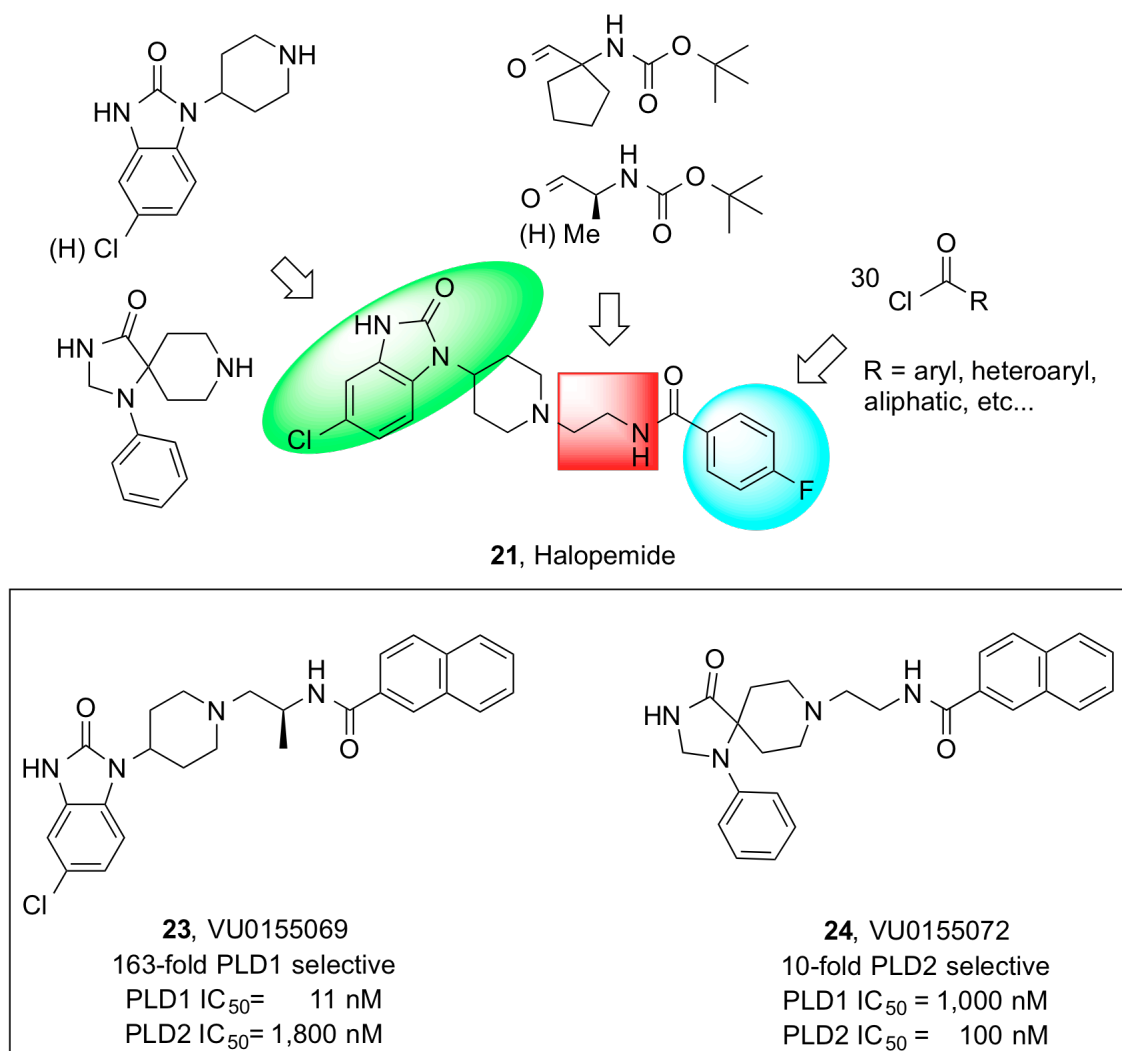


Figure 5. Initial SAR studies on halopemide (Figure reproduced with permission from Selvy *et al.* 2011).

Optimization of halopemide for PLD1 specificity

The impact of various halogenated privileged structures on PLD1 potency and selectivity

Initial PLD inhibitor libraries based on halopemide (**21**) were diversity-oriented in an effort to explore a broad chemical space and identify molecular entities that would engender PLD isoform-selective inhibition. Subsequent optimization strategies were

more focused and driven from a medicinal chemistry perspective (**Figure 6**) to improve PLD1 and PLD2 potency and selectivity within **25** and **26**, respectively.

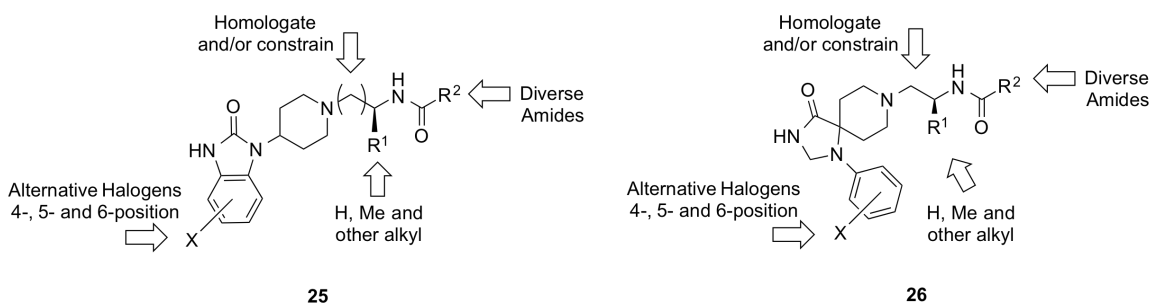


Figure 6. Focused lead optimization strategy to improve PLD1 potency and selectivity within scaffold **25**, and parallel strategy to improve PLD2 potency and selectivity within scaffold **26** (Figure reproduced with permission from Selvy *et al.* 2011).

Several important pieces of information were discovered or confirmed in this round of analog synthesis based on **25**: (1) homologation of the ethylenediamine linker of an analog by just one carbon to a propyl chain eliminated all activity; (2) heteroaromatic and aromatic amides on the right side of analogs confer excellent potency; (3) a racemic trans-cyclopropyl phenyl amide dramatically increased PLD1 selectivity; (4) a 5-bromo substituted benzimidazolone increased potency and PLD1 selectivity.

The synthetic route to nearly all of the compounds reported in Scott *et al.* 2009 was straightforward and all materials used were commercially available (**Figure 5**). With the help of the VICB synthesis core (primarily Dr. Kwangho Kim) we explored the impact of halogenating the benzimidazolone scaffold present in **21** at various positions. After receiving the halogenated scaffolds these libraries were straightforward to prepare. We followed the general approach reported by Monovich *et. al* in their 2007 paper (Monovich, 2007).

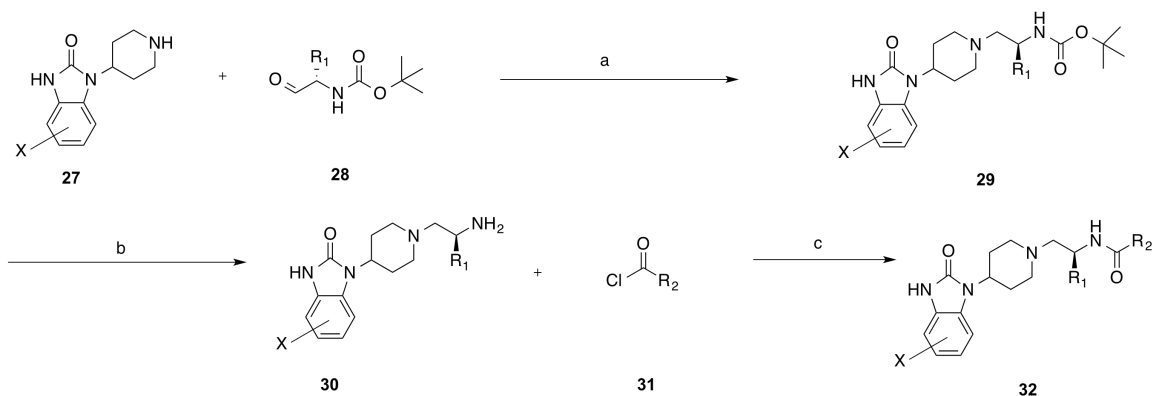


Figure 7. Synthetic scheme for various halogenated benzimidazolones. Reagents and conditions: (a) MP-B(Oac)₃ DCE/MeOH, rt, 16 h (75-95%); (b) 4N HCl/dioxane, MeOH (98%); (c) DMF/DCM, DIPEA, rt, 1 hour (50-95%)

In the initial report by Scott *et al.* a compound ~163-fold selective for PLD1 over PLD2 in a cell-based assay was described (Scott et al., 2009). In an attempt to gain improved PLD1 selectivity we prepared compounds containing a variety of halogenated privileged structures including the 4-F, 5-F, 5-Cl, 5-Br, and 6-F congeners (**Figure 8**). We initially acquired these scaffolds from the VICB synthesis core (except the 5-Cl which was commercially available), but eventually I prepared multigram quantities of the 5-Br scaffold in the complete synthesis of the most PLD1 selective compound described to date, VU0359595.

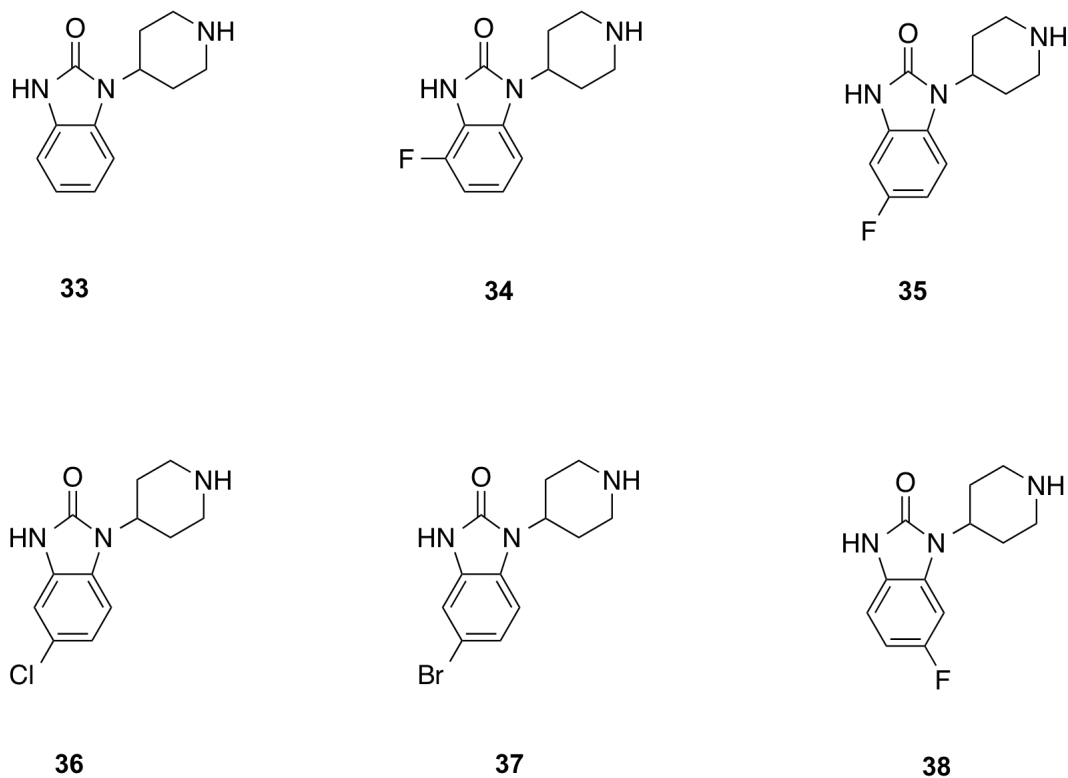
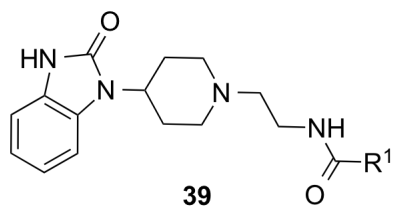


Figure 8. Chemical structures of plain, 4-F, 5-F, 5-Cl, 5-Br, and 6-F benzimidazolone scaffolds used in an attempt to improve PLD1 potency and selectivity.

We prepared several hundred compounds according to scheme shown in **Figure 7** and colleagues in the Brown lab (primarily Dr. Sarah Scott) assayed them for inhibitory activity against PLD1 and PLD2. Many representative compounds, including the most isoform-selective compound, are shown on the following pages. For comparison, a small subset of compounds and corresponding potency values containing the unsubstituted 1-(piperidin-4-yl)-1*H*-benzo[*d*]imidazol-2(3*H*)-one are shown below (**Figure 9**).



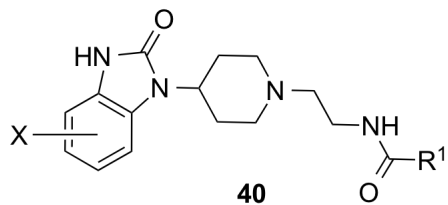
Cmpd	R ¹	PLD1 IC ₅₀ (nM) ^a	PLD2 IC ₅₀ (nM) ^b	Fold PLD1- selective
39a		21	380	18
39b		35	3,900	111
39c		8	42	5.1
39d		40	730	18
39e		70	740	10.5
39f		110	860	7.8
39g		120	850	7

^aCellular PLD1 assay with Calu-1 Cells; ^bCellular assay with 293-PLD2 cells.

Figure 9. Chemical structures and activities of various unsubstituted 1-(piperidin-4-yl)-1*H*-benzo[*d*]imidazol-2(3*H*)-ones. Chemical synthesis performed by Jana Lewis, Jason Buck, and myself. Enzyme activity assays performed by Sarah Scott (Figure adapted with permission from Lewis *et al.* 2009).

In terms of the unsubstituted 1-(piperidin-4-yl)-1*H*-benzo[*d*]imidazol-2(3*H*)-one, aromatic/heteroaromatic moieties off of the eastern amide tend to confer good potency. Interestingly, the *trans*-phenyl cyclopropane-containing compound **39b** showed a noticeable increase in PLD1 selectivity compared to any other functional groups prepared

and tested (**Figure 9**). Next, we evaluated the various halogenated benzimidazolones lacking a chiral (*S*)-methyl group in the ethylenediamine linker (**Figure 10**).



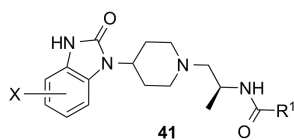
Cmpd	X	R ¹	PLD1 IC ₅₀ (nM) ^a	PLD2 IC ₅₀ (nM) ^b	Fold PLD1- selective
40a	5-Cl		21	300	14.2
40b	5-Cl		10	240	24
40c	5-Cl		2	520	250
40d	5-F		4	140	35
40e	5-F		12	290	24
40f	5-F		18	61	3.3
40g	5-Br		3	97	32
40h	5-Br		4	76	19
40i	6-F		7	42	6
40j	6-F		4	14	3.2

^aCellular PLD1 assay with Calu-1 Cells; ^bCellular assay with 293-PLD2 cells.

Figure 10. Chemical structures and activities of various halogenated 1-(piperidin-4-yl)-1*H*-benzo[*d*]imidazol-2(3*H*)-ones. Chemical synthesis performed by Jana Lewis, Jason Buck, and myself. Enzyme activity assays performed by Sarah Scott (Figure adapted with permission from Lewis *et al.* 2009).

Incorporation of a key (*S*)-methyl group that allows for the 1,700-fold PLD1 selective inhibitor VU0359595

The various halogenations shown in **Figure 10** confirmed previous SAR with respect to the eastern amide cap and ethylenediamine linker. In general, halogen substitution increased PLD1 potency to the low nanomolar range regardless of the position of the halogen; however, PLD2 potency also increased as well. Next, we turned to exploring the effects of various halogen substitutions combined with a chiral (*S*)-methyl group in the ethylenediamine linker (**Figure 11**).



Cmpd	X	R ¹	PLD1 IC ₅₀ (nM) ^a	PLD2 IC ₅₀ (nM) ^b	Fold PLD1- selective
41a	5-Cl		46	933	163
41b	4-F		43	12,000	280
41c	4-F		130	10,000	77
41d	4-F		38	14,000	370
41e	4-F		66	13,000	200
41f	4-F		100	>20,000	>200
41g	5-F		11	3,100	180
41h	5-F		7.4	1,040	140
41i	5-Cl		10	1,400	140
41j	5-Cl		6.4	1,200	190
41k	5-Cl		8	1,150	140
41l	5-Cl		3	730	240
41m	5-Br		3.5	187	53
41n	5-Br		5.5	3,900	700
41o	5-Br		4	890	222
41p	5-Br		3.7	6,400	1,700
41q	6-F		2	360	180
41r	6-F		6	2,700	450

^aCellular PLD1 assay with Calu-1 Cells; ^bCellular assay with 293-PLD2 cells.

Figure 11. Chemical structures and activities of various halogenated 1-(piperidin-4-yl)-1*H*-benzo[*d*]imidazol-2(3*H*)-ones coupled to an ethylenediamine linker containing a chiral (*S*)-methyl group. Chemical synthesis performed by Jana Lewis, Jason Buck, and myself. Enzyme activity assays performed by Sarah Scott (Figure adapted with permission from Lewis *et al.* 2009).

Incorporation of a chiral (*S*)-methyl group in the ethylenediamine linker had an astounding effect on PLD1 selectivity. For many compounds, the addition of the chiral (*S*)-methyl group drove PLD1 potency into the low, single-digit nanomolar range and simultaneously drove PLD2 potency up into the micromolar range (**Figure 11**). In terms of potency and selectivity, the 5-Br (**41m-p**) substituted benzimidazolones provided the best results, providing PLD1 IC₅₀ values ranging from about 3 nM to 6 nM and with extraordinarily high PLD1 selectivity. Of all of these analogs, **41p** (VU0359595) was the standout molecule and possesses unprecedented selectivity for PLD1. Compound **41p** (VU0359595), with the 5-bromo-1-(piperidin-4-yl)-1,3-dihydro-2*H*-benzo[*d*]imidazol-2-one scaffold, the (*S*)-methyl group linker and the *trans*-phenyl cyclopropane amide is the most potent (IC₅₀ = 3.7 nM) and selective versus PLD2 (IC₅₀ = 6.4 μM, ~1,700-fold selective) PLD1 inhibitor ever described. The concentration-response-curves for **41p** (VU0359595) in cellular PLD1 (Calu-1) and PLD2 (293-PLD2) enzyme assays are shown below (**Figure 12**).

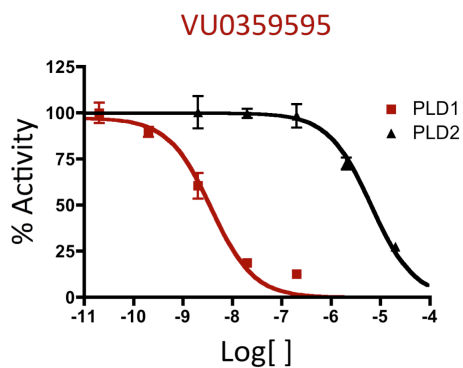


Figure 12. Concentration response curves for **41p** (VU0359595) in the cellular PLD1 and PLD2 enzyme activity assays. Enzyme activity assays performed by Sarah Scott (Figure adapted with permission from Lewis *et al.* 2009).

Summary of the SAR leading to VU0359595

At this point it is useful to review the steps taken to go from halopemide, essentially a dual isoform PLD inhibition, to **41p** (VU0359595), a highly selective PLD1 inhibitor. We synthesized and assayed several hundred compounds in order to develop robust SAR that ultimately led to the development of **41p** (VU0359595). A visual overview of the PLD1 SAR we established is shown below (**Figure 13**).

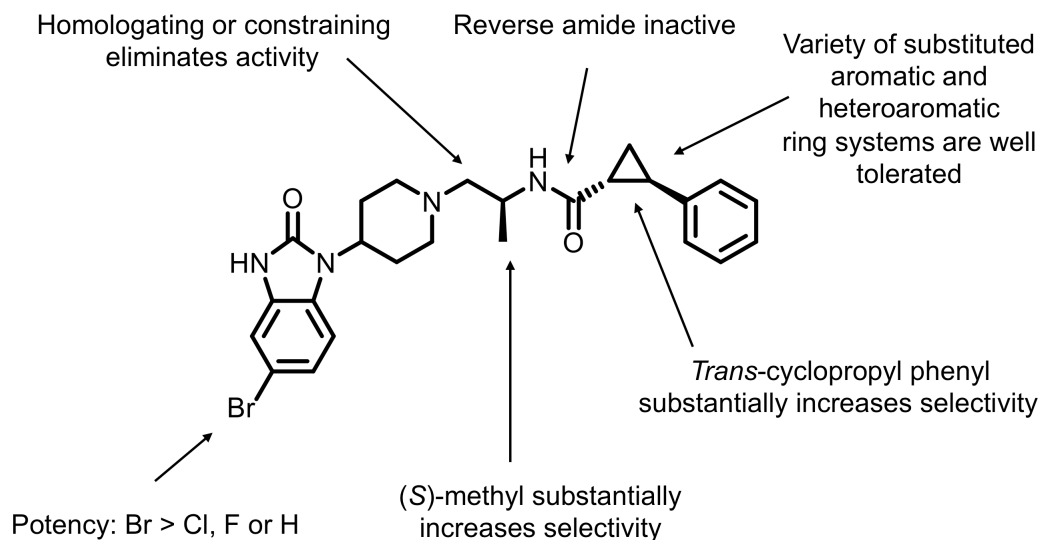


Figure 13. Key structure activity relationships that led to the development of **41p** (VU0359595).

In our initial libraries we coupled a large number of eastern amide caps to the benzimidazolone scaffold and determined that, in general, aromatic or heteroaromatic functional groups conferred the most potency. However, these functional groups offered little in the way of PLD1 selectivity. We did discover that the incorporation of *trans*-phenyl cyclopropane amide increased PLD1 specificity quite substantially. Also, by exploring various halogenations about the benzimidazolone scaffold we identified the 5-Br congener as giving excellent potency and selectivity. Ultimately, it was the installation of the (*S*)-methyl group in the ethylenediamine linker that facilitated a massive increase in PLD1 selectivity. We also discovered several clear steric constraints. Any homologation of the ethylenediamine linker resulted in a completely inactive compound. Likewise, methylating the amides or reversing them resulted in massive losses in potency. The key changes that enabled continuous improvements in both PLD1 potency and selectivity are shown below, highlighted in red (**Figure 14**).

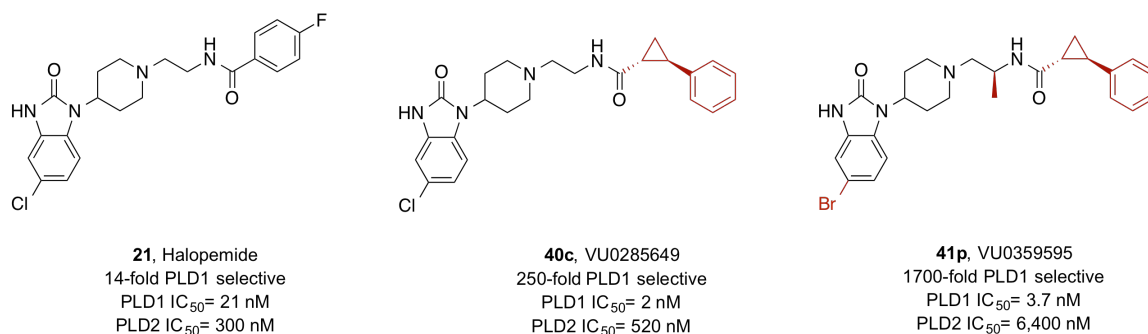


Figure 14. Key structural modifications (shown in red) that led to the development of **41p** (VU0359595) (Figure adapted with permission from Selvy *et al.* 2011).

Synthesis and characterization of VU0359595

Chemical synthesis of VU0359595

Initially we obtained various halogenated 1-(piperidin-4-yl)-1*H*-benzo[*d*]imidazol-2(3*H*)-ones from the VICB chemical synthesis core. However, after we identified **41p** (VU0359595) as our most potent, selective PLD1 inhibitor I synthesized a considerable amount of this compound (and fully characterized every synthetic intermediate) from commercially available starting materials (my staff scientist colleagues also prepared future batches of various compounds). Additionally, we were able to resolve the diastereomers of VU0359595 using supercritical fluid chromatography (and a chiral column).

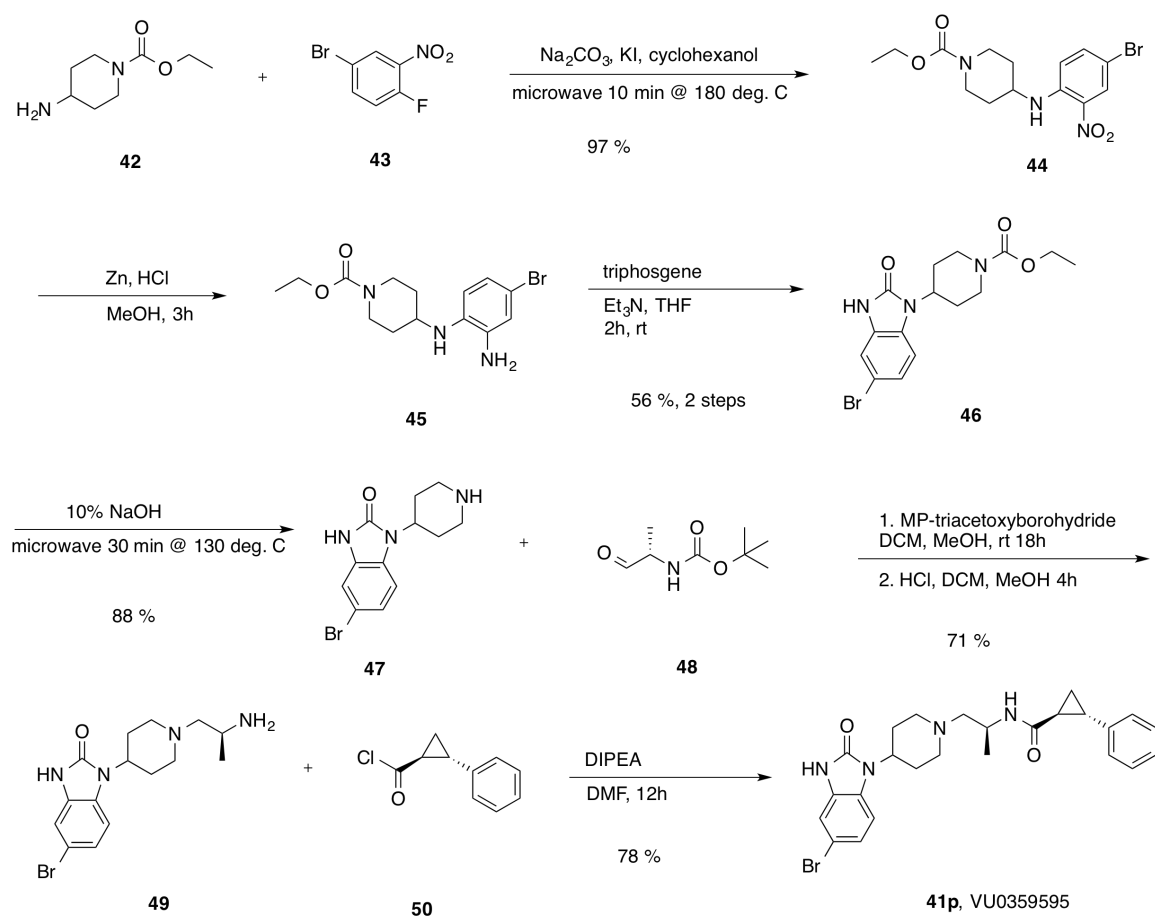


Figure 15. Chemical synthesis of **41p** (VU0359595) from commercially available starting materials.

The synthesis of VU0359595 in 7 steps at a 26% overall yield proceeds as shown above (**Figure 15**). First, a microwave synthesizer is utilized to perform a nucleophilic aromatic substitution reaction followed by a zinc-mediated reduction of a nitro group to an aniline. Triphosgene is utilized to close a ring thereby forming the benzimidazolone scaffold portion of the compound. A microwave synthesizer is again utilized to facilitate the removal of an ethyl carbamate. The rest of the synthesis is identical to the scheme shown in **Figure 7**; reductive amination, BOC deprotection and an amide coupling.

Chiral resolution of VU0359595 diastereomers and PLD inhibitory activities thereof

VU0359595 (described up to this point) is actually present as a mixture of two diastereomers, because the *trans*-2-phenylcyclopropanecarbonyl chloride **50** used to acylate the free amine **49** is actually *trans*-racemic (**Figure 16**). In order to assess the relative contributions of each stereoisomer we utilized supercritical fluid chromatography (and a chiral column) to separate the diastereomers and assay their inhibitory activity against PLD1 and PLD2.

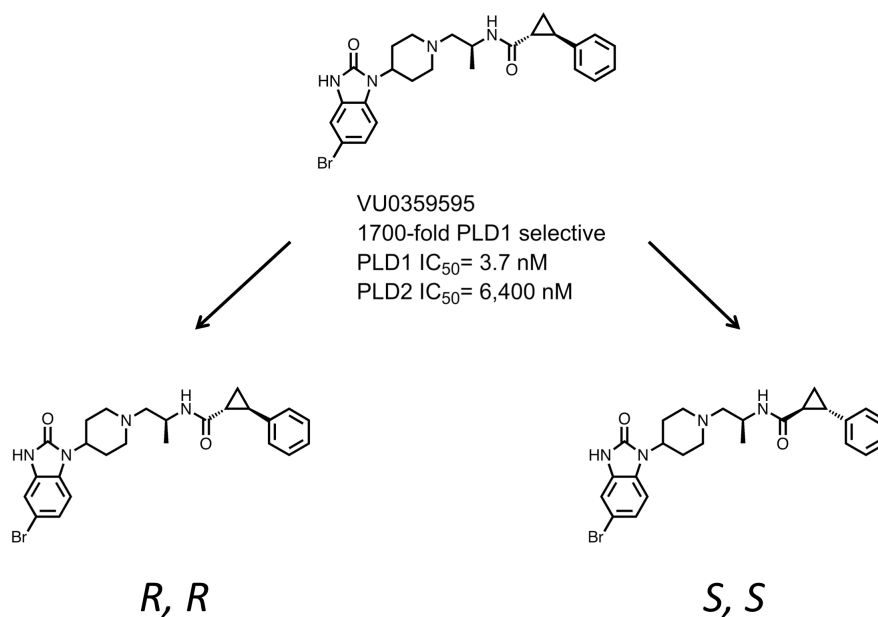


Figure 16. Chemical structures of the two diastereomers of **41p** (VU0359595).

After screening several chiral columns we determined that an isocratic run utilizing ethanol and liquid CO₂ on a Regiscell™ column allowed for excellent separation of the two diastereomers (**Figure 17**). Based on the UV absorbance data it appears that the diastereomers are present in a roughly 1:1 ratio; they eluted roughly 2 minutes apart.

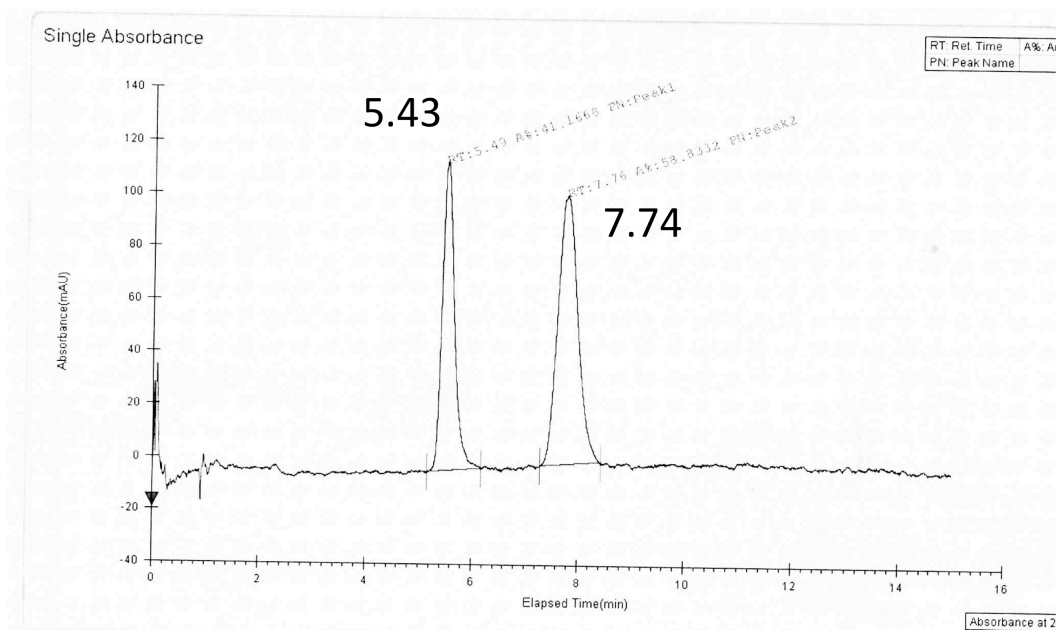


Figure 17. UV absorbance trace showing the separation of the two diastereomers of **41p** (VU0359595). Supercritical fluid chromatography performed by Nathan Kett.

After separating the diastereomers via stacked injections we analyzed each collected peak for purity (**Figure 18**). We were able to completely resolve the two diastereomers.

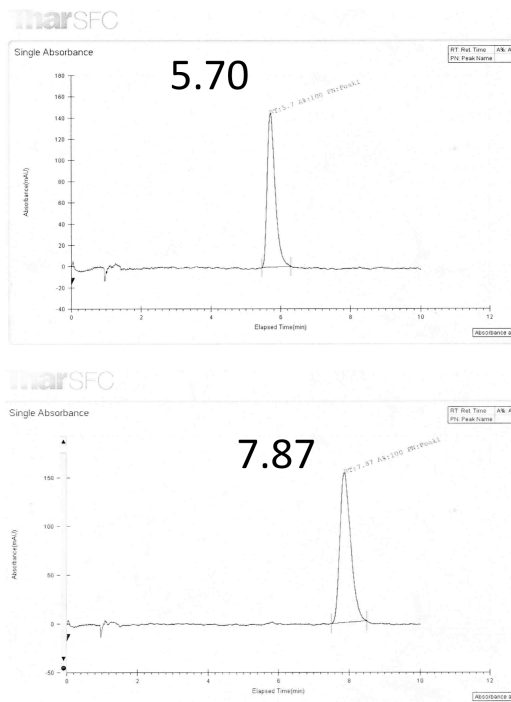


Figure 18. UV absorbance trace showing the purity of each diastereomer of **41p** (VU0359595). Supercritical fluid chromatography performed by Nathan Kett.

Ultimately, we wanted to determine if all of the activity resided in one stereoisomer of **41p** (VU0359595). Previous SAR work had shown us that the (*S*)-methyl group in the middle of the compound was superior to the (*R*)-methyl version; however, we had not examined if different stereochemistry about the cyclopropane ring conferred different activity.

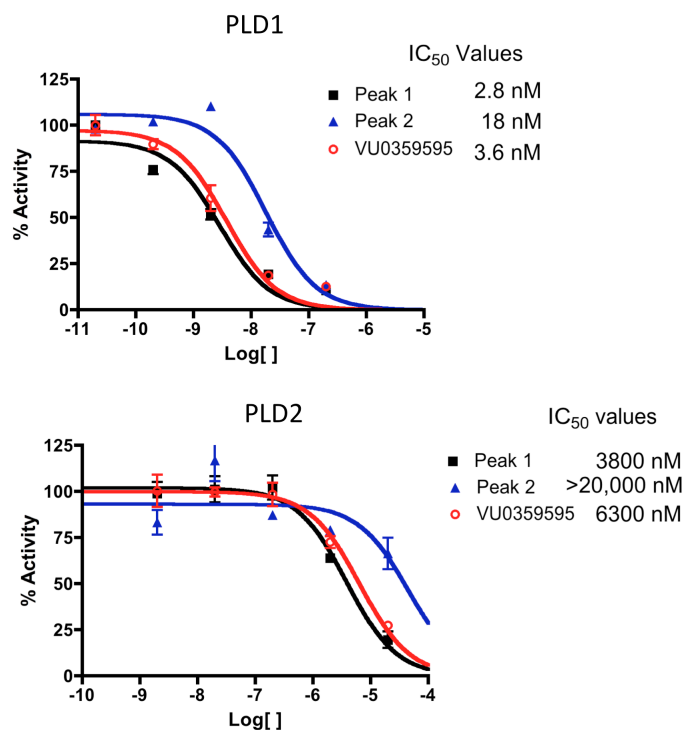


Figure 19. Concentration response curves for each diastereomer of **41p** (VU0359595) in the cellular PLD1 and PLD2 enzyme activity assays. Supercritical fluid chromatography performed by Nathan Kett. Enzyme activity assays performed by Sarah Scott.

Somewhat surprisingly, the diastereomers were roughly equipotent with respect to PLD1 inhibition (**Figure 19**). The only significant difference compared to the 1:1 mixture of diastereomers was an apparent decrease in potency for PLD2 in the stereoisomer that eluted as the second peak; however, given such high selectivity present with VU0359595 (present as a mixture of diastereomers) we saw no need to pursue an enantioselective synthesis of VU0359595.

Optimization of an alternative scaffold that confers PLD2 selectivity

Initial SAR containing the 1,3,8-triazaspiro[4,5]decan-4-one privileged structure

Halopemide (**21**) proved to be a viable starting point for a PLD1 specific inhibitor optimization campaign that ultimately led to VU0359595, a 1,700-fold PLD1 selective

inhibitor. However, even after preparing ~500 compounds based on halopemide (**21**) PLD2 selective inhibitors remained elusive. In a limited diversity-oriented synthesis effort we identified the 1,3,8-triazaspiro[4,5]decan-4-one privileged structure (**52**) as being able to confer slight PLD2 selectivity (**Figure 20**).

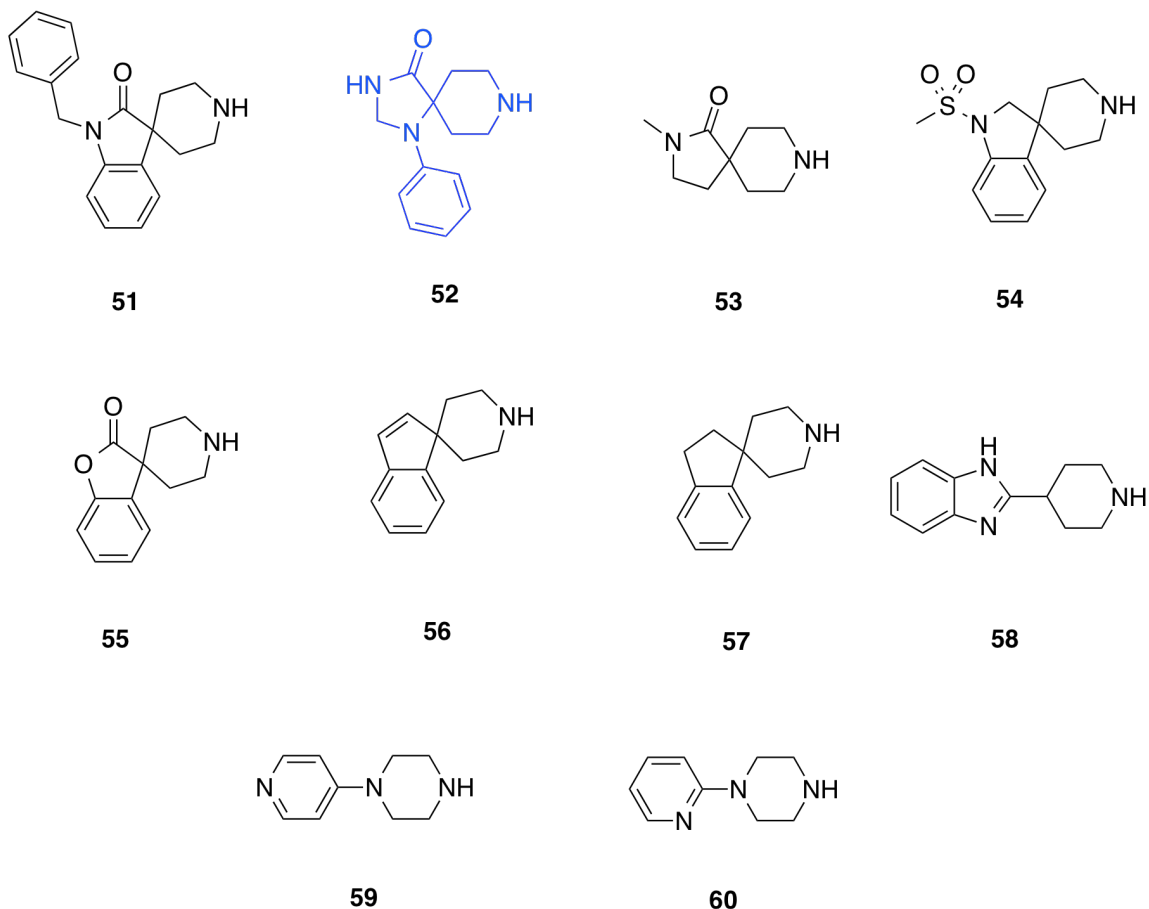


Figure 20. Chemical structures of various scaffolds tested for their ability to confer PLD2 selectivity.

We prepared a variety of compounds in much the same fashion as we initially did for PLD1 (**Figure 7**); these initial compounds consisted essentially of the 1,3,8-triazaspiro[4,5]decan-4-one privileged structure, an ethylenediamine linker, and an amide cap (**Figure 21**).

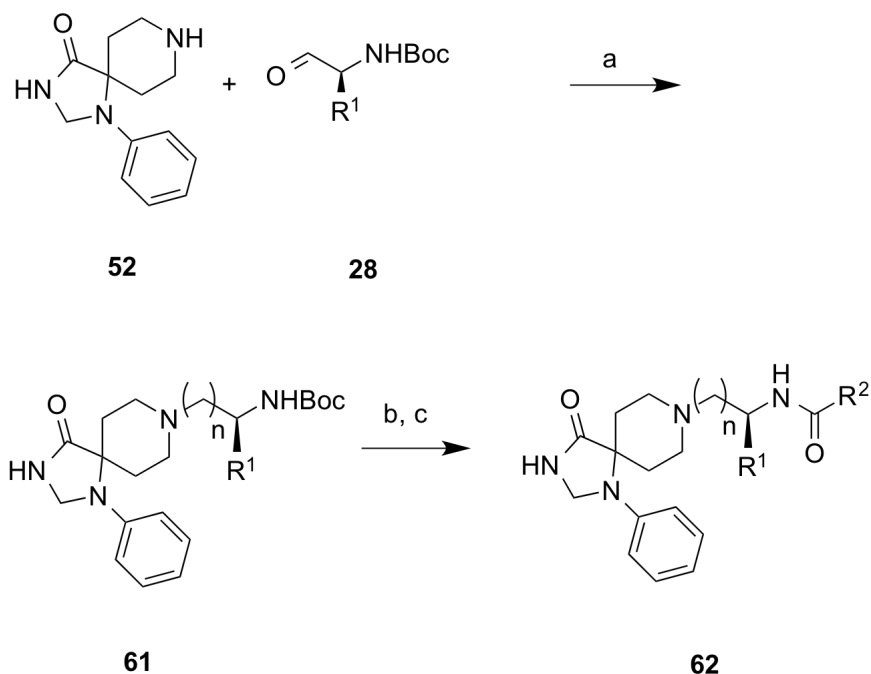
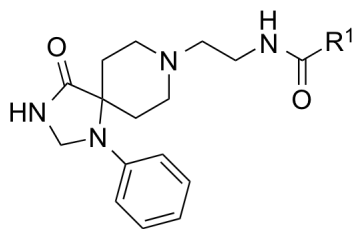


Figure 21. Synthetic scheme for various 1,3,8-triazaspiro[4,5]decan-4-one-containing PLD inhibitors. Reagents and conditions: (a) MP-B(Oac)₃, DCE/MeOH, rt, 16 h (75-95%); (b) 4N HCl/dioxane, MeOH (98%); (c) R₂COCl, DMF/DCM, DIPEA, rt, 1 hour (50-95%). (Figure adapted with permission from Lavieri *et al.* 2009).

All materials used in this initial PLD2 SAR work were commercially available and the syntheses were straightforward. As we observed in the previous series of PLD1 selective inhibitors the ethylenediamine linker was absolutely required. Homologations of the linker to the corresponding 3- and 4-carbon tethers (or longer) yielded inactive compounds, as did cyclic constraints. **Figure 22** highlights unsubstituted ethylenediamine linker congeners **63** without the (*S*)-methyl group and examines only alternative amides. Compound **63a** was our lead PLD2-preferring compound previously identified in our diversity-oriented synthesis campaign, with a PLD2 IC₅₀ of 110 nM and ~9-fold selectivity versus PLD1 (IC₅₀ = 1,000 nM). In general, analogs **63** with PLD inhibitory activity were PLD2-preferring (1- to 20-fold). Incorporation of the PLD1 preferring *trans*-phenyl cyclopropane amide moiety, provides **63b**, and a complete loss of

PLD inhibition. The most potent analog in the series, **63e** (PLD2 IC₅₀ = 30 nM), incorporated a 2-benzothiophene amide, but displayed only 5-fold PLD2 selectivity. A 2-quinoline amide congener (**63c**) displayed comparable PLD 2 potency (PLD2 IC₅₀ = 90 nM) to the lead **63a** but selectivity versus PLD1 (PLD1 IC₅₀ = 1,990 nM) was improved (>20-fold). Interestingly, incorporation of a second nitrogen atom to provide the corresponding quinoxaline derivative (**63h**) results in a complete loss of PLD inhibitory activity. Compound **63c** was the most PLD2-selective inhibitor to come out of this round of analogs aimed at improving PLD2 selectivity.



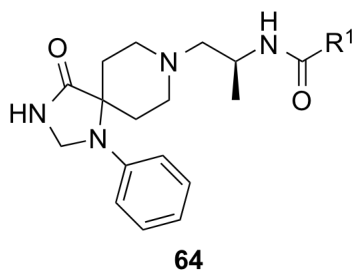
63

Cmpd	R ¹	PLD1 IC ₅₀ (nM) ^a	PLD2 IC ₅₀ (nM) ^b	Fold PLD2- selective
63a		1,000	110	9.1
63b		>20,000	>20,000	-
63c		1,900	90	21.1
63d		2,100	1,600	1.3
63e		150	30	5.0
63f		4,250	990	7.8
63g		5,900	550	10.7
63h		>20,000	>20,000	-

^aCellular PLD1 assay with Calu-1 Cells; ^bCellular assay with HEK293-gfp PLD2 cells.

Figure 22. Chemical structures and activities of various 1,3,8-triazaspiro[4,5]decan-4-ones. Chemical synthesis performed by Jana Lewis and myself. Enzyme activity assays performed by Sarah Scott (Figure adapted with permission from Lavieri *et al.* 2009).

While we were highly encouraged about being able to continue to improve PLD2 selectivity within this series the results from a directed library exploring the impact of incorporation of the (*S*)-methyl group (PLD1-preferring moiety) on the ethylenediamine linker with the 1,3,8-triazaspiro[4,5]decan-4-one scaffold (PLD2-preferring) were quite surprising. Incorporation of the (*S*)-methyl group into analogs **64** had significant impact, providing few active compounds, but PLD1 inhibitory activity was dramatically increased within a PLD2-preferring privileged structure (**Figure 23**). For example, compound **64a**, the (*S*)-methyl analog of the ~9-fold PLD2 selective **63a**, displayed comparable PLD2 inhibitory activity (PLD2 IC₅₀ = 140 nM), but PLD1 inhibitory activity increased 40-fold (PLD1 IC₅₀ = 25 nM), relative to **63a**. Thus, **64a** is considered a PLD1/2 dual inhibitor, and the *in vitro* biochemical enzyme activity assay verified this result (PLD1 IC₅₀ = 299 nM, PLD2 IC₅₀ = 235 nM). Another well-established PLD1-preferring moiety, the *trans*-phenyl cyclopropane moiety of VU0359595, was inactive on both PLD isoforms in analogs such as **63b**, but in combination with the (*S*)-methyl group, congener **64b** now possessed measureable PLD1 inhibitory activity (PLD1 IC₅₀ = 2.6 μM) with no effect, relative to **63b**, on PLD2 inhibition.



Cmpd	R ¹	PLD1 IC ₅₀ (nM) ^a	PLD2 IC ₅₀ (nM) ^b
64a		25	140
64b		2,600	30,000
64c		150	200
64d		3,400	27,000

^aCellular PLD1 assay with Calu-1 Cells; ^bCellular assay with HEK293-gfpPLD2 cells.

Figure 23. Chemical structures and activities of various 1,3,8-triazaspiro[4,5]decan-4-ones. Chemical synthesis performed by Jana Lewis and myself. Enzyme activity assays performed by Sarah Scott (Figure adapted with permission from Lavieri *et al.* 2009).

PLD inhibitor **63c** (Cellular assay: PLD IC₅₀ = 1,900 nM, PLD2 IC₅₀ = 90 nM, 21-fold selective; *In vitro* biochemical assay: PLD IC₅₀ = >20,000 nM, PLD2 IC₅₀ = 500 nM, >40-fold selective) represents a significant milestone in working toward a PLD2 selective inhibitor. Indeed, until we were able to identify a scaffold other than the benzimidazolone scaffold we were not able to obtain any preference for PLD2 inhibition. Next, I completed more involved syntheses of analogs of **63c** in an attempt to further improve PLD2 selectivity within the 1,3,8-triazaspiro[4,5]decan-4-one series.

Synthesis of various 3 and/or 4 halogenated 1,3,8-triazaspiro[4,5]decan-4-ones

From the initial SAR described above we gleaned that we did not have much room for variability/optimization with respect to the eastern amide moiety in **63a**. We decided to focus on functionalization of the 1,3,8-triazaspiro[4,5]decan-4-one scaffold by the incorporation of various halogens, as this proved successful in the benzimidazolone-based PLD1 inhibitor **41p** (VU0359595). Only the unsubstituted 1-phenyl-1,3,8-triazaspiro[4,5]decan-4-one was commercially available, so while known in the literature, the halogenated congeners had to be synthesized. As shown in **Figure 24**, *N*-benzyl piperidinone **65** underwent a Strecker reaction with 3-fluoroaniline to provide **66a**, and acidic hydrolysis delivered the carboxamide **67a** in 68% yield for the two steps. Closing of the spirocyclic five-membered ring required forcing microwave-assisted conditions (150 °C for 15 minutes in AcOH), followed by reduction to provide **68a** in 12% yield. A final hydrogenation with Pd/C removed the benzyl protecting group affording the key scaffold **69a** in 96% yield. In a similar manner, key scaffolds **69b-f** were prepared in overall yields from **65** averaging about 8%.

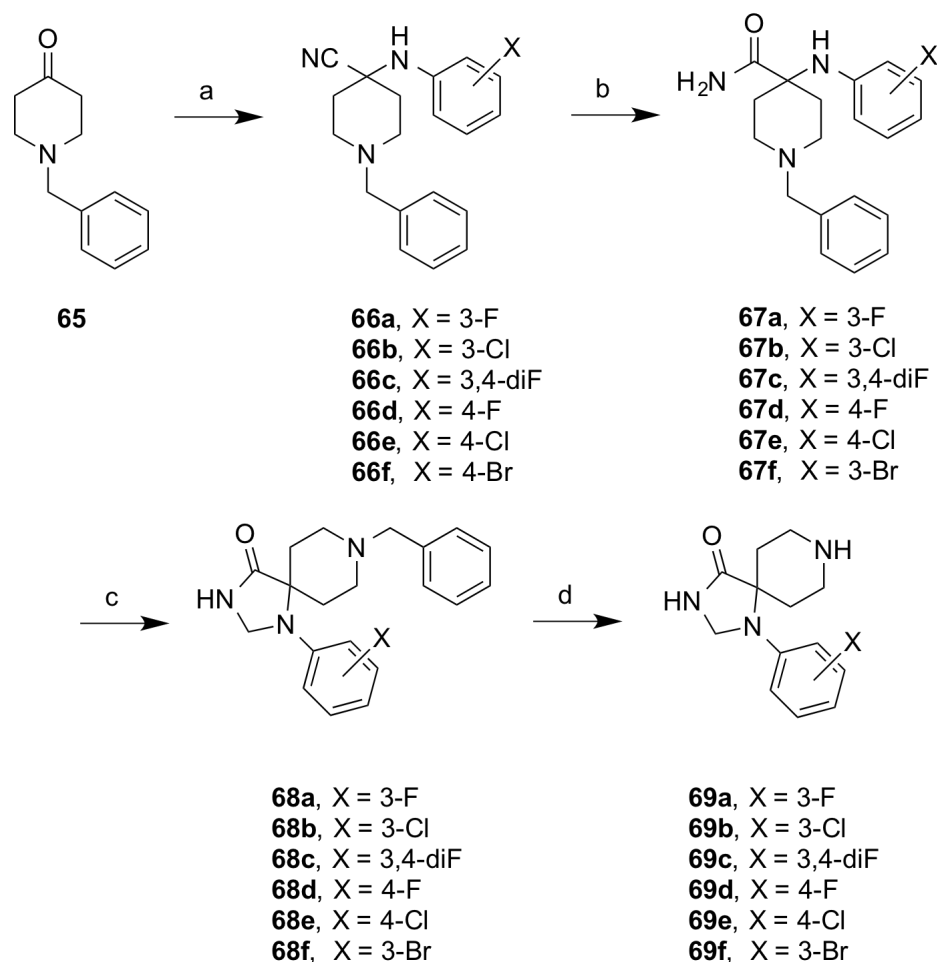


Figure 24. Chemical synthesis of various halogen substituted 1,3,8-triazaspiro[4,5]decan-4-ones. Reagents and conditions: (a) KCN, AcOH, 12 h, rt; (b) H₂SO₄, 12 h, 68%-74% for two steps; (c) *i.*) trimethyl orthoformate, AcOH, microwave, 150 °C, 15 min; *ii.*) NaBH₄, MeOH, 3 hr, 12%-20%; (d) H₂, Pd/C, MeOH, AcOH, 20 hr, 89-96% (Figure adapted with permission from Lavieri *et al.* 2010).

With the requisite synthetically derived halogenated congeners **69a-f** in hand, we initiated the synthesis of a 4x6 matrix library of twenty-four analogs based on the PLD2 preferring inhibitor **63a** (Figure 22). Accordingly, 1,3,8-triazaspiro[4,5]decan-4-ones **69a-f** underwent a reductive amination reaction with *tert*-butyl 2-oxoethylcarbamate to provide, after deprotection, amines **70a-f** in 58-78% yields (Figure 25). Then, the six amines **70a-f** were acylated with four acid chlorides (2-naphthyl, 3-quinolyl, 4-

fluorobenzoyl and 5-fluoro-2-indolyl) to deliver the 24-member library of analogs **71(a-d)** - **76(a-d)** in 75-85% yields.

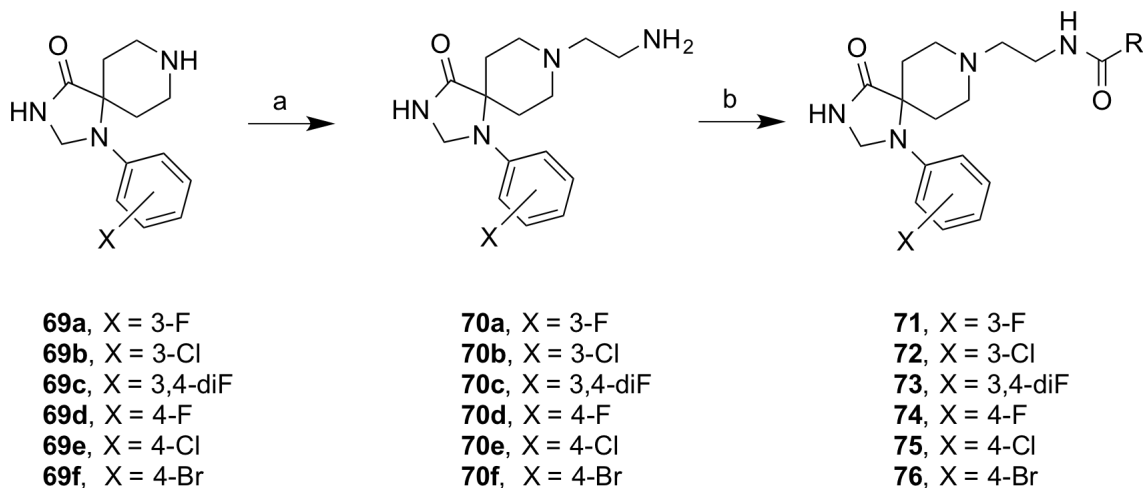
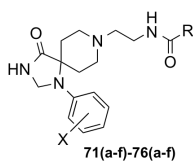


Figure 25. Chemical synthesis of various halogen substituted 1,3,8-triazaspiro[4,5]decan-4-one-containing PLD2 inhibitors. Reagents and conditions: (a) *i*. tert-butyl 2-oxoethylcarbamate, MP-B(OAc)₃H, DCM, MeOH, 18 hr, *ii*. 4.0M HCl/dioxane, DCM, MeOH, 4 hr, 58-78%; (b) RCOCl, DIEA, DMF, rt, 4 hr, 75-85%. (Figure adapted with permission from Lavieri *et al.* 2010).

All library members **71(a-d)** - **76(a-d)** were evaluated for their ability to inhibit PLD1 and PLD2 in a cellular assay (Calu-1 and HEK293-gfpPLD2, respectively) as well as a biochemical assay with recombinant PLD1 and PLD2 enzymes. The cellular assays drove the SAR, with routine confirmation in the *in vitro* biochemical assay to ensure compounds were direct acting inhibitors. SAR for the 24-member library marked a clear departure from the SAR of the earlier PLD1 selective benzimidazolone-based inhibitors, and all but two of the analogs **71(a-d)** - **76(a-d)** displayed a preference for PLD2 inhibition, with the two exceptions, **75c** and **76c**, being dual PLD1/2 inhibitors with comparable PLD1 and PLD2 inhibition.



Cmpd	X	R	PLD1 IC ₅₀ (nM) ^a	PLD2 IC ₅₀ (nM) ^b	Fold PLD2 Selective	Cmpd	X	R	PLD1 IC ₅₀ (nM) ^a	PLD2 IC ₅₀ (nM) ^b	Fold PLD2 Selective
71a	3-F		1,500	20	75	74a	4-F		1,700	80	21
71b			2,500	63	40	74b			2,000	40	50
71c			12,000	6,700	1.8	74c			14,000	610	23
71d			210	25	8	74d			290	30	9
72a	3-Cl		1,200	290	4	75a	4-Cl		2,270	655	3.5
72b			870	165	5	75b			3,500	200	17
72c			3,470	70	50	75c			5,590	5,670	~1
72d			250	73	3.4	75d			335	50	7
73a	3,4-diF		2,800	120	23	76a	4-Br		5,900	350	17
73b			2,060	70	30	76b			2,700	360	8
73c			5,780	660	9	76c			10,000	8,000	~1
73d			390	100	4	76d			2,660	100	27

^aCellular PLD1 assay with Calu-1 cells. ^bCellular assay with HEK293-gfp PLD2 cells. Cell-based assays were used to develop CRCs (from 200 pM to 20 uM) and determine IC₅₀s for all compounds in Calu-1 or HEK293-gfpPLD2 cell lines. The geometric mean of the standard errors of the log(IC₅₀) values from the curve fits of all compounds were computed and compared to the IC₅₀s themselves. There were levels of ~30% error for Calu-1 and ~70% for HEK293-gfpPLD2 IC₅₀s. Despite the variance in the absolute values over a large number of assays, the reproducibility of the effects and relative potency of the inhibitors were found to be robust.

Figure 26. Chemical structures and activities of various 1,3,8-triazaspiro[4,5]decan-4-one-containing PLD2 inhibitors. Cellular enzyme activity assays performed by Sarah Scott; *in vitro* enzyme activity assays performed by Paige E. Selvy. (Figure adapted with permission from Lavieri *et al.* 2010).

Both PLD2 potency and selectivity were dependent on the halogen employed, the substitution pattern on the phenyl ring of the 1,3,8-triazaspiro[4,5]decan-4-one scaffold and on the nature of the eastern amide moiety. As with many allosteric ligands, SAR was shallow and somewhat unpredictable. However, this matrix library approach identified several PLD2 inhibitors that represented a significant improvement over the original PLD2 inhibitor **63a**, and highlights the power and utility of a matrix library approach, as the SAR would not have informed a singleton approach towards optimal PLD2 inhibitors.

For example, **72c** and **74b** displayed ~50-fold selectivity for PLD2, with PLD2 IC₅₀s of 70 nM and 40 nM, respectively; interestingly, **72c** contains the 3-Cl moiety and a 4-fluorophenyl amide whereas **74b** is based on a 4-F scaffold and a 3-quinolinyl amide. Any other combination within these scaffolds results in a decrease of either PLD2 potency or PLD2 selectivity.

From this effort we discovered the most potent and selective PLD2 inhibitor to date, **71a** (VU0364739), with a PLD2 IC₅₀ of 20 nM and possessing 75-fold selectivity versus PLD1 in the cellular assay (**Figure 27A**).

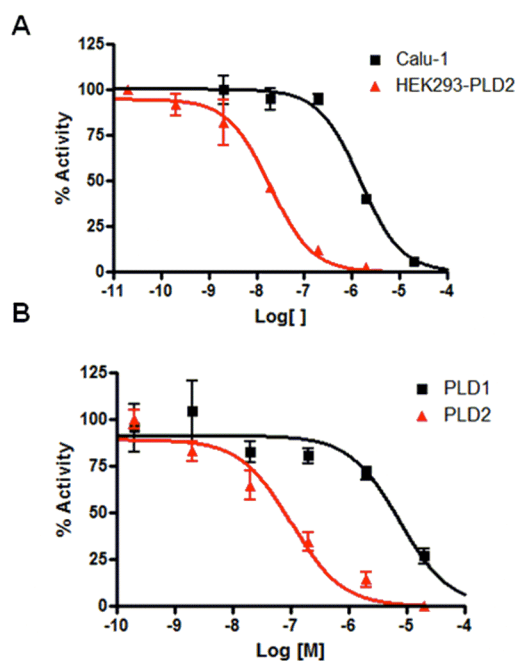


Figure 27. Concentration-Response-Curves (CRCs) for A) cellular PLD1 ■ (Calu-1) assay and PLD2 ▲ (HEK293-gfpPLD2) assay and B) biochemical inhibition assay CRCs with purified ■ PLD1 and ▲ PLD2 highlighting the unprecedented 75-fold PLD2 versus PLD1 selectivity for **71a** (VU0364739) in both PLD assays. Cellular enzyme activity assays performed by Sarah Scott; *in vitro* enzyme activity assays performed by Paige E. Selvy. (Figure adapted with permission from Lavieri *et al.* 2010).

In our *in vitro* biochemical assay using purified PLD1 and PLD2, **71a** possessed a PLD1 IC₅₀ of 7,500 nM and a PLD2 IC₅₀ of 100 nM, replicating the unprecedented 75-fold selectivity for PLD2 (**Figure 27B**). Subsequent efforts to replace the halogens with alternative functional groups (nitriles, heterocycles, cycloalkyls and numerous polar functionalities) led to a complete loss of PLD2 potency. While we could not replicate the 1,700-fold PLD1 selectivity of **41p** (VU0359595) in a PLD2 preferring inhibitor, the 75-fold PLD2 selectivity of **71a** (VU0364739) afforded a small molecule probe to effectively evaluate PLD2 pharmacology in various systems.

Preliminary evaluation of N-(2-(1-(3-Fluorophenyl)-4-oxo-1,3,8-triazaspiro[4.5]decan -8-yl)ethyl)-2-naphthamide (VU0364739) and VU0359595

Biological activity

In earlier work with moderately isoform selective PLD inhibitors we found that inhibitors selective for both isoforms blocked the *in vitro* invasive migration of a triple negative breast cancer cell line (MDA-MB-231); however, siRNA studies indicated that PLD2 played a dominant role. With significantly improved isoform selective PLD1 (VU0359595) and PLD2 (VU0364739) inhibitors, we extended our previous work to dissect the roles of PLD1 and PLD2 in regulating cell proliferation and apoptosis in MDA-MB-231 breast cancer cells.

PLD2 inhibitor **71a** (VU0364739) provided a striking effect in a 48 hour cell proliferation assay, wherein inhibition of PLD2 causes a pronounced decrease in cell proliferation of MDA-MB-231 cells, as compared to an equivalent 10 μ M concentration of the PLD1 inhibitor **41p** (VU0359595) (**Figure 28A**). When cultured under serum free

conditions, the same assay in MDA-MB-231 cells resulted in almost a complete blockade of proliferation with **71a** (VU0364739), and under these conditions, PLD1 inhibition has a significant effect as well (**Figure 28B**). These data do show a preferential sensitization of MDA-MB-231 cells to PLD2 inhibition.

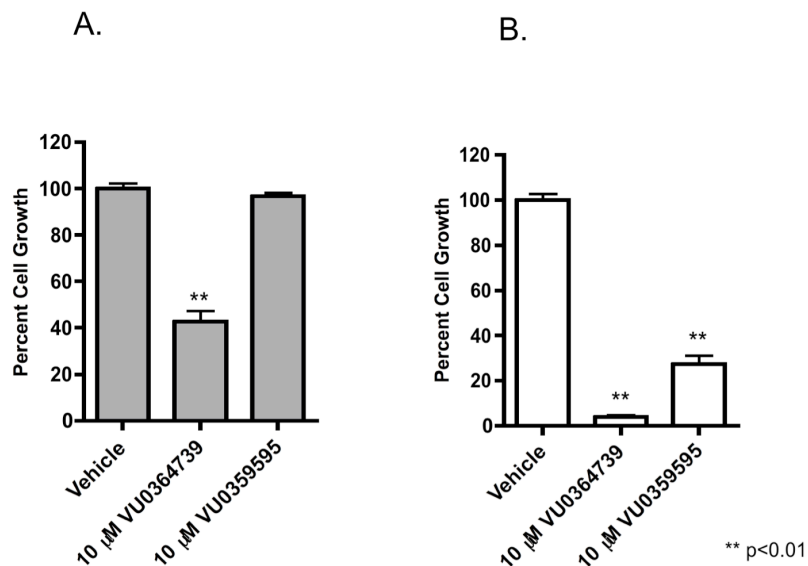


Figure 28. Inhibition of PLD2 with **71a** (VU0364739) leads to decreased proliferation of MDA-MB-231 cells. MDA-MB-231 cells were cultured in the presence of PLD inhibitor for 48 hours after which cell viability was assayed using WST-1 cell proliferation reagent. **A.** MDA-MB-231 cells cultured in the presence of 10% FBS were fairly resistant to PLD inhibitor treatment with only 10 μM **71a** (VU0364739) treatment leading to a significant decrease in cell proliferation. **B.** MDA-MB-231 cells cultured under serum free conditions had a more pronounced response to PLD inhibition with both PLD1 **41p** (VU0359595) and PLD2 **71a** (VU0364739) selective compounds significantly decreasing cell proliferation. Cell proliferation assays performed by Sarah Scott. (Figure adapted with permission from Lavieri *et al.* 2010).

We also evaluated the effect of **71a** (VU0364739) on cell proliferation in MDA-MB-231 cells over a 96 hour time course and with a dose-response paradigm (**Figure 29**). In the presence of 10% FBS, **71a** (VU0364739) displayed a dose-dependent decrease in cell proliferation over the time course, with significant effects at both a 5 μM

and 10 μ M dose (**Figure 29A**). Under serum free conditions (**Figure 29B**), a more pronounced effect was observed at in a dose (1 μ M, 5 μ M and 10 μ M) and time dependent manner. Importantly, **71a** (VU0364739) was significantly less cytotoxic in standard cell viability assays in non-transformed cells (data not shown).

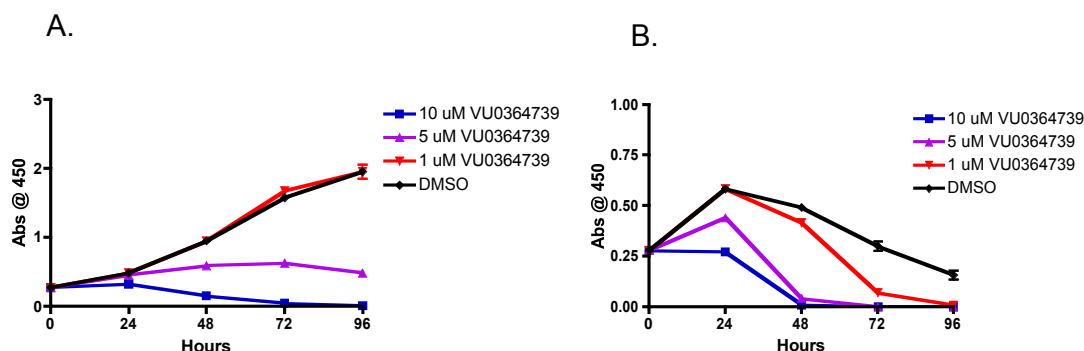


Figure 29. Inhibition of PLD2 leads to a time-dependent decrease in proliferation of MDA-MB-231 cells. MDA-MB-231 cells were cultured in the presence of PLD inhibitor and cell viability was assayed using WST-1 cell proliferation reagent over 96 hours. **A.** MDA-MB-231 cells cultured in the presence of 10% FBS showed a dose dependent attenuation of cell proliferation over time. Cultures with 10 and 5 μ M **71a** (VU0364739) treatment led to a significant decrease in cell proliferation while 1 mM inhibitor had no effect. **B.** MDA-MB-231 cells cultured in the absence of serum had a more pronounced response to PLD inhibition with all concentrations of the PLD2 selective compound significantly decreasing cell proliferation in a dose and time dependent manner. WST-1 Cell proliferation assays performed by Sarah Scott. (Figure adapted with permission from Lavieri *et al.* 2010).

Next, we evaluated the role of PLD1 and PLD2 inhibition on apoptosis in MDA-MB-231 with and without serum, employing Caspase 3 and 7 as a surrogate marker for apoptosis (**Figure 30**). Once again, our isoform selective inhibitors were able to distinguish differential roles for PLD1 and PLD2. In the standard 48 hour apoptosis assay, a 10 μ M dose of PLD2 inhibitor **71a** (VU0364739) provided a significant (3-fold increase) increase in Caspase 3 and 7 activity, whereas inhibition of PLD1 with **41p** (VU0359595) led to a marginal increase in Caspase 3 and 7 activity (**Figure 30A**). Under serum free conditions, both **41p** (VU0359595) and **71a** (VU0364739) had similar effects on Caspase 3 and 7 activity (**Figure 30B**). These data again suggest that PLD2

signaling plays a critical role in the invasive migration, proliferation and survival of MDA-MB-231 breast cancer cells.

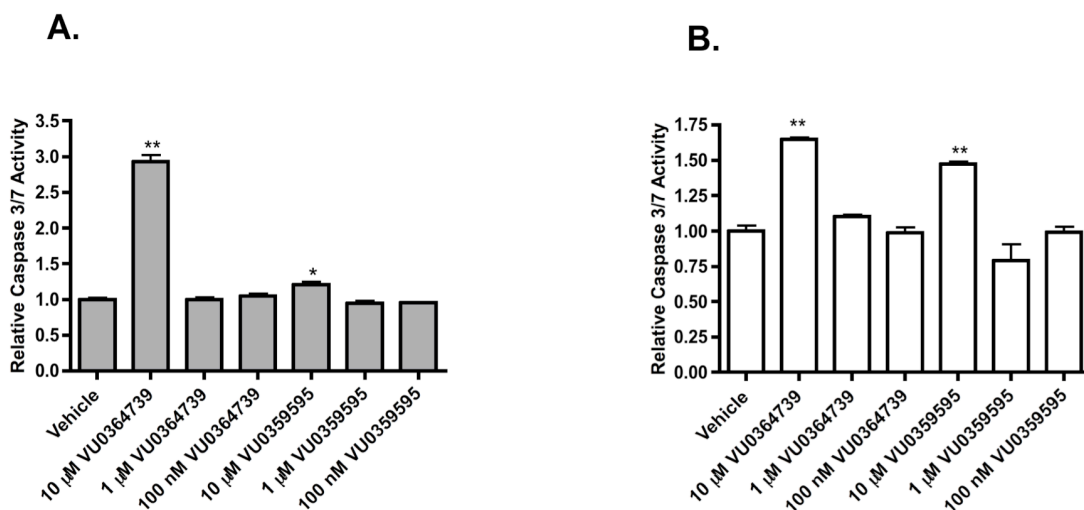


Figure 30. Inhibition of PLD2 leads to increased apoptosis in MDA-MB-231 cells compared with minimal effect of PLD1 inhibition. MDA-MB-231 cells were cultured in the presence of PLD inhibitor for 48 hours after which time Caspase 3 & 7 activity was measured. **A.** MDA-MB-231 cells cultured in the presence of 10% FBS were fairly resistant to PLD inhibitor treatment (**41p** or **71a**) with only 10 μ M **71a** (VU0364739) treatment leading to a significant increase in Caspase 3 & 7 activity compared to vehicle control. **B.** MDA-MB-231 cells cultured under serum free conditions had increased Caspase 3 & 7 activity upon 10 μ M PLD inhibitor treatment as compared to the vehicle control. Caspase assays performed by Sarah Scott (Figure adapted with permission from Lavieri *et al.* 2010).

Pharmacokinetics

We evaluated **41p** (VU0359595) and **71a** (VU0364739) in a battery of *in vitro* and *in vivo* DMPK assays to determine if these isoform selective PLD inhibitors would be suitable candidates with which to dissect PLD function *in vivo*. PLD1 inhibitor **41p** (VU0359595) was lipophilic (clogP = 4.5), yet possessed ~2% free fraction in rat and human plasma protein binding experiments (equilibrium dialysis) and was easily formulated into acceptable vehicles. In rat iv PK experiments, **41p** (VU0359595) was found to be a highly cleared compound (Cl = 60 mL/min/kg) with a moderate half-life ($t_{1/2}$ = 0.75 hr) and high volume of distribution (V_{dss} = 4.7 L/kg) (**Figure 31**). A similar

profile was obtained for PLD2 inhibitor **71a** (VU0364739). While less lipophilic ($\text{clogP} = 3.2$), **71a** (VU0364739) also displayed ~2% free fraction in rat and human plasma protein binding experiments (equilibrium dialysis) and was easily formulated into acceptable vehicles. In rat iv PK experiments, **71a** (VU0364739) was found to be a highly cleared compound ($\text{Cl} = 61 \text{ mL/min/kg}$) with a moderate half-life ($t_{1/2} = 1.5 \text{ hr}$) and high volume of distribution ($V_{\text{dss}} = 8.1 \text{ L/kg}$).

Cmpd	plasma protein binding (% bound)	IV (pharmacokinetics) ^a				PO (plasma & brain levels) ^b			
		dose (mg/kg)	CL (mL/min/kg)	$t_{1/2}$ (h)	V_{dss} (L/kg)	dose (mg/kg)	Plasma (ng/mL)	Brain (ng/mL)	Brain/Plasma
41p	98.1	1	60.7	0.78	4.7	10	29	BLQ	BLQ
71a	97.9	1	61.5	1.52	8.1	10	39.9	29	0.73

Figure 31. Pharmacokinetic profile of **41p** (VU0359595) and **71a** (VU0364739) in rat. Pharmacokinetic analyses performed by Satyawan Jadhav, Ryan Morrison and J. Scott Daniels (Figure adapted with permission from Lavieri *et al.* 2010).

Recent genetic and knock-out studies have suggested therapeutic roles for PLD inhibition in Alzheimer's disease and stroke; therefore, centrally penetrant PLD inhibitors would be of great value for preclinical target validation. To address this, both **41p** (VU0359595) and **71a** (VU0364739) were dosed at 10 mpk po in a standard 90 minute single point brain:plasma (PBL) study. While levels of **41p** (VU0359595) were below quantitation in the brain, **71a** (VU0364739) displayed a Brain/Plasma ratio of 0.73 thereby representing the first centrally penetrant PLD inhibitor we have prepared. Due to their overall PK properties, **41p** (VU0359595) and **71a** (VU0364739) remain important *in vitro* tools to probe and dissect the differential roles and pharmacology of PLD1 and PLD2; however, additional optimization is required to develop robust *in vivo* proof-of-

concept compounds. Specifically, the clearance values that are approximately equal to liver blood flow in a rat need to be improved.

A (*S*)-methyl group dramatically increases PLD1 potency within a PLD2-preferring chemotype

The addition of a (*S*)-methyl group dramatically increased isoform selectivity in the PLD1-selective benzimidazolone series culminating in the identification of **41p** (VU0359595). Installation of the (*S*)-methyl group into the modestly PLD2-preferring **63a** (PLD1 IC₅₀ = 1,000 nM, PLD2 IC₅₀ = 110 nM), within the triazaspirone series (Figure 32), resulted in **64a** with enhanced (40-fold) PLD1 inhibition and essentially no effect on PLD2 activity (PLD1 IC₅₀ = 25 nM, PLD2 IC₅₀ = 140 nM).

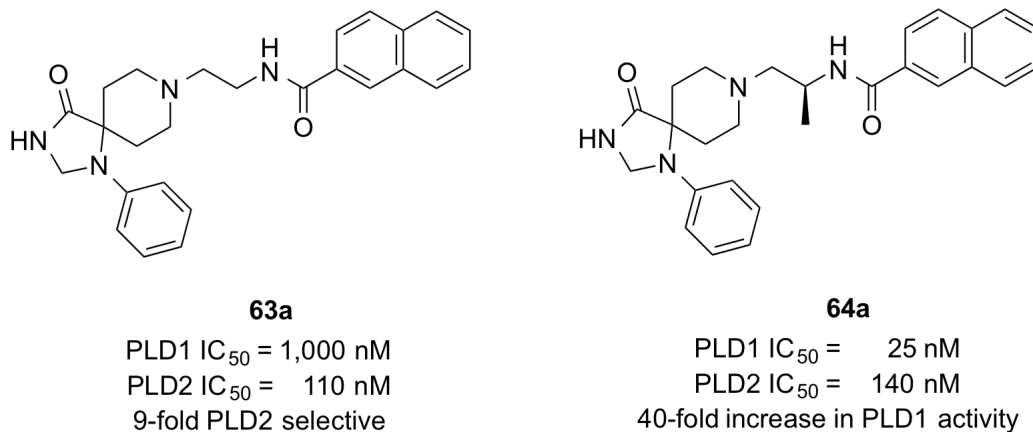


Figure 32. Chemical structures and activities of PLD2 preferring inhibitor **63a** and the impact of adding a chiral (*S*)-methyl group providing **64a** and a 40-fold increase in PLD1 inhibitory activity (Figure adapted with permission from Lavieri *et al.* 2010).

This type of ‘molecular switch’ has been noted before for allosteric modulators of GPCRs engendering either subtype selectivity or reversing the mode of pharmacology (NAM to PAM or PAM to NAM). Thus, we wanted to evaluate if the addition of the PLD1-preferring (*S*)-methyl ‘molecular switch’ would increase PLD1 inhibitory activity

in a highly PLD2 preferring compound such as **71a** (VU0364739). We prepared an analog **77** of **71a** (VU0364739) containing the relevant (*S*)-methyl group (**Figure 33**). Evaluation of **77** in PLD1 and PLD2 cellular enzyme activity assays further showcased the impact of the (*S*)-methyl group as a ‘molecular switch’, providing a 150-fold increase in PLD1 inhibitory activity (PLD1 IC₅₀ = 10 nM) while maintaining PLD2 activity (PLD2 IC₅₀ = 60 nM). Thus, a 75-fold PLD2 preferring inhibitor **71a** (VU0364739) is converted into a potent dual PLD1/2 inhibitor **77** by the addition of a single (*S*)-methyl group.

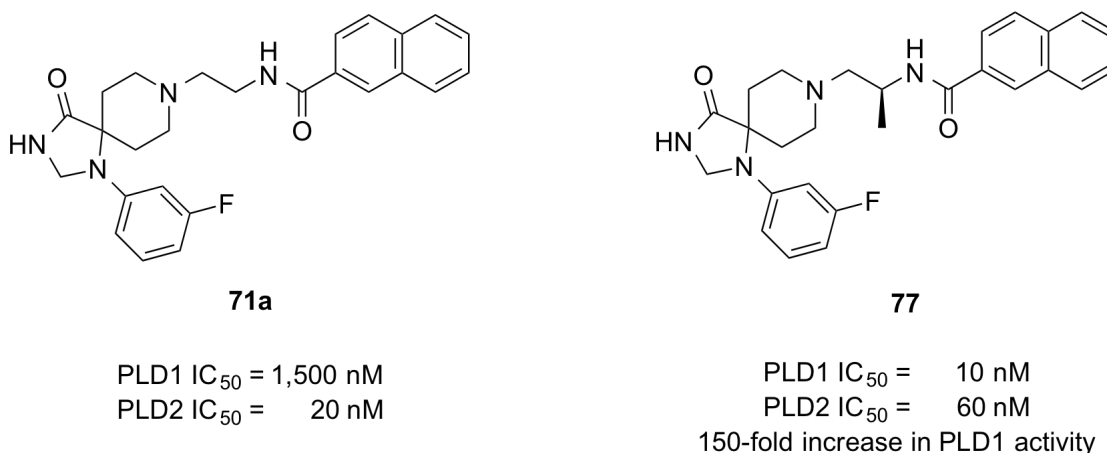


Figure 33. Chemical structures and activities of PLD2 preferring inhibitor **71a** (VU0364739) and the impact of adding a chiral (*S*)-methyl group providing **77** and a 150-fold increase in PLD1 inhibitory activity. Enzyme activity assays performed by Sarah Scott (Figure adapted with permission from Lavieri *et al.* 2010).

While we were not able to match the 1,700-fold selectivity for PLD1 present in **41p** (VU0359595) we able to prepare a centrally penetrant, potent (PLD2 IC₅₀ = 20 nM), 75-fold selective PLD2 inhibitor, **71a** (VU0364739). It was not until the identification of the 1,3,8-triazaspiro[4,5]decan-4-one scaffold that we were able to make progress toward the 75-fold selective PLD2 inhibitor, **71a** (VU0364739) (**Figure 34**).

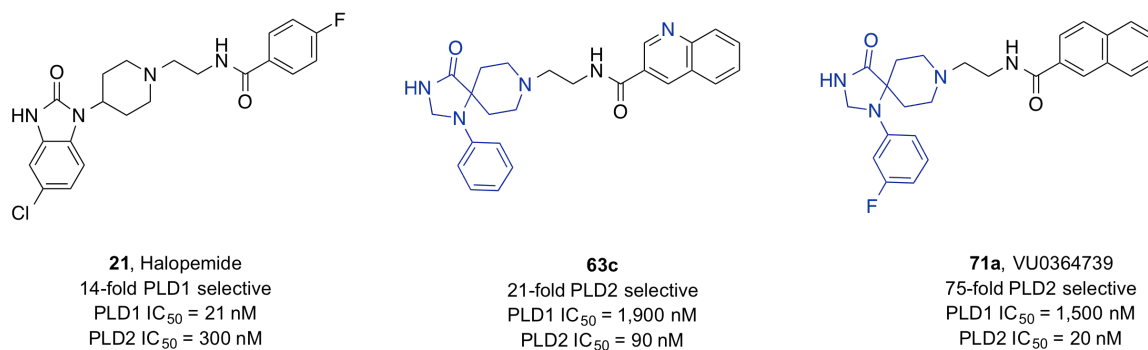


Figure 34. Key structural modifications (shown in blue) that led to the development of **71a** (VU0364739) (Figure adapted with permission from Selvy *et al.* 2012).

Interestingly, introduction of a ‘molecular switch’, in the form of a (*S*)-methyl group, to **71a** (VU0364739) increased PLD1 activity 150-fold providing a potent PLD1/2 inhibitor **77**. Both **41p** (VU0359595) and **71a** (VU0364739) should prove useful as tools to study the role(s) of PLD1 and PLD2 in various cell lines/tissues. Future compounds optimized for DMPK properties may prove useful for *in vivo* target validation and perhaps even as therapeutics for diseases such as cancer, schizophrenia, stroke and Alzheimer’s disease, where aberrant PLD activity has been noted.

Materials and methods

Cell culture

Calu-1, and MDA-231 cells were purchased from American Type Culture Collection (Manassas, VA). Calu-1 and MDA-231 cells were maintained in DMEM supplemented with 10% FBS, 100 µg/mL penicillin-streptomycin and 0.25 µg/mL amphotericin. HEK293 cells stably expressing GFP tagged human PLD2A were generated in the lab. To sustain selection pressure low passage-number HEK293-gfpPLD2 cells were maintained in DMEM supplemented with 10% FBS, 100 µg/mL

penicillin-streptomycin, 2 µg/mL puromycin and 600 µg/mL G418. All HEK293-gfpPLD2 experiments were done on tissue culture plates that had been coated with low levels of poly-lysine. All cells were maintained in a humidified 5% CO₂ incubator at 37°C.

Endogenous PLD enzyme activity assay

Endogenous PLD activity was determined using a modified *in vivo* deuterated 1-butanol PLD assay. All cell types aside from the stable HEK293-gfpPLD2 cells were serum-starved 18 h before experiment. Cells were pretreated with PLD inhibitor or DMSO for 5 min at room temperature (20 °C). After pretreatment, Calu-1 cells were treated with 1 mM PMA + 0.3% (v/v) 1-butanol-D₁₀ and either PLD inhibitor or DMSO, or medium alone for 30 min at 37 °C. HEK293-gfpPLD2 cells were treated in the presence of 0.3% 1-butanol- D₁₀ and PLD inhibitor or vehicle. After treatment, samples were extracted and internal standard was added. The resulting lipids were dried and resuspended in MS solvent. Samples were directly injected into a Finnigan TSQ Quantum triple quadrupole MS and data were collected in negative ion mode. Data were analyzed as a ratio of major phosphatidylbutanol-D₉ lipid products and internal standard. Background signal was subtracted using cells not treated with 1-butanol-D₁₀ as a negative control. The data were then expressed as percent of PMA-stimulated PLD activity or as percent of basal PLD activity and IC₅₀ values for each compound were estimated from concentration response curves in both cell types.

Assessment of cell proliferation via WST-1 assay

Cells are plated into 96-well tissue culture plates at 15,000 cells/well in tissue culture treated 96-well black wall/clear bottom assay plates (Corning Inc. Costar plates) in complete growth medium and allowed to grow overnight. After 24 hours of growth media was removed and cells are treated with PLD inhibitor or DMSO vehicle control in 100 μ L of DMEM 1% AA either +/- 10% FBS. Media and inhibitor are replenished every 24 hours and after 48 hours cells were treated with 10 μ L/well of a modified MTT reagent, WST-1 Cell Proliferation Reagent (Roche Diagnostics Corporation, Indianapolis, IN). Plates were then incubated for 1 hr at 37 °C. After incubation UV absorbance was measured at 450 nm with, BioTek Synergy HT plate reader (BioTek Inc., Winooski, VT). Background signal was subtracted from wells with no cells present. Data is expressed as absorbance at 450 nm. For time course experiments cells were seeded at 7,500 cells/well into media containing PLD inhibitor or DMSO vehicle control. Media was removed and replaced every 24 hours and at set time points (24, 48, 72, and 96 hours) cells were treated with WST-1 reagent as described above.

Assessment of caspase 3/7 activity

Caspase-3/7 activity was measured using a homogeneous bioluminescent method according to manufacturer's directions (Caspase-Glo 3/7 Assay, Promega, Madison, WI). In this assay, caspase-3/7 activity is measured by the ability to cleave the proluminescent Caspase 3/7 specific DEVD-aminoluciferin substrate to liberate the free aminoluciferin which is then consumed by luciferase generating a luminescent signal. The luminescent signal is directly proportional to the amount of Caspase 3/7 activity. Cells were plated at

15,000 cells/well in tissue culture treated 96-well black wall/clear bottom assay plates (Corning Inc. Costar plates) in 50 μ L growth medium at 37 °C. After 24 hours media was removed and replaced with DMEM, 1%AA, +/- 10% FBS with either PLD inhibitor or DMSO vehicle control. Media was replenished every 24 hours to account for metabolism of the compounds. After 48 hours growth in the presence of PLD inhibitor 50 μ L Caspase-Glo 3/7 reagent was added to each well, plates were incubated at room temperature for 1 h, and luminescent signal was then detected with BioTek Synergy HT plate reader (BioTek Inc.; Winooski, VT). Caspase 3/7 activity was normalized to vehicle control and expressed as fold stimulation of Caspase activity.

***In vitro* pharmacokinetic studies**

The metabolism of PLD inhibitors, **41p** (VU0359595) and **71a** (VU0364739), was investigated in rat hepatic microsomes (BD Biosciences, Billerica, MA) using substrate depletion methodology (% test article remaining). A potassium phosphate-buffered reaction mixture (0.1 M, pH 7.4) of test article (1 μ M) and microsomes (0.5 mg/mL) was pre-incubated (5 min) at 37°C prior to the addition of NADPH (1 mM). The incubations, performed in 96-well plates, were continued at 37°C under ambient oxygenation and aliquots (80 μ L) were removed at selected time intervals (0, 3, 7, 15, 25 and 45 min). Protein was precipitated by the addition of chilled acetonitrile (160 μ L), containing glyburide as an internal standard (50 ng/mL), and centrifuged at 3000 rpm (4°C) for 10 min. Resulting supernatants were transferred to new 96-well plates in preparation for LC/MS/MS analysis. The *in vitro* half-life ($t_{1/2}$, min, Eq. 1), intrinsic clearance (CL_{int} ,

mL/min/kg, Eq. 2) and subsequent predicted hepatic clearance (CL_{hep} , mL/min/kg, Eq. 3) was determined employing the following equations:

$$(1) t_{1/2} = \text{Ln}(2) / k ; \text{ where } k \text{ represents the slope from linear regression analysis}$$

(% test article remaining)

$$(2) CL_{\text{int}} = (0.693 / t_{1/2}) (\text{rxn volume} / \text{mg of microsomes}) (45 \text{ mg microsomes} / \text{gram of liver}) (20^a \text{ gm of liver} / \text{kg body weight}); ^a \text{scale-up factors of 20 (human) and 45 (rat)}$$

$$(3) CL_{\text{hep}} = \frac{Q \cdot CL_{\text{int}}}{Q + CL_{\text{int}}}$$

***In vivo* pharmacokinetic studies**

Male Sprague-Dawley rats (n=2) weighing around 300g were purchased from Harlon laboratories (Indianapolis, IN) and implanted with catheters in the carotid artery and jugular vein. The cannulated animals were acclimated to their surroundings for approximately one week before dosing and provided food and water *ad libitum*. Compounds **41p** (VU0359595) and **71a** (VU0364739) were administered intravenously (IV) to rats via the jugular vein catheter in 20% DMSO/80% saline at a dose of 1 mg/kg and a dose volume of 1 mL/kg. Blood collections via the carotid artery were performed at pre-dose, and at 2 min, 7 min, 15 min, 30 min, and 1, 2, 4, 7 and 24 hrs post dose. Samples were collected into chilled, EDTA-fortified tubes, centrifuged for 10 minutes at 3000 rpm (4°C), and resulting plasma aliquoted into 96-well plates for LC/MS/MS analysis. All pharmacokinetic analysis was performed employing noncompartmental analysis. For oral exposure studies, measuring both systemic plasma and CNS tissue exposure, compounds **41p** (VU0359595) and **71a** (VU0364739) were administered (oral

gavage) to fasted rats (n=2) as suspensions in 10% tween 80/0.5% methylcellulose at a dose of 10 mg/kg and in a dosing volume of 10 mL/kg; blood and whole brain samples were collected at 1.5h post dose. Blood was collected into chilled, EDTA-fortified tubes, centrifuged for 10 minutes at 3000 rpm (4°C) and stored at -80°C until LC/MS/MS analysis. The brain samples were rinsed in PBS, snap frozen and stored at -80°C. Prior to LC/MS/MS analysis, brain samples were thawed to room temperature and subjected to mechanical homogenation employing a Mini-Beadbeater™ and 1.0 mm Zirconia/Silica Beads (BioSpec Products). All animal studies were approved by the Vanderbilt University Medical Center Institutional Animal Care and Use Committee. The animal care and use program is fully accredited by the Association for Assessment and Accreditation of Laboratory Animal Care, International.

Plasma protein binding

Protein binding of the PLD inhibitors, **41p** (VU0359595) and **71a** (VU0364739), was determined in rat plasma via equilibrium dialysis employing Single-Use RED Plates with inserts (ThermoFisher Scientific, Rochester, NY). Briefly plasma (220 µL) was added to the 96 well plate containing test article (5 µL) and mixed thoroughly. Subsequently, 200 µL of the plasma-test article mixture was transferred to the *cis* chamber (red) of the RED plate, with an accompanying 350 µL of phosphate buffer (25 mM, pH 7.4) in the *trans* chamber. The RED plate was sealed and incubated 4 h at 37°C with shaking. At completion, 50 µL aliquots from each chamber were diluted 1:1 (50 µL) with either plasma (*cis*) or buffer (*trans*) and transferred to a new 96 well plate, at which time ice-cold acetonitrile (2 volumes) was added to extract the matrices. The plate

was centrifuged (3000 rpm, 10 min) and supernatants transferred to a new 96 well plate. The sealed plate was stored at -20°C until LC/MS/MS analysis.

Liquid chromatography/mass spectrometry analysis for pharmacokinetic experiments

In vivo experiments

PLD inhibitors, **41p** (VU0359595) and **71a** (VU0364739), were analyzed via electrospray ionization (ESI) on an AB Sciex API-4000 (Foster City, CA) triple-quadrupole instrument that was coupled with Shimadzu LC-10AD pumps (Columbia, MD) and a Leap Technologies CTC PAL auto-sampler (Carrboro, NC). Analytes were separated by gradient elution using a Fortis C18 2.1 x 50 mm, 3.5 µm column (Fortis Technologies Ltd, Cheshire, UK) thermostated at 40°C. HPLC mobile phase A was 0.1% NH₄OH (pH unadjusted), mobile phase B was acetonitrile. The gradient started at 30% B after a 0.2 min hold and was linearly increased to 90% B over 0.8 min; held at 90% B for 0.5 min and returned to 30% B in 0.1 min followed by a re-equilibration (0.9 min). The total run time was 2.5 min and the HPLC flow rate was 0.5 mL/min. The source temperature was set at 500°C and mass spectral analyses were performed using multiple reaction monitoring (MRM), with transitions for **41p** (VU0359595) (m/z 497.5→202.3) and **71a** (VU0364739) (m/z 447.4→198.1) utilizing a Turbo-Ionspray® source in positive ionization mode (5.0 kV spray voltage). All data were analyzed using AB Sciex Analyst 1.4.2 software.

In vitro experiments

The PLD inhibitors were analyzed similarly to that described above (*In vivo*) with the following exceptions: LC/MS/MS analysis was performed employing a TSQ Quantum^{ULTRA} that was coupled to a ThermoSurveyor LC system (Thermoelectron Corp., San Jose, CA) and a Leap Technologies CTC PAL auto-sampler (Carrboro, NC). Chromatographic separation of analytes was achieved with an Acquity BEH C18 2.1 x 50 mm, 1.7 μm column (Waters, Taunton, MA).

Medicinal chemistry

General synthetic methods

All reactions were carried out employing standard chemical techniques. Unless otherwise noted, reactions were run in anhydrous solvents. Solvents for extraction, washing and chromatography were HPLC grade. All reagents were purchased from Sigma-Aldrich and Biotage at the highest commercial quality and were used without purification. Microwave-assisted reactions were conducted using a Biotage Initiator-60 single mode microwave synthesizer.

All NMR spectra were recorded on a 400 MHz Bruker AMX NMR. ¹H chemical shifts are reported as δ values in ppm downfield from the solvent residual peak (MeOD = 3.31, DMSO-d₆ = 2.50, CDCl₃ = 7.26). Data are reported as follows: chemical shift, multiplicity (s = singlet, d = doublet, t = triplet, q = quartet, m = multiplet), coupling constant (Hz), and integration. ¹³C chemical shifts are reported as δ values in ppm downfield from the solvent residual peak (MeOD = 49.0, DMSO-d₆ = 39.5, CDCl₃ = 77.16). Low resolution mass spectra were obtained on an Agilent 1200 LCMS with

electrospray ionization equipped with a YMC Jsphere H-80 S-4 3.0 x 50 mm column running a gradient of 5-95% (over 4 minutes) acetonitrile in 0.1% trifluoroacetic acid in water. High-resolution mass spectra were recorded on a Waters QTOF-API-US plus Acquity system with electrospray ionization. Analytical thin layer chromatography was performed on 250 μ m silica gel 60 F254 plates. Automated flash column chromatography was performed on a Teledyne ISCO combiflash Rf system. Analytical HPLC was performed on an Agilent 1200 analytical LCMS equipped with a YMC Jsphere H-80 S-4 3.0 x 50 mm column running a gradient of 5-95% (at a flow rate of 1.25 mL/min over 4 minutes) acetonitrile in 0.1% trifluoroacetic acid in water, and UV detection at 214 nm and 254 nm along with ELSD detection.

Preparative purification of library compounds was performed on a custom Agilent 1200 preparative LCMS with collection triggered by mass detection or alternatively compounds were purified on a Gilson 215 preparative LC system equipped with a Phenomenx Luna 5u C18 50 x 30 mm column by running a gradient of 20-60% acetonitrile in 0.1% trifluoroacetic acid in water at a flow rate of 50 mL/min over approximately 5 minutes. All yields refer to analytically pure and fully characterized materials (^1H NMR, ^{13}C NMR, analytical LCMS and HRMS).

For the purposes of compound tracking and organization all final library compounds were transferred to barcoded vials and diluted to 10 mM in DMSO. Large preparations of compounds such as **41p** (VU0359595) and **71a** (VU0364739) were stored as powders (typically hydrochloride salts) at 0 °C and diluted at the time of use. Each new compound was registered into a central computer database system, which assigned a unique VU identification number to each compound. In the text, arbitrary number codes

for compounds (e.g. **41p**) are specific for each chapter and are often used alongside the full VU registration code (e.g. VU0359595).

Chemical experimentals

***N*-(2-(4-(5-chloro-2-oxo-2,3-dihydro-1*H*-benzo[*d*]imidazol-1-yl)piperidin-1-yl)ethyl)-4-fluorobenzamide (21).** 1-(1-(2-aminoethyl)piperidin-4-yl)-5-chloro-1*H*-benzo[*d*]imidazol-2(3*H*)-one dihydrochloride (465 mg, 1.26 mmol), 4-fluorobenzoyl chloride (200 mg, 1.26 mmol) and *N,N*-diisopropylethylamine (0.770 mL, 4.41 mmol) were all dissolved in *N,N*-dimethylformamide (10 mL) at 0 degrees Celsius. The reaction mixture was allowed to warm to room temperature and stirred for about 12 hours. The product was precipitated via the addition of water and then isolated via filtration. The product was then washed 4 times with a solution of lithium chloride (3M) and dried under reduced pressure to afford a light tan solid (210 mg, 0.5 mmol, 40 %). ¹H NMR (400.1 MHz, DMSO-*d*₆) δ (ppm): 11.07 (s, 1H), 8.59 (br s, 1H), 7.97 - 7.91 (m, 2H), 7.34 - 7.23 (m, 3H), 7.02 - 6.97 (m, 2H), 4.29 - 4.15 (m, 1H), 3.51 - 3.43 (m, 2H), 3.24-3.13 (m, 2H), 2.74 - 2.64 (m, 2H), 2.47 - 2.31 (m, 4H), 1.70 (d, *J* = 7 Hz, 2H); ¹³C NMR (100.6 MHz, DMSO-*d*₆) δ (ppm): 165.2, 162.6, 153.6, 130.9, 129.9, 129.8, 129.6, 128.0, 124.9, 120.0, 115.3, 115.1, 109.8, 108.8, 56.3, 52.4 (2C), 49.5, 36.5, 27.8 (2C); HRMS (TOF, ESI) C₂₁H₂₃N₄O₂FCl [M+H]⁺ calculated 417.1494, found 417.1496; LC-MS: rt (min) = 2.006; LRMS (ESI) m/z = 417.1.

VU0155056. *N*-(2-(4-(2-oxo-2,3-dihydro-1*H*-benzo[*d*]imidazol-1-yl)piperidin-1-yl)ethyl)-2-naphthamide hydrochloride (39a). *N*-(2-(4-(2-oxo-2,3-dihydro-1*H*-benzo[*d*]imidazol-1-yl)piperidin-1-yl)ethyl)-2-naphthamide (908 mg, 2.19 mmol) was

stirred in methanol (10 mL) at room temperature and treated with hydrochloric acid (4M in dioxane, 2 mL). After about 25 minutes the compound was dried under reduced pressure to afford a pink solid (908 mg, 1.86 mmol, 88 %). ^1H NMR (400.1 MHz, $\text{DMSO-}d_6$) δ (ppm): 10.99 (s, 1H), 9.18 (t, $J = 6$ Hz, 1H), 8.63 (s, 1H) 8.08 - 7.96 (m, 4H), 7.68 - 7.56 (m, 3H), 7.03 - 6.96 (m, 3H), 4.66 - 4.55 (m, 1H), 4.12 (s, 1H), 3.86 - 3.73 (m, 4H), 3.67 - 3.53 (m, 2H), 3.31 - 3.20 (m, 2H), 2.98 - 2.88 (m, 2H), 1.90 (d, $J = 12$ Hz, 2H); ^{13}C NMR (100.6 MHz, $\text{DMSO-}d_6$) δ (ppm): 166.6, 153.5, 134.3, 132.1, 131.2, 128.9 (2C), 128.4, 127.9 (2C), 127.7, 127.6, 126.8, 124.2, 120.9, 120.5, 109.4, 109.1, 55.5, 51.4 (2C), 46.5, 35.8, 25.4 (2C); HRMS (TOF, ESI) $\text{C}_{25}\text{H}_{27}\text{N}_4\text{O}_2$ $[\text{M}+\text{H}]^+$ calculated 415.2134, found 415.2133; LC-MS: rt (min) = 2.074; LRMS (ESI) $m/z = 415.2$.

Ethyl 4-((4-bromo-2-nitrophenyl)amino)piperidine-1-carboxylate (44). A mixture of ethyl-4-amino-1-piperidine (6.027 g, 35 mmol), 4-bromo-1-fluoro-2-nitrobenzene (7.699 g, 35 mmol), sodium carbonate (3.709 g, 35 mmol) and potassium iodide (581 mg, 3.5 mmol) dissolved in cyclohexanol (30 mL) was subjected to microwave irradiation at 180 degrees celsius for 10 minutes in a biotage initiator single-mode microwave synthesizer. The crude reaction mixture was diluted with toluene, washed 4 times with water, dried with magnesium sulfate, filtered and concentrated under reduced pressure. The crude compound was dissolved in dichloromethane, further purified by filtration and concentrated under reduced pressure to afford a bright orange solid (12.58 g, 33.8 mmol, 97 %). ^1H NMR (400.1 MHz, CDCl_3) δ (ppm): 8.31 (d, $J = 2$ Hz, 1H), 8.05 (d, $J = 7$ Hz, 1H), 7.48 (dd, $J = 2, 9$ Hz, 1H), 6.78 (d, $J = 9$ Hz, 1H), 4.14 (q, $J = 7$ Hz, 2H), 4.11 - 4.01 (m, 2H), 3.70 - 3.60 (m, 1H), 3.14 - 3.05 (m, 2H), 2.10 -

2.01 (m, 2H), 1.61 - 1.50 (m, 2H), 1.27(t, $J = 7$ Hz, 3H); ^{13}C NMR (100.6 MHz, CDCl_3) δ (ppm): 155.5, 143.2, 139.0, 132.5, 129.4, 115.7, 106.7, 61.7, 49.5, 42.2 (2C), 31.7 (2C), 14.8; HRMS (TOF, ESI) $\text{C}_{14}\text{H}_{19}\text{N}_3\text{O}_4\text{Br}$ $[\text{M}+\text{H}]^+$ calculated 372.0559, found 372.0559; LC-MS: rt (min) = 3.015; LRMS (ESI) $m/z = 372.0$.

ethyl 4-(5-bromo-2-oxo-2,3-dihydro-1H-benzo[d]imidazol-1-yl)piperidine-1-carboxylate (46). Ethyl 4-((4-bromo-2-nitrophenyl)amino)piperidine-1-carboxylate (12.36 g, 33.2 mmol) was dissolved in a solution of hydrochloric acid (150 mL, 1M in methanol) at 0 degrees Celsius. Zinc dust (10.7 g, 166 mmol) was added and the reaction was monitored via TLC (1:1 ethyl acetate:hexanes). After the reaction reached completion the methanol was removed under reduced pressure, water was added and the mixture was extracted into ethyl acetate 3 times dried, filtered and concentrated under reduced pressure. This material was then dissolved in tetrahydrofuran (200 mL) at 0 degrees Celsius. Triphosgene (9.8 g, 33.2 mmol) was added and allowed to dissolve over 15 minutes. Finally, triethylamine (11.5 mL, 83 mmol) was added slowly over 15 minutes. The reaction completed after about 30 minutes and was then diluted with water and a solution of hydrochloric acid (1M). The reaction mixture was extracted into dichloromethane and dried under reduced pressure. The material was chromatographed on a 330 g flash column (UV monitored at 292 nm) running a gradient of 0-45% ethyl acetate in hexanes to afford a light pink solid (6.94 g, 18.8 mmol, 56 %). ^1H NMR (400.1 MHz, $\text{DMSO}-d_6$) δ (ppm): 11.03 (s, 1H), 7.21 (d, $J = 8$ Hz, 1H), 7.14 - 7.09 (m, 2H), 4.37-4.28 (m, 1H), 4.17 - 4.02 (m, 4H), 2.91 (br s, 2H), 2.23 - 2.10 (m, 2H), 1.68 (d, $J = 11$ Hz, 2H), 1.20 (t, $J = 7$ Hz, 3H); ^{13}C NMR (100.6 MHz, $\text{DMSO}-d_6$) δ (ppm): 154.6, 153.5, 129.9, 128.6, 122.9, 112.4, 111.4, 110.3, 60.8, 50.1, 43.0 (2C), 28.5 (2C), 14.6;

HRMS (TOF, ESI) C₁₅H₁₉N₃O₃Br [M+H]⁺ calculated 368.0610, found 368.0608; LC-MS: rt (min) = 2.460; LRMS (ESI) m/z = 368.0.

5-bromo-1-(piperidin-4-yl)-1*H*-benzo[*d*]imidazol-2(3*H*)-one (47). ethyl 4-(5-bromo-2-oxo-2,3-dihydro-1*H*-benzo[*d*]imidazol-1-yl)piperidine-1-carboxylate (6.0 g, 16.3 mmol) was dissolved in sodium hydroxide (30 mL, 2M) and subjected to microwave irradiation for 1.75 h at 130 degrees Celsius. The reaction mixture was diluted with water and then adjusted to pH 1 with hydrochloric acid (14 M). The reaction mixture was then carefully adjusted to pH 12 with solid sodium carbonate. The resulting precipitate was then filtered and dried under reduced pressure to afford a tan solid (4.27 g, 14.42 mmol, 88 %). ¹H NMR (400.1 MHz, DMSO-*d*₆) δ (ppm): 7.24 (d, *J* = 8 Hz, 1H), 7.15 - 7.09 (m, 2H), 4.25 - 4.14 (m, 1H), 3.36 (br s, 2H), 3.03 (d, *J* = 12 Hz, 2H), 2.59 - 2.51 (m, 2H), 2.19 - 2.06 (m, 2H), 1.56 (d, *J* = 10 Hz, 2H); ¹³C NMR (100.6 MHz, DMSO-*d*₆) δ (ppm): 153.5, 129.9, 128.5, 122.7, 112.2, 111.3, 110.5, 50.6, 45.8 (2C), 30.0 (2C); HRMS (TOF, ESI) C₁₂H₁₅N₃OBr [M+H]⁺ calculated 296.0398, found 296.0388; LC-MS: rt (min) = 1.605; LRMS (ESI) m/z = 298.0.

(*S*)-1-(1-(2-aminopropyl)piperidin-4-yl)-5-bromo-1*H*-benzo[*d*]imidazol-2(3*H*)-one dihydrochloride (49). (*S*)-*tert*-butyl (1-(4-(5-bromo-2-oxo-2,3-dihydro-1*H*-benzo[*d*]imidazol-1-yl)piperidin-1-yl)propan-2-yl)carbamate (3.77 g, 8.33 mmol) was dissolved in dichloromethane (35 mL) and a minimal amount of methanol added dropwise. Hydrochloric acid was added (4M in dioxane, 21 mL) and the reaction was stirred for approximately 16 hours at room temperature. The reaction was concentrated under reduced pressure to afford a white solid (3.06 g, 7.18 mmol, 86 %). ¹H NMR (400.1 MHz, DMSO-*d*₆) δ (ppm): 11.05 (s, 1H), 8.62 (s, 3H), 7.58 (d, *J* = 8 Hz, 1H), 7.16

- 7.10 (m, 2H), 4.67 - 4.52 (m, 1H), 3.98 - 3.78 (m 2H), 3.69 - 3.56 (m, 1H), 3.38 - 3.13 (m, 4H), 2.94 - 2.76 (m, 2H), 1.91 (d, $J = 12$ Hz, 2H), 1.35 (d, $J = 6$ Hz, 3H); ^{13}C NMR (100.6 MHz, DMSO- d_6) δ (ppm): 153.7, 130.5, 128.1, 123.1, 113.1, 112.1, 111.1, 59.6, 53.1, 52.1, 46.7, 42.9, 25.7, 25.5, 17.7; HRMS (TOF, ESI) $\text{C}_{15}\text{H}_{22}\text{N}_4\text{OBr}$ $[\text{M}+\text{H}]^+$ calculated 353.0977, found 353.0979; LC-MS: rt (min) = 1.480; LRMS (ESI) $m/z = 355.1$.

VU0359595.

trans-N-((S)-1-(4-(5-bromo-2-oxo-2,3-dihydro-1H

benzo[*d*]imidazol-1-yl)piperidin-1-yl)propan-2-yl)-2

phenylcyclopropanecarboxamide (41p). (*S*)-1-(1-(2-aminopropyl)piperidin-4-yl)-5-bromo-1*H*-benzo[*d*]imidazol-2(3*H*)-one dihydrochloride (2.95 g, 6.92 mmol), *trans*-2-phenylcyclopropanecarbonyl chloride (1.25 g, 6.92 mmol) and *N,N*-diisopropylethylamine (4.22 mL, 24.22 mmol) were all dissolved in *N,N*-dimethylformamide (30 mL) at 0 degrees Celsius. The reaction mixture was allowed to warm to room temperature and stirred for about 12 hours. The reaction mixture was diluted with water and extracted into dichloromethane 5 times. The dichloromethane layer was then washed 3 times with a solution of lithium chloride (3M) and dried under reduced pressure. The reaction mixture was chromatographed on a 120 g flash column eluting in a gradient of 0-10 % methanol in dichloromethane to afford a white solid (2.69 g, 5.4 mmol, 78 %). ^1H NMR (400.1 MHz, DMSO- d_6) δ (ppm): 11.02 (s, 1H), 7.94 (dd, $J = 3, 8$ Hz, 1H), 7.27 (t, $J = 8$ Hz, 2H), 7.19 - 7.05 (m, 6H), 4.15 - 4.04 (m, 1H), 4.01 - 3.92 (m, 1H), 2.99 - 2.91 (m, 2H), 2.39 - 2.17 (m, 5H), 2.15 - 2.03 (m, 2H), 1.90 - 1.83 (m, 1H), 1.67 - 1.56 (m, 2H), 1.39 - 1.31 (m, 1H), 1.22 - 1.14 (m, 1H), 1.07 (dd, $J = 2, 7$ Hz, 3H); ^{13}C NMR (100.6 MHz, DMSO- d_6) δ (ppm): 170.1, 153.5, 141.3, 129.9, 128.6,

128.3 (2C), 125.9, 125.8, 125.7, 122.8, 112.2, 111.3, 110.1, 63.0, 52.7, 50.4 (2C), 42.4, 28.6 (2C), 25.9, 23.7, 19.2, 15.1; HRMS (TOF, ESI) $C_{25}H_{30}N_4O_2Br$ $[M+H]^+$ calculated 497.1552, found 497.1545; LC-MS: rt (min) = 2.092; LRMS (ESI) m/z = 497.1.

1-benzyl-4-((3-fluorophenyl)amino)piperidine-4-carboxamide (67a). To a solution of 1-benzylpiperidin-4-one (13.25 g, 70 mmol) in glacial acetic acid (70 mL) and water (12 mL) cooled to 0 degrees Celsius was added 3-fluoroaniline (8.55 g, 77 mmol) and potassium cyanide (4.55 g, 70 mmol). The reaction was allowed to warm to room temperature and agitated for approximately 12 hours. The reaction was then cooled to 0 degrees Celsius and ammonium hydroxide (18 M) was added dropwise until the solution pH was 11 or greater. The mixture was then extracted into dichloromethane and dried under reduced pressure to yield the crude product as a tan oil (20.5 g). The crude product was then immediately cooled to 0 degrees Celsius and concentrated sulfuric acid (18 M, 120 mL) was added dropwise. The reaction was allowed to warm to room temperature and agitated for approximately 12 hours. The reaction was then cooled to 0 degrees Celsius and ammonium hydroxide (18 M) was added dropwise until the solution pH was 11 or greater. The mixture was then extracted into dichloromethane and dried under reduced pressure to afford a tan solid (15.78 g, 48.25 mmol, 68 %). 1H NMR (400.1 MHz, $CDCl_3$) δ (ppm): 7.51 - 7.37 (m, 7H), 6.67 - 6.47 (m, 4H), 4.27 (s, 1H), 3.64 (s, 2H), 2.95 - 2.87 (m, 2H), 2.53 - 2.44 (m, 2H), 2.29 - 2.21 (m, 2H), 2.07 (d, $J = 13$ Hz, 2H); ^{13}C NMR (100.6 MHz, $CDCl_3$) δ (ppm): 178.0, 162.6, 145.7, 138.3, 130.5, 129.1 (2C), 128.4 (2C), 127.2, 111.8, 106.1, 103.1, 63.1, 58.5, 48.7 (2C), 34.8, 31.5; HRMS (TOF, ESI) $C_{19}H_{23}N_3OF$ $[M+H]^+$ calculated 328.1825, found 328.1827; LC-MS: rt (min) = 1.855; LRMS (ESI) m/z = 328.2.

1-(3-fluorophenyl)-1,3,8-triazaspiro[4.5]decan-4-one (69a). 1-Benzyl-4-((3-fluorophenyl)amino)piperidine-4-carboxamide (15.78 g, 48.25 mmol), trimethyl orthoformate (80 mL), and glacial acetic acid (40 mL) were combined and subjected to microwave irradiation at 150 degrees Celsius for 15 minutes. The mixture was adjusted to pH 12 with ammonium hydroxide (18 M) and extracted into dichloromethane and dried under reduced pressure. This material was then added to a suspension of sodium borohydride (4.56 g, 120.6 mmol) in methanol (150 mL) and stirred for about 3 hours. The reaction was quenched with water, extracted into dichloromethane, and dried under reduced pressure. The material was then chromatographed on a 330 g flash column (Teledyne) as follows: (1) a gradient from 0-80 % ethyl acetate in hexanes over 10 minutes was run, and on the same column (2) a gradient from 0-10 % methanol in dichloromethane was run. The purity of the isolated intermediate compound was established via LCMS, rt (min) 1.723; LRMS (ESI) m/z = 340.1. This intermediate (1.94 g) was immediately dissolved in methanol (40 mL) and glacial acetic acid (10 mL), and treated with palladium on carbon (cat., 80 mg) under an atmosphere of hydrogen. After about 36 hours the reaction mixture was filtered through celite, concentrated under reduced pressure, diluted with water, made alkaline with saturated sodium bicarbonate and extracted 8 times into dichloromethane to afford a white solid (1.37 g, 5.49 mmol, 11 %). ¹H NMR (400.1 MHz, DMSO-*d*₆) δ (ppm): 8.67 (s, 1H), 7.20 (q, *J* = 8 Hz, 1H), 6.73 (d, *J* = 8 Hz, 1H), 6.62 (d, *J* = 13 Hz, 1H), 6.52 - 6.46 (m, 1H), 4.57 (s, 2H), 3.20 - 3.09 (m, 3H), 2.91 - 2.82 (m, 2H), 2.46 - 2.36 (m, 2H), 1.48 (d, *J* = 14 Hz, 2H); ¹³C NMR (100.6 MHz, DMSO-*d*₆) δ (ppm): 176.0, 164.3, 145.0, 130.1, 109.3, 103.1, 100.2, 58.8,

58.6, 42.1 (2C), 28.9 (2C); HRMS (TOF, ESI) C₁₃H₁₇N₃OF [M+H]⁺ calculated 250.1356, found 250.1351; LC-MS: rt (min) = 1.394; LRMS (ESI) m/z = 250.1.

8-(2-aminoethyl)-1-(3-fluorophenyl)-1,3,8-triazaspiro[4.5]decan-4-one

dihydrochloride (70a). 1-(3-fluorophenyl)-1,3,8-triazaspiro[4.5]decan-4-one (1370 mg, 5.49 mmol) and *tert*-butyl (2-oxoethyl)carbamate (961 mg, 6.03 mmol) were combined and dissolved in dichloromethane (25 mL) and methanol (10 mL) and stirred for about 30 minutes at room temperature. After about 30 minutes macroporous triacetoxyborohydride (3 g, 7.26 mmol) was added to the reaction and after 14 hours an additional amount of *tert*-butyl (2-oxoethyl)carbamate (200 mg, 1.25 mmol) was added to drive the reaction to completion. After about 24 hours the reaction mixture was filtered through celite and concentrated under reduced pressure. The crude compound was chromatographed on an 80 g flash column eluting in a gradient of 0-10 % methanol in dichloromethane to afford a white solid (1.64 g, 4.18 mmol, 76 %). ¹H NMR (400.1 MHz, DMSO-*d*₆) δ (ppm): 8.69 (s, 1H), 7.22 (q, *J* = 8 Hz, 1H), 6.72 - 6.63 (m, 2H), 6.60 - 6.49 (m, 2H), 4.58 (s, 2H), 2.83 - 2.75 (m, 2H), 2.74 - 2.65 (m, 2H), 2.61 - 2.48 (m, 2H), 2.42 - 2.35 (m, 2H), 1.91 (s, 2H), 1.55 (d, *J* = 13 Hz, 2H), 1.39 (s, 9H); ¹³C NMR (100.6 MHz, DMSO-*d*₆) δ (ppm): 175.8, 161.9, 155.6, 145.0, 130.4, 109.4, 103.2, 100.3, 77.5, 58.7, 58.1, 57.4, 49.3 (2C), 37.6, 28.3 (3C), 28.1 (2C); HRMS (TOF, ESI) C₂₀H₃₀N₄O₃F [M+H]⁺ calculated 393.2302, found 393.2301; LC-MS: rt (min) = 1.966; LRMS (ESI) m/z = 393.2. *tert*-butyl (2-(1-(3-fluorophenyl)-4-oxo-1,3,8-triazaspiro[4.5]decan-8-yl)ethyl)carbamate (1.64 g, 4.18 mmol) was dissolved in dichloromethane (40 mL) and a minimal amount of methanol added dropwise. Hydrochloric acid was added (4M in dioxane, 20 mL) and the reaction was stirred for

approximately 36 hours at room temperature. The reaction was concentrated under reduced pressure to afford a white solid (1.34 g, 3.66 mmol, 88 %). ^1H NMR (400.1 MHz, $\text{DMSO-}d_6$) δ (ppm): 9.12 (s, 1H), 8.47 (s, 2H), 7.18 (q, $J = 8$ Hz, 1H), 7.07 - 7.02 (m, 1H), 6.79 - 6.72 (m, 1H), 6.57 - 6.50 (m, 1H), 4.63 (s, 2H), 3.72 - 3.56 (m, 4H), 3.45 - 3.38 (m, 4H), 3.10 - 3.00 (m, 2H), 1.90 (d, $J = 15$ Hz, 2H); ^{13}C NMR (100.6 MHz, $\text{DMSO-}d_6$) δ (ppm): 174.4, 162.3, 144.4, 130.3, 109.8, 103.8, 100.2, 69.0, 56.5, 53.3, 49.1 (2C), 33.8, 25.6 (2C); HRMS (TOF, ESI) $\text{C}_{15}\text{H}_{22}\text{N}_4\text{OF}$ $[\text{M}+\text{H}]^+$ calculated 293.1778, found 293.1776; LC-MS: rt (min) = 1.405; LRMS (ESI) $m/z = 293.1$.

VU0364739. *N*-(2-(1-(3-fluorophenyl)-4-oxo-1,3,8-triazaspiro[4.5]decan-8-yl)ethyl)-2-naphthamide (71a). 8-(2-aminoethyl)-1-(3-fluorophenyl)-1,3,8-triazaspiro[4.5]decan-4-one dihydrochloride **70a** (1.23 g, 3.37 mmol), 2-naphthoyl chloride (641 mg, 3.37 mmol) and *N,N*-diisopropylethylamine (2.05 mL, 11.7 mmol) were all dissolved in *N,N*-dimethylformamide (20 mL) at 0 degrees Celsius. The reaction mixture was allowed to warm to room temperature and stirred for about 12 hours. The reaction mixture was diluted with water and extracted into dichloromethane 5 times. The dichloromethane layer was then washed 3 times with a solution of lithium chloride (3M) and dried under reduced pressure. The reaction mixture was chromatographed on an 80 g flash column eluting in 0-5 % methanol in dichloromethane to afford a white solid (1.25 g, 2.80 mmol, 83 %). ^1H NMR (400.1 MHz, $\text{DMSO-}d_6$) δ (ppm): 8.69 (s, 1H), 8.60 (t, $J = 5$ Hz, 1H), 8.45 (s, 1H), 8.04 - 7.92 (m, 4H), 7.64 - 7.56 (m, 2H), 7.11 (q, $J = 8$ Hz, 1H), 6.68 - 6.63 (m, 1H), 6.58 - 6.52 (m, 1H), 6.49 - 6.43 (m, 1H), 4.58 (s, 2H), 3.48 (q, $J = 6$ Hz, 2H), 2.91 - 2.83 (m, 2H), 2.80 - 2.72 (m, 2H), 2.64 - 2.53 (m, 4H), 1.58 (d, $J = 14$ Hz, 2H); ^{13}C NMR (100.6 MHz, $\text{DMSO-}d_6$) δ (ppm): 175.9, 166.2, 164.3, 161.9, 145.0,

134.1, 132.2, 130.3, 128.8, 127.8, 127.6, 127.5, 127.3, 126.7, 124.1, 109.3, 103.3, 100.3, 58.7, 58.1, 56.9, 49.4 (2C), 37.3, 28.2 (2C); HRMS (TOF, ESI) C₂₆H₂₈N₄O₂F [M+H]⁺ calculated 447.2196, found 447.2195; LC-MS: rt (min) = 2.287; LRMS (ESI) m/z = 447.2. Analogs **22b-d** were made following the same protocol starting from **21a** and were purified via reversed-phase chromatography to greater than 95% purity (as trifluoroacetate salts) as analyzed by ELSD and UV at both 214 and 254 nm.

***N*-(2-(1-(3-fluorophenyl)-4-oxo-1,3,8-triazaspiro[4.5]decan-8-yl)ethyl)-2-naphthamide hydrochloride (71a-HCl).** *N*-(2-(1-(3-fluorophenyl)-4-oxo-1,3,8-triazaspiro[4.5]decan-8-yl)ethyl)-2-naphthamide **71a** (1.25 mg, 2.80 mmol) was stirred in methanol (30 mL) at room temperature and treated with hydrochloric acid (4M in dioxane, 4 mL). After about 25 minutes the compound was dried under reduced pressure to afford a white solid (1.31 g, 2.72 mmol, 97 %). ¹H NMR (400.1 MHz, DMSO-*d*₆) δ (ppm): 10.99 (s, 1H), 9.14 (t, *J* = 5 Hz, 1H), 9.11 (s, 1H), 8.60 (s, 1H), 8.06 - 7.97 (m, 4H), 7.65 - 7.57 (m, 2H), 7.21 (q, *J* = 8 Hz, 1H), 7.05 - 7.01 (m, 1H), 6.83 - 6.77 (m, 1H), 6.58 - 6.52 (m, 1H), 4.64 (s, 2H), 3.85 - 3.75 (m, 2H), 3.74 - 3.64 (m, 4H), 3.41-3.36 (m, 2H), 3.11 - 2.99 (m, 2H), 1.92 (d, *J* = 14 Hz, 2H); ¹³C NMR (100.6 MHz, DMSO-*d*₆) δ (ppm): 174.4, 166.6, 164.6, 162.2, 144.6, 134.3, 132.1, 131.2, 130.5, 128.9, 127.9, 127.8, 127.6, 126.8, 124.2, 109.9, 104.0, 100.3, 59.0, 56.6, 55.7, 48.7 (2C), 34.4, 25.7 (2C); HRMS (TOF, ESI) C₂₆H₂₈N₄O₂F [M+H]⁺ calculated 447.2196, found 447.2186; LC-MS: rt (min) = 2.264; LRMS (ESI) m/z = 447.2.

8-(2-aminoethyl)-1-(3-chlorophenyl)-1,3,8-triazaspiro[4.5]decan-4-one dihydrochloride (70b). 1-(3-chlorophenyl)-1,3,8-triazaspiro[4.5]decan-4-one **69b** (127 mg, 0.47 mmol) and *tert*-butyl (2-oxoethyl)carbamate (83.8 mg, 0.51 mmol) were

combined and dissolved in dichloromethane (1.5 mL) and methanol (0.05 mL) and stirred for about 30 minutes at room temperature. After about 30 minutes macroporous triacetoxyborohydride (600 mg, 1.4 mmol) was added to the reaction and after 14 hours an additional amount of *tert*-butyl (2-oxoethyl)carbamate (41.9 mg, 0.25 mmol) was added to drive the reaction to completion. After about 24 hours the reaction mixture was filtered through celite and concentrated under reduced pressure. The crude compound was chromatographed on a 12 g flash column eluting in a gradient of 0-10 % methanol in dichloromethane to afford a white solid (72 mg, 0.18 mmol, 37 %). ¹H NMR (400.1 MHz, MeOD) δ (ppm): 7.21 (t, *J* = 9 Hz, 1H), 6.95 - 6.90 (m, 2H), 6.86 - 6.78 (m, 1H), 4.69 (s, 2H), 3.23 - 3.02 (m, 4H), 2.81 - 2.67 (m, 4H), 1.97 (s, 2H), 1.78 (d, *J* = 14 Hz, 2H), 1.45 (s, 9H); ¹³C NMR (100.6 MHz, MeOD) δ (ppm): 178.2, 158.5, 145.8, 136.2, 141.3, 119.5, 115.4, 114.2, 80.3, 60.4, 60.1, 58.4, 50.7 (2C), 38.1, 29.2 (2C), 28.7 (3C); HRMS (TOF, ESI) C₂₀H₃₀N₄O₃Cl [M+H]⁺ calculated 409.2006, found 409.1996; LC-MS: rt (min) = 1.984; LRMS (ESI) *m/z* = 409.2. *tert*-butyl (2-(1-(3-chlorophenyl)-4-oxo-1,3,8-triazaspiro[4.5]decan-8-yl)ethyl)carbamate (72 mg, 0.17 mmol) was dissolved in dichloromethane (5 mL) and a minimal amount of methanol added dropwise. Hydrochloric acid was added (4M in dioxane, 1.0 mL) and the reaction was stirred for approximately 16 hours at room temperature. The reaction was concentrated under reduced pressure to afford a white solid (60 mg, 0.16 mmol, 93 %). ¹H NMR (400.1 MHz, MeOD) δ (ppm): 7.25 (t, *J* = 8 Hz, 1H), 7.20 - 7.15 (m, 1H), 6.88 - 6.81 (m, 2H), 4.74 (s, 2H), 3.96 - 3.86 (m, 2H), 3.73 - 3.65 (m, 2H), 3.51 (s, 4H), 3.20 - 3.10 (m, 2H), 2.05 (d, *J* = 15 Hz, 2H); ¹³C NMR (100.6 MHz, MeOD) δ (ppm): 176.9, 145.2, 135.6, 131.5, 119.9, 115.1, 114.4, 60.5, 58.4, 54.9, 51.2 (2C), 35.4, 27.8 (2C); HRMS (TOF,

ESI) C₁₅H₂₂N₄OCl [M+H]⁺ calculated 309.1482, found 308.1480; LC-MS: rt (min) = 1.413; LRMS (ESI) m/z = 309.1.

***N*-(2-(1-(3-chlorophenyl)-4-oxo-1,3,8-triazaspiro[4.5]decan-8-yl)ethyl)-2-naphthamide 2,2,2-trifluoroacetate (72a).** 8-(2-aminoethyl)-1-(3-chlorophenyl)-1,3,8-triazaspiro[4.5]decan-4-one dihydrochloride **70b** (60 mg, 0.15 mmol), 2-naphthoyl chloride (30.0 mg, 0.15 mmol) and *N,N*-diisopropylethylamine (0.115 mL, 0.66 mmol) were all dissolved in *N,N*-dimethylformamide (1 mL) at 0 degrees Celsius. The reaction mixture was allowed to warm to room temperature and stirred for about 12 hours. The reaction mixture was diluted with water and extracted into dichloromethane 5 times. The dichloromethane layer was then washed 3 times with a solution of lithium chloride (3M) and dried under reduced pressure. The reaction mixture was subjected to reversed-phase chromatography to afford a white solid (43.4 mg, 0.075 mmol, 50 %). ¹H NMR (400.1 MHz, DMSO-*d*₆) δ (ppm): 9.32 (s, 1H), 9.13 (s, 1H), 9.01 (t, *J* = 5 Hz, 1H), 8.50 (s, 1H), 8.06 - 7.94 (m, 4H), 7.66 - 7.58 (m, 2H), 7.22 (t, *J* = 8 Hz, 1H), 6.98 - 6.94 (m, 1H), 6.86 - 6.80 (m, 2H), 4.65 (s, 2H), 3.79 - 3.68 (m, 6H), 3.44 - 3.39 (m, 2H), 2.88 - 2.75 (m, 2H), 1.97 (d, *J* = 15 Hz, 2H); ¹³C NMR (100.6 MHz, DMSO-*d*₆) δ (ppm): 174.3, 167.0, 158.6, 144.2, 134.3, 134.2, 132.1, 131.2, 130.4, 128.9 (2C), 128.0, 127.8, 127.7 (2C), 126.9, 124.1, 117.7, 113.2, 112.5, 59.0, 56.6, 55.3, 48.9 (2C), 34.6, 26.0 (2C); HRMS (TOF, ESI) C₂₆H₂₈N₄O₂Cl [M+H]⁺ calculated 463.1901, found 463.1894; LC-MS: rt (min) = 2.266; LRMS (ESI) m/z = 463.1. Analogs **72b-d** were made following the same protocol starting from **70b** and were purified via reversed-phase chromatography to greater than 95% purity (as trifluoroacetate salts) as analyzed by ELSD and UV at both 214 and 254 nM.

8-(2-aminoethyl)-1-(3,4-difluorophenyl)-1,3,8-triazaspiro[4.5]decan-4-one dihydrochloride (70c). 1-(3,4-difluorophenyl)-1,3,8-triazaspiro[4.5]decan-4-one (100 mg, 0.37 mmol) and *tert*-butyl (2-oxoethyl)carbamate (65.5 mg, 0.41 mmol) were combined and dissolved in dichloromethane (1.5 mL) and methanol (0.05 mL) and stirred for about 30 minutes at room temperature. After about 30 minutes macroporous triacetoxylborohydride (600 mg, 1.4 mmol) was added to the reaction and after 14 hours an additional amount of *tert*-butyl (2-oxoethyl)carbamate (32.75 mg, 0.21 mmol) was added to drive the reaction to completion. After about 24 hours the reaction mixture was filtered through celite and concentrated under reduced pressure. The crude compound was chromatographed on a 12 g flash column eluting in a gradient of 0-10 % methanol in dichloromethane to afford a white solid (67 mg, 0.16 mmol, 44 %). ¹H NMR (400.1 MHz, MeOD) δ (ppm): 7.15 (q, *J* = 10 Hz, 1H), 6.99 - 6.92 (m, 1H), 6.76 - 6.70 (m, 1H), 4.67 (s, 2H), 3.30 - 3.25 (m, 2H) 3.24 - 3.13 (m, 2H), 2.87 - 2.76 (m, 2H), 2.72 - 2.60 (m, 2H), 1.97 (s, 2H), 1.83 (d, *J* = 14 Hz, 2H), 1.45 (s, 9H); ¹³C NMR (100.6 MHz, MeOD) δ (ppm): 177.9, 158.4, 152.9, 150.4, 141.6, 118.4, 113.0, 106.1, 80.4, 60.8, 59.9, 58.2, 50.5 (2C), 37.6, 29.0 (2C), 28.7 (3C); HRMS (TOF, ESI) C₂₀H₂₉N₄O₃F₂ [M+H]⁺ calculated 411.2208, found 411.2209; LC-MS: rt (min) = 1.942; LRMS (ESI) *m/z* = 411.2. *tert*-butyl (2-(1-(3,4-difluorophenyl)-4-oxo-1,3,8-triazaspiro[4.5]decan-8-yl)ethyl)carbamate (67 mg, 0.16 mmol) was dissolved in dichloromethane (5 mL) and a minimal amount of methanol added dropwise. Hydrochloric acid was added (4M in dioxane, 1.0 mL) and the reaction was stirred for approximately 16 hours at room temperature. The reaction was concentrated under reduced pressure to afford a white solid (58 mg, 0.15 mmol, 95 %). ¹H NMR (400.1 MHz, DMSO-*d*₆) δ (ppm): 9.12 (s, 1H), 8.50 (br s, 2H), 7.18 (q, *J* =

10 Hz, 1H), 7.11 - 7.03 (m, 1H), 7.00 - 6.94 (m, 1H), 4.60 (s, 2H), 3.69 - 3.57 (m, 4H), 3.45 - 3.38 (m, 4H), 3.02 - 2.91 (m, 2H), 1.90 (d, $J = 15$ Hz, 2H); ^{13}C NMR (100.6 MHz, DMSO- d_6) δ (ppm): 174.4, 151.2, 149.1, 139.9, 117.4, 110.2, 103.1, 59.2, 56.5, 53.2, 49.0 (2C), 33.7, 25.6 (2C); HRMS (TOF, ESI) $\text{C}_{15}\text{H}_{21}\text{N}_4\text{OF}_2$ $[\text{M}+\text{H}]^+$ calculated 311.1683, found 311.1681; LC-MS: rt (min) = 1.334; LRMS (ESI) $m/z = 311.1$.

***N*-(2-(1-(3,4-difluorophenyl)-4-oxo-1,3,8-triazaspiro[4.5]decan-8-yl)ethyl)-2-naphthamide 2,2,2-trifluoroacetate (73a).** 8-(2-aminoethyl)-1-(3,4-difluorophenyl)-1,3,8-triazaspiro[4.5]decan-4-one dihydrochloride (46 mg, 0.12 mmol), 2-naphthoyl chloride (22.8 mg, 0.12 mmol) and *N,N*-diisopropylethylamine (0.091 mL, 0.52 mmol) were all dissolved in *N,N*-dimethylformamide (1 mL) at 0 degrees Celsius. The reaction mixture was allowed to warm to room temperature and stirred for about 12 hours. The reaction mixture was diluted with water and extracted into dichloromethane 5 times. The dichloromethane layer was then washed 3 times with a solution of lithium chloride (3M) and dried under reduced pressure. The reaction mixture was subjected to reversed-phase chromatography to afford a white solid (26 mg, 0.04 mmol, 37 %). ^1H NMR (400.1 MHz, DMSO- d_6) δ (ppm): 9.85 (s, 1H), 9.10 (s, 1H), 9.00 (t, $J = 5$ Hz, 1H), 8.49 (s, 1H), 8.06 - 7.94 (m, 4H), 7.66 - 7.58 (m, 2H), 7.28 (q, $J = 10$ Hz, 1H), 7.04 - 6.96 (m, 1H), 6.75-6.69 (m, 1H), 4.61 (s, 2H), 3.77 - 3.65 (m, 6H), 3.44 - 3.38 (m, 2H), 2.76 - 2.64 (m, 2H), 1.97 (d, $J = 14$ Hz, 2H); ^{13}C NMR (100.6 MHz, DMSO- d_6) δ (ppm): 174.4, 167.0, 158.5, 148.7, 140.2, 134.3, 132.1, 131.2, 128.9, 128.0, 127.8, 127.7 (2C), 126.9, 124.1, 117.7, 117.5, 110.6, 103.8, 103.6, 59.2, 56.6, 55.2, 49.0 (2C), 34.6, 26.0 (2C); HRMS (TOF, ESI) $\text{C}_{26}\text{H}_{27}\text{N}_4\text{O}_2\text{F}_2$ $[\text{M}+\text{H}]^+$ calculated 465.2102, found 465.2102; LC-MS: rt (min) = 2.230; LRMS (ESI) $m/z = 465.2$. Analogs **73b-d** were made following the same protocol

starting from **70c** and were purified via reversed-phase chromatography to greater than 95% purity (as trifluoroacetate salts) as analyzed by ELSD and UV at both 214 and 254 nM.

8-(2-aminoethyl)-1-(4-fluorophenyl)-1,3,8-triazaspiro[4.5]decan-4-one

dihydrochloride (70d). 1-(4-fluorophenyl)-1,3,8-triazaspiro[4.5]decan-4-one **69d** (54.8 mg, 0.22 mmol) and *tert*-butyl (2-oxoethyl)carbamate (38.2 mg, 0.24 mmol) were combined and dissolved in dichloromethane (1.5 mL) and methanol (0.05 mL) and stirred for about 30 minutes at room temperature. After about 30 minutes macroporous triacetoxylborohydride (600 mg, 1.4 mmol) was added to the reaction and after 14 hours an additional amount of *tert*-butyl (2-oxoethyl)carbamate (19.1 mg, 0.12 mmol) was added to drive the reaction to completion. After about 24 hours the reaction mixture was filtered through celite and concentrated under reduced pressure. The crude compound was chromatographed on a 12 g flash column eluting in a gradient of 0-10 % methanol in dichloromethane to afford a white solid (41 mg, 0.10 mmol, 47 %). ¹H NMR (400.1 MHz, MeOD) δ (ppm): 7.10 - 7.02 (m, 4H), 4.67 (s, 2H), 3.28 - 3.24 (m, 2H), 3.20 - 3.12 (m, 2H) 2.86 - 2.80 (m, 2H), 2.44 - 2.37 (m, 2H), 1.95 (s, 2H), 1.88 (d, *J* = 14 Hz, 2H), 1.44 (s, 9H); ¹³C NMR (100.6 MHz, MeOD) δ (ppm): 178.4, 160.7, 158.4, 140.8, 122.3, 122.2, 116.7, 116.5, 80.4, 61.2, 60.1, 58.1, 50.6 (2C), 37.5, 29.5 (2C), 28.7 (3C); HRMS (TOF, ESI) C₂₀H₃₀N₄O₃F [M+H]⁺ calculated 393.2302, found 393.2300; LC-MS: rt (min) = 1.850; LRMS (ESI) *m/z* = 393.2. *tert*-butyl (2-(1-(4-fluorophenyl)-4-oxo-1,3,8-triazaspiro[4.5]decan-8-yl)ethyl)carbamate (41 mg, 0.10 mmol) was dissolved in dichloromethane (5 mL) and a minimal amount of methanol added dropwise. Hydrochloric acid was added (4M in dioxane, 0.5 mL) and the reaction was stirred for

approximately 16 hours at room temperature. The reaction was concentrated under reduced pressure to afford a white solid (34 mg, 0.093 mmol, 93 %). ^1H NMR (400.1 MHz, MeOD) δ (ppm): 7.16 - 7.08 (m, 2H), 7.08 - 7.00 (m, 2H), 4.72 (s, 2H), 3.92 - 3.81 (m, 2H), 3.72 - 3.63 (m, 2H), 3.50 (s, 4H), 2.93-2.81 (m, 2H), 2.05 (d, J = 15 Hz, 2H); ^{13}C NMR (100.6 MHz, MeOD) δ (ppm): 177.3, 160.3, 140.1, 120.5, 120.4, 116.9, 116.7, 61.1, 58.6, 54.9, 51.3 (2C), 35.4, 28.5 (2C); HRMS (TOF, ESI) $\text{C}_{15}\text{H}_{22}\text{N}_4\text{OF}$ $[\text{M}+\text{H}]^+$ calculated 293.1778, found 293.1769; LC-MS: rt (min) = 1.260; LRMS (ESI) m/z = 293.2.

***N*-(2-(1-(4-fluorophenyl)-4-oxo-1,3,8-triazaspiro[4.5]decan-8-yl)ethyl)-2-naphthamide 2,2,2-trifluoroacetate (74a).** 8-(2-aminoethyl)-1-(4-fluorophenyl)-1,3,8-triazaspiro[4.5]decan-4-one dihydrochloride (34 mg, 0.09 mmol), 2-naphthoyl chloride (17.8 mg, 0.09 mmol) and *N,N*-diisopropylethylamine (0.067 mL, 0.385 mmol) were all dissolved in *N,N*-dimethylformamide (1 mL) at 0 degrees Celsius. The reaction mixture was allowed to warm to room temperature and stirred for about 12 hours. The reaction mixture was diluted with water and extracted into dichloromethane 5 times. The dichloromethane layer was then washed 3 times with a solution of lithium chloride (3M) and dried under reduced pressure. The reaction mixture was subjected to reversed-phase chromatography to afford a white solid (25.8 mg, 0.04 mmol, 51 %). ^1H NMR (400.1 MHz, $\text{DMSO}-d_6$) δ (ppm): 9.92 (s, 1H), 9.02 (s, 1H), 8.97 (t, J = 5 Hz, 1H), 8.48 (s, 1H), 8.06 - 7.94 (m, 4H), 7.66 - 7.58 (m, 2H), 7.09 (t, J = 9 Hz, 2H), 7.03 - 6.97 (m, 2H), 4.61 (s, 2H), 3.76 - 3.63 (m, 6H), 3.38 - 3.34 (m, 2H), 2.63 - 2.51 (m, 2H), 1.97 (d, J = 14 Hz, 2H); ^{13}C NMR (100.6 MHz, $\text{DMSO}-d_6$) δ (ppm): 174.7, 166.9, 157.6, 155.3, 139.3, 134.3, 132.1, 131.2, 128.9 (2C), 128.0, 127.8, 127.7 (2C), 126.9, 124.1, 118.2, 118.1,

115.7, 115.5, 59.2, 56.7, 55.3, 50.0 (2C), 34.6, 26.5 (2C); HRMS (TOF, ESI) $C_{26}H_{28}N_4O_2F$ $[M+H]^+$ calculated 447.2196, found 447.2196; LC-MS: rt (min) = 2.140; LRMS (ESI) m/z = 447.2. Analogs **74b-d** were made following the same protocol starting from **70d** and were purified via reversed-phase chromatography to greater than 95% purity (as trifluoroacetate salts) as analyzed by ELSD and UV at both 214 and 254 nM.

8-(2-aminoethyl)-1-(4-chlorophenyl)-1,3,8-triazaspiro[4.5]decan-4-one

dihydrochloride (70e). 1-(4-chlorophenyl)-1,3,8-triazaspiro[4.5]decan-4-one **69e** (152 mg, 0.57 mmol) and *tert*-butyl (2-oxoethyl)carbamate (100 mg, 0.63 mmol) were combined and dissolved in dichloromethane (1.5 mL) and methanol (0.05 mL) and stirred for about 30 minutes at room temperature. After about 30 minutes macroporous triacetoxymethylborohydride (600 mg, 1.4 mmol) was added to the reaction and after 14 hours an additional amount of *tert*-butyl (2-oxoethyl)carbamate (76 mg, 0.32 mmol) was added to drive the reaction to completion. After about 24 hours the reaction mixture was filtered through celite and concentrated under reduced pressure. The crude compound was chromatographed on a 12 g flash column eluting in a gradient of 0-10 % methanol in dichloromethane to afford a white solid (108 mg, 0.26 mmol, 46 %). 1H NMR (400.1 MHz, MeOD) δ (ppm): 7.23 (d, J = 9 Hz, 2H), 6.96 (d, J = 9 Hz, 2H), 4.69 (s, 2H), 3.39 - 3.32 (m, 2H), 3.26 - 3.17 (m, 2H), 2.90 - 2.83 (m, 2H), 2.78 - 2.67 (m, 2H), 1.97 (s, 2H), 1.84 (d, J = 14 Hz, 2H), 1.45 (s, 9H); ^{13}C NMR (100.6 MHz, MeOD) δ (ppm): 178.0, 158.5, 143.1, 130.1 (2C), 125.4, 118.1 (2C), 80.5, 60.6, 59.6, 58.2, 50.6 (2C), 37.6, 28.8 (2C), 28.7 (3C); HRMS (TOF, ESI) $C_{20}H_{30}N_4O_3Cl$ $[M+H]^+$ calculated 409.2006, found 409.2006; LC-MS: rt (min) = 2.002; LRMS (ESI) m/z = 409.2. *tert*-butyl (2-(1-(4-

chlorophenyl)-4-oxo-1,3,8-triazaspiro[4.5]decan-8-yl)ethyl)carbamate (108 mg, 0.26 mmol) was dissolved in dichloromethane (5 mL) and a minimal amount of methanol added dropwise. Hydrochloric acid was added (4M in dioxane, 1.5 mL) and the reaction was stirred for approximately 16 hours at room temperature. The reaction was concentrated under reduced pressure to afford a white solid (94 mg, 0.25 mmol, 95 %). ¹H NMR (400.1 MHz, MeOD) δ (ppm): 7.25 (d, *J* = 9 Hz, 2H), 7.06 (d, *J* = 9 Hz, 2H), 4.73 (s, 2H), 3.95 - 3.85 (m, 2H), 3.72 - 3.64 (m, 2H), 3.51 (s, 4H), 3.19 - 3.08 (m, 2H), 2.03 (d, *J* = 15 Hz, 2H); ¹³C NMR (100.6 MHz, MeOD) δ (ppm): 177.1, 142.5, 130.3 (2C), 125.3, 117.5 (2C), 60.6, 58.4, 55.0, 51.3 (2C), 35.5, 27.8 (2C); HRMS (TOF, ESI) C₁₅H₂₂N₄OCl [M+H]⁺ calculated 309.1482, found 309.1479; LC-MS: rt (min) = 1.420; LRMS (ESI) m/z = 309.1.

***N*-(2-(1-(4-chlorophenyl)-4-oxo-1,3,8-triazaspiro[4.5]decan-8-yl)ethyl)-2-naphthamide 2,2,2-trifluoroacetate (75a).** 8-(2-aminoethyl)-1-(4-chlorophenyl)-1,3,8-triazaspiro[4.5]decan-4-one dihydrochloride **70e** (94 mg, 0.24 mmol), 2-naphthoyl chloride (47.1 mg, 0.24 mmol) and *N,N*-diisopropylethylamine (0.182 mL, 1.05 mmol) were all dissolved in *N,N*-dimethylformamide (1 mL) at 0 degrees Celsius. The reaction mixture was allowed to warm to room temperature and stirred for about 12 hours. The reaction mixture was diluted with water and extracted into dichloromethane 5 times. The dichloromethane layer was then washed 3 times with a solution of lithium chloride (3M) and dried under reduced pressure. The reaction mixture was subjected to reversed-phase chromatography to afford a white solid (62.9 mg, 0.11 mmol, 45 %). ¹H NMR (400.1 MHz, DMSO-*d*₆) δ (ppm): 10.24 (s, 1H), 9.10 (s, 1H), 9.01 (t, *J* = 5 Hz, 1H), 8.49 (s, 1H), 8.06 - 7.94 (m, 4H), 7.65 - 7.57 (m, 2 H), 7.23 (d, *J* = 9 Hz, 2H), 6.94 (d, *J* = 9 Hz,

2H), 4.63 (s, 2H), 3.78 - 3.65 (m, 6H), 3.40 - 3.33 (m, 2H), 2.85 - 2.72 (m, 2H), 1.96 (d, $J = 14$ Hz, 2H); ^{13}C NMR (100.6 MHz, DMSO- d_6) δ (ppm): 174.5, 166.9, 158.9, 141.7, 134.3, 132.1, 131.2, 128.9 (2C), 128.7 (2C), 128.0 (2C), 127.8, 127.7 (2C), 126.8, 124.1, 122.1, 115.7, 59.0, 56.5, 55.2, 48.9 (2C), 34.6, 26.0 (2C); HRMS (TOF, ESI) HRMS (TOF, ESI) $\text{C}_{26}\text{H}_{28}\text{N}_4\text{O}_2\text{Cl}$ $[\text{M}+\text{H}]^+$ calculated 463.1901, found 463.1897; LC-MS: rt (min) = 2.249; LRMS (ESI) $m/z = 463.2$. Analogs **75b-d** were made following the same protocol starting from **70e** and were purified via reversed-phase chromatography to greater than 95% purity (as trifluoroacetate salts) as analyzed by ELSD and UV at both 214 and 254 nm.

8-(2-aminoethyl)-1-(4-bromophenyl)-1,3,8-triazaspiro[4.5]decan-4-one

dihydrochloride (70f). 1-(4-bromophenyl)-1,3,8-triazaspiro[4.5]decan-4-one **69f** (177 mg, 0.57 mmol) and *tert*-butyl (2-oxoethyl)carbamate (100 mg, 0.63 mmol) were combined and dissolved in dichloromethane (1.5 mL) and methanol (0.05 mL) and stirred for about 30 minutes at room temperature. After about 30 minutes macroporous triacetoxyborohydride (600 mg, 1.4 mmol) was added to the reaction and after 14 hours an additional amount of *tert*-butyl (2-oxoethyl)carbamate (76 mg, 0.32 mmol) was added to drive the reaction to completion. After about 24 hours the reaction mixture was filtered through celite and concentrated under reduced pressure. The crude compound was chromatographed on a 12 g flash column eluting in a gradient of 0-10 % methanol in dichloromethane to afford a white solid (163 mg, 0.36 mmol, 63 %). ^1H NMR (400.1 MHz, MeOD) δ (ppm): 7.35 (d, $J = 9$ Hz, 2H), 6.90 (d, $J = 9$ Hz, 2H), 4.68 (s, 2H), 3.29 - 3.21 (m, 2H), 3.20 - 3.10 (m, 2H), 2.86 - 2.68 (m, 4H), 1.97 (s, 2H), 1.80 (d, $J = 14$ Hz, 2H), 1.45 (s, 9H); ^{13}C NMR (100.6 MHz, MeOD) δ (ppm): 176.2, 155.6, 143.4, 129.0

(2C), 117.6, 114.3 (2C), 77.5, 58.6, 58.2, 57.4, 49.3 (2C), 37.7, 28.3 (2C), 28.3 (3C); HRMS (TOF, ESI) C₂₀H₃₀N₄O₃Br [M+H]⁺ calculated 453.1501, found 453.1504; LC-MS: rt (min) = 2.048; LRMS (ESI) m/z = 455.1. *tert*-butyl (2-(1-(4-bromophenyl)-4-oxo-1,3,8-triazaspiro[4.5]decan-8-yl)ethyl)carbamate (163 mg, 0.35 mmol) was dissolved in dichloromethane (5 mL) and a minimal amount of methanol added dropwise. Hydrochloric acid was added (4M in dioxane, 1.5 mL) and the reaction was stirred for approximately 16 hours at room temperature. The reaction was concentrated under reduced pressure to afford a white solid (140 mg, 0.33 mmol, 94 %). ¹H NMR (400.1 MHz, DMSO-*d*₆) δ (ppm): 9.09 (s, 1H), 8.48 (br s, 2H), 7.29 (d, *J* = 9 Hz, 2H), 7.09 (d, *J* = 9 Hz, 2H), 4.61 (s, 2H), 3.71 - 3.58 (m, 4H), 3.47 - 3.38 (m, 4H), 3.09 - 2.97 (m, 2H), 1.89 (d, *J* = 14 Hz, 2H); ¹³C NMR (100.6 MHz, DMSO-*d*₆) δ (ppm): 174.5, 141.8, 131.5 (2C), 115.9 (2C), 109.1, 58.9, 56.4, 53.3, 49.2 (2C), 33.7, 25.5 (2C); HRMS (TOF, ESI) C₁₅H₂₂N₄OBr [M+H]⁺ calculated 353.0977, found 353.0977; LC-MS: rt (min) = 1.467; LRMS (ESI) m/z = 353.1.

***N*-(2-(1-(4-bromophenyl)-4-oxo-1,3,8-triazaspiro[4.5]decan-8-yl)ethyl)-2-naphthamide 2,2,2-trifluoroacetate (76a).** 8-(2-aminoethyl)-1-(4-bromophenyl)-1,3,8-triazaspiro[4.5]decan-4-one dihydrochloride **70f** (66 mg, 0.15 mmol), 2-naphthoyl chloride (29.5 mg, 0.15 mmol) and *N,N*-diisopropylethylamine (0.126 mL, 0.73 mmol) were all dissolved in *N,N*-dimethylformamide (1 mL) at 0 degrees Celsius. The reaction mixture was allowed to warm to room temperature and stirred for about 12 hours. The reaction mixture was diluted with water and extracted into dichloromethane 5 times. The dichloromethane layer was then washed 3 times with a solution of lithium chloride (3M) and dried under reduced pressure. The reaction mixture was subjected to reversed-phase

chromatography to afford a white solid (66.1 mg, 0.11 mmol, 71 %). ¹H NMR (400.1 MHz, DMSO-*d*₆) δ (ppm): 10.23 (s, 1H), 9.10 (s, 1H), 9.00 (t, *J* = 5 Hz, 1H), 8.49 (s, 1H), 8.06 - 7.93 (m, 4H), 7.65 - 7.58 (m, 2H), 7.34 (d, *J* = 9 Hz, 2H), 6.89 (d, *J* = 9 Hz, 2H), 4.62 (s, 2H), 3.78 - 3.66 (m, 6H), 3.46 - 3.40 (m, 2H), 2.86 - 2.74 (m, 2H), 1.95 (d, *J* = 14 Hz, 2H); ¹³C NMR (100.6 MHz, DMSO-*d*₆) δ (ppm): 174.5, 166.9, 158.9, 142.1, 134.3, 132.1, 131.6 (2C), 131.2, 128.9 (2C), 128.0 (2C), 127.8, 127.7 (2C), 126.8, 124.1, 116.1, 109.6, 58.9, 56.5, 55.2, 48.9 (2C), 34.6, 25.9 (2C); HRMS (TOF, ESI) HRMS (TOF, ESI) C₂₆H₂₈N₄O₂Br [M+H]⁺ calculated 507.1396, found 507.1393; LC-MS: rt (min) = 2.279; LRMS (ESI) *m/z* = 507.1. Analogs **76b-d** were made following the same protocol starting from **70f** and were purified via reversed-phase chromatography to greater than 95% purity (as trifluoroacetate salts) as analyzed by ELSD and UV at both 214 and 254 nM.

***N*-(2-(4-oxo-1-phenyl-1,3,8-triazaspiro[4.5]decan-8-yl)ethyl)-2-naphthamide 2,2,2-trifluoroacetate (63a).** 8-(2-aminoethyl)-1-phenyl-1,3,8-triazaspiro[4.5]decan-4-one dihydrochloride (100 mg, 0.28 mmol), 2-naphthoyl chloride (60.2 mg, 0.31 mmol) and *N,N*-diisopropylethylamine (0.170 mL, 0.98 mmol) were all dissolved in *N,N*-dimethylformamide (1 mL) at 0 degrees Celsius. The reaction mixture was allowed to warm to room temperature and stirred for about 12 hours. The reaction mixture was diluted with water and extracted into dichloromethane 5 times. The dichloromethane layer was then washed 3 times with a solution of lithium chloride (3M) and dried under reduced pressure. The reaction mixture was subjected to reversed-phase chromatography to afford a white solid (88 mg, 0.16 mmol, 58 %). ¹H NMR (400.1 MHz, DMSO-*d*₆) δ (ppm): 9.79 (s, 1H), 9.04 (s, 1H), 8.97 (m, 1H), 8.49 (s, 1H), 8.06 - 7.94 (m, 4H), 7.67 -

7.58 (m, 2H), 7.24 (t, $J = 8$ Hz, 2H), 6.94 (d, $J = 8$ Hz, 2H), 6.81 (t, $J = 7$ Hz, 1H), 4.64 (s, 2H), 3.78 - 3.66 (m, 6H), 3.42 - 3.37 (m, 2H), 2.86 - 2.74 (m, 2H), 1.95 (d, $J = 14$ Hz, 2H); ^{13}C NMR (100.6 MHz, DMSO- d_6) δ (ppm): 174.8, 167.0, 142.8, 134.3, 132.1, 131.2, 129.1 (2C), 128.9 (2C), 128.0 (2C), 127.8, 127.7 (2C), 126.9, 124.1, 118.5, 114.7 (2C), 58.9, 56.5, 55.3, 49.1 (2C), 34.7, 26.2 (2C); HRMS (TOF, ESI) $\text{C}_{26}\text{H}_{29}\text{N}_4\text{O}_2$ $[\text{M}+\text{H}]^+$ calculated 429.2291, found 429.2293; LC-MS: rt (min) = 2.148; LRMS (ESI) $m/z = 429.2$.

(S)-N-(1-(1-(3-fluorophenyl)-4-oxo-1,3,8-triazaspiro[4.5]decan-8-yl)propan-2-yl)-2-naphthamide 2,2,2-trifluoroacetate (77). (S)-8-(2-aminopropyl)-1-(3-fluorophenyl)-1,3,8-triazaspiro[4.5]decan-4-one dihydrochloride (140 mg, 0.37 mmol), 2-naphthoyl chloride (76 mg, 0.40 mmol) and *N,N*-diisopropylethylamine (0.225 mL, 1.29 mmol) were all dissolved in *N,N*-dimethylformamide (5 mL) at 0 degrees Celsius. The reaction mixture was allowed to warm to room temperature and stirred for about 12 hours. The reaction mixture was diluted with water and extracted into dichloromethane 5 times. The dichloromethane layer was then washed 3 times with a solution of lithium chloride (3M) and dried under reduced pressure. The reaction mixture was subjected to reversed-phase chromatography to afford a white solid (19.3 mg, 0.03 mmol, 9 %). ^1H NMR (400.1 MHz, DMSO- d_6) δ (ppm): 9.74 (s, 1H), 9.10 (s, 1H), 8.78 (d, $J = 8$ Hz, 1H), 8.50 (s, 1H), 8.06 - 7.95 (m, 4H), 7.66 - 7.58 (m, 2H), 7.20 (q, $J = 8$ Hz, 1H), 6.76 - 6.69 (m, 2H), 6.60 - 6.53 (m, 1H), 4.62 (s, 2H), 3.88 - 3.69 (m, 3H), 3.61 - 3.54 (m, 1H), 3.43 - 3.33 (m, 3H), 2.93 - 2.71 (m, 2H), 2.01 - 1.82 (m, 2H), 1.31 (d, $J = 7$ Hz, 3H); ^{13}C NMR (100.6 MHz, DMSO- d_6) δ (ppm): 174.4, 166.7, 162.1, 144.7, 134.3, 132.1, 131.4, 130.6, 130.5, 128.9, 127.9 (2C), 127.8 (2C), 127.7, 126.9, 124.4, 109.8, 104.3, 100.9, 60.8, 59.0, 56.6,

49.8, 48.7, 41.3, 26.0, 25.8, 19.0; HRMS (TOF, ESI) $C_{27}H_{30}N_4O_2F$ $[M+H]^+$ calculated
461.2353, found 461.2354; LC-MS: rt (min) = 0.445; LRMS (ESI) m/z = 461.2.

Chapter III

DEVELOPMENT OF AZIDE AND DIAZIRINE-CONTAINING PLD PHOTOPROBES AND A STRATEGY TO VERIFY COVALENT LABELING OF THE ENZYME

Introduction

Photoaffinity labeling of proteins

Overview

The concept of photoaffinity labeling was first described by Singh, Thornton and Westheimer in the 1960s (Singh et al., 1962). Since this initial report, many groups have utilized various photoaffinity labeling techniques to characterize important biological phenomena. Interactions such as protein-ligand, protein-protein, protein-nucleic acid and protein-cofactor have all been successfully targeted in recent years (Dubinsky et al., 2012).

In theory, photoaffinity labeling is remarkably simple; however, in practice successful application of the technique to a specific situation can be quite challenging. First, a ligand containing a photoactivatable group must be prepared. This ligand is incubated with its target macromolecule(s) forming a noncovalent ligand-target complex. After complex formation, UV irradiation causes a photolysis reaction to occur thereby generating a highly reactive intermediate that can covalently modify the target macromolecule. The adducted macromolecule can then be analyzed via methods such as SDS-PAGE and/or various mass spectrometry techniques (**Figure 1**) (Robinette et al., 2006).

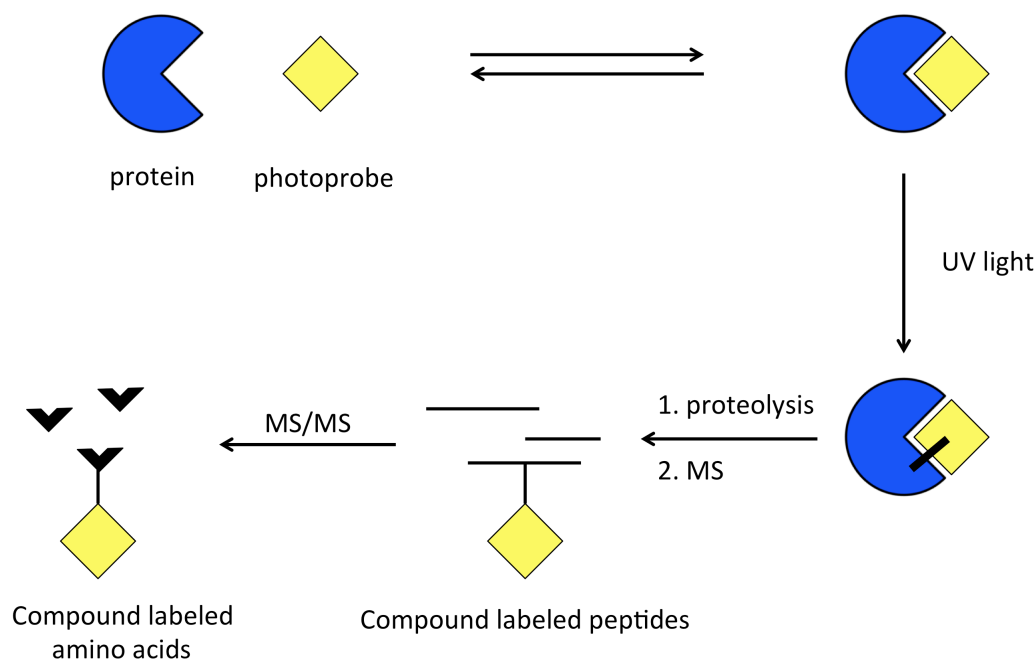


Figure 1. Idealized workflow for a photoaffinity labeling experiment. In this case the molecular target (blue circle) is covalently labeled by a photoprobe (yellow square).

The information obtained from a successful photoaffinity labeling experiment can provide several useful pieces of information depending on the specific methods employed. It is possible to use analogs of naturally occurring compounds, such as cholesterol, to identify previously unknown molecular targets of a naturally occurring compound (Hulce et al., 2013). In much the same way, the molecular target(s) of natural products from various animal and plant sources can be investigated (Dubinsky et al., 2012). When photoaffinity labeling techniques are combined with modern mass spectrometry techniques one can potentially ascertain receptor-ligand stoichiometry, a map of a ligand binding pocket and even the precise amino acids involved in a protein-ligand interaction (Robinette et al., 2006).

Commonly utilized photoactivatable functional groups

The most commonly used photoactivatable groups are: **(1)** benzophenones, **(2)** azides and **(3)** diazirines (Dubinsky et al., 2012) (**Figure 2**). Benzophenones **(1)** form triplet carbonyls upon irradiation. Benzophenones have a few advantages in that they are activated at relatively long wavelengths that do not damage biological molecules (e.g. proteins) and are quite stable in a variety of solvents. However, one significant (and obvious) problem with benzophenones is that they are much larger than the other photoactivatable groups (**Figure 2**). In the case of many allosteric ligands the known SAR may not allow for the incorporation of such a large functional group. Arylazides form nitrenes and various other reactive intermediates upon irradiation. Despite the small size of an azide (relative to a benzophenone) the wavelength required to activate an azide is relatively short and can damage proteins and other biomolecules. Diazirines **(3)** possess a number of important advantages compared to **(1)** benzophenones and **(2)** azides; the photochemistry of diazirines is discussed below.

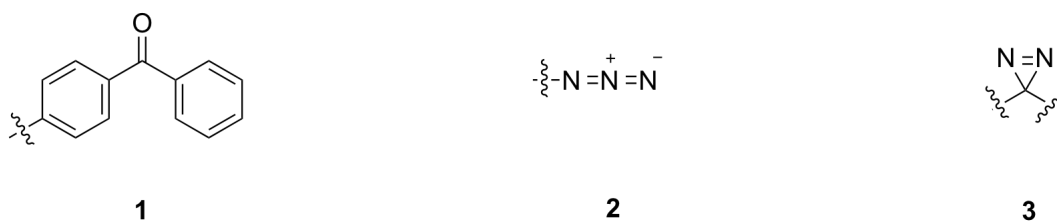


Figure 2. The three most commonly used photoactivatable groups: **(1)** benzophenones, **(2)** azides and **(3)** diazirines.

Diazirine-based photoaffinity labeling

The binding pocket on a protein for a given small molecule almost always has size/steric limitations. As discussed in chapter II, the extension of the ethylenediamine linker region by a single carbon atom in compounds such as VU0364739 completely

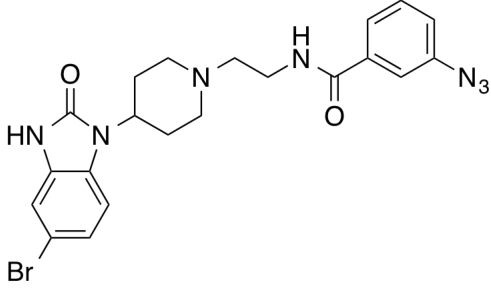
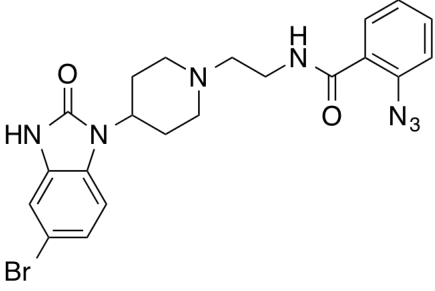
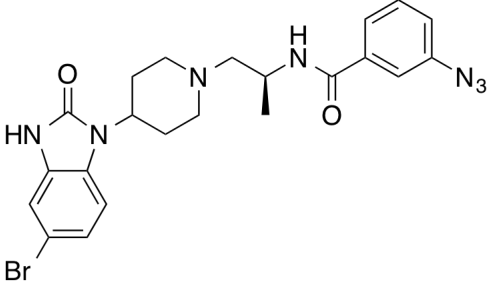
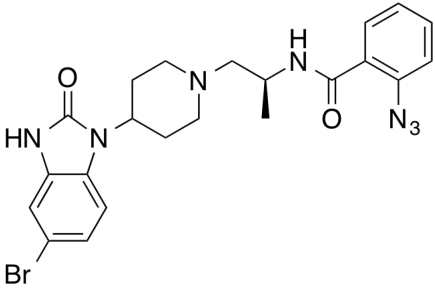
eliminated PLD inhibitory activity. Therefore, a small photoactivatable group is often ideal. Even then, some SAR development work is almost certainly necessary to ensure the photoactivatable group does not completely alter or destroy the activity of the photoprobe relative to the original ligand. Of all commonly used photoactivatable groups diazirines (**3**) are the smallest (**Figure 2**). Upon UV light exposure, diazirines react to form carbenes. The resultant carbene possesses two non-bonding orbitals and there are two possible ways to divide the two electrons among these orbitals; the singlet carbene with two spin-paired electrons and the triplet carbene with electrons possessing parallel spin states (Dubinsky et al., 2012).

A key feature of a carbene is its ability to quickly form a covalent bond with the nearest target molecule through C-C, C-H, O-H and X-H insertion reactions. The carbene is so reactive that any portion of it that is not covalently bound to a protein should be quenched with water; in theory, this decreases nonspecific labeling. In addition to its relatively small size the diazirine group has several other advantages: stability at room temperature, relative stability in the presence of nucleophiles, photoactivation at longer wavelengths (350-365 nm) that do not damage biomolecules, and relatively high reactivity (Dubinsky et al., 2012). Singlet aryldiazirines such as those formed from phenyldiazirine undergo photoisomerization and one of the undesired side reactions includes a linear diazo compound. In order to avoid this outcome a commonly utilized carbene precursor is the trifluoromethylaryldiazirine moiety. In recent years numerous improved methods for preparing trifluoromethylaryldiazirines have been reported and many photoaffinity projects have utilized trifluoromethylaryldiazirines (Dubinsky et al., 2012).

Azide-containing PLD photoaffinity probes

Cellular and *in vitro* potency

In our initial photoaffinity labeling effort we utilized arylazide-containing compounds (**Figure 3**). Compounds **4** and **5** displayed reasonable potency for both PLD1 and PLD2 in the cellular enzyme activity assay, whereas the addition of a (*S*)-methyl group in compounds **6** and **7** resulted in almost a complete loss of activity with respect to PLD2. Clearly, there is some amount of preference for the azide to be located in the meta position instead of the ortho position in terms of PLD2 inhibition. With these first generation arylazide photoprobes we had compounds that appeared to display good PLD1 potency and moderate PLD2 potency (**Figure 3**).

Cmpd	PLD1 IC ₅₀ (nM) ^a	PLD2 IC ₅₀ (nM) ^b
<p>4</p> 	23	630
<p>5</p> 	24	2,000
<p>6</p> 	30	13,000
<p>7</p> 	93	18,350

^aCellular PLD1 assay with Calu-1 Cells; ^bCellular assay with HEK293-gfpPLD2 cells.

Figure 3. First generation PLD photoaffinity probes containing arylazides. Chemical synthesis performed by Bruce Melancon and enzyme activity assays performed by Sarah Scott.

We noticed a general trend that the exact potency values from the cellular enzyme activity assay and the *in vitro* biochemical activity assay performed with purified proteins were not always exactly identical. Typically, these values were relatively close and in nearly every case (hundreds of compounds) the potency of various compounds compared to each other in one assay matched the rank order of potency in the other assay. However, because I would be using the compounds to attempt to label recombinant, truncated forms of PLD1 (PLD1c.d311) and PLD2 (PLD2.d308) I checked their potency on both constructs. HFMT.PLD1c.d311 has been routinely expressed and purified in the Brown laboratory for a number of years; however, I performed all steps from molecular biology to the recombinant expression and purification of HFMT.PLD2.d308. Compound **6** had an IC₅₀ for PLD1c.d311 of about 6 μM and compound **4** had an IC₅₀ for PLD2.d308 of about 2 μM. As we expected based on previous experiments, removing the N-terminus of PLD1 or PLD2 causes a significant decrease in potency; however, we used these constructs because we are able to express and purify reasonable amounts of them to near homogeneity, this is not the case for the full length constructs.

Verification of the photolysis reaction in a model system

Prior to attempting to covalently label proteins I wanted to verify that the photolysis of the azide (and presumably formation of a nitrene) was occurring. A 1000 watt mercury lamp connected to a monochromator was utilized for all photochemistry experiments (Porter laboratory). This instrument was ideal for its power and ability to precisely select the wavelength of light to which a sample was exposed. After first photolyzing a commercially available aryl azide (which worked as expected) I then setup

an analytical reaction in which compound **4** was activated by UV light at 310 nm in the presence of benzylamine **8** (**Figure 4**). The likely products formed are shown below.

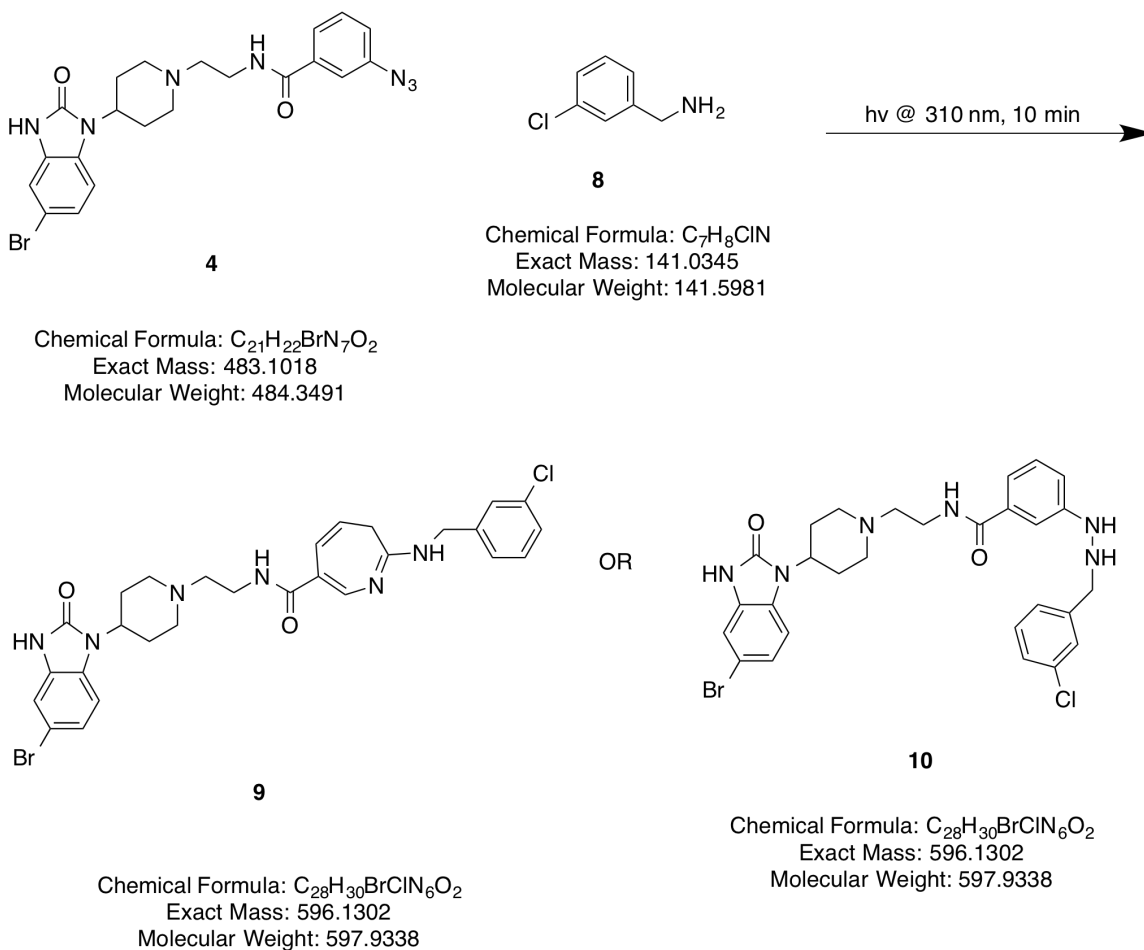


Figure 4. Photolysis reaction of compound **4** and subsequent insertion of a nitrene into compound **8**.

An LC-MS analysis of a reaction mixture that was not exposed to UV light showed no product formation, as was expected. An LC-MS analysis of a reaction mixture that was exposed to UV light gave clear evidence that a photolysis reaction, and subsequent nitrene insertion had occurred (**Figure 5**). This reaction was performed on an analytical scale in the buffer in which the actual protein labeling experiment would eventually be performed. Therefore, structural characterization of the products was not practical. Based on the analytical LC-MS data and literature precedent it is likely that

compounds **9** and/or **10** were formed in the reaction (**Figure 5**). A product appears displaying the correct m/z of 597 (M+1), and also shows the isotopic distribution characteristic of a bromine-containing compound.

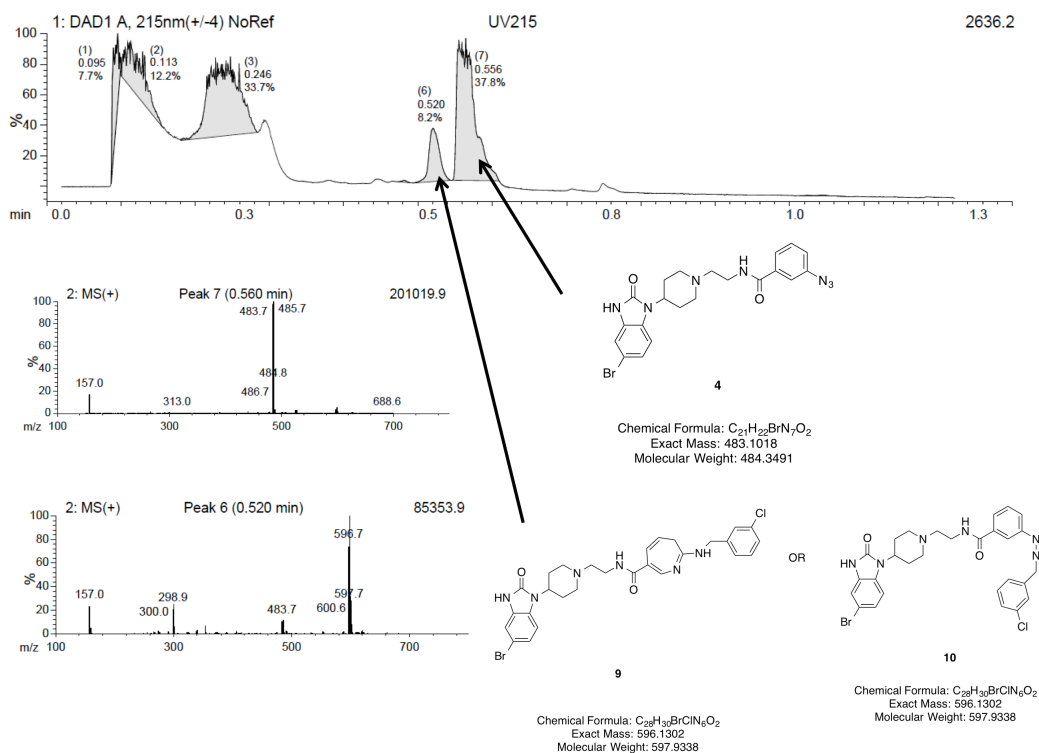


Figure 5. LC-MS characterization of the photolysis reaction of compound **4** and subsequent insertion of a nitrene into compound **8**.

Verification of protein stability during UV irradiation

In addition to demonstrating that nitrene formation was occurring I also wanted to examine if the UV light treatment was damaging the protein, and if so to what extent. In these experiments a truncated PLD2 construct missing the first 308 amino acids, PLD2.d308, was irradiated under the same conditions that the actual labeling experiment would entail. After being subjected to UV light for various amounts of time samples were immediately placed on ice and then assayed for enzyme activity (**Figure 6**). While there was some loss of enzyme activity (presumably due to protein damage) that appears

to be time/dose dependent this loss was by no means complete or prohibitive of future photoaffinity labeling experiments.

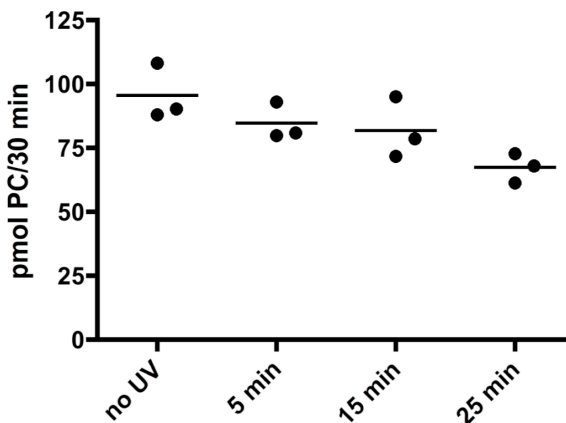


Figure 6. PLD enzyme activity in response to UV irradiation at 310 nm.

Development of a strategy to confirm covalent labeling of PLD

Enzyme activity assay following dialysis of a known noncovalent inhibitor

There are a variety of ways to confirm covalent labeling of a protein with a photoprobe. If the protein is small enough and/or probe large enough it may be possible to simply run an SDS-PAGE gel and observe a band shift. In our case the molecular weight of the HFMT.PLD2.d308 protein, with affinity tags present, was about 110 kDa and the weight of the photoprobe is about 0.5 kDa (the MW of the protein without affinity tags attached is ~70 kDa). As I expected, it was not possible to see a clear band shift on a SDS-PAGE gel (**Figure 7**). Other methods such as incorporating radioactivity into the photolabel and then testing for radioactivity in a band on a gel have also been utilized. I decided to try a few ways to look at irreversible inhibition using the *in vitro* biochemical reconstitution assay that has been discussed/referenced extensively in the previous chapters.

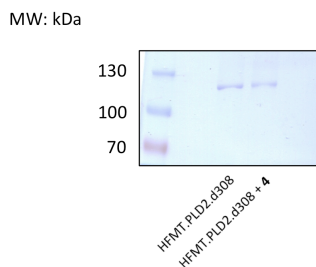
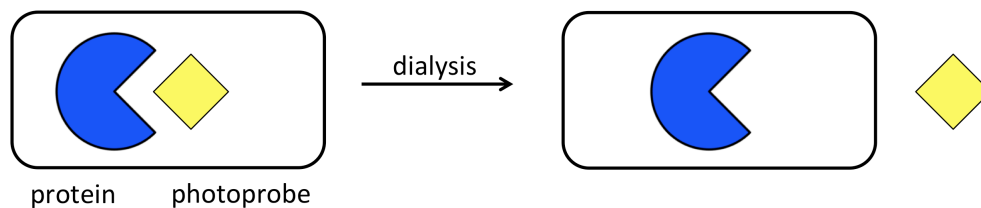


Figure 7. SDS-PAGE gel comparing the mobility of untreated and treated HFMT.PLD2.d308, this is a 6% gel.

My general plan was to physically separate noncovalently bound inhibitor/photoprobe from the enzyme and then compare the enzyme activity in that sample to a sample where the compound/photoprobe had not been removed. Initially, I tried to do this by attaching HFMT.PLD2.d308 to an affinity resin and subsequently washing the compound away, but this approach was unsuccessful. Ultimately I was able to reduce this concept to practice via a dialysis approach (**Figure 8**).

No covalent labeling of enzyme



Covalent labeling of enzyme

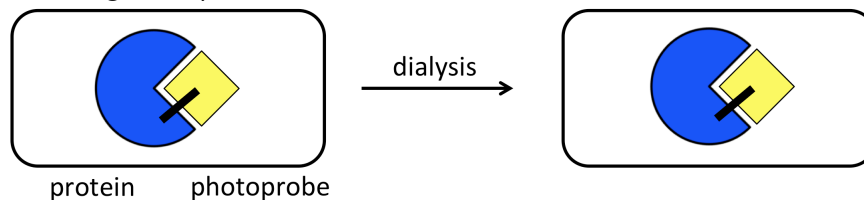


Figure 8. Dialysis based strategy to determine if PLD has been covalently labeled by a photoprobe. **A.** No covalent bond is formed and the small molecule can diffuse out of the dialysis tubing **B.** A covalent bond is formed the small molecule-protein conjugate is much too large to diffuse out of the dialysis tubing.

By using dialysis tubing with a molecular weight cutoff of 10 kDa a 110 kDa protein and 0.5 kDa small molecule were, in theory, easily separable. I planned to then assay the enzyme activity present inside the dialysis tubing as a way to determine if the inhibitor/photoprobe was covalently bound to the enzyme. If a binding event is not covalent then enzyme activity should be able to be recovered after dialysis (**Figure 8, panel A**), but if a binding event resulted in a covalent bond being formed then dialysis of that sample should yield lower enzyme activity compared to a dialyzed control sample (**Figure 8, panel B**).

In order to determine if this idea would work I setup a pilot experiment using a well-characterized noncovalent PLD2 inhibitor VU0364739 (compound **71a** from chapter II) and HFMT.PLD2.d308. In this experiment HFMT.PLD2.d308 was incubated with either DMSO or 20 μ M VU0364739 (total sample volume of 400 μ l) overnight either in a tube at 4 °C or in dialysis tubing with a 10 kDa molecular weight cutoff that was dialyzed against 1 L of buffer (MW cutoff approximately 20 times the weight of VU0364739). After approximately 16 hours 2 μ l from each sample were assayed in the *in vitro* PLD activity assay (after dilution into the assay tube, inhibitor concentration was nominally 600 nM). Results indicated that the compound completely diffused out of the dialysis tubing, as would be expected with a noncovalent enzyme inhibitor (**Figure 9**).

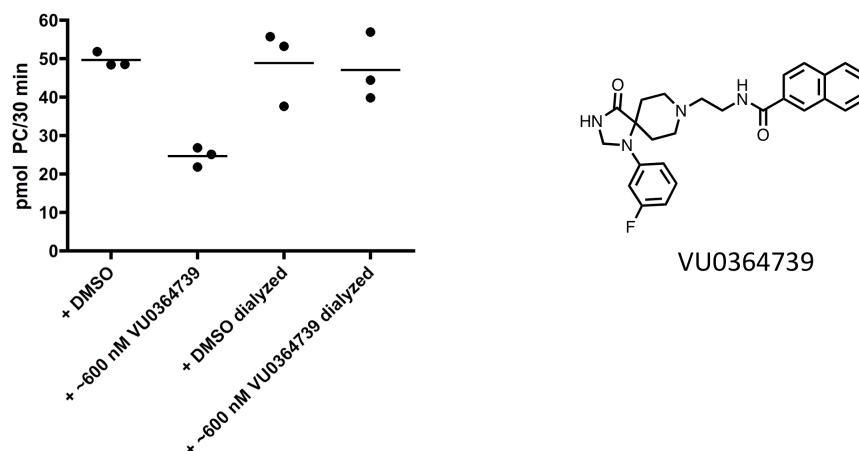


Figure 9. VU0364739 binding to HFMT.PLD2.d308 is reversible and this reversibility can be measured via an enzyme activity assay following dialysis.

Enzyme activity following dialysis of an azide-containing photoprobe

Given data that indicated my idea to verify covalent labeling via the approach described in **Figures 8 and 9** could possibly work I attempted to label HFMT.PLD2.d308 with arylazide compound **4**. In this experiment samples were prepared in essentially the same fashion as the experiment shown in **Figure 9**, except that some samples were treated with UV light at 310 nm. As shown below, compound **4** appears to covalently label HFMT.PLD2.d308 (**Figure 10**). The three samples on the left side of the graph were not dialyzed; even when not photoactivated compound **4** inhibits HFMT.PLD2.d308 (as it should), and after photoactivation **4** appears to inhibit HFMT.PLD2.d308 more potently. This can be explained by some portion of the protein being irreversibly inhibited, and the remaining portion being inhibited to the same degree as in the sample not exposed to UV light. The three samples on the right side of the graph were all dialyzed; there is almost no difference in activity between the DMSO treated and sample and the sample treated with **4** (but not with UV light). This appears to indicate that, absent a covalent bond being formed, compound **4** diffuses out of the dialysis tubing

containing the HFMT.PLD2.d308 enzyme. Conversely, in the sample containing compound **4** that is exposed to UV light the enzyme activity is significantly lower than both a control sample treated with light and DMSO, and the sample treated with compound **4** (but not UV light).

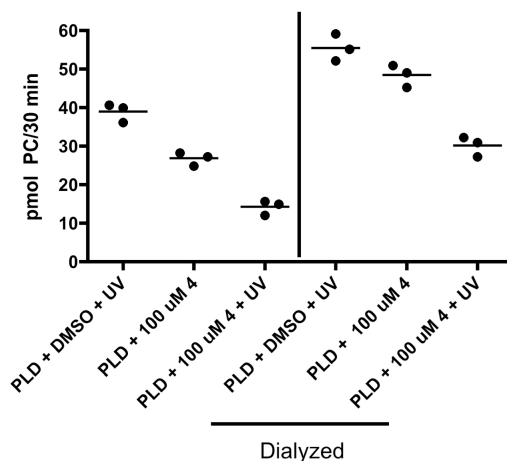


Figure 10. Arylazide compound **4** covalently labels HFMT.PLD2.d308 in a UV light exposure-dependent manner. Representative example from 3 independent experiments.

Proteolysis and CID MS/MS analysis of arylazide-labeled, truncated PLD1 and PLD2 constructs

Analysis of arylazide photoprobe fragments under CID conditions

In order to obtain some idea about which fragments of **4** would possibly appear under collision induced dissociation (CID) while **4** was attached to a peptide I attempted to covalently label the c-myc peptide (Glu-Gln-Lys-Leu-Ile-Ser-Glu-Glu-Asp-Leu) in a phosphate buffer. Unfortunately, we did not ever observe a labeled c-myc peptide. This is likely due to the fact that there is essentially no affinity between **4** and c-myc, and the highest practical concentrations of c-myc to even use are probably μM amounts (I used

10 μM) and the concentration of H_2O in the buffer was $\sim 55 \text{ M}$. Not surprisingly, we observed the formation of hydroxylamine **11** upon UV treatment (**Figure 11**). The mass spectrum of **11** clearly shows the characteristic $\sim 1:1$ distribution of the $M+1$ and $M+3$ peaks for the bromine-containing **11** (**Figure 11 panel B**).

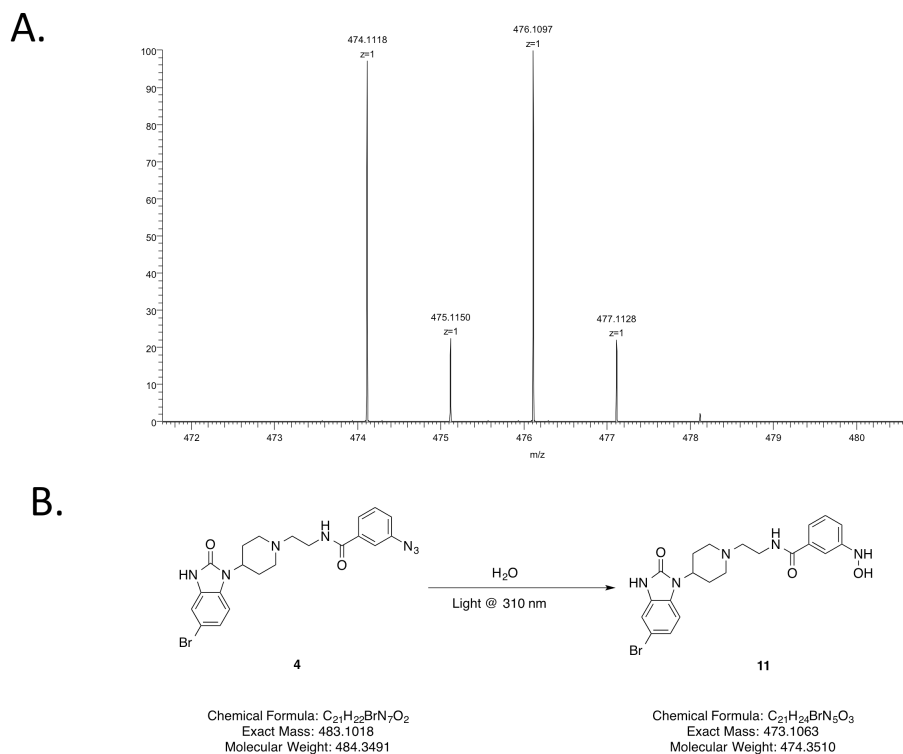


Figure 11. Compound **4** reacts with water to form a hydroxylamine after being activated by UV light. **A.** Mass spectrum of hydroxylamine **11**. **B.** UV dependent formation of **11** in water. Mass spectrometry performed by Kristie Rose.

With the help of Kristie Rose in the proteomics core facility we examined the MS2 fragments from both peaks of **11**, m/z 474.1118 and m/z 476.1097, corresponding to compounds containing the different isotopes of bromine. Three prominent fragments from the fragmentation of m/z peak at 474 are shown below (**Figure 12**). Fragment **12** does not contain a bromine atom, whereas both **13** and **14** do contain bromine atoms. This is made clear by examination of the MS2 spectrum from the m/z 476 fragment

(Figure 13). Fragment 12 shows up at the same mass to charge ratio (179) whether it comes from the m/z 474 or m/z 476 peak of compound 11. However, both fragment 13 and fragment 14 show up at a m/z 2 units larger in the m/z 476 peak compared to the m/z 474 peak, indicating they contain bromine atoms (Figures 12 and 13).

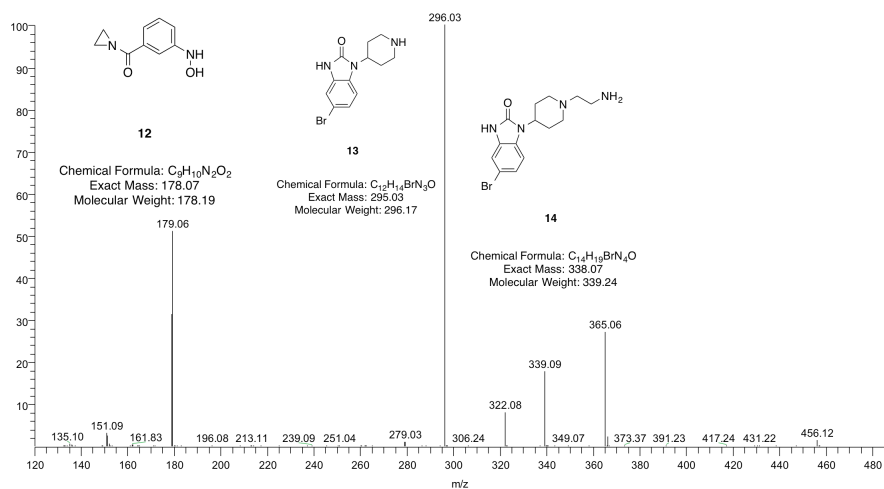


Figure 12. MS2 fragments formed from the m/z 474 peak corresponding to compound 11. Mass spectrometry performed by Kristie Rose. Assistance in determining fragment identification provided by Pavlina Ivanova and Thomas Mathews.

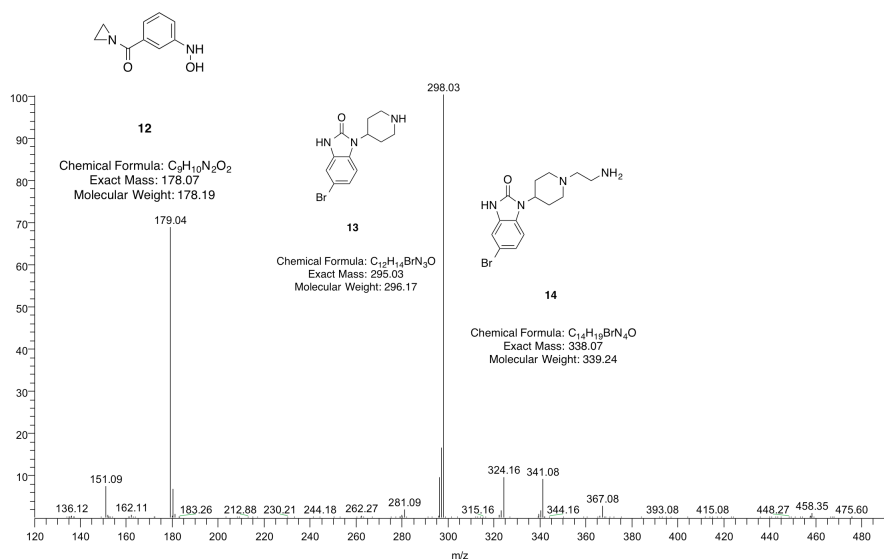


Figure 13. MS2 fragments formed from the m/z 476 peak corresponding to compound 11. Mass spectrometry performed by Kristie Rose. Assistance in determining fragment identification provided by Pavlina Ivanova and Thomas Mathews.

In-gel trypsin digestion

After having obtained independent evidence that the protein was being covalently labeled by compound **4** (**Figure 10**) and identifying some possible fragments of **4** I initially attempted to label both HFMT.PLD2.d308 and HFMT.PLD1c.d311 with compound **4**. Both control samples (DMSO) and samples for each protein incubated with 10 μ M or 100 μ M **4** were all irradiated at 310 nm for 30 minutes. Following this treatment 1 μ g of each protein was run on a SDS-PAGE gel. The protein was digested with trypsin in the gel, peptides were extracted and these samples were analyzed in the proteomics core facility.

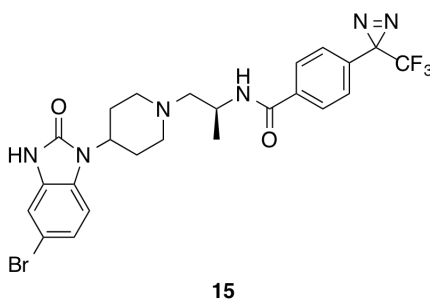
We obtained about 70% sequence coverage from the in-gel digests, which is reasonable for this approach, but in order to obtain more sequence coverage I performed some in-solution trypsin digests. While the in-solution digests improved sequence coverage to greater than 90% we were not able to easily identify an adducted peptide despite utilizing a number of advanced data analysis techniques. We also attempted a MALDI-TOF experiment knowing it would provide much lower (~30%) sequence coverage, but could possibly give us a labeled peptide. We did not detect a labeled peptide from the MALDI-TOF experiment. At this point I also became concerned that if the nitrene was reacting with a nitrogen or oxygen atom (which was impossible to know or rule out) the resulting N-N or N-O bond could break apart under before the adducted peptide even makes it to the linear ion trap. That would be the worst-case scenario, because then the labeled peptide would be “unlabeled” before it ever entered the mass spectrometer. For these reasons my colleagues in the Lindsley lab prepared a

trifluoromethylaryldiazirine compound and I began a series of experiments utilizing the trifluoromethylaryldiazirine compound.

Trifluoromethylaryldiazirine-containing PLD photoaffinity probes

Rationale for the use of a carbene

As was discussed above carbenes are highly reactive, and in practice capable of labeling any part of a protein. While this level of reactivity may also be present in a nitrene, as we would expect to form from **4**, there is at least one key difference. It is possible (and unknowable *a priori*) that a nitrene may form a relatively weak N-N or N-O bond and that this bond could break apart under electrospray ionization before the adducted peptide even makes it into the mass spectrometer. With a carbene we would expect any number of possible adducts ranging from a C-C bond to a C-O or C-N bond; the bond energies of the carbon-containing bonds are substantially higher than the bond energies of the nitrogen-containing bonds. For this reason I began working with the trifluoromethylaryldiazirine compound **15** (Figure 14).



Chemical Formula: C₂₄H₂₄BrF₃N₆O₂
Exact Mass: 564.1096
Molecular Weight: 565.3952

Figure 14. Chemical structure of compound **15** (VU0487289). Chemical synthesis performed by Jeremy (Wandong) Wen.

Truncated PLD1c *in vitro* potency and specificity

In a similar fashion as with the azide-containing compound **4** I examined the potency of **15** on both HFMT.PLD1c.d311 and HFMT.PLD2.d308. Interestingly, **15** displayed near-complete inhibition of the PLD1 construct at 25 μ M; however, even at 100 μ M **15** did not inhibit the PLD2 construct at all (**Figure 15**). I did not examine the potency of **15** in more detail, because I had planned to use a large molar excess of **15** (compared to protein) in order to err on the side of too much nonspecific labeling as opposed to no labeling at all. Due to this difference in potency, I chose to focus on photolabelling truncated, recombinant PLD1 protein.

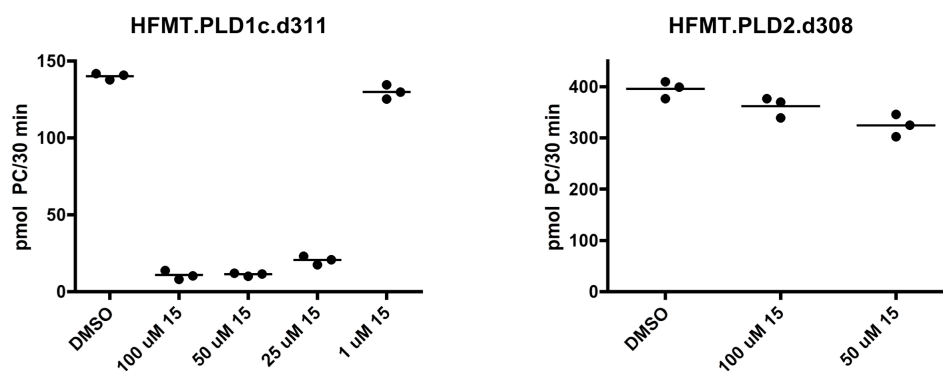


Figure 15. *In vitro* enzyme activity assays of recombinant PLD1 and PLD2 constructs in response to compound **15** (VU0487289) treatment. **A.** HFMT.PLD1c.d311 **B.** HFMT.PLD2.d308. Portions of each of these experiments were repeated at least 5 times as part of other independent experiments.

Confirmation of photolysis via LC-MS

Methods used to verify photolysis chemistry occurring were similar to those used with compound **4**. Briefly, a small amount of compound **15** at 10 mM in DMSO was added to MeOH. This mixture was irradiated with UV light at 365 nm for about 10 minutes. An aliquot of this reaction mixture was then injected directly and analyzed via

LC-MS (**Figure 16**). On a qualitative level, the chemistry is occurring as expected and the expected product **16** can be observed.

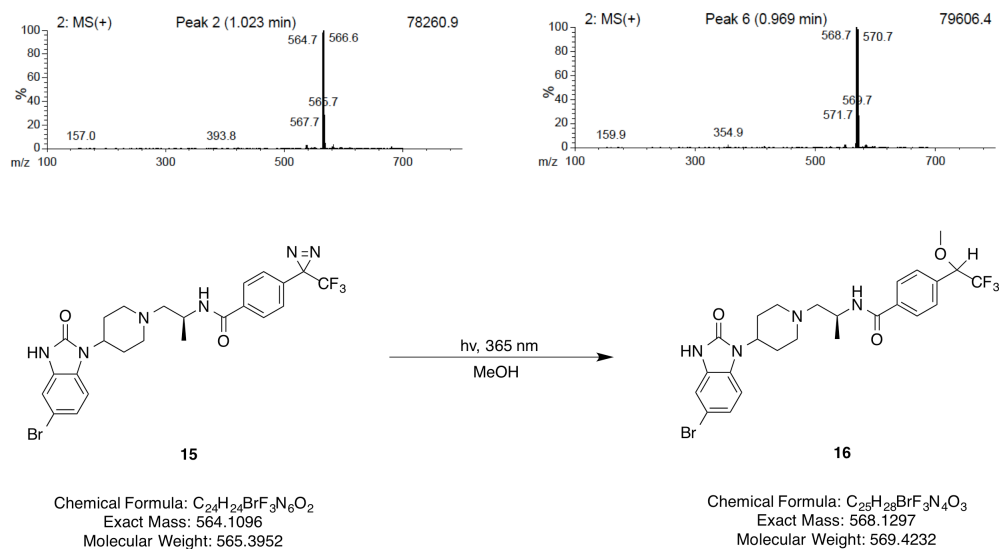


Figure 16. LC-MS characterization of the photolysis reaction of compound **15** and subsequent reaction of the carbene with methanol.

Verification of protein stability during UV irradiation

In the previous experiments conducted with arylazide **4** the protein was irradiated at 310 nm. The wavelength used to activate trifluoromethylaryldiazirine **15** was 365 nm and protein stability was verified at this different wavelength when samples were treated with light for 15 minutes. UV light at 365 nm has no measurable effect on PLD stability, as measured by an *in vitro* activity assay (**Figure 17**). Surprisingly, in two different samples each containing the protein and the photoprobe (at different concentrations) that were treated with UV light the activity present in the UV light treated samples was actually higher than in the samples containing the protein and the photoprobe (but not treated with UV light). This is in contrast to what was observed with arylazide **4** (**Figure 10**) where UV light appeared to effectively increase the potency of the compound. This is not completely unreasonable, because the carbene formation and subsequent reactions

occur quite quickly so any compound **15** that does not covalently modify the enzyme is almost certainly quenched with water (~55 M) and it would seem the resulting alcohol is not a potent inhibitor. This interesting observation would prove to hold true across many subsequent, independent experiments.

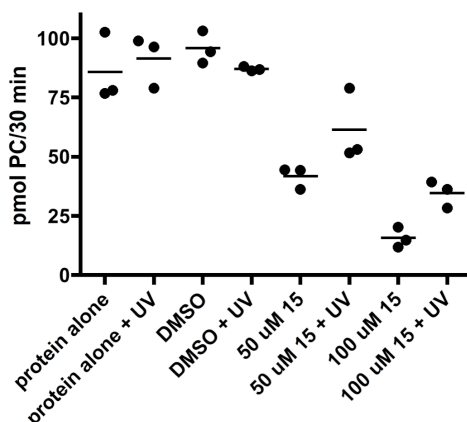


Figure 17. *In vitro* enzyme activity assay of recombinant PLD1c.d311 in response to UV treatment at 365 nm and various concentrations of **15** plus/minus UV light.

Verification of covalent labeling via dialysis and enzyme activity assay

In a similar manner (**Figure 8**) as described for compound **4** I utilized dialysis coupled with an *in vitro* enzyme activity assay to test for covalent labeling of PLD1c.d311 by **15**. Some of these experiments were repeated up to 6 times (independent experiments on different days) and in some experiments there were as many as 3 separate samples of the identical condition each assayed in triplicate. In the examples shown below all raw data points are shown to illustrate precision and reproducibility.

In the first example shown below I chose to include three separate samples (each analyzed in triplicate) of the protein incubated with **15** and treated with UV light (**Figure 18**). In this experiment, as in **Figure 17**, treating **15** with UV light actually causes an apparent loss in potency. Also, independent of UV light treatment **15** appears to

covalently label HFMT.PLD1c.d311. Notably, the 3 samples all treated with light containing **15** give essentially identical enzyme activity values. This is not entirely unexpected, because the trifluoromethylaryldiazirine carbon will be somewhat electrophilic, and even if stable to the protein I did not take extreme caution to keep the samples in absolute darkness so some UV light from ambient sources may have caused some level of photolysis to occur.

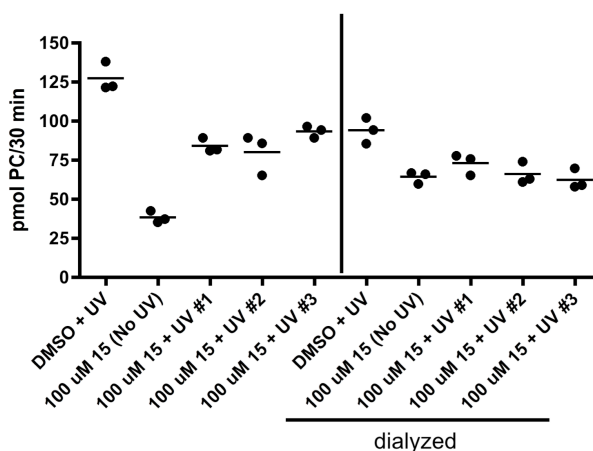


Figure 18. Trifluoromethylaryldiazirine compound **15** covalently labels HFMT.PLD2.d308 in a UV light exposure-independent manner. Samples to the right of the vertical line were dialyzed after UV irradiation. Representative example from 5 independent experiments.

After the initial experiment (**Figure 18**) and some repeats of that experiment I performed a rather large experiment containing a number of important controls. All of the findings in the original experiment (**Figure 18**) were reproducible and the additional controls yielded the expected results (**Figure 19**). As expected, the noncovalent inhibitor VU0359595 could be dialyzed away from the protein and UV light treatment had no effect on VU0359595. Again, **15** irreversibly inhibited HFMT.PLD1c.d311 independent of UV irradiation. I attempted to block labeling of the protein by using the noncovalent inhibitor, VU0359595, in the presence of **15**, but was not successful. In an ideal situation, I would have included a large molar excess of VU0359595, but given that **15**

was at 100 μM this was simply not possible due to limitations such as solubility and the volume of DMSO I would have had to add to the sample.

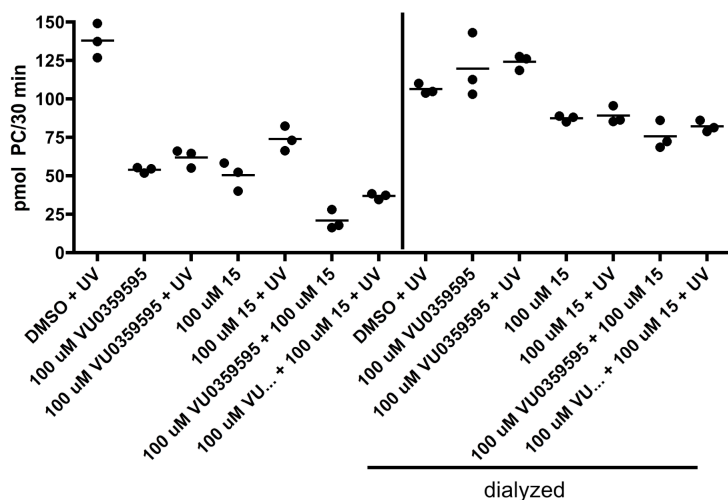


Figure 19. Trifluoromethylaryldiazirine compound **15** covalently labels HFMT.PLD2.d308 in a UV light exposure-independent manner. Additional controls are included compared to **Figure 18**. Samples to the right of the vertical line were dialyzed after UV irradiation.

Fragmentation of the diazirine-containing probe with CID and HCD to identify fragments

CID fragments

In order to gain some understanding of what fragments we might encounter in a photoprobe labeled sample we fragmented **15** using both CID and higher-energy collisional dissociation (HCD). In both cases **15** appears to undergo an intense neutral loss upon electrospray ionization (**Figure 20**). The MS2 spectrum of the m/z 565 peak using either fragmentation approach simply yields an m/z of 537. However, the MS2 spectrum of the m/z 537 peak provided significant useful information.

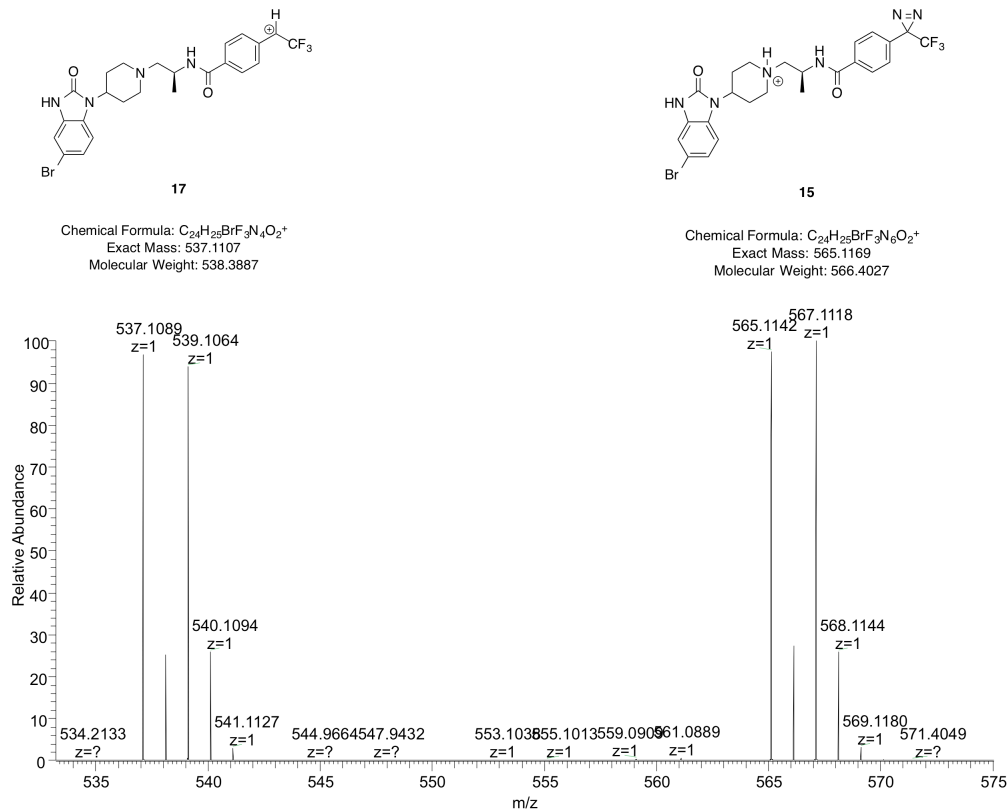


Figure 20. MS1 spectrum (zoomed) of **15**. Mass spectrometry performed by Kristie Rose in the proteomics core facility.

The MS2 spectrum resulting from the fragmentation of the m/z 537 peak was relatively straightforward to interpret and includes many fragments we expected to see based on the fragmentation of **11** (**Figure 12**) under CID conditions (**Figure 21**). While knowing these fragments was useful, it actually turned out that using HCD conditions to fragment the peptides would prove to be more useful for our purposes so we also examined the fragmentation of the m/z 537 peak from compound **15** using HCD.

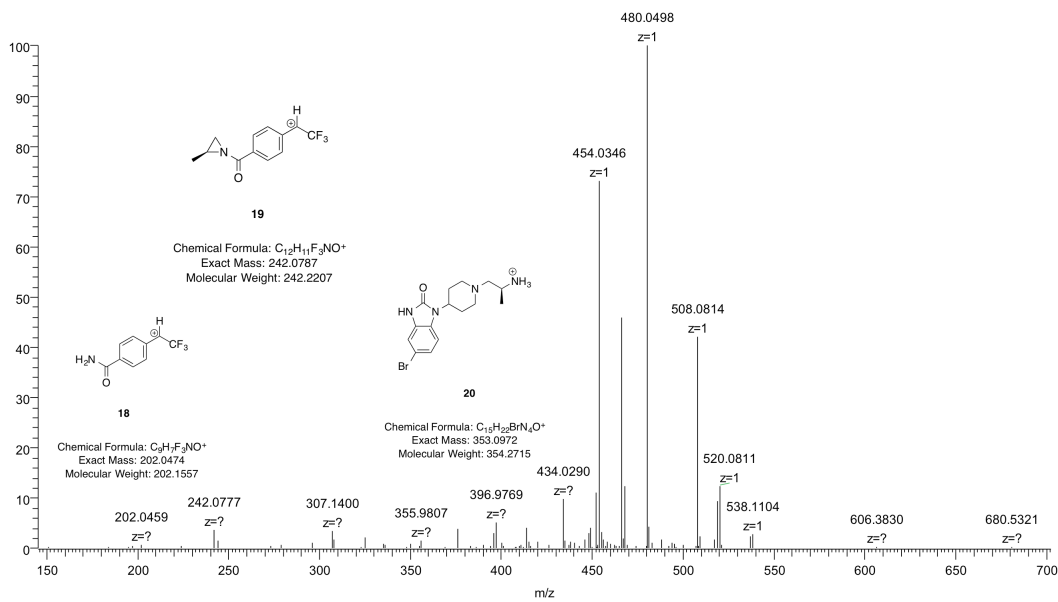


Figure 21. MS2 spectrum of m/z 537 from **15** under CID conditions. Mass spectrometry performed by Kristie Rose in the proteomics core facility. Input on observed fragments provided by Thomas Mathews and Pavlina Ivanova.

HCD fragments

One issue that can come up in these types of experiments is that if there is a highly labile bond on the adducted photoprobe it may break under CID and the amide bonds in the backbone of the peptide may not break. This would make identifying the labeled amino acid/peptide extremely challenging if not impossible. One approach to circumvent this issue is to use HCD in order to break apart the peptide even if the probe breaks apart as well. The various m/z peaks observed for **15** in an HCD experiment are shown below (**Figure 22**).

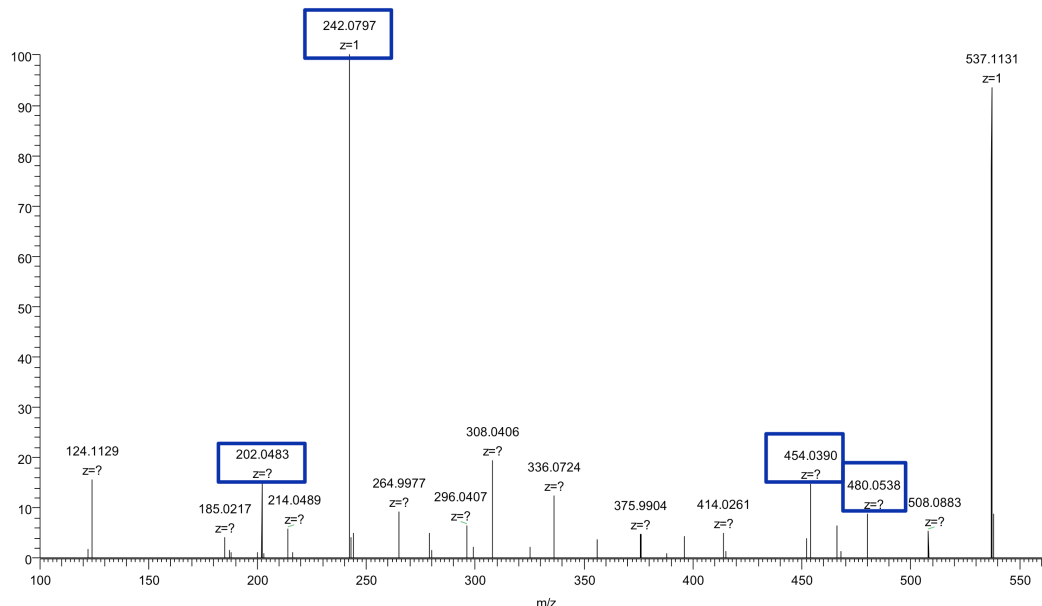


Figure 22. MS2 spectrum of m/z 537 from **15** under HCD conditions. Blue boxes indicated fragments identical to those displayed in **Figure 21**. Mass spectrometry performed by Kristie Rose in the proteomics core facility.

In-solution proteolysis with trypsin to increase data quality and sequence coverage (compared to in-gel digests)

After initially attempting to label protein with the arylazide **4** and performing an in-gel digest I switched to using the trifluoromethylaryldiazirine **15** and performing an in-solution trypsin digestion. This was possible because I was able to purify HFMT.PLD1c.d311, and later PLD1c.d311 (affinity tags removed), to essentially a single band via coomassie stained SDS-PAGE. Performing an in-solution trypsin digestion allowed us to sequence cover nearly the entire PLD1c.d311 protein (in multiple experiments) as compared to only about 60-70% sequence coverage using in-gel digestion methods. Procedures for both methods of proteolysis with trypsin are described in more details below in the “materials and methods” section of this chapter.

Proteomic analysis of diazirine-labeled, truncated PLD1c

HCD MS/MS analysis

While we did perform both CID and HCD experiments using both **4** and **15** we focused primarily on HCD experiments using **15**. Shown below is a base peak chromatogram from a 90-minute LC run of the proteolyzed PLD1c.d311 (no affinity tags present, and not treated with photoprobe) alone (**Figure 23**).

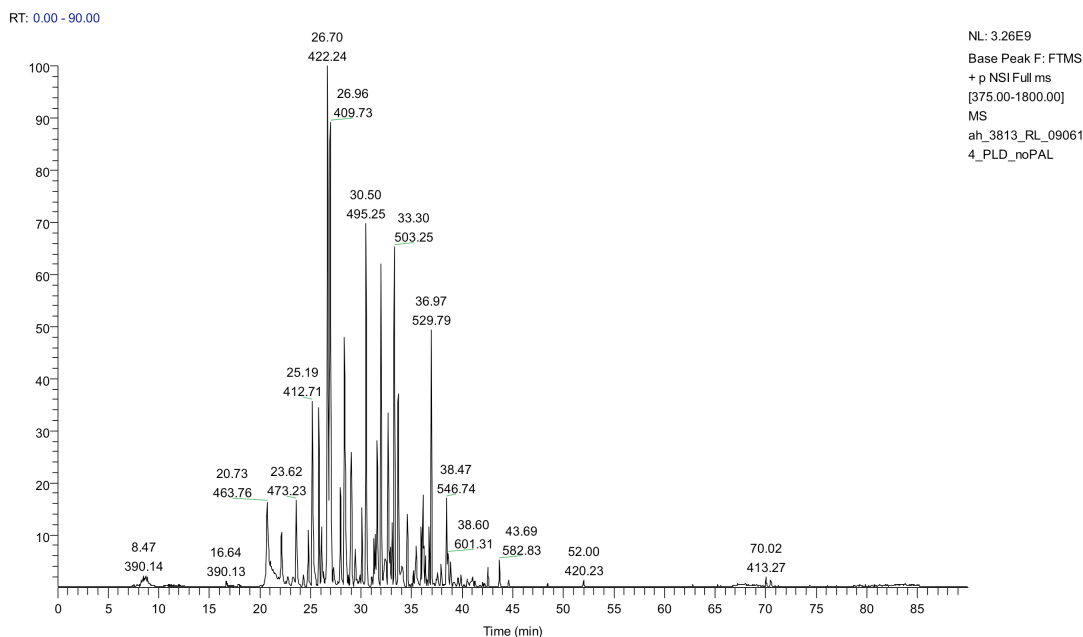


Figure 23. Base peak chromatogram of trypsin digested PLD1c.d311. Mass spectrometry performed by Kristie Rose in the proteomics core facility.

In the introduction to this chapter I alluded to the idea that any carbene molecules that are not covalently bound to the target protein should immediately be quenched with water (~55 M); this should, in theory, decrease nonspecific labeling of the target protein. The expected product from the reaction of **15** with water is shown below.

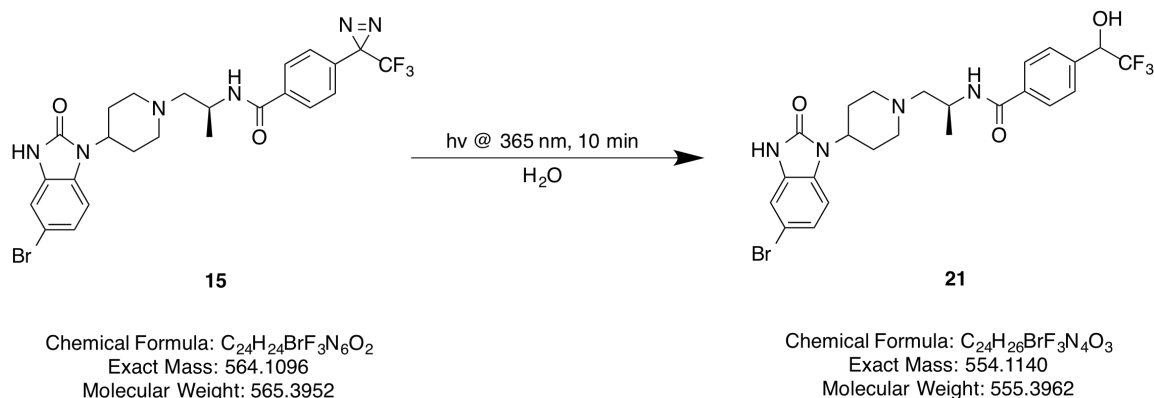


Figure 24. The carbene formed from the photoactivation of trifluoromethylaryldiazirine **15** reacts with water to form an alcohol.

Indeed, when comparing the base peak chromatogram from the proteolyzed PLD1c.d311 protein alone sample (**Figure 23**) to the base peak chromatogram from PLD1c.d311 plus a very large molar excess of **15** (treated with UV light) there are two new peaks at m/z 565 and m/z 555/557 (**Figure 25**). As shown below, these new peaks correspond to unreacted **15**, and **15** that has been quenched with water. Note, the photolysis reaction is essentially going to completion as the intensity of the water quenched-peak for **15** is many orders of magnitude larger than the unreacted **15**. This is an excellent result, because combined with the earlier enzyme activity data these data indicated that the probe is likely either labeling one or a few sites on the protein or it is being completely being quenched with water.

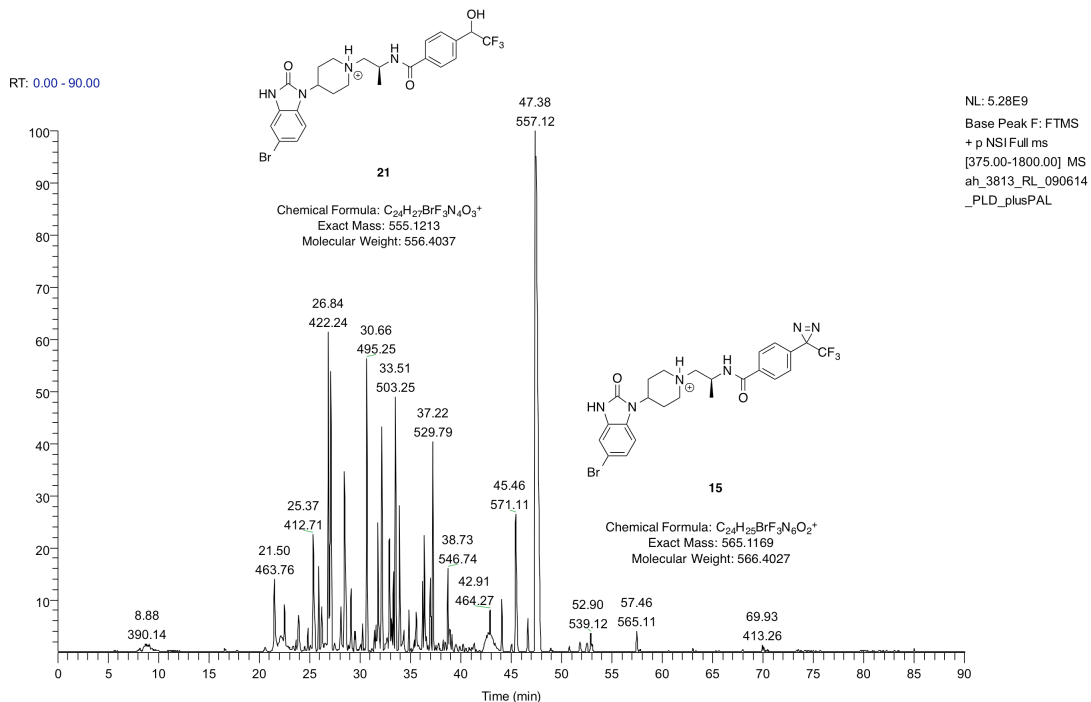


Figure 25. Base peak chromatogram of trypsin digested PLD1c.d311 plus a large molar excess of **15** (treated with UV light). Mass spectrometry performed by Kristie Rose in the proteomics core facility.

To further confirm the identity of **15** and **21** we examined the isotopic distribution in each of the sets of peaks corresponding to **15** and **21**. We would expect to see the isotopic distribution unique to bromine in both of these peaks if they are in fact the unreacted **15** and water quenched-product **21**. Indeed for the m/z 565 peak corresponding to the unreacted **15** we observed a roughly equal relative abundance of the M+1 and M+3 peaks, characteristic of a bromine-containing species (**Figure 26**). Similarly, for the m/z 555 peak corresponding to the expected product **21** we observed a roughly equal relative abundance of M+1 and M+3 peaks, characteristic of a bromine-containing species (**Figure 26**).

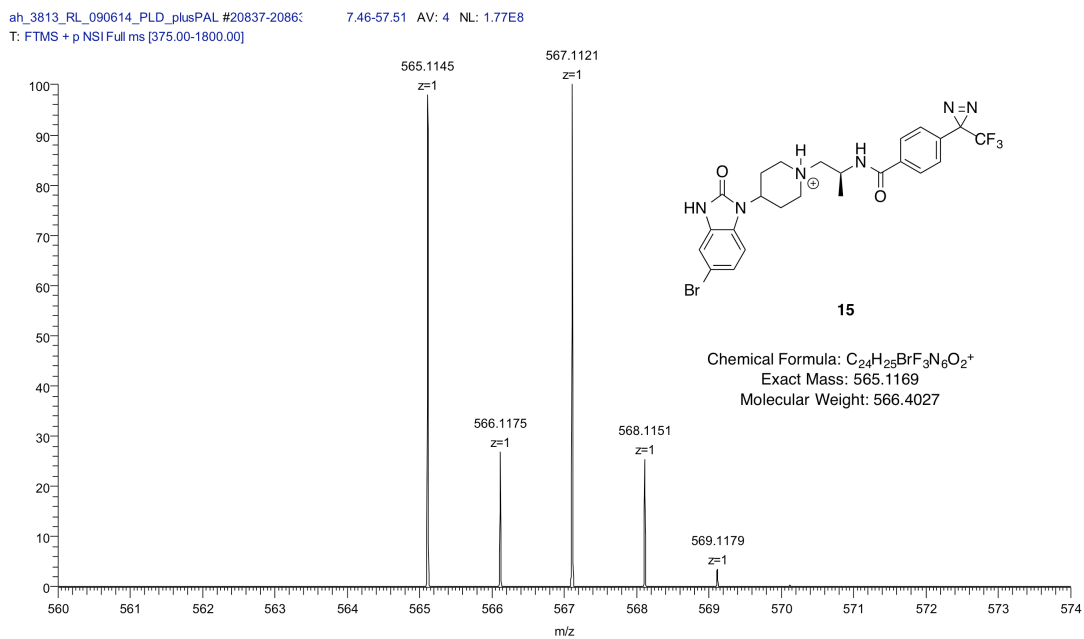


Figure 26. Zoomed view of m/z 565 peak from **Figure 25**. Mass spectrometry performed by Kristie Rose in the proteomics core facility.

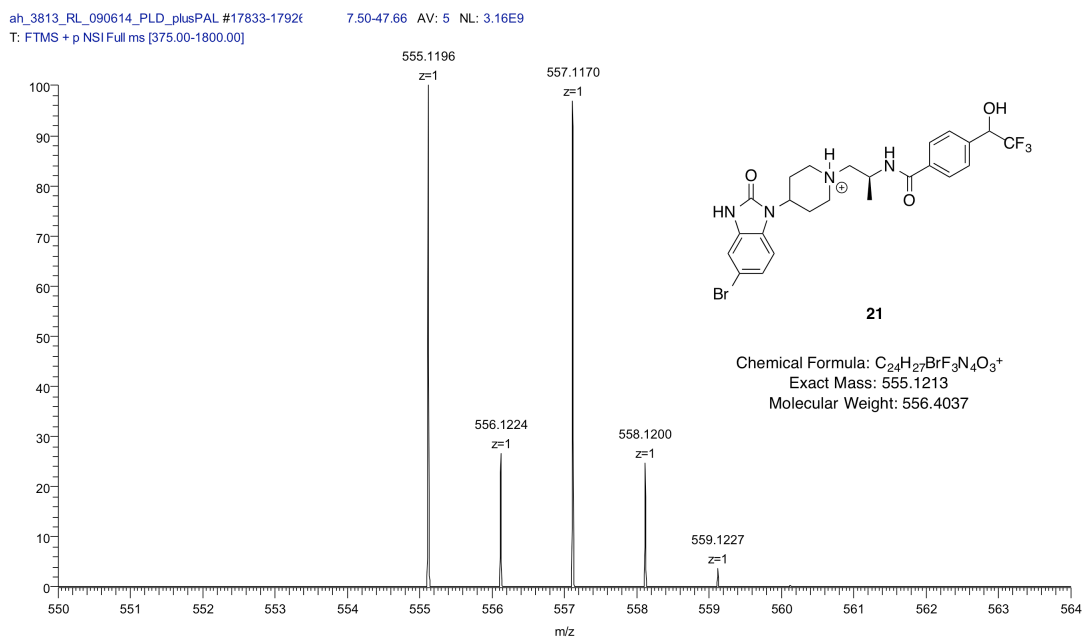


Figure 27. Zoomed view of m/z 555/557 peak from **Figure 25**. Mass spectrometry performed by Kristie Rose in the proteomics core facility.

Data analysis

The data analysis for an experiment like the one shown above in **Figures 23 and 25** is extremely complicated. There are literally dozens of reasons that the PLD1c.d311 enzyme could be covalently labeled by **15** and it would not be possible to definitively identify an adducted peptide/amino acid. Kristie Rose and her colleague Tina Tsui in the proteomics core facility performed a large amount of data analysis in an effort to find an adducted peptide/amino acid. The general problem is that there are tens of thousands of spectra generated per experiment and in some of the MS2 spectra there is no y and b ion series present. In this case, it is virtually impossible to reliably determine from which MS1 precursor a given ion/peptide came.

One of the reasons we decided to perform HCD experiments was that we were fairly confident (based on experiments with the free compound in solution, **Figure 22**) the photoprobe **15** (or an adduct) would break apart under HCD conditions. The details of how **15** would fragment under HCD conditions allowed us to devise a data mining strategy that would take advantage of searching for unique MS2 product ions that could only have come from **15**.

Tina Tsui analyzed the data by using MATLAB to extract a list of all peaks from the RAW files obtained from the experiment. She then wrote a script to search through the entire peak list looking for fragments that must have come from **15**. Based on the experiment in **Figure 22**, we identified five m/z peaks as being reasonable to search for: 264.9977, 308.0406, 336.0724, 375.9904, 454.0390. Tina set the tolerance for identifying these peaks at ± 20 ppm and we decided to require at least 2 of these peaks be present to flag a spectrum as a candidate hit (in order to decrease false positives). Kristie

then generated a list of all of the theoretical peptides that could be obtained from a trypsin digestion of PLD1c.d311, including missed cleavages, various oxidations, etc. Both the no probe and probe treated sample data sets were then analyzed against this database of theoretical peptides. MS2 spectra that contained at least 2 of the relevant peaks and originated from a precursor ion that matched the m/z of a theoretical peptide were flagged as possible hits.

As one would expect if this whole approach were valid, there were essentially no hits from the protein alone sample. Note, Kristie has to manually examine the primary data/spectra for each potential hit, because the spectra quality is enormously variable. There actually are a handful of hits from the probe treated sample. Some of them are false positives due to reasons such as incorrect charge states on the precursor ion, but some of them may actually be real adducts. The issue so far has been that even when a MS2 spectrum appears to contain 2 or more ions from the candidate list and came from a MS1 precursor ion that matched the m/z of a theoretical peptide there were no y/b ions present and the intensity of the MS1 precursor ion is so low that without sequence information (which can't even be obtained manually) we can't be sure the data are believable.

Interestingly, all of these potential hits elute off of the column near the end of the LC gradient which actually makes sense, because we are labeling (what we think is) a hydrophobic peptide with a very hydrophobic compound (even by small molecule standards). The photoprobe itself elutes well after most of the peptides do on the LC run (**Figure 25**). For these reasons we modified the chromatography to include an extended isocratic hold at 99% ACN at the end of the run in an effort to ensure that we elute all of

the hydrophobic (potentially made even more so by the addition of **15**) peptides off of the column. It would be quite unfortunate if we haven't detected an adduct, because the labeled peptide was never injected into the mass spectrometer (an astute comment made by Professor David Tabb). At the time of this writing I had prepared new samples with PLD1c.d311 (no affinity tags present) and Kristie had run the samples using more aggressive chromatography aimed at eluting highly nonpolar compounds, but the data analysis is in process.

Materials and methods

HFMT.PLD2.d308 expression and purification

Amino acids 309-933 of human PLD2 were amplified and ligated into a pDEST derived vector containing an N-terminal 6x-His, Flag, MBP, TEV protease cut site sequence. HFMT.PLD2.d308 in pDEST8 was used to create bacmid DNA and ultimately high titer baculovirus according to the manufacturers directions. HFMT.PLD2.d308 expression and enzyme activity in *Sf21* cell lysates were verified via western blot and PLD *in vitro* enzyme activity assay respectively.

Monolayer cultures (150 mm plates) of *Sf21* cells were infected with the appropriate amount of baculovirus (typically 150-200 ul, based on batch of P3 virus) and harvested 72 hours later. Alternatively, suspension cultures of *Sf21* cells were used, but expression was not as reliable in this system. Cells were scraped, resuspended and collected via centrifugation at 500 x g for 5 minutes. Cells were lysed via sonication in a lysis buffer (8.1 mM Na₂HPO₄, 1.5 mM KH₂PO₄ pH 7.5, 137 mM NaCl, 2.5 mM KCl, 0.5 mM DTT and Roche complete (EDTA free) protease inhibitor cocktail). Lysates

were clarified by ultracentrifugation at 100,000 x g for 60 min at 4 °C. Clarified lysates were filtered through a 0.2 micron filter and loaded onto a 1 ml bed volume HiTrap nickel chelating column that had previously been equilibrated with the lysis buffer minus DTT and protease inhibitors. The column was washed until the UV absorbance at 280 nm returned to base line. Non-specific proteins were eluted using a 32 mM imidazole step gradient. HFMT.PLD2.d308 was eluted using a linear gradient from 32-400 mM imidazole over 10-20 column volumes.

At this point, if the protein was to be used with the affinity tags present, then it was pooled, concentrated to about 0.5 ml and run over a 24 ml Sephadex 200 (GE) size exclusion column that had previously been equilibrated with the wash buffer from the nickel affinity column (8.1 mM Na₂HPO₄, 1.5 mM KH₂PO₄ pH 7.5, 137 mM NaCl, 2.5 mM KCl). Note, after the affinity column DTT was added to a final concentration at 1 mM, and again DTT was added to the final purified protein after size exclusion chromatography at 1 mM.

If the protein was to be used without the affinity tags present the protein was pooled, concentrated and incubated with TEV protease at 16 °C overnight (0.1 mg TEV per 1 mg of PLD enzyme). The next day this material was incubated with amylose resin (NEB) in order to scavenge the free HFMT tag and uncleaved protein. The resin was pelleted and supernatant was then filtered through a 0.2 micron filter and run over a 24 ml Sephadex 200 (GE) size exclusion column that had previously been equilibrated with the wash buffer from the nickel affinity column (8.1 mM Na₂HPO₄, 1.5 mM KH₂PO₄ pH 7.5, 137 mM NaCl, 2.5 mM KCl). As described above, DTT was kept present at 1 mM to ensure protein stability. Note, HFMT.PLD1c.d311 will lose activity in a matter of

hours if DTT is not present, but HFMT.PLD2.d308 appears to be much more stable, even in the absence of DTT.

Modifications to PLD1c.d311 chromatography

HFMT.PLD1c.d311 used for proteomics purposes was purified in an essentially identical manner to that described above for HFMT.PLD2.d308. Originally the protocol for removing the HFMT affinity tag called for rerunning that material over a nickel affinity column to remove the free HFMT tag and uncleaved protein; however, I found the amylose resin scavenging approach described above to be both much faster and more effective.

Dialysis assay procedure

Various proteins (described above) were diluted to various concentrations (approximately 30-40 ng/ul) in a phosphate buffer (8.1 mM Na₂HPO₄, 1.5 mM KH₂PO₄ pH 7.5, 137 mM NaCl, 2.5 mM KCl, 1 mM DTT). Approximately 400 µl per sample was treated with relevant compounds and/or UV light. For each sample, 50 µl was set aside and stored at 4 °C overnight while the remaining 350 µl was put into 10 kDa MW cutoff dialysis tubing and dialyzed against 1 L of phosphate buffer (8.1 mM Na₂HPO₄, 1.5 mM KH₂PO₄ pH 7.5, 137 mM NaCl, 2.5 mM KCl, 1 mM DTT) at 4 °C overnight. At the end of the dialysis procedure equivalent volumes from the dialyzed and nondialyzed samples were assayed *in vitro* for PLD enzyme activity (typically 10 µl).

Photolabeling procedure

UV irradiation

Various proteins, typically at a concentration of about 2.5 μM , were incubated with azide or diazirine-containing photoprobes, typically at a concentration of 100 μM , for 15-20 minutes on ice and then 20 minutes at room temperature. Samples were placed in a quartz cuvette and irradiated at either 310 or 365 nm (azide or diazirine activation respectively) for approximately 20 minutes. The UV light source was a 1000 watt mercury lamp with an inline monochromator. Samples were then kept on ice until proteolysis.

In-gel trypsin digestion

Various proteins, typically 1 μg per lane, were run on NuPAGE gradient gels following the manufacturers protocols. Gels were stained with coomassie R250 according to well-established methods. Special care was taken during the entire procedure to avoid contaminating samples with keratin from human skin and hair. Bands of interest were excised from the gel via a methanol-rinsed blade and subsequently chopped into small cubes.

Gel pieces were transferred to 1.5 ml tubes and destained. To each tube was added ~ 100 μl of 100 μM ammonium bicarbonate/acetonitrile (1:1, vol/vol). Tubes were agitated and washed 3 times for 10 minutes each. Next, 200-500 μl of acetonitrile was added and then completely removed after 10 minutes. Approximately 100 μl of 10 mM DTT was added and the tube was agitated for 1 hour, then 500 μl of acetonitrile was added and then completely removed after 10 minutes. To alkylate cysteine residues ~ 100

μl 55 mM iodoacetamide (enough to cover gel material) was added and samples were agitated for 20 min at room temperature, in the dark. Samples were washed with $\sim 100 \mu\text{l}$ of 100 mM ammonium bicarbonate for a few minutes and then all liquid was removed. Next, $\sim 100 \mu\text{l}$ of 100% acetonitrile, and samples were agitated for 5 minutes and all liquid was removed. Gel pieces were dried in under vacuum for 10-15 minutes to remove all acetonitrile.

Fresh trypsin (12.5 ng/ μl) from a frozen stock (500 ng/ μl stock, stored at -80°C) was prepared by adding 10 μl of trypsin to 190 μl of 100 mM ammonium bicarbonate and 190 μl of water. Gel pieces were covered in the trypsin solution and chilled/rehydrated on ice for 30 minutes. Enough 100 mM ammonium bicarbonate was added to cover the gels pieces in liquid. Samples were incubated/proteolyzed overnight at 37°C .

All subsequent extracts were saved and combined for analysis. Supernatant was removed and saved. To each tube was added 100 μl of water. Samples were heated to 37°C for 5 minutes, vortexed for 5 minutes, centrifuged briefly at 2,000 x g and liquid transferred to a new tube. Next, 100 μl of 5% formic acid/acetonitrile (1:1, vol/vol) was added to gel slices, they were heat to 37°C for 5 minutes, vortexed for 5 minutes, centrifuged briefly at 2,000 x g and the liquid was transferred to a new tube (this was performed twice). Samples were dried under vacuum for several hours. After samples were dried they were resuspended in 10-60 μl of 0.1% formic acid. Samples were then ready for analysis and handed off to Kristie Rose in the proteomics core facility.

This protocol was adapted from:

1. Vanderbilt Mass Spectrometry Research Center protocol # MSRC-R-031

2. In-gel digestion for mass spectromic characterization of proteins and proteomes.

Shevchenko et al. *Nature protocols*. **2006**.

In-solution trypsin digestion

Various proteins, at about 2.5 - 5 μM , were first reduced with 200 μM DTT and then alkylated with 600 μM iodoacetamide (each added in the smallest volume practical, usually 1 μl). Trypsin was used as described above in a 1:30 ratio w/w with the various enzymes. Samples were then ready for analysis and handed off to Kristie Rose in the proteomics core facility.

Proteomics methods and data analysis

Proteolytically digested PLD1 was loaded onto a capillary reverse phase analytical column (360 μm O.D. x 100 μm I.D.) using an Eksigent NanoLC Ultra HPLC and autosampler. The analytical column was packed with 20 cm of C18 reverse phase material (Jupiter, 3 μm beads, 300 \AA , Phenomenox), directly into a laser-pulled emitter tip. Peptides were gradient-eluted at a flow rate of 500 nl/min, and the mobile phase solvents consisted of 0.1% formic acid, 99.9% water (solvent A) and 0.1% formic acid, 99.9% acetonitrile (solvent B). A 90-minute gradient was performed, consisting of the following: 0-10 min (sample loading via autosampler onto column), 2% B; 10-50 min, 2-40% B; 55-66 min, 40-99% B; 60-75 min, 99% B; 75-80 min 99-2% B; 80-90 min (column equilibration), 2% B. Eluting peptides were mass analyzed on a Q Exactive mass spectrometer (Thermo Scientific), equipped with a nanoelectrospray ionization source. The Q Exactive was operated in the data-dependent mode acquiring HCD

MS/MS scans ($R = 17,500$) after each MS1 scan ($R = 70,000$) on the 18 most abundant ions using an MS1 ion target of 3×10^6 ions and an MS2 target of 1×10^5 ions. The maximum ion time for MS/MS scans was set to 100 ms, the HCD-normalized collision energy was set to 27, and dynamic exclusion was set to 10 s.

Chapter IV

SUMMARY AND FUTURE DIRECTIONS

I was incredibly fortunate to have become involved in studying PLD enzymology and pharmacology when I did. PLD enzyme activity in mammalian tissues was initially described in the 1970s (Saito and Kanfer, 1973), but human PLD1 (Hammond et al., 1995) and PLD2 were not cloned until the late 1990s (Colley et al., 1997). While a provocative paper published in 2005 showed PLD played a major role in Ras driven tumorigenesis *in vivo* (Buchanan et al., 2005) PLD1 and PLD2 knockout mice were not reported until 2010, while I was in graduate school (Dall'armi et al., 2010; Elvers et al., 2010; Oliveira et al., 2010). The first drug-like, small molecule PLD inhibitor was published in 2007, the same year I began graduate school (Monovich, 2007). It is hard for me to imagine a better time to start working toward developing potent small molecule, drug-like, isoform-selective PLD inhibitors.

Our interest in developing drug-like, small molecule PLD inhibitors stemmed, in part, from the fact that there were not any. The most utilized class of chemical compounds to study PLD function over the past several decades has been primary alcohols (e.g., *n*-butanol). Alcohols are often, incorrectly described in the literature as “PLD inhibitors.” It is important to emphasize that alcohols are not PLD inhibitors, rather *n*-butanol (as well as some other primary alcohols) blocks PLD-catalyzed PtdOH production by competing with water as a nucleophile, thereby causing the formation of phosphatidylbutanol in a transphosphatidylation reaction. It should come as no surprise that using a primary alcohol at a concentration described in percent amounts may not be a

completely “specific” approach. To be fair, many studies utilized RNA interference techniques and/or dominant negative constructs; however, these types of studies do not allow us to learn much about the potential druggability of a target.

The first drug-like PLD inhibitor to be identified was disclosed in 2007 by a group at Novartis that ran a high throughput screen to identify PLD2 inhibitors. Their effort identified halopemide (**1**), a psychotropic agent originally reported by Janssen in the late 1970s and early 1980s for numerous neuroscience indications, as a PLD2 inhibitor with an IC_{50} value of 1.5 μ M (**Figure 1**) (Monovich, 2007).

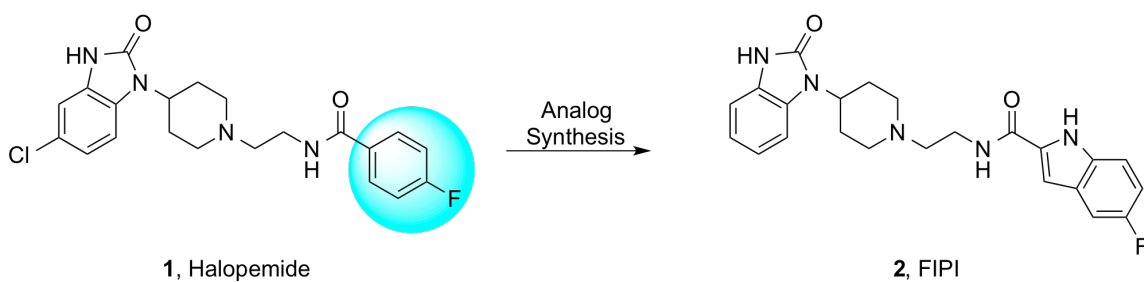


Figure 1. Structure of halopemide (**1**) and an optimized analog called FIPI (**2**) (Figure adapted with permission from Selvy *et al.* 2011).

This short report was limited to a succinct description of the synthesis of fourteen halopemide analogs where alternative amide moieties were surveyed, resulting in the discovery of **2**, later coined FIPI, with an IC_{50} of 200 nM and good rat pharmacokinetics. However, there was no mention of PLD1 inhibition in this initial paper, but it was subsequently found that halopemide (**1**) potently inhibits both PLD1 (cellular IC_{50} = 21 nM, *in vitro* IC_{50} = 220 nM) and PLD2 (cellular IC_{50} = 300 nM, *in vitro* IC_{50} = 310 nM) as does **22** (PLD1 cellular IC_{50} = 1 nM, *in vitro* IC_{50} = 9.5 nM; PLD2 cellular IC_{50} = 44 nM, *in vitro* IC_{50} = 17 nM) (Scott *et al.*, 2009). Thus, halopemide (**1**) and all the halopemide analogs presented in this initial report are more accurately described as dual

PLD1/2 inhibitors, and even show a slight preference for PLD1 inhibition. Despite these issues, the halopemide (**1**) scaffold is an excellent starting point for a PLD inhibitor development campaign due to its potent PLD inhibition, favorable preclinical drug metabolism and pharmacokinetic profile, and most importantly, extensive history in multiple clinical trials (Loonen and Soudijn, 1985).

Halopemide (**1**) was evaluated in five separate clinical trials with over 100 schizophrenic, oligophrenic and autistic patients receiving the drug (Loonen and Soudijn, 1985). Efficacy was observed in the majority of patients, and importantly, no adverse side effects or toxicities were noted, despite achieving plasma exposures of 100 ng/mL to 360 ng/mL from the 20 mg/kg and 60 mg/kg doses of 21, respectively (van Rooij et al., 1979). At these plasma concentrations, PLD1 was clearly inhibited, suggesting inhibition of PLD by this chemotype in humans is a safe and therapeutically viable approach.

At the time when I was just beginning to work in the Lindsley lab members of the Brown and Lindsley labs collaborated to publish the first significant SAR campaign based on halopemide (**1**) (Scott et al., 2009). This broad, first generation effort did yield the first PLD1-selective inhibitor, VU0155069 (**3**), in which the chiral (*S*)-methyl group significantly enhanced PLD1 preference to ~163-fold over PLD2 in a cell-based assay (**Figure 2**). Subsequent iterations of lead optimization reinforced the initial observation that the chiral (*S*)-methyl group increased PLD1 inhibition. While the piperidinyl benzimidazolone-containing analogs failed to display any preference for PLD2 inhibition, a triazaspirone congener uniformly increased PLD2 inhibition to provide the first PLD2 (10-fold PLD2 preferring) selective inhibitor, VU0155072 (**4**) (**Figure 2**).

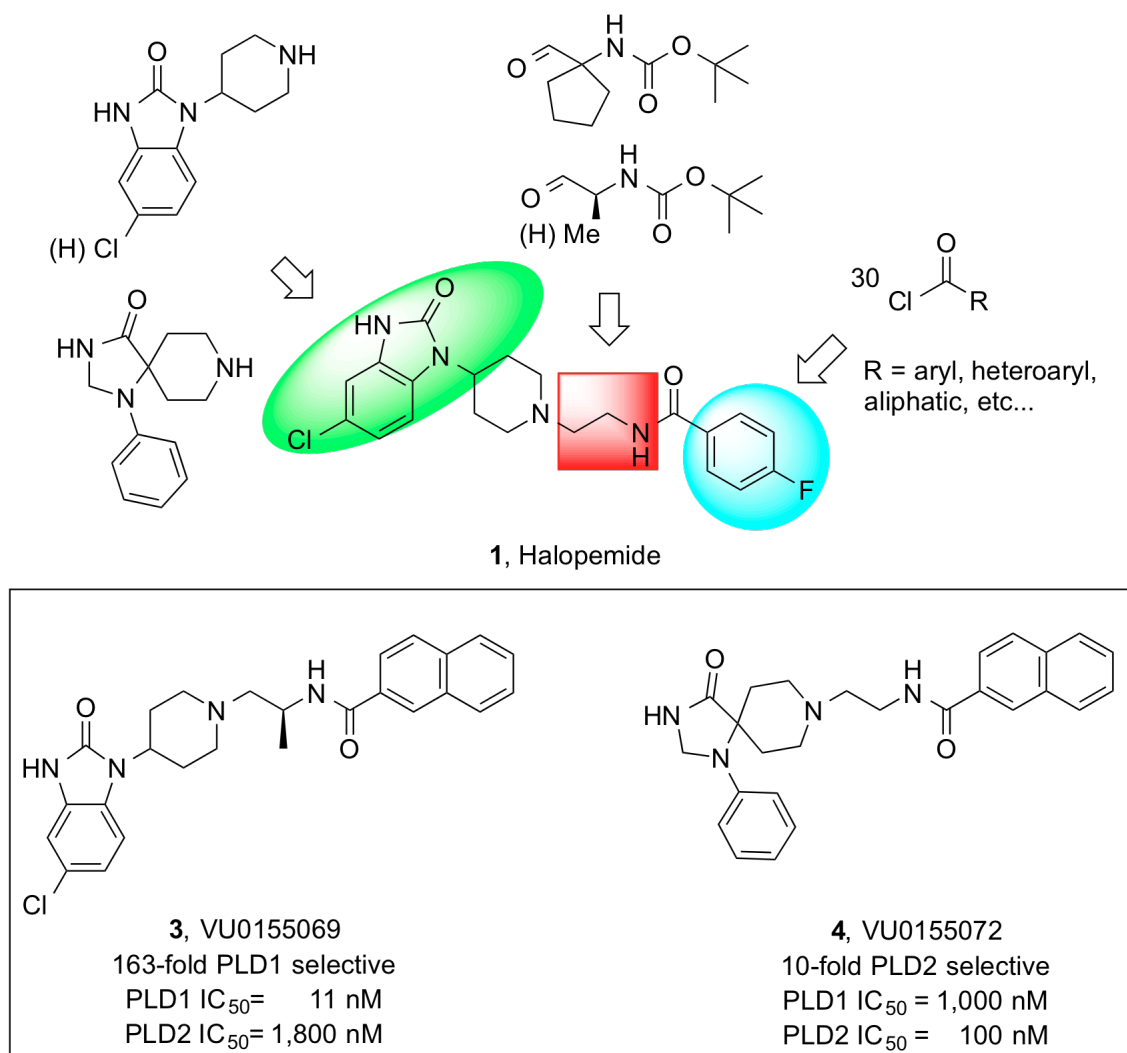


Figure 2. Initial SAR studies on halopemide (Figure adapted with permission from Selvy *et al.* 2011).

In our initial libraries we coupled a large number of eastern amide caps to the benzimidazolone scaffold and determined that, in general, aromatic or heteroaromatic functional groups conferred the most potency. However, these functional groups did not provide any gains in PLD1 selectivity. We did discover that the incorporation of *trans*-phenyl cyclopropane amide, as in compound **5**, increased PLD1 specificity quite substantially (**Figure 3**). Also, by exploring various halogenations about the benzimidazolone scaffold we identified the 5-Br congener as conferring excellent

potency and selectivity. Ultimately, it was the installation of the (*S*)-methyl group in the ethylenediamine linker that facilitated a dramatic increase in PLD1 selectivity. The key changes that enabled continuous improvements in both PLD1 potency and selectivity ultimately leading to VU0359595 are shown below, highlighted in red (**Figure 3**).

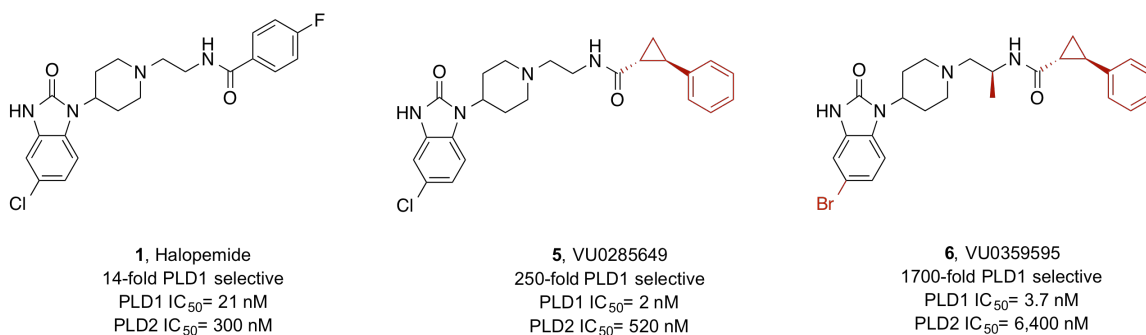


Figure 3. Key structural modifications (shown in red) that led to the development of **6** (VU0359595) (Figure adapted with permission from Selvy *et al.* 2012).

With a potent, and highly selective PLD1 inhibitor in hand (VU0359595) I spearheaded an effort to improve upon the PLD2 selectivity in **4**. From the initial SAR depicted above (**Figure 2**) we gleaned that we did not have much room for variability/optimization with respect to the eastern amide moiety in **4**. We decided to focus on functionalization of the 1,3,8-triazaspiro[4,5]decan-4-one scaffold by the incorporation of various halogens, as this proved successful in the benzimidazolone-based PLD1 inhibitor **6** (VU0359595). Only the unsubstituted 1-phenyl-1,3,8-triazaspiro[4,5]decan-4-one was commercially available, so while known in the literature, the halogenated congeners had to be synthesized. I prepared the requisite halogenated congeners and ultimately used them to prepare a targeted 4 x 6 matrix library of twenty four analogs based on the PLD2 preferring inhibitor **4** (**Figure 2**). While we were not able to match the 1,700-fold selectivity for PLD1 present in **6** (VU0359595) we were able to prepare a centrally penetrant, potent (PLD2 IC₅₀ = 20 nM), 75-fold selective

PLD2 inhibitor, **8** (VU0364739). It was not until the identification of the 1,3,8-triazaspiro[4,5]decan-4-one scaffold, as in **7**, that we were able to make progress toward the 75-fold selective PLD2 inhibitor, **8** (VU0364739) (**Figure 4**).

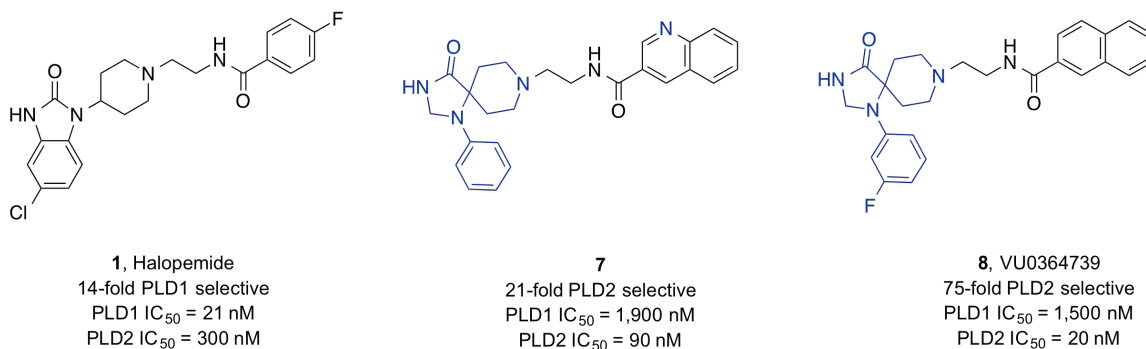


Figure 4. Key structural modifications (shown in blue) that led to the development of **8** (VU0364739) (Figure adapted with permission from Selvy *et al.* 2012).

Clearly, a further increase in PLD2 selectivity would be advantageous from a chemical probe standpoint, but it is unlikely that any massive improvements will be made within the 1,3,8-triazaspiro[4,5]decan-4-one scaffold. Indeed, a recent paper from the Brown and Lindsley labs contained a compound very similar in structure to VU0364739 that appears not to inhibit PLD1 at all (IC₅₀ > 20 μM) but the compound's potency with respect to PLD2 decreased noticeably compared to VU0364739 (IC₅₀ of 355 nM versus IC₅₀ of 20 nM for VU0364739) (O'Reilly *et al.*, 2013). In order to obtain significant improvements in PLD2 selectivity it may be necessary to optimize an entirely different chemotype. In the absence of structural information, one possible way to do this would be to run a new high throughput screen for both PLD1 and PLD2.

We evaluated VU0359595 and VU0364739 in a battery of *in vitro* and *in vivo* DMPK assays to determine if these isoform selective PLD inhibitors would be suitable candidates with which to dissect PLD function *in vivo*. PLD1 inhibitor VU0359595 was

lipophilic (clogP = 4.5), yet possessed ~2% free fraction in rat and human plasma protein binding experiments (equilibrium dialysis) and was easily formulated into acceptable vehicles. In rat iv PK experiments, VU0359595 was found to be a highly cleared compound (Cl = 60 mL/min/kg) with a moderate half-life ($t_{1/2}$ = 0.75 hr) and high volume of distribution (V_{dss} = 4.7 L/kg) (**Figure 5**). A similar profile was obtained for PLD2 inhibitor VU0364739. While less lipophilic (clogP = 3.2), VU0364739 also displayed ~2% free fraction in rat and human plasma protein binding experiments (equilibrium dialysis) and was easily formulated into acceptable vehicles. In rat iv PK experiments, VU0364739 was found to be a highly cleared compound (Cl = 61 mL/min/kg) with a moderate half-life ($t_{1/2}$ = 1.5 hr) and high volume of distribution (V_{dss} = 8.1 L/kg).

Cmpd	plasma protein binding (% bound)	IV (pharmacokinetics) ^a				PO (plasma & brain levels) ^b			
		dose (mg/kg)	CL (mL/min/kg)	$t_{1/2}$ (h)	V_{dss} (L/kg)	dose (mg/kg)	Plasma (ng/mL)	Brain (ng/mL)	Brain/Plasma
VU0359595	98.1	1	60.7	0.78	4.7	10	29	BLQ	BLQ
VU0364739	97.9	1	61.5	1.52	8.1	10	39.9	29	0.73

Figure 5. Pharmacokinetic profile of VU0359595 and VU0364739 in rat. Pharmacokinetic analyses performed by Satyawan Jadhav, Ryan Morrison and J. Scott Daniels (Figure adapted with permission from Lavieri *et al.* 2010).

Recent genetic and knock-out studies have suggested therapeutic potential for PLD inhibition in Alzheimer's disease and stroke. Additionally, there is some interest in targeting certain brain cancers with PLD inhibitors. Therefore, centrally penetrant PLD inhibitors would be of great value for preclinical target validation. To address this, both VU0359595 and VU0364739 were dosed at 10 mpk po in a standard 90 minute single point brain:plasma (PBL) study. While levels of VU0359595 were below the level of quantitation in the brain, VU0364739 displayed a Brain/Plasma ratio of 0.73 thereby

representing the first centrally penetrant PLD inhibitor we have characterized (**Figure 5**). Unfortunately, the clearance values of both VU0359595 and VU0364739 are approximately equal to liver blood flow in a rat. Notably, I did not perform a lead optimization campaign with the explicit goal of improving the compounds' *in vivo* disposition; however, some amount of DMPK optimization would certainly allow us to make stronger arguments about the drug-likeness potential of these compounds.

In addition to the chemical synthesis and optimization of the compounds described in this dissertation I also endeavored to gain some understanding of how these compounds inhibit PLD. Given that no human PLD enzyme has ever been crystallized I knew it was extremely unlikely we would be able to obtain a cocrystal with one of these inhibitors during my time in graduate school. I actually attempted to gain some insight into how the compounds work via a wide range of biochemical approaches, many of which were not discussed herein. I made a variety of constructs missing portions of the N-terminus of PLD1 and screened them for their sensitivity to VU0359595; none of these constructs were resistant to VU0359595. I also individually mutated about 3-dozen amino acids in a portion of the enzyme we suspected to be involved in binding VU0359595; again no constructs displayed resistance to VU0359595.

In order to directly answer the more general question about the mechanism of inhibition of the compounds I setup a Michaelis-Menten type assay in which the concentration of a short chain lipid substrate was increased (but kept monomeric, well below its CMC) while PLD enzyme concentration was held constant. I had planned to then add various inhibitors to determine if they were competitive, uncompetitive inhibitors or mixed inhibitors. Unfortunately, after optimizing various experimental

parameters I discovered that PLD2.d308 displays substrate inhibition kinetics (and not Michaelis-Menten kinetics) (**Figure 6**). While it is possible to determine the mode of inhibition of an inhibitor in a system that displays substrate inhibition kinetics it would have been extraordinarily expensive to do so in our case, so much so that we decided not to pursue those experiments.

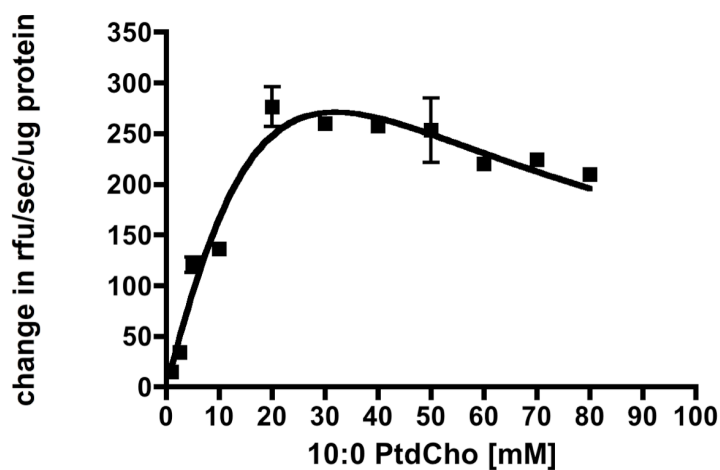


Figure 6. HFMT.PLD2.d308 displays substrate inhibition kinetics.

Finally, I turned my attention to photoaffinity labeling as means to potentially identify a region on PLD where the compound could be binding. I utilized both azide **9** and diazirine **10**-containing photoprobes in an attempt to label PLD1c.d311 (**Figure 7**). While I was able to show acceptable potency for both photoprobes on recombinant PLD1c.d311 protein; show the photochemistry occurring in solution; and develop a method to show covalent labeling of the protein we were not, at the time of my writing, able to definitively identify a tryptic peptide labeled with either photoprobe. There are many, many possible reasons for this and I will address a few of the most likely reasons and what we have done, and could do, in order to solve the relevant problems. Nearly all

of the data analysis for the proteomics data was carried out by Kristie Rose and her colleagues in the proteomics core facility.

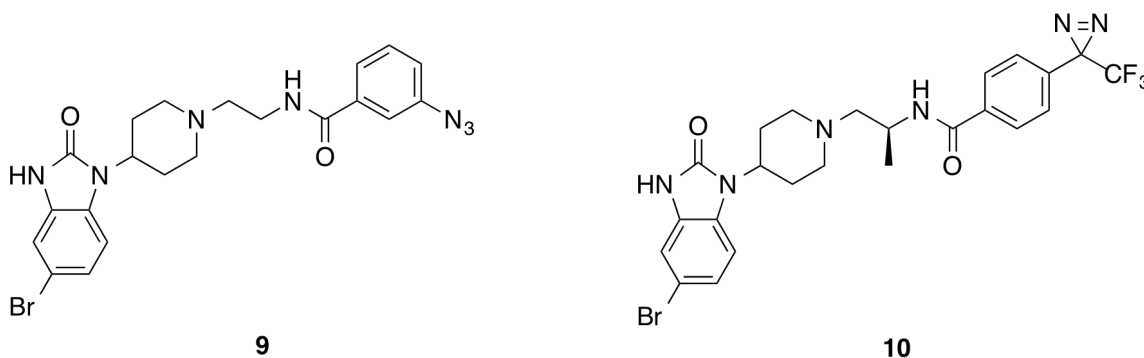
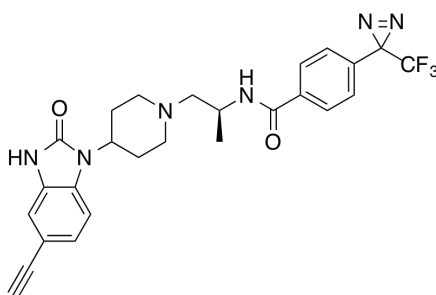


Figure 7. Chemical structures of azide **9** and diazirine **10**-containing photoprobes.

It is possible that the photoprobe is breaking off of the labeled peptide before analysis in the mass spectrometer. Even if this were true for the nitrogen-containing bond formed by compound **9**, the carbon-containing bond formed by **10** should remedy this issue. It may also simply be the case that we have not sequence covered the amino acid(s) labeled by the photoprobe; however, this seems unlikely because we have covered almost 100% of PLD1c.d311 (over multiple samples). Finally, a more simple and concerning issue may have to do with the chromatography and not the MS/MS analysis itself. The probe itself elutes off of the column used for the trypsin-digested protein sample toward the end of a long LC run. This may be a serious issue because if the already quite hydrophobic probe is adducted to a large, hydrophobic peptide the labeled peptide may never even come off of the column. In that case, the adducted peptide would never be injected into the mass spectrometer. In an attempt to remedy this Kristie has modified the chromatography to much more aggressively elute nonpolar compounds, and those experiments are being performed at the time of this writing.

I thought of an alternative approach to labeling and possibly identifying/isolating a compound labeled peptide based on an application of click chemistry. Unfortunately, it appeared the incorporation of an alkyne into the diazirine-containing photoprobe, as in compound **11**, caused essentially a complete loss of inhibitory activity (**Figure 8**). Had this compound maintained some level of potency I would have used it to “click” (copper-catalyzed 1-4 dipolar azide-alkyne cycloaddition) on any number of commercially available azide-containing compounds, which I would then be able to detect in various ways. Initially, I planned to use an azide-biotin compound and simply do a western blot using a streptavidin-HRP conjugate to determine if the PLD protein had been covalently labeled with the alkyne-containing photoprobe. Then, it may have been possible to pull out a labeled peptide containing the peptide-photoprobe-biotin conjugate and identify it via MS/MS. Clearly, an area of future work could be to explore the tolerance for an alkyne on different regions of compounds like **11** in an effort to pursue this click chemistry approach. This approach of using a clickable photoprobe has been used before and an excellent, recent example from the Cravatt lab was recently published in *Nature Methods* (Hulce et al., 2013).



11

Figure 8. Chemical structure of alkyne-containing photoprobe **11**.

In summary, the body of work described herein has resulted in the identification of key structure activity relationships that allowed for the chemical synthesis of drug-like, small molecule, isoform-selective PLD inhibitors. These compounds have been and continue to be used as chemical probes with which to study the various signaling roles of PLD acting in concert with proteins such as mTOR and Akt. Additionally, the SAR described herein allowed for the development of both azide and diazirine-containing photoactivatable probes. Even though the biology of PLD has been studied for decades targeted pharmacological modulation of PLD has only recently become possible.

COPYRIGHT PERMISSIONS

Significant portions of this dissertation are based on work that was published in the four journal articles listed below. Each journal's policy explicitly allows for the reproduction, in part or in full, of published articles as part of a dissertation. In addition to this explicit permission the formal permission for reuse from each publisher is included on the following pages:

Reproduced in part with permission from Selvy, P.E., Lavieri, R.R., Lindsley, C.W., Brown, H.A. Phospholipase D: Enzymology, Functionality, and Chemical Modulation. *Chemical Reviews*. **2011**, *111*, 6064-6119. Copyright 2011 American Chemical Society. <http://pubs.acs.org/doi/abs/10.1021/cr200296t>

Reproduced in part with permission from Lavieri, R.R., Scott, S.A., Selvy, P.E., Kim, K., Jadhav, S., Morrison, R.D., Daniels, J.S., Brown, H.A., Lindsley, C.W. Design, Synthesis and Biological Evaluation of Halogenated N-(2-(4-oxo-1-phenyl-1,3,8-triazaspiro[4.5]decan-8-yl)ethyl)benzamides: Discovery of an Isoform-Selective Small Molecule Phospholipase D2 (PLD2) Inhibitor. *Journal of Medicinal Chemistry*. **2010**, *53*, 6706-6719. Copyright 2010 American Chemical Society. <http://pubs.acs.org/doi/abs/10.1021/jm100814g>

Reproduced in part with permission from Lavieri, R.R., Scott, S.A., Lewis, J.A., Selvy, P.E., Armstrong, M.D., Brown, H.A., Lindsley, C.W. Design and synthesis of isoform-selective phospholipase D (PLD) inhibitors. Part II: Identification of the 1,3,8-triazaspiro[4.5]decan-4-one privileged structure that engenders PLD2 selectivity. *Bioorganic & Medicinal Chemistry Letters*. **2009**, *19*, 2240-2243. Copyright 2009 Elsevier Ltd. <http://www.sciencedirect.com/science/article/pii/S0960894X09002467>

Reproduced in part with permission from Lewis, J.A., Scott, S.A., **Lavieri, R.R.**, Buck, J.R., Selvy, P.E., Stoops, S.L., Armstrong, M.D., Brown, H.A., Lindsley, C.W. Design and synthesis of isoform-selective phospholipase D (PLD) inhibitors. Part I: Impact of alternative halogenated privileged structures for PLD1 specificity. *Bioorganic & Medicinal Chemistry Letters*. **2009**, *19*, 1916-1920. Copyright 2009 Elsevier Ltd. <http://www.sciencedirect.com/science/article/pii/S0960894X0900211X>



Title: Phospholipase D: Enzymology, Functionality, and Chemical Modulation

Author: Paige E. Selvy, Robert R. Lavieri, Craig W. Lindsley, and H. Alex Brown

Publication: Chemical Reviews

Publisher: American Chemical Society

Date: Oct 1, 2011

Copyright © 2011, American Chemical Society

Logged in as:
Robert Lavieri

[LOGOUT](#)

PERMISSION/LICENSE IS GRANTED FOR YOUR ORDER AT NO CHARGE

This type of permission/license, instead of the standard Terms & Conditions, is sent to you because no fee is being charged for your order. Please note the following:

- Permission is granted for your request in both print and electronic formats, and translations.
- If figures and/or tables were requested, they may be adapted or used in part.
- Please print this page for your records and send a copy of it to your publisher/graduate school.
- Appropriate credit for the requested material should be given as follows: "Reprinted (adapted) with permission from (COMPLETE REFERENCE CITATION). Copyright (YEAR) American Chemical Society." Insert appropriate information in place of the capitalized words.
- One-time permission is granted only for the use specified in your request. No additional uses are granted (such as derivative works or other editions). For any other uses, please submit a new request.

[BACK](#)

[CLOSE WINDOW](#)

**Title:**

Design, Synthesis, and Biological Evaluation of Halogenated N-(2-(4-Oxo-1-phenyl-1,3,8-triazaspiro[4.5]decan-8-yl)ethyl)benzamides: Discovery of an Isoform-Selective Small Molecule Phospholipase D2 Inhibitor

Author:

Robert R. Lavieri, Sarah A. Scott, Paige E. Selvy, Kwangho Kim, Satyawant Jadhav, Ryan D. Morrison, J. Scott Daniels, H. Alex Brown, and Craig W. Lindsley

Publication: Journal of Medicinal Chemistry

Publisher: American Chemical Society

Date: Sep 1, 2010

Copyright © 2010, American Chemical Society

Logged in as:
Robert Lavieri

LOGOUT

PERMISSION/LICENSE IS GRANTED FOR YOUR ORDER AT NO CHARGE

This type of permission/license, instead of the standard Terms & Conditions, is sent to you because no fee is being charged for your order. Please note the following:

- Permission is granted for your request in both print and electronic formats, and translations.
- If figures and/or tables were requested, they may be adapted or used in part.
- Please print this page for your records and send a copy of it to your publisher/graduate school.
- Appropriate credit for the requested material should be given as follows: "Reprinted (adapted) with permission from (COMPLETE REFERENCE CITATION). Copyright (YEAR) American Chemical Society." Insert appropriate information in place of the capitalized words.
- One-time permission is granted only for the use specified in your request. No additional uses are granted (such as derivative works or other editions). For any other uses, please submit a new request.

BACK

CLOSE WINDOW



Title: Design and synthesis of isoform-selective phospholipase D (PLD) inhibitors. Part II. Identification of the 1,3,8-triazaspiro[4,5]decan-4-one privileged structure that engenders PLD2 selectivity

Author: Robert Lavieri, Sarah A. Scott, Jana A. Lewis, Paige E. Selvy, Michelle D. Armstrong, H. Alex Brown, Craig W. Lindsley

Publication: Bioorganic & Medicinal Chemistry Letters

Publisher: Elsevier

Date: 15 April 2009

Copyright © 2009 Elsevier Ltd. All rights reserved.

Logged in as:
Robert Lavieri

LOGOUT

Order Completed

Thank you very much for your order.

This is a License Agreement between Robert R Lavieri ("You") and Elsevier ("Elsevier"). The license consists of your order details, the terms and conditions provided by Elsevier, and the [payment terms and conditions](#).

[Get the printable license.](#)

License Number	3440970640194
License date	Aug 02, 2014
Licensed content publisher	Elsevier
Licensed content publication	Bioorganic & Medicinal Chemistry Letters
Licensed content title	Design and synthesis of isoform-selective phospholipase D (PLD) inhibitors. Part II. Identification of the 1,3,8-triazaspiro[4,5]decan-4-one privileged structure that engenders PLD2 selectivity
Licensed content author	Robert Lavieri, Sarah A. Scott, Jana A. Lewis, Paige E. Selvy, Michelle D. Armstrong, H. Alex Brown, Craig W. Lindsley
Licensed content date	15 April 2009
Licensed content volume number	19
Licensed content issue number	8
Number of pages	4
Type of Use	reuse in a thesis/dissertation
Portion	full article
Format	both print and electronic
Are you the author of this Elsevier article?	Yes
Will you be translating?	No
Title of your thesis/dissertation	SYNTHESIS, DEVELOPMENT AND BIOCHEMICAL CHARACTERIZATION OF SMALL-MOLECULE, ISOFORM-SELECTIVE PHOSPHOLIPASE D INHIBITORS AND PHOTOACTIVATABLE PROBES
Expected completion date	Oct 2014
Estimated size (number of pages)	200
Elsevier VAT number	GB 494 6272 12
Permissions price	0.00 USD
VAT/Local Sales Tax	0.00 USD / 0.00 GBP
Total	0.00 USD

ORDER MORE...

CLOSE WINDOW

Copyright © 2014 [Copyright Clearance Center, Inc.](#) All Rights Reserved. [Privacy statement.](#)
Comments? We would like to hear from you. E-mail us at customer@copyright.com



Title: Design and synthesis of isoform-selective phospholipase D (PLD) inhibitors. Part I: Impact of alternative halogenated privileged structures for PLD1 specificity

Author: Jana A. Lewis, Sarah A. Scott, Robert Lavieri, Jason R. Buck, Paige E. Selvy, Sydney L. Stoops, Michelle D. Armstrong, H. Alex Brown, Craig W. Lindsley

Publication: Bioorganic & Medicinal Chemistry Letters

Publisher: Elsevier

Date: 1 April 2009

Copyright © 2009 Elsevier Ltd. All rights reserved.

Logged in as:
Robert Lavieri

[LOGOUT](#)

Order Completed

Thank you very much for your order.

This is a License Agreement between Robert R Lavieri ("You") and Elsevier ("Elsevier"). The license consists of your order details, the terms and conditions provided by Elsevier, and the [payment terms and conditions](#).

[Get the printable license.](#)

License Number	3440970393052
License date	Aug 02, 2014
Licensed content publisher	Elsevier
Licensed content publication	Bioorganic & Medicinal Chemistry Letters
Licensed content title	Design and synthesis of isoform-selective phospholipase D (PLD) inhibitors. Part I: Impact of alternative halogenated privileged structures for PLD1 specificity
Licensed content author	Jana A. Lewis, Sarah A. Scott, Robert Lavieri, Jason R. Buck, Paige E. Selvy, Sydney L. Stoops, Michelle D. Armstrong, H. Alex Brown, Craig W. Lindsley
Licensed content date	1 April 2009
Licensed content volume number	19
Licensed content issue number	7
Number of pages	5
Type of Use	reuse in a thesis/dissertation
Portion	full article
Format	both print and electronic
Are you the author of this Elsevier article?	Yes
Will you be translating?	No
Title of your thesis/dissertation	SYNTHESIS, DEVELOPMENT AND BIOCHEMICAL CHARACTERIZATION OF SMALL-MOLECULE, ISOFORM-SELECTIVE PHOSPHOLIPASE D INHIBITORS AND PHOTOACTIVATABLE PROBES
Expected completion date	Oct 2014
Estimated size (number of pages)	200
Elsevier VAT number	GB 494 6272 12
Permissions price	0.00 USD
VAT/Local Sales Tax	0.00 USD / 0.00 GBP
Total	0.00 USD

[ORDER MORE...](#)

[CLOSE WINDOW](#)

Copyright © 2014 [Copyright Clearance Center, Inc.](#) All Rights Reserved. [Privacy statement.](#)
Comments? We would like to hear from you. E-mail us at customer@copyright.com

REFERENCES

- Abergel, C., Abousalham, A., Chenivresse, S., Riviere, M., Moustacas-Gardies, A. M., and Verger, R. (2001). Crystallization and preliminary crystallographic study of a recombinant phospholipase D from cowpea (*Vigna unguiculata* L. Walp). *Acta Crystallogr D Biol Crystallogr* 57, 320-322.
- Agwu, D. E., McPhail, L. C., Sozzani, S., Bass, D. A., and McCall, C. E. (1991). Phosphatidic acid as a second messenger in human polymorphonuclear leukocytes. Effects on activation of NADPH oxidase. *Journal of Clinical Investigation* 88, 531-539.
- Ahn, B. H., Rhim, H., Kim, S. Y., Sung, Y. M., Lee, M. Y., Choi, J. Y., Wolozin, B., Chang, J. S., Lee, Y. H., Kwon, T. K., *et al.* (2002). alpha-Synuclein interacts with phospholipase D isozymes and inhibits pervanadate-induced phospholipase D activation in human embryonic kidney-293 cells. *J Biol Chem* 277, 12334-12342.
- Andrews, B., Bond, K., Lehman, J. A., Horn, J. M., Dugan, A., and Gomez-Cambronero, J. (2000). Direct inhibition of in vitro PLD activity by 4-(2-aminoethyl)-benzenesulfonyl fluoride. *Biochem Biophys Res Commun* 273, 302-311.
- Aoki, J., Taira, A., Takanezawa, Y., Kishi, Y., Hama, K., Kishimoto, T., Mizuno, K., Saku, K., Taguchi, R., and Arai, H. (2002). Serum lysophosphatidic acid is produced through diverse phospholipase pathways. *J Biol Chem* 277, 48737-48744.
- Arous, C., Naimi, M., and Van Obberghen, E. (2011). Oleate-mediated activation of phospholipase D and mammalian target of rapamycin (mTOR) regulates proliferation and rapamycin sensitivity of hepatocarcinoma cells. *Diabetologia*.
- Athenstaedt, K., and Daum, G. (1999). Phosphatidic acid, a key intermediate in lipid metabolism. *Eur J Biochem* 266, 1-16.
- Athenstaedt, K., Weys, S., Paltauf, F., and Daum, G. (1999). Redundant systems of phosphatidic acid biosynthesis via acylation of glycerol-3-phosphate or dihydroxyacetone phosphate in the yeast *Saccharomyces cerevisiae*. *J Bacteriol* 181, 1458-1463.
- Avila-Flores, A., Santos, T., Rincon, E., and Merida, I. (2005). Modulation of the mammalian target of rapamycin pathway by diacylglycerol kinase-produced phosphatidic acid. *J Biol Chem* 280, 10091-10099.
- Babior, B. M., Lambeth, J. D., and Nauseef, W. (2002). The neutrophil NADPH oxidase. *Arch Biochem Biophys* 397, 342-344.
- Bacac, M., and Stamenkovic, I. (2008). Metastatic cancer cell. *Annu Rev Pathol* 3, 221-247.
- Bai, X., Cerimele, F., Ushio-Fukai, M., Waqas, M., Campbell, P. M., Govindarajan, B., Der, C. J., Battle, T., Frank, D. A., Ye, K., *et al.* (2003). Honokiol, a small molecular

weight natural product, inhibits angiogenesis in vitro and tumor growth in vivo. *J Biol Chem* 278, 35501-35507.

Bhattacharya, M., Babwah, A. V., Godin, C., Anborgh, P. H., Dale, L. B., Poulter, M. O., and Ferguson, S. S. (2004). Ral and phospholipase D2-dependent pathway for constitutive metabotropic glutamate receptor endocytosis. *J Neurosci* 24, 8752-8761.

Blaskovich, M. A., Yendluri, V., Lawrence, H. R., Lawrence, N. J., Sebti, S. M., and Springett, G. M. (2013). Lysophosphatidic acid acyltransferase beta regulates mTOR signaling. *PLoS One* 8, e78632.

Bonifacino, J. S., and Glick, B. S. (2004). The mechanisms of vesicle budding and fusion. *Cell* 116, 153-166.

Borgna, J. L., and Rochefort, H. (1981). Hydroxylated metabolites of tamoxifen are formed in vivo and bound to estrogen receptor in target tissues. *J Biol Chem* 256, 859-868.

Boureaux, A., Vignal, E., Faure, S., and Fort, P. (2007). Evolution of the Rho family of ras-like GTPases in eukaryotes. *Mol Biol Evol* 24, 203-216.

Brown, F. D., Thompson, N., Saqib, K. M., Clark, J. M., Powner, D., Thompson, N. T., Solari, R., and Wakelam, M. J. (1998). Phospholipase D1 localises to secretory granules and lysosomes and is plasma-membrane translocated on cellular stimulation. *Curr Biol* 8, 835-838.

Brown, H. A. (2007). Biochemical analysis of phospholipase D. *Methods Enzymol* 434, 49-87.

Brown, H. A., Gutowski, S., Kahn, R. A., and Sternweis, P. C. (1995). Partial purification and characterization of Arf-sensitive phospholipase D from porcine brain. *J Biol Chem* 270, 14935-14943.

Brown, H. A., Gutowski, S., Moomaw, C. R., Slaughter, C., and Sternweis, P. C. (1993). ADP-ribosylation factor, a small GTP-dependent regulatory protein, stimulates phospholipase D activity. *Cell* 75, 1137-1144.

Brown, H. A., Henage, L. G., Preininger, A. M., Xiang, Y., and Exton, J. H. (2007). Biochemical analysis of phospholipase D. *Methods Enzymol* 434, 49-87.

Brunner, G., Zalkow, L., Burgess, E., Rifkin, D. B., Wilson, E. L., Gruszecka-Kowalik, E., and Powis, G. (1996). Inhibition of glycosylphosphatidylinositol (GPI) phospholipase D by suramin-like compounds. *Anticancer Res* 16, 2513-2516.

Buchanan, F. G., McReynolds, M., Couvillon, A., Kam, Y., Holla, V. R., Dubois, R. N., and Exton, J. H. (2005). Requirement of phospholipase D1 activity in H-RasV12-induced transformation. *Proc Natl Acad Sci U S A* 102, 1638-1642.

- Burch, J., McKenna, C., Palmer, S., Norman, G., Glanville, J., Sculpher, M., and Woolacott, N. (2009). Rimonabant for the treatment of overweight and obese people. *Health Technol Assess 13 Suppl 3*, 13-22.
- Buser, C. A., and McLaughlin, S. (1998). Ultracentrifugation technique for measuring the binding of peptides and proteins to sucrose-loaded phospholipid vesicles. *Methods Mol Biol 84*, 267-281.
- Cai, S., and Exton, J. H. (2001). Determination of interaction sites of phospholipase D1 for RhoA. *Biochem J 355*, 779-785.
- Campa, F., and Randazzo, P. A. (2008). Arf GTPase-activating proteins and their potential role in cell migration and invasion. *Cell Adh Migr 2*, 258-262.
- Cao, J. X., Koop, B. F., and Upton, C. (1997). A human homolog of the vaccinia virus HindIII K4L gene is a member of the phospholipase D superfamily. *Virus Res 48*, 11-18.
- Carman, G. M., Deems, R. A., and Dennis, E. A. (1995). Lipid signaling enzymes and surface dilution kinetics. *J Biol Chem 270*, 18711-18714.
- Carnero, A., Cuadrado, A., del Peso, L., and Lacal, J. C. (1994). Activation of type D phospholipase by serum stimulation and ras-induced transformation in NIH3T3 cells. *Oncogene 9*, 1387-1395.
- Chalasanani, N., Vuppalanchi, R., Raikwar, N. S., and Deeg, M. A. (2006). Glycosylphosphatidylinositol-specific phospholipase d in nonalcoholic Fatty liver disease: a preliminary study. *J Clin Endocrinol Metab 91*, 2279-2285.
- Chen, J. S., and Exton, J. H. (2004). Regulation of phospholipase D2 activity by protein kinase C alpha. *J Biol Chem 279*, 22076-22083.
- Chen, J. S., and Exton, J. H. (2005). Sites on phospholipase D2 phosphorylated by PKCalpha. *Biochem Biophys Res Commun 333*, 1322-1326.
- Chen, Y., Rodrik, V., and Foster, D. A. (2005). Alternative phospholipase D/mTOR survival signal in human breast cancer cells. *Oncogene 24*, 672-679.
- Chen, Y., Zheng, Y., and Foster, D. A. (2003). Phospholipase D confers rapamycin resistance in human breast cancer cells. *Oncogene 22*, 3937-3942.
- Chen, Y. G., Siddhanta, A., Austin, C. D., Hammond, S. M., Sung, T. C., Frohman, M. A., Morris, A. J., and Shields, D. (1997). Phospholipase D stimulates release of nascent secretory vesicles from the trans-Golgi network. *J Cell Biol 138*, 495-504.
- Choi, S. Y., Huang, P., Jenkins, G. M., Chan, D. C., Schiller, J., and Frohman, M. A. (2006). A common lipid links Mfn-mediated mitochondrial fusion and SNARE-regulated exocytosis. *Nat Cell Biol 8*, 1255-1262.

Chu, M., Patel, M. G., Pai, J.-K., Das, P. R., and Puar, M. S. (1996). Sch 53823 and Sch 53825, novel fungal metabolites with phospholipase D inhibitory activity. *Bioorganic & medicinal chemistry letters* *6*, 579-584.

Chu, M., Truumees, I., Patel, M. G., Gullo, V. P., Pai, J.-K., Das, P. R., and Puar, M. S. (1994). Two new phospholipase d inhibitors, sch 49211 and sch 49212, produced by the fungus *nattrasia mangirferae*. *Bioorganic & medicinal chemistry letters* *4*, 1539-1542.

Clair, T., Aoki, J., Koh, E., Bandle, R. W., Nam, S. W., Ptaszynska, M. M., Mills, G. B., Schiffmann, E., Liotta, L. A., and Stracke, M. L. (2003). Autotaxin hydrolyzes sphingosylphosphorylcholine to produce the regulator of migration, sphingosine-1-phosphate. *Cancer Res* *63*, 5446-5453.

Clair, T., Lee, H. Y., Liotta, L. A., and Stracke, M. L. (1997). Autotaxin is an exoenzyme possessing 5'-nucleotide phosphodiesterase/ATP pyrophosphatase and ATPase activities. *J Biol Chem* *272*, 996-1001.

Clark, A. M., El-Feraly, F. S., and Li, W. S. (1981). Antimicrobial activity of phenolic constituents of *Magnolia grandiflora* L. *J Pharm Sci* *70*, 951-952.

Clevers, H. (2006). Wnt/beta-catenin signaling in development and disease. *Cell* *127*, 469-480.

Cockcroft, S., Thomas, G. M., Fensome, A., Geny, B., Cunningham, E., Gout, I., Hiles, I., Totty, N. F., Truong, O., and Hsuan, J. J. (1994). Phospholipase D: a downstream effector of ARF in granulocytes. *Science* *263*, 523-526.

Cozy, E., Borgna, J. L., and Rochefort, H. (1982). Tamoxifen and metabolites in MCF7 cells: correlation between binding to estrogen receptor and inhibition of cell growth. *Cancer Res* *42*, 317-323.

Colley, W. C., Sung, T. C., Roll, R., Jenco, J., Hammond, S. M., Altshuller, Y., Bar-Sagi, D., Morris, A. J., and Frohman, M. A. (1997). Phospholipase D2, a distinct phospholipase D isoform with novel regulatory properties that provokes cytoskeletal reorganization. *Curr Biol* *7*, 191-201.

Cox, D. A., and Cohen, M. L. (1997). Amyloid beta-induced neurotoxicity is associated with phospholipase D activation in cultured rat hippocampal cells. *Neurosci Lett* *229*, 37-40.

Cuevas, W. A., and Songer, J. G. (1993). *Arcanobacterium haemolyticum* phospholipase D is genetically and functionally similar to *Corynebacterium pseudotuberculosis* phospholipase D. *Infect Immun* *61*, 4310-4316.

Cummings, R., Parinandi, N., Wang, L., Usatyuk, P., and Natarajan, V. (2002). Phospholipase D/phosphatidic acid signal transduction: role and physiological significance in lung. *Mol Cell Biochem* *234-235*, 99-109.

- Dall'armi, C., Hurtado-Lorenzo, A., Tian, H., Morel, E., Nezu, A., Chan, R. B., Yu, W. H., Robinson, K. S., Yeku, O., Small, S. A., *et al.* (2010). The phospholipase D1 pathway modulates macroautophagy. *Nat Commun* *1*, 142.
- Davies, D. R., Interthal, H., Champoux, J. J., and Hol, W. G. (2002a). Insights into substrate binding and catalytic mechanism of human tyrosyl-DNA phosphodiesterase (Tdp1) from vanadate and tungstate-inhibited structures. *J Mol Biol* *324*, 917-932.
- Davies, D. R., Interthal, H., Champoux, J. J., and Hol, W. G. (2002b). The crystal structure of human tyrosyl-DNA phosphodiesterase, Tdp1. *Structure* *10*, 237-248.
- Davies, D. R., Interthal, H., Champoux, J. J., and Hol, W. G. (2003). Crystal structure of a transition state mimic for Tdp1 assembled from vanadate, DNA, and a topoisomerase I-derived peptide. *Chem Biol* *10*, 139-147.
- de Giuseppe, P. O., Ullah, A., Silva, D. T., Gremski, L. H., Wille, A. C., Chaves Moreira, D., Ribeiro, A. S., Chaim, O. M., Murakami, M. T., Veiga, S. S., and Arni, R. K. (2011). Structure of a novel class II phospholipase D: catalytic cleft is modified by a disulphide bridge. *Biochem Biophys Res Commun* *409*, 622-627.
- Deeg, M. A., Bowen, R. F., Williams, M. D., Olson, L. K., Kirk, E. A., and LeBoeuf, R. C. (2001). Increased expression of GPI-specific phospholipase D in mouse models of type 1 diabetes. *Am J Physiol Endocrinol Metab* *281*, E147-154.
- Deeg, M. A., Raikwar, N. S., Johnson, C., and Williams, C. D. (2007). Statin therapy reduces serum levels of glycosylphosphatidylinositol-specific phospholipase D. *Transl Res* *150*, 153-157.
- Deems, R. A. (2000). Interfacial enzyme kinetics at the phospholipid/water interface: practical considerations. *Anal Biochem* *287*, 1-16.
- Dharmalingam, K., and Jayaraman, J. (1971). Mechanism of glucose repression of mitochondriogenesis: induction of phospholipases. *Biochem Biophys Res Commun* *45*, 1115-1118.
- Di Fulvio, M., Frondorf, K., Henkels, K. M., Lehman, N., and Gomez-Cambronero, J. (2007). The Grb2/PLD2 interaction is essential for lipase activity, intracellular localization and signaling in response to EGF. *J Mol Biol* *367*, 814-824.
- Disse, J., Vitale, N., Bader, M.-F., and Gerke, V. (2009). Phospholipase D1 is specifically required for regulated secretion of von Willebrand factor from endothelial cells. *Blood* *113*, 973-980.
- Diwu, Z., Zimmermann, J., Meyer, T., and Lown, J. W. (1994). Design, synthesis and investigation of mechanisms of action of novel protein kinase C inhibitors: perylenequinonoid pigments. *Biochem Pharmacol* *47*, 373-385.

- Doti, N., Cassese, A., Marasco, D., Paturzo, F., Sabatella, M., Viparelli, F., Dathan, N., Monti, S. M., Miele, C., Formisano, P., *et al.* (2010). Residues 762-801 of PLD1 mediate the interaction with PED/PEA15. *Mol Biosyst* *6*, 2039-2048.
- Du, G., Altshuler, Y. M., Vitale, N., Huang, P., Chasserot-Golaz, S., Morris, A. J., Bader, M. F., and Frohman, M. A. (2003). Regulation of phospholipase D1 subcellular cycling through coordination of multiple membrane association motifs. *J Cell Biol* *162*, 305-315.
- Du, G., Huang, P., Liang, B. T., and Frohman, M. A. (2004). Phospholipase D2 localizes to the plasma membrane and regulates angiotensin II receptor endocytosis. *Mol Biol Cell* *15*, 1024-1030.
- Dubinsky, L., Krom, B. P., and Meijler, M. M. (2012). Diazirine based photoaffinity labeling. *Bioorg Med Chem* *20*, 554-570.
- Eisen, S. F., and Brown, H. A. (2002). Selective estrogen receptor (ER) modulators differentially regulate phospholipase D catalytic activity in ER-negative breast cancer cells. *Mol Pharmacol* *62*, 911-920.
- Elias, M., Potocky, M., Cvrckova, F., and Zarsky, V. (2002). Molecular diversity of phospholipase D in angiosperms. *BMC Genomics* *3*, 2.
- Ella, K. M., Dolan, J. W., and Meier, K. E. (1995). Characterization of a regulated form of phospholipase D in the yeast *Saccharomyces cerevisiae*. *Biochem J* *307* (Pt 3), 799-805.
- Ella, K. M., Dolan, J. W., Qi, C., and Meier, K. E. (1996). Characterization of *Saccharomyces cerevisiae* deficient in expression of phospholipase D. *Biochem J* *314* (Pt 1), 15-19.
- Elvers, M., Stegner, D., Hagedorn, I., Kleinschnitz, C., Braun, A., Kuijpers, M. E., Boesl, M., Chen, Q., Heemskerk, J. W., Stoll, G., *et al.* (2010). Impaired alpha(IIb)beta(3) integrin activation and shear-dependent thrombus formation in mice lacking phospholipase D1. *Sci Signal* *3*, ra1.
- Fang, Y., Vilella-Bach, M., Bachmann, R., Flanigan, A., and Chen, J. (2001). Phosphatidic acid-mediated mitogenic activation of mTOR signaling. *Science* *294*, 1942-1945.
- Fisher, G. J., Henderson, P. A., Voorhees, J. J., and Baldassare, J. J. (1991). Epidermal growth factor-induced hydrolysis of phosphatidylcholine by phospholipase D and phospholipase C in human dermal fibroblasts. *Journal of Cellular Physiology* *146*, 309-317.
- Foster, D. A. (2009). Phosphatidic acid signaling to mTOR: signals for the survival of human cancer cells. *Biochim Biophys Acta* *1791*, 949-955.

- Foster, D. A., and Xu, L. (2003). Phospholipase D in cell proliferation and cancer. *Mol Cancer Res* 1, 789-800.
- Frankel, P., Ramos, M., Flom, J., Bychenok, S., Joseph, T., Kerkhoff, E., Rapp, U. R., Feig, L. A., and Foster, D. A. (1999). Ral and Rho-dependent activation of phospholipase D in v-Raf-transformed cells. *Biochem Biophys Res Commun* 255, 502-507.
- Futrell, J. M. (1992). Loxoscelism. *Am J Med Sci* 304, 261-267.
- Garcia, A., Zheng, Y., Zhao, C., Toschi, A., Fan, J., Shraibman, N., Brown, H. A., Bar-Sagi, D., Foster, D. A., and Arbiser, J. L. (2008). Honokiol suppresses survival signals mediated by Ras-dependent phospholipase D activity in human cancer cells. *Clinical Cancer Research* 14, 4267-4274.
- Ghosh, S., Moore, S., Bell, R. M., and Dush, M. (2003). Functional analysis of a phosphatidic acid binding domain in human Raf-1 kinase: mutations in the phosphatidate binding domain lead to tail and trunk abnormalities in developing zebrafish embryos. *J Biol Chem* 278, 45690-45696.
- Ghosh, S., Strum, J. C., Sciorra, V. A., Daniel, L., and Bell, R. M. (1996). Raf-1 kinase possesses distinct binding domains for phosphatidylserine and phosphatidic acid. Phosphatidic acid regulates the translocation of Raf-1 in 12-O-tetradecanoylphorbol-13-acetate-stimulated Madin-Darby canine kidney cells. *J Biol Chem* 271, 8472-8480.
- Gibellini, F., and Smith, T. K. (2010). The Kennedy pathway--De novo synthesis of phosphatidylethanolamine and phosphatidylcholine. *IUBMB Life* 62, 414-428.
- Gorentla, B. K., Wan, C. K., and Zhong, X. P. (2011). Negative regulation of mTOR activation by diacylglycerol kinases. *Blood* 117, 4022-4031.
- Gottlin, E. B., Rudolph, A. E., Zhao, Y., Matthews, H. R., and Dixon, J. E. (1998). Catalytic mechanism of the phospholipase D superfamily proceeds via a covalent phosphohistidine intermediate. *Proc Natl Acad Sci U S A* 95, 9202-9207.
- Grossman, S., Cogley, J., Hogue, P. K., Kearney, E. B., and Singer, T. P. (1973). Relation of phospholipase D activity to the decay of succinate dehydrogenase and of covalently bound flavin in yeast cells undergoing glucose repression. *Arch Biochem Biophys* 158, 744-753.
- Gruchalla, R. S., Dinh, T. T., and Kennerly, D. A. (1990). An indirect pathway of receptor-mediated 1,2-diacylglycerol formation in mast cells. I. IgE receptor-mediated activation of phospholipase D. *J Immunol* 144, 2334-2342.
- Hammond, S. M., Altshuler, Y. M., Sung, T. C., Rudge, S. A., Rose, K., Engebrecht, J., Morris, A. J., and Frohman, M. A. (1995). Human ADP-ribosylation factor-activated phosphatidylcholine-specific phospholipase D defines a new and highly conserved gene family. *J Biol Chem* 270, 29640-29643.

- Hammond, S. M., Jenco, J. M., Nakashima, S., Cadwallader, K., Gu, Q., Cook, S., Nozawa, Y., Prestwich, G. D., Frohman, M. A., and Morris, A. J. (1997). Characterization of two alternately spliced forms of phospholipase D1. Activation of the purified enzymes by phosphatidylinositol 4,5-bisphosphate, ADP-ribosylation factor, and Rho family monomeric GTP-binding proteins and protein kinase C- α . *J Biol Chem* *272*, 3860-3868.
- Hanahan, D. J., and Chaikoff, I. L. (1947a). A new phospholipide-splitting enzyme specific for the ester linkage between the nitrogenous base and the phosphoric acid grouping. *J Biol Chem* *169*, 699-705.
- Hanahan, D. J., and Chaikoff, I. L. (1947b). The phosphorus-containing lipides of the carrot. *J Biol Chem* *168*, 233-240.
- Hanahan, D. J., and Chaikoff, I. L. (1948). On the nature of the phosphorus-containing lipides of cabbage leaves and their relation to a phospholipide-splitting enzyme contained in these leaves. *J Biol Chem* *172*, 191-198.
- Harkins, A. L., London, S. D., and Dolan, J. W. (2008). An upstream regulator and downstream target of phospholipase D1 activity during pheromone response in *Saccharomyces cerevisiae*. *FEMS Yeast Res* *8*, 237-244.
- Harkins, A. L., Yuan, G., London, S. D., and Dolan, J. W. (2010). An oleate-stimulated, phosphatidylinositol 4,5-bisphosphate-independent phospholipase D in *Schizosaccharomyces pombe*. *FEMS Yeast Res* *10*, 717-726.
- Haslam, R. J., and Coorssen, J. R. (1993). Evidence that activation of phospholipase D can mediate secretion from permeabilized platelets. *Programmed Cell Death in Cancer Progression and Therapy* *344*, 149-164.
- Hatcher, H., Planalp, R., Cho, J., Torti, F. M., and Torti, S. V. (2008). Curcumin: from ancient medicine to current clinical trials. *Cellular and Molecular Life Sciences* *65*, 1631-1652.
- Hegde, V. R., Silver, J., Patel, M. G., Bryant, R., Pai, J., Das, P. R., Puar, M. S., and Cox, P. A. (1995). Phospholipase D inhibitors from a *Myrsine* species. *J Nat Prod* *58*, 1492-1497.
- Henage, L. G., Exton, J. H., and Brown, H. A. (2006). Kinetic analysis of a mammalian phospholipase D: allosteric modulation by monomeric GTPases, protein kinase C, and polyphosphoinositides. *J Biol Chem* *281*, 3408-3417.
- Henkels, K. M., Peng, H. J., Frondorf, K., and Gomez-Cambronero, J. (2010). A comprehensive model that explains the regulation of phospholipase D2 activity by phosphorylation-dephosphorylation. *Mol Cell Biol* *30*, 2251-2263.
- Herbst, R. S. (2004). Review of epidermal growth factor receptor biology. *Int J Radiat Oncol Biol Phys* *59*, 21-26.

- Hodgson, A. L., Bird, P., and Nisbet, I. T. (1990). Cloning, nucleotide sequence, and expression in *Escherichia coli* of the phospholipase D gene from *Corynebacterium pseudotuberculosis*. *J Bacteriol* *172*, 1256-1261.
- Hodgson, A. L., Krywult, J., Corner, L. A., Rothel, J. S., and Radford, A. J. (1992). Rational attenuation of *Corynebacterium pseudotuberculosis*: potential cheesy gland vaccine and live delivery vehicle. *Infect Immun* *60*, 2900-2905.
- Honda, A., Nogami, M., Yokozeki, T., Yamazaki, M., Nakamura, H., Watanabe, H., Kawamoto, K., Nakayama, K., Morris, A. J., Frohman, M. A., and Kanaho, Y. (1999). Phosphatidylinositol 4-phosphate 5-kinase alpha is a downstream effector of the small G protein ARF6 in membrane ruffle formation. *Cell* *99*, 521-532.
- Hong, Y., Zhang, W., and Wang, X. (2010). Phospholipase D and phosphatidic acid signalling in plant response to drought and salinity. *Plant Cell Environ* *33*, 627-635.
- Honigberg, S. M., Conicella, C., and Esposito, R. E. (1992). Commitment to meiosis in *Saccharomyces cerevisiae*: involvement of the SPO14 gene. *Genetics* *130*, 703-716.
- Hu, T., and Exton, J. H. (2003). Mechanisms of regulation of phospholipase D1 by protein kinase Calpha. *J Biol Chem* *278*, 2348-2355.
- Hughes, W. E., and Parker, P. J. (2001). Endosomal localization of phospholipase D 1a and 1b is defined by the C-termini of the proteins, and is independent of activity. *Biochem J* *356*, 727-736.
- Hui, L., Abbas, T., Pielak, R. M., Joseph, T., Bargonetti, J., and Foster, D. A. (2004). Phospholipase D elevates the level of MDM2 and suppresses DNA damage-induced increases in p53. *Molecular and Cellular Biology* *24*, 5677-5686.
- Hui, L., Zheng, Y., Yan, Y., Bargonetti, J., and Foster, D. A. (2006). Mutant p53 in MDA-MB-231 breast cancer cells is stabilized by elevated phospholipase D activity and contributes to survival signals generated by phospholipase D. *Oncogene* *25*, 7305-7310.
- Hulce, J. J., Cognetta, A. B., Niphakis, M. J., Tully, S. E., and Cravatt, B. F. (2013). Proteome-wide mapping of cholesterol-interacting proteins in mammalian cells. *Nat Methods* *10*, 259-264.
- Imamura, F. (1993). Induction of in vitro tumor cell invasion of cellular monolayers by lysophosphatidic acid or phospholipase D. *Biochem Biophys Res Commun* *193*, 497-503.
- Imamura, S., and Horiuti, Y. (1979). Purification of *Streptomyces chromofuscus* phospholipase D by hydrophobic affinity chromatography on palmitoyl cellulose. *J Biochem* *85*, 79-95.
- Jaiyesimi, I. A., Buzdar, A. U., Decker, D. A., and Hortobagyi, G. N. (1995). Use of tamoxifen for breast cancer: twenty-eight years later. *J Clin Oncol* *13*, 513-529.

- Jang, Y. H., Ahn, B. H., Namkoong, S., Kim, Y. M., Jin, J. K., Kim, Y. S., and Min do, S. (2008a). Differential regulation of apoptosis by caspase-mediated cleavage of phospholipase D isozymes. *Cell Signal* 20, 2198-2207.
- Jang, Y. H., Namkoong, S., Kim, Y. M., Lee, S. J., Park, B. J., and Min, D. S. (2008b). Cleavage of phospholipase D1 by caspase promotes apoptosis via modulation of the p53-dependent cell death pathway. *Cell Death Differ* 15, 1782-1793.
- Jenco, J. M., Rawlingson, A., Daniels, B., and Morris, A. J. (1998). Regulation of phospholipase D2: selective inhibition of mammalian phospholipase D isoenzymes by alpha- and beta-synucleins. *Biochemistry* 37, 4901-4909.
- Jin, J. K., Ahn, B. H., Na, Y. J., Kim, J. I., Kim, Y. S., Choi, E. K., Ko, Y. G., Chung, K. C., Kozlowski, P. B., and Min do, S. (2007). Phospholipase D1 is associated with amyloid precursor protein in Alzheimer's disease. *Neurobiol Aging* 28, 1015-1027.
- Jones, D. R., Avila, M. A., Sanz, C., and Varela-Nieto, I. (1997). Glycosyl-phosphatidylinositol-phospholipase type D: a possible candidate for the generation of second messengers. *Biochem Biophys Res Commun* 233, 432-437.
- Jones, D. R., and Varela-Nieto, I. (1998). The role of glycosyl-phosphatidylinositol in signal transduction. *Int J Biochem Cell Biol* 30, 313-326.
- Jordan, V. C., Collins, M. M., Rowsby, L., and Prestwich, G. (1977). A monohydroxylated metabolite of tamoxifen with potent antioestrogenic activity. *J Endocrinol* 75, 305-316.
- Joseph, T., Bryant, A., Frankel, P., Wooden, R., Kerkhoff, E., Rapp, U. R., and Foster, D. A. (2002). Phospholipase D overcomes cell cycle arrest induced by high-intensity Raf signaling. *Oncogene* 21, 3651-3658.
- Kaelin, W. G., Jr. (2007). The von Hippel-Lindau tumor suppressor protein and clear cell renal carcinoma. *Clin Cancer Res* 13, 680s-684s.
- Kam, Y., and Exton, J. H. (2001). Phospholipase D Activity Is Required for Actin Stress Fiber Formation in Fibroblasts. *Mol Cell Biol* 21, 4055-4066.
- Kanfer, J. N., Singh, I. N., Pettegrew, J. W., McCartney, D. G., and Sorrentino, G. (1996). Phospholipid metabolism in Alzheimer's disease and in a human cholinergic cell. *J Lipid Mediat Cell Signal* 14, 361-363.
- Kang, D. W., Choi, K. Y., and Min, D. S. (2011). Phospholipase D Meets Wnt Signaling: A New Target for Cancer Therapy. *Cancer Res*.
- Kang, D. W., Lee, J. Y., Oh, D. H., Park, S. Y., Woo, T. M., Kim, M. K., Park, M. H., Jang, Y. H., and Min do, S. (2009). Triptolide-induced suppression of phospholipase D expression inhibits proliferation of MDA-MB-231 breast cancer cells. *Experimental and Molecular Medicine* 41, 678-685.

Kang, D. W., Lee, S. H., Yoon, J. W., Park, W. S., Choi, K. Y., and Min do, S. (2010). Phospholipase D1 drives a positive feedback loop to reinforce the Wnt/beta-catenin/TCF signaling axis. *Cancer Res* 70, 4233-4242.

Kang, D. W., and Min do, S. (2010). Positive feedback regulation between phospholipase D and Wnt signaling promotes Wnt-driven anchorage-independent growth of colorectal cancer cells. *PLoS One* 5, e12109.

Kato, Y. (2005). Acidic extracellular pH induces matrix metalloproteinase-9 expression in mouse metastatic melanoma cells through the phospholipase D-mitogen-activated protein kinase signaling. *J Biol Chem* 280, 10938-10944.

Kato, M. (2005). WNT/PCP signaling pathway and human cancer (review). *Oncol Rep* 14, 1583-1588.

Kennedy, E. P. (1958). The biosynthesis of phospholipids. *Am J Clin Nutr* 6, 216-220.

Kim, J. H., Lee, S. D., Han, J. M., Lee, T. G., Kim, Y., Park, J. B., Lambeth, J. D., Suh, P. G., and Ryu, S. H. (1998). Activation of phospholipase D1 by direct interaction with ADP-ribosylation factor 1 and RalA. *FEBS Lett* 430, 231-235.

Kim, Y., Han, J. M., Park, J. B., Lee, S. D., Oh, Y. S., Chung, C., Lee, T. G., Kim, J. H., Park, S. K., Yoo, J. S., *et al.* (1999). Phosphorylation and activation of phospholipase D1 by protein kinase C in vivo: determination of multiple phosphorylation sites. *Biochemistry* 38, 10344-10351.

Kinchen, J. M., Doukoumetzidis, K., Almendinger, J., Stergiou, L., Tosello-Trampont, A., Sifri, C. D., Hengartner, M. O., and Ravichandran, K. S. (2008). A pathway for phagosome maturation during engulfment of apoptotic cells. *Nat Cell Biol* 10, 556-566.

Kishida, M., and Shimoda, C. (1986). Genetic mapping of eleven spo genes essential for ascospore formation in the fission yeast *Schizosaccharomyces pombe*. *Curr Genet* 10, 443-447.

Kiss, Z., and Anderson, W. H. (1997). Inhibition of phorbol ester-stimulated phospholipase D activity by chronic tamoxifen treatment in breast cancer cells. *FEBS Lett* 400, 145-148.

Kitzen, J. J., de Jonge, M. J., Lamers, C. H., Eskens, F. A., van der Biessen, D., van Doorn, L., Ter Steeg, J., Brandely, M., Puozzo, C., and Verweij, J. (2009). Phase I dose-escalation study of F60008, a novel apoptosis inducer, in patients with advanced solid tumours. *European Journal of Cancer* 45, 1764-1772.

Knoepp, S. M., Chahal, M. S., Xie, Y. H., Zhang, Z. H., Brauner, D. J., Hallman, M. A., Robinson, S. A., Han, S. J., Imai, M., Tomlinson, S., and Meier, K. E. (2008). Effects of active and inactive phospholipase D2 on signal transduction, adhesion, migration, invasion, and metastasis in EL4 lymphoma cells. *Molecular Pharmacology* 74, 574-584.

- Kobayashi, M., and Kanfer, J. N. (1987). Phosphatidylethanol formation via transphosphatidylation by rat brain synaptosomal phospholipase D. *J Neurochem* *48*, 1597-1603.
- Koch, T., Brandenburg, L. O., Liang, Y., Schulz, S., Beyer, A., Schroder, H., and Holtt, V. (2004). Phospholipase D2 modulates agonist-induced mu-opioid receptor desensitization and resensitization. *J Neurochem* *88*, 680-688.
- Koch, T., Brandenburg, L. O., Schulz, S., Liang, Y., Klein, J., and Holtt, V. (2003). ADP-ribosylation factor-dependent phospholipase D2 activation is required for agonist-induced mu-opioid receptor endocytosis. *J Biol Chem* *278*, 9979-9985.
- Kohn, A. D., and Moon, R. T. (2005). Wnt and calcium signaling: beta-catenin-independent pathways. *Cell Calcium* *38*, 439-446.
- Kook, S., and Exton, J. H. (2005). Identification of interaction sites of protein kinase Calpha on phospholipase D1. *Cell Signal* *17*, 1423-1432.
- Koonin, E. V. (1996). A duplicated catalytic motif in a new superfamily of phosphohydrolases and phospholipid synthases that includes poxvirus envelope proteins. *Trends Biochem Sci* *21*, 242-243.
- Kruger, R., Kuhn, W., Muller, T., Woitalla, D., Graeber, M., Kosel, S., Przuntek, H., Epplen, J. T., Schols, L., and Riess, O. (1998). Ala30Pro mutation in the gene encoding alpha-synuclein in Parkinson's disease. *Nature Genetics* *18*, 106-108.
- LaLonde, M., Janssens, H., Yun, S., Crosby, J., Redina, O., Olive, V., Altshuller, Y. M., Choi, S. Y., Du, G., Gergen, J. P., and Frohman, M. A. (2006). A role for Phospholipase D in *Drosophila* embryonic cellularization. *BMC Dev Biol* *6*, 60.
- LaLonde, M. M., Janssens, H., Rosenbaum, E., Choi, S. Y., Gergen, J. P., Colley, N. J., Stark, W. S., and Frohman, M. A. (2005). Regulation of phototransduction responsiveness and retinal degeneration by a phospholipase D-generated signaling lipid. *J Cell Biol* *169*, 471-479.
- Lavieri, R., Scott, S. A., Lewis, J. A., Selvy, P. E., Armstrong, M. D., Alex Brown, H., and Lindsley, C. W. (2009). Design and synthesis of isoform-selective phospholipase D (PLD) inhibitors. Part II. Identification of the 1,3,8-triazaspiro[4,5]decan-4-one privileged structure that engenders PLD2 selectivity. *Bioorganic & medicinal chemistry letters* *19*, 2240-2243.
- Lavieri, R. R., Scott, S. A., Selvy, P. E., Kim, K., Jadhav, S., Morrison, R. D., Daniels, J. S., Brown, H. A., and Lindsley, C. W. (2010). Design, synthesis, and biological evaluation of halogenated n-(2-(4-oxo-1-phenyl-1,3,8-triazaspiro[4.5]decan-8-yl)ethyl)benzamides: discovery of an isoform-selective small molecule phospholipase D2 inhibitor. *Journal of Medicinal Chemistry* *53*, 6706-6719.

- Lee, M. J., Oh, J. Y., Park, H. T., Uhlinger, D. J., and Kwak, J. Y. (2001). Enhancement of phospholipase D activity by overexpression of amyloid precursor protein in P19 mouse embryonic carcinoma cells. *Neurosci Lett* *315*, 159-163.
- Lehman, N., Ledford, B., Di Fulvio, M., Frondorf, K., McPhail, L. C., and Gomez-Cambrero, J. (2007). Phospholipase D2-derived phosphatidic acid binds to and activates ribosomal p70 S6 kinase independently of mTOR. *FASEB J* *21*, 1075-1087.
- Leicht, D. T., Balan, V., Kaplun, A., Singh-Gupta, V., Kaplun, L., Dobson, M., and Tzivion, G. (2007). Raf kinases: function, regulation and role in human cancer. *Biochimica Et Biophysica Acta* *1773*, 1196-1212.
- Leiros, I., Hough, E., D'Arrigo, P., Carrea, G., Pedrocchi-Fantoni, G., Secundo, F., and Servi, S. (2000a). Crystallization and preliminary X-ray diffraction studies of phospholipase D from *Streptomyces* sp. *Acta Crystallogr D Biol Crystallogr* *56*, 466-468.
- Leiros, I., McSweeney, S., and Hough, E. (2004). The reaction mechanism of phospholipase D from *Streptomyces* sp. strain PMF. Snapshots along the reaction pathway reveal a pentacoordinate reaction intermediate and an unexpected final product. *J Mol Biol* *339*, 805-820.
- Leiros, I., Secundo, F., Zambonelli, C., Servi, S., and Hough, E. (2000b). The first crystal structure of a phospholipase D. *Structure* *8*, 655-667.
- Leone, M., Crowell, K. J., Chen, J., Jung, D., Chiang, G. G., Sareth, S., Abraham, R. T., and Pellecchia, M. (2006). The FRB domain of mTOR: NMR solution structure and inhibitor design. *Biochemistry* *45*, 10294-10302.
- Leong, S. L., Cappai, R., Barnham, K. J., and Pham, C. L. (2009). Modulation of alpha-synuclein aggregation by dopamine: a review. *Neurochemical Research* *34*, 1838-1846.
- Leung, D., Saghatelian, A., Simon, G. M., and Cravatt, B. F. (2006). Inactivation of N-acyl phosphatidylethanolamine phospholipase D reveals multiple mechanisms for the biosynthesis of endocannabinoids. *Biochemistry* *45*, 4720-4726.
- Levy, B. D. (2005). Novel polyisoprenyl phosphates block phospholipase D and human neutrophil activation in vitro and murine peritoneal inflammation in vivo. *Br J Pharmacol* *146*, 344-351.
- Levy, B. D., Clark, J. M., Wakelam, M. J. O., and Serhan, C. N. (1999). Polyisoprenyl phosphate signaling inhibits phospholipase D: Novel intracellular "stop" signals. *Am J Resp Crit Care* *159*, A188-A188.
- Lewis, J. A., Scott, S. A., Lavieri, R., Buck, J. R., Selvy, P. E., Stoops, S. L., Armstrong, M. D., Brown, H. A., and Lindsley, C. W. (2009). Design and synthesis of isoform-selective phospholipase D (PLD) inhibitors. Part I: Impact of alternative halogenated privileged structures for PLD1 specificity. *Bioorganic & medicinal chemistry letters* *19*, 1916-1920.

- Li, J. Y., Hollfelder, K., Huang, K. S., and Low, M. G. (1994). Structural features of GPI-specific phospholipase D revealed by proteolytic fragmentation and Ca²⁺ binding studies. *J Biol Chem* 269, 28963-28971.
- Li, M., Hong, Y., and Wang, X. (2009). Phospholipase D- and phosphatidic acid-mediated signaling in plants. *Biochim Biophys Acta* 1791, 927-935.
- Liscovitch, M., Chalifa, V., Pertile, P., Chen, C. S., and Cantley, L. C. (1994). Novel function of phosphatidylinositol 4,5-bisphosphate as a cofactor for brain membrane phospholipase D. *J Biol Chem* 269, 21403-21406.
- Liscovitch, M., Czarny, M., Fiucci, G., and Tang, X. (2000). Phospholipase D: molecular and cell biology of a novel gene family. *Biochem J* 345 Pt 3, 401-415.
- Liu, L. X., Spoerke, J. M., Mulligan, E. L., Chen, J., Reardon, B., Westlund, B., Sun, L., Abel, K., Armstrong, B., Hardiman, G., *et al.* (1999). High-throughput isolation of *Caenorhabditis elegans* deletion mutants. *Genome Res* 9, 859-867.
- Liu, M. Y., Gutowski, S., and Sternweis, P. C. (2001). The C terminus of mammalian phospholipase D is required for catalytic activity. *J Biol Chem* 276, 5556-5562.
- Loonen, A. J., Soe-Agnie, C. J., and Soudijn, W. (1981). Effects of halopemide on GABA receptor binding, uptake and release. *Brain Res* 210, 485-492.
- Loonen, A. J. M., and Soudijn, W. (1985). Halopemide, a New Psychotropic Agent - Cerebral Distribution and Receptor Interactions. *Pharmaceutisch Weekblad-Scientific Edition* 7, 1-9.
- Lopez, I., Arnold, R. S., and Lambeth, J. D. (1998). Cloning and initial characterization of a human phospholipase D2 (hPLD2). ADP-ribosylation factor regulates hPLD2. *J Biol Chem* 273, 12846-12852.
- Lucas, E. A., Billington, S. J., Carlson, P., McGee, D. J., and Jost, B. H. (2010). Phospholipase D promotes *Arcanobacterium haemolyticum* adhesion via lipid raft remodeling and host cell death following bacterial invasion. *BMC Microbiol* 10, 270.
- Luo, J. Q., Liu, X., Hammond, S. M., Colley, W. C., Feig, L. A., Frohman, M. A., Morris, A. J., and Foster, D. A. (1997). RalA interacts directly with the Arf-responsive, PIP2-dependent phospholipase D1. *Biochem Biophys Res Commun* 235, 854-859.
- Matthies, D. S., Fleming, P. A., Wilkes, D. M., and Blakely, R. D. (2006). The *Caenorhabditis elegans* choline transporter CHO-1 sustains acetylcholine synthesis and motor function in an activity-dependent manner. *J Neurosci* 26, 6200-6212.
- McCubrey, J. A., Steelman, L. S., Chappell, W. H., Abrams, S. L., Wong, E. W., Chang, F., Lehmann, B., Terrian, D. M., Milella, M., Tafuri, A., *et al.* (2007). Roles of the Raf/MEK/ERK pathway in cell growth, malignant transformation and drug resistance. *Biochimica Et Biophysica Acta* 1773, 1263-1284.

- McDonald, L. A., Barbieri, L. R., Bernan, V. S., Janso, J., Lassota, P., and Carter, G. T. (2004). 07H239-A, a new cytotoxic eremophilane sesquiterpene from the marine-derived xylariaceous fungus LL-07H239. *Journal of Natural Products* *67*, 1565-1567.
- McNamara, P. J., Bradley, G. A., and Songer, J. G. (1994). Targeted mutagenesis of the phospholipase D gene results in decreased virulence of *Corynebacterium pseudotuberculosis*. *Mol Microbiol* *12*, 921-930.
- McNamara, P. J., Cuevas, W. A., and Songer, J. G. (1995). Toxic phospholipases D of *Corynebacterium pseudotuberculosis*, *C. ulcerans* and *Arcanobacterium haemolyticum*: cloning and sequence homology. *Gene* *156*, 113-118.
- McPhail, L. C., Waite, K. A., Regier, D. S., Nixon, J. B., Qualliotine-Mann, D., Zhang, W. X., Wallin, R., and Sergeant, S. (1999). A novel protein kinase target for the lipid second messenger phosphatidic acid. *Biochimica Et Biophysica Acta* *1439*, 277-290.
- Miller, R. R., Jr., Yates, J. W., and Geer, B. W. (1993). Dietary ethanol stimulates the activity of phosphatidylcholine-specific phospholipase D and the formation of phosphatidylethanol in *Drosophila melanogaster* larvae. *Insect Biochem Mol Biol* *23*, 749-755.
- Mitchell, R., McCulloch, D., Lutz, E., Johnson, M., MacKenzie, C., Fennell, M., Fink, G., Zhou, W., and Sealfon, S. C. (1998). Rhodopsin-family receptors associate with small G proteins to activate phospholipase D. *Nature* *392*, 411-414.
- Monovich, L. (2007). Optimization of halopemide for phospholipase D2 inhibition. *Bioorg Med Chem Lett* *17*, 2310-2311.
- Motoike, T., Bieger, S., Wiegandt, H., and Unsicker, K. (1993). Induction of phosphatidic acid by fibroblast growth factor in cultured baby hamster kidney fibroblasts. *FEBS Lett* *332*, 164-168.
- Murakami, M. T., Fernandes-Pedrosa, M. F., Tambourgi, D. V., and Arni, R. K. (2005). Structural basis for metal ion coordination and the catalytic mechanism of sphingomyelinases D. *J Biol Chem* *280*, 13658-13664.
- Murakami-Murofushi, K., Kaji, K., Kano, K., Fukuda, M., Shioda, M., and Murofushi, H. (1993). Inhibition of cell proliferation by a unique lysophosphatidic acid, PHYLPA, isolated from *Physarum polycephalum*: signaling events of antiproliferative action by PHYLPA. *Cell Struct Funct* *18*, 363-370.
- Nakashima, S., Hisamoto, N., Banno, Y., Matsumoto, K., Nozawa, Y. (2000). *Worm Breeder's Gazette* *16*, 1-2.
- Neiman, A. M. (1998). Prospore membrane formation defines a developmentally regulated branch of the secretory pathway in yeast. *J Cell Biol* *140*, 29-37.

- Noh, D. Y., Ahn, S. J., Lee, R. A., Park, I. A., Kim, J. H., Suh, P. G., Ryu, S. H., Lee, K. H., and Han, J. S. (2000). Overexpression of phospholipase D1 in human breast cancer tissues. *Cancer Lett* 161, 207-214.
- Norton, L. J., Zhang, Q., Saqib, K. M., Schrewe, H., Macura, K., Anderson, K. E., Lindsley, C. W., Brown, H. A., Rudge, S. A., and Wakelam, M. J. (2011). PLD1 rather than PLD2 regulates phorbol-ester-, adhesion-dependent and Fc{gamma}-receptor-stimulated ROS production in neutrophils. *J Cell Sci* 124, 1973-1983.
- O'Reilly, M. C., Scott, S. A., Brown, K. A., Oguin, T. H., 3rd, Thomas, P. G., Daniels, J. S., Morrison, R., Brown, H. A., and Lindsley, C. W. (2013). Development of dual PLD1/2 and PLD2 selective inhibitors from a common 1,3,8-Triazaspiro[4.5]decane Core: discovery of MI298 and MI299 that decrease invasive migration in U87-MG glioblastoma cells. *J Med Chem* 56, 2695-2699.
- Ogino, C., Daido, H., Ohmura, Y., Takada, N., Itou, Y., Kondo, A., Fukuda, H., and Shimizu, N. (2007). Remarkable enhancement in PLD activity from *Streptovorticillium cinnamoneum* by substituting serine residue into the GG/GS motif. *Biochim Biophys Acta* 1774, 671-678.
- Ohguchi, K., Banno, Y., Nakagawa, Y., Akao, Y., and Nozawa, Y. (2005). Negative regulation of melanogenesis by phospholipase D1 through mTOR/p70 S6 kinase 1 signaling in mouse B16 melanoma cells. *Journal of Cellular Physiology* 205, 444-451.
- Ohguchi, K., Banno, Y., Nakashima, S., and Nozawa, Y. (1996). Regulation of membrane-bound phospholipase D by protein kinase C in HL60 cells - Synergistic action of small GTP-binding protein RhoA. *Journal of Biological Chemistry* 271, 4366-4372.
- Ohh, M. (2006). Ubiquitin pathway in VHL cancer syndrome. *Neoplasia* 8, 623-629.
- Okamoto, Y., Morishita, J., Tsuboi, K., Tonai, T., and Ueda, N. (2004). Molecular characterization of a phospholipase D generating anandamide and its congeners. *J Biol Chem* 279, 5298-5305.
- Oliveira, T. G., Chan, R. B., Tian, H., Laredo, M., Shui, G., Staniszewski, A., Zhang, H., Wang, L., Kim, T. W., Duff, K. E., *et al.* (2010). Phospholipase d2 ablation ameliorates Alzheimer's disease-linked synaptic dysfunction and cognitive deficits. *J Neurosci* 30, 16419-16428.
- Oliveira, T. G., and Di Paolo, G. (2010). Phospholipase D in brain function and Alzheimer's disease. *Biochim Biophys Acta* 1801, 799-805.
- Orth, E. S., Brandao, T. A., Souza, B. S., Pliego, J. R., Vaz, B. G., Eberlin, M. N., Kirby, A. J., and Nome, F. (2010). Intramolecular catalysis of phosphodiester hydrolysis by two imidazoles. *J Am Chem Soc* 132, 8513-8523.
- Osisami, M., Ali, W., and Frohman, M. A. (2012). A role for phospholipase D3 in myotube formation. *PLoS One* 7, e33341.

- Pacher, P., Batkai, S., and Kunos, G. (2006). The endocannabinoid system as an emerging target of pharmacotherapy. *Pharmacol Rev* 58, 389-462.
- Park, M. H., Ahn, B. H., Hong, Y. K., and Min, D. S. (2009). Overexpression of phospholipase D enhances matrix metalloproteinase-2 expression and glioma cell invasion via protein kinase C and protein kinase A/NF-kappa B/Sp1-mediated signaling pathways. *Carcinogenesis* 30, 356-365.
- Park, S. K., Min, D. S., and Exton, J. H. (1998). Definition of the protein kinase C interaction site of phospholipase D. *Biochem Biophys Res Commun* 244, 364-367.
- Perry, R. R., Kang, Y., and Greaves, B. (1995). Effects of tamoxifen on growth and apoptosis of estrogen-dependent and -independent human breast cancer cells. *Annals of Surgical Oncology* 2, 238-245.
- Pertwee, R. G. (2008). The diverse CB1 and CB2 receptor pharmacology of three plant cannabinoids: delta9-tetrahydrocannabinol, cannabidiol and delta9-tetrahydrocannabivarin. *Br J Pharmacol* 153, 199-215.
- Plevin, R., Cook, S. J., Palmer, S., and Wakelam, M. J. (1991). Multiple sources of sn-1,2-diacylglycerol in platelet-derived-growth-factor-stimulated Swiss 3T3 fibroblasts. Evidence for activation of phosphoinositidase C and phosphatidylcholine-specific phospholipase D. *Biochem J* 279 (Pt 2), 559-565.
- Plonk, S. G., Park, S. K., and Exton, J. H. (1998). The alpha-subunit of the heterotrimeric G protein G13 activates a phospholipase D isozyme by a pathway requiring Rho family GTPases. *J Biol Chem* 273, 4823-4826.
- Polymeropoulos, M. H., Lavedan, C., Leroy, E., Ide, S. E., Dehejia, A., Dutra, A., Pike, B., Root, H., Rubenstein, J., Boyer, R., *et al.* (1997). Mutation in the alpha-synuclein gene identified in families with Parkinson's disease. *Science* 276, 2045-2047.
- Ponting, C. P., and Kerr, I. D. (1996). A novel family of phospholipase D homologues that includes phospholipid synthases and putative endonucleases: identification of duplicated repeats and potential active site residues. *Protein Sci* 5, 914-922.
- Poste, G., and Fidler, I. J. (1980). The pathogenesis of cancer metastasis. *Nature* 283, 139-146.
- Pritchard, C. A., Bolin, L., Slattery, R., Murray, R., and McMahon, M. (1996). Post-natal lethality and neurological and gastrointestinal defects in mice with targeted disruption of the A-Raf protein kinase gene. *Curr Biol* 6, 614-617.
- Qin, C., and Wang, X. (2002). The Arabidopsis phospholipase D family. Characterization of a calcium-independent and phosphatidylcholine-selective PLD zeta 1 with distinct regulatory domains. *Plant Physiol* 128, 1057-1068.

- Qin, K., Dong, C., Wu, G., and Lambert, N. A. (2011). Inactive-state preassembly of G(q)-coupled receptors and G(q) heterotrimers. *Nature chemical biology* 7, 740-747.
- Raghu, P., Coessens, E., Manifava, M., Georgiev, P., Pettitt, T., Wood, E., Garcia-Murillas, I., Okkenhaug, H., Trivedi, D., Zhang, Q., *et al.* (2009a). Rhabdomere biogenesis in *Drosophila* photoreceptors is acutely sensitive to phosphatidic acid levels. *J Cell Biol* 185, 129-145.
- Raghu, P., Manifava, M., Coadwell, J., and Ktistakis, N. T. (2009b). Emerging findings from studies of phospholipase D in model organisms (and a short update on phosphatidic acid effectors). *Biochim Biophys Acta* 1791, 889-897.
- Raikwar, N. S., Bowen, R. F., and Deeg, M. A. (2005). Mutating His29, His125, His133 or His158 abolishes glycosylphosphatidylinositol-specific phospholipase D catalytic activity. *Biochem J* 391, 285-289.
- Rana, R. S., and Hokin, L. E. (1990). Role of phosphoinositides in transmembrane signaling. *Physiological Reviews* 70, 115-164.
- Rappley, I., Gitler, A. D., Selvy, P. E., LaVoie, M. J., Levy, B. D., Brown, H. A., Lindquist, S., and Selkoe, D. J. (2009). Evidence that alpha-synuclein does not inhibit phospholipase D. *Biochemistry* 48, 1077-1083.
- Raymond, F. D., Fortunato, G., Moss, D. W., Castaldo, G., Salvatore, F., and Impallomeni, M. (1994). Inositol-specific phospholipase D activity in health and disease. *Clin Sci (Lond)* 86, 447-451.
- Reich, R., Blumenthal, M., and Liscovitch, M. (1995). Role of phospholipase D in laminin-induced production of gelatinase A (MMP-2) in metastatic cells. *Clin Exp Metastasis* 13, 134-140.
- Ren, J., Xiao, Y. J., Singh, L. S., Zhao, X., Zhao, Z., Feng, L., Rose, T. M., Prestwich, G. D., and Xu, Y. (2006). Lysophosphatidic acid is constitutively produced by human peritoneal mesothelial cells and enhances adhesion, migration, and invasion of ovarian cancer cells. *Cancer Res* 66, 3006-3014.
- Rhee, S. G. (2001). Regulation of phosphoinositide-specific phospholipase C. *Annu Rev Biochem* 70, 281-312.
- Riebeling, C., Bourgoin, S., and Shields, D. (2008). Caspase cleavage of phospholipase D1 in vitro alters its regulation and reveals a novel property of the "loop" region. *Biochim Biophys Acta* 1781, 376-382.
- Riese, D. J., 2nd, Gallo, R. M., and Settleman, J. (2007). Mutational activation of ErbB family receptor tyrosine kinases: insights into mechanisms of signal transduction and tumorigenesis. *Bioessays* 29, 558-565.

- Rizzo, M. A. (1999). Phospholipase D and its product, phosphatidic acid, mediate agonist-dependent raf-1 translocation to the plasma membrane and the activation of the mitogen-activated protein kinase pathway. *J Biol Chem* 274, 1131-1139.
- Rizzo, M. A., Shome, K., Watkins, S. C., and Romero, G. (2000). The recruitment of Raf-1 to membranes is mediated by direct interaction with phosphatidic acid and is independent of association with Ras. *J Biol Chem* 275, 23911-23918.
- Robinette, D., Neamati, N., Tomer, K. B., and Borchers, C. H. (2006). Photoaffinity labeling combined with mass spectrometric approaches as a tool for structural proteomics. *Expert Rev Proteomics* 3, 399-408.
- Rose, K., Rudge, S. A., Frohman, M. A., Morris, A. J., and Engebrecht, J. (1995). Phospholipase D signaling is essential for meiosis. *Proc Natl Acad Sci U S A* 92, 12151-12155.
- Rossi, F., Grzeskowiak, M., Della Bianca, V., Calzetti, F., and Gandini, G. (1990). Phosphatidic acid and not diacylglycerol generated by phospholipase D is functionally linked to the activation of the NADPH oxidase by FMLP in human neutrophils. *Biochem Biophys Res Commun* 168, 320-327.
- Roth, M. G. (2008). Molecular mechanisms of PLD function in membrane traffic. *Traffic* 9, 1233-1239.
- Rudolph, A. E., Stuckey, J. A., Zhao, Y., Matthews, H. R., Patton, W. A., Moss, J., and Dixon, J. E. (1999). Expression, characterization, and mutagenesis of the *Yersinia pestis* murine toxin, a phospholipase D superfamily member. *J Biol Chem* 274, 11824-11831.
- Sabatini, D. M. (2006). mTOR and cancer: insights into a complex relationship. *Nature Reviews Cancer* 6, 729-734.
- Sadler, J. E. (1998). Biochemistry and genetics of von Willebrand factor. *Annu Rev Biochem* 67, 395-424.
- Saito, M., and Kanfer, J. (1973). Solubilization and properties of a membrane-bound enzyme from rat brain catalyzing a base-exchange reaction. *Biochem Biophys Res Commun* 53, 391-398.
- Saliba, A. E., Vonkova, I., Ceschia, S., Findlay, G. M., Maeda, K., Tischer, C., Deghou, S., van Noort, V., Bork, P., Pawson, T., *et al.* (2014). A quantitative liposome microarray to systematically characterize protein-lipid interactions. *Nat Methods* 11, 47-50.
- Schmid, P. C., Reddy, P. V., Natarajan, V., and Schmid, H. H. (1983). Metabolism of N-acyl ethanolamine phospholipids by a mammalian phosphodiesterase of the phospholipase D type. *J Biol Chem* 258, 9302-9306.
- Schofield, J. N., Stephens, J. W., Hurel, S. J., Bell, K. M., deSouza, J. B., and Rademacher, T. W. (2002). Insulin reduces serum glycosylphosphatidylinositol

phospholipase D levels in human type I diabetic patients and streptozotocin diabetic rats. *Mol Genet Metab* 75, 154-161.

Schreck, R., and Rapp, U. R. (2006). Raf kinases: oncogenesis and drug discovery. *Int J Cancer* 119, 2261-2271.

Sciorra, V. A., Hammond, S. M., and Morris, A. J. (2001). Potent direct inhibition of mammalian phospholipase D isoenzymes by calphostin-c. *Biochemistry* 40, 2640-2646.

Sciorra, V. A., Rudge, S. A., Prestwich, G. D., Frohman, M. A., Engebrecht, J., and Morris, A. J. (1999). Identification of a phosphoinositide binding motif that mediates activation of mammalian and yeast phospholipase D isoenzymes. *EMBO J* 18, 5911-5921.

Sciorra, V. A., Rudge, S. A., Wang, J., McLaughlin, S., Engebrecht, J., and Morris, A. J. (2002). Dual role for phosphoinositides in regulation of yeast and mammalian phospholipase D enzymes. *J Cell Biol* 159, 1039-1049.

Scott, S. A., Selvy, P. E., Buck, J. R., Cho, H. P., Criswell, T. L., Thomas, A. L., Armstrong, M. D., Arteaga, C. L., Lindsley, C. W., and Brown, H. A. (2009). Design of isoform-selective phospholipase D inhibitors that modulate cancer cell invasiveness. *Nature chemical biology* 5, 108-117.

Selvy, P. E., Lavieri, R. R., Lindsley, C. W., and Brown, H. A. (2011). Phospholipase D: enzymology, functionality, and chemical modulation. *Chem Rev* 111, 6064-6119.

Shen, Q., Stanton, M. L., Feng, W., Rodriguez, M. E., Ramondetta, L., Chen, L., Brown, R. E., and Duan, X. (2010). Morphoproteomic analysis reveals an overexpressed and constitutively activated phospholipase D1-mTORC2 pathway in endometrial carcinoma. *Int J Clin Exp Pathol* 4, 13-21.

Shen, Y., Xu, L., and Foster, D. A. (2001). Role for phospholipase D in receptor-mediated endocytosis. *Molecular and Cellular Biology* 21, 595-602.

Shi, M., Zheng, Y., Garcia, A., Xu, L., and Foster, D. A. (2007). Phospholipase D provides a survival signal in human cancer cells with activated H-Ras or K-Ras. *Cancer Lett* 258, 268-275.

Shigemura, K., Arbiser, J. L., Sun, S. Y., Zayzafoon, M., Johnstone, P. A., Fujisawa, M., Gotoh, A., Weksler, B., Zhau, H. E., and Chung, L. W. (2007). Honokiol, a natural plant product, inhibits the bone metastatic growth of human prostate cancer cells. *Cancer* 109, 1279-1289.

Singer, W. D., Brown, H. A., Bokoch, G. M., and Sternweis, P. C. (1995). Resolved phospholipase D activity is modulated by cytosolic factors other than Arf. *J Biol Chem* 270, 14944-14950.

- Singh, A., Thornton, E. R., and Westheimer, F. H. (1962). The photolysis of diazoacetylchymotrypsin. *J Biol Chem* *237*, 3006-3008.
- Snider, A. J., Zhang, Z., Xie, Y., and Meier, K. E. (2010). Epidermal growth factor increases lysophosphatidic acid production in human ovarian cancer cells: roles for phospholipase D2 and receptor transactivation. *Am J Physiol Cell Physiol* *298*, C163-170.
- Song, J., Jiang, Y. W., and Foster, D. A. (1994). Epidermal growth factor induces the production of biologically distinguishable diglyceride species from phosphatidylinositol and phosphatidylcholine via the independent activation of type C and type D phospholipases. *Cell Growth Differ* *5*, 79-85.
- Soucek, A., and Souckova, A. (1974). Toxicity of bacterial sphingomyelinases D. *J Hyg Epidemiol Microbiol Immunol* *18*, 327-335.
- Stace, C. L., and Ktistakis, N. T. (2006). Phosphatidic acid- and phosphatidylserine-binding proteins. *Biochim Biophys Acta* *1761*, 913-926.
- Stanacev, N. Z., and Stuhne-Sekalec, L. (1970). On the mechanism of enzymatic phosphatidylation. Biosynthesis of cardiolipin catalyzed by phospholipase D. *Biochim Biophys Acta* *210*, 350-352.
- Steed, P. M., Clark, K. L., Boyar, W. C., and Lasala, D. J. (1998). Characterization of human PLD2 and the analysis of PLD isoform splice variants. *FASEB J* *12*, 1309-1317.
- Stieglitz, K., Seaton, B., and Roberts, M. F. (1999). The role of interfacial binding in the activation of *Streptomyces chromofuscus* phospholipase D by phosphatidic acid. *J Biol Chem* *274*, 35367-35374.
- Stuckey, J. A., and Dixon, J. E. (1999). Crystal structure of a phospholipase D family member. *Nat Struct Biol* *6*, 278-284.
- Su, W., Yeku, O., Olepu, S., Genna, A., Park, J. S., Ren, H., Du, G., Gelb, M. H., Morris, A. J., and Frohman, M. A. (2009). 5-Fluoro-2-indolyl des-chlorohalopemide (FIPI), a phospholipase D pharmacological inhibitor that alters cell spreading and inhibits chemotaxis. *Mol Pharmacol* *75*, 437-446.
- Sugars, J. M., Cellek, S., Manifava, M., Coadwell, J., and Ktistakis, N. T. (1999). Fatty acylation of phospholipase D1 on cysteine residues 240 and 241 determines localization on intracellular membranes. *J Biol Chem* *274*, 30023-30027.
- Sun, Y., Fang, Y., Yoon, M. S., Zhang, C., Roccio, M., Zwartkuis, F. J., Armstrong, M., Brown, H. A., and Chen, J. (2008). Phospholipase D1 is an effector of Rheb in the mTOR pathway. *Proc Natl Acad Sci U S A* *105*, 8286-8291.
- Sung, T. C., Altshuller, Y. M., Morris, A. J., and Frohman, M. A. (1999). Molecular analysis of mammalian phospholipase D2. *J Biol Chem* *274*, 494-502.

- Tambourgi, D. V., Magnoli, F. C., van den Berg, C. W., Morgan, B. P., de Araujo, P. S., Alves, E. W., and Da Silva, W. D. (1998). Sphingomyelinases in the venom of the spider *Loxosceles intermedia* are responsible for both dermonecrosis and complement-dependent hemolysis. *Biochem Biophys Res Commun* 251, 366-373.
- Tanaka, M., Okudaira, S., Kishi, Y., Ohkawa, R., Iseki, S., Ota, M., Noji, S., Yatomi, Y., Aoki, J., and Arai, H. (2006). Autotaxin stabilizes blood vessels and is required for embryonic vasculature by producing lysophosphatidic acid. *J Biol Chem* 281, 25822-25830.
- Tang, J. H., He, W. J., Huang, H., Tan, C. C., Duan, Q., Wang, K. J., Yuan, X. Y., and Zhu, X. J. (2009). Important roles of glycosylphosphatidylinositol (GPI)-specific phospholipase D and some GPI-anchored proteins in the pathogenesis of hepatocellular carcinoma. *Clin Biochem* 42, 400-407.
- Tania, M., Khan, A., Zhang, H., Li, J., and Song, Y. (2010). Autotaxin: a protein with two faces. *Biochem Biophys Res Commun* 401, 493-497.
- Taniguchi, Y. Y., Taniguchi, M., Tsuge, T., Oka, A., and Aoyama, T. (2010). Involvement of *Arabidopsis thaliana* phospholipase Dzeta2 in root hydrotropism through the suppression of root gravitropism. *Planta* 231, 491-497.
- Titov, D. V., Gilman, B., He, Q. L., Bhat, S., Low, W. K., Dang, Y., Smeaton, M., Demain, A. L., Miller, P. S., Kugel, J. F., *et al.* (2011). XPB, a subunit of TFIIH, is a target of the natural product triptolide. *Nature chemical biology*.
- Tokumura, A., Majima, E., Kariya, Y., Tominaga, K., Kogure, K., Yasuda, K., and Fukuzawa, K. (2002). Identification of human plasma lysophospholipase D, a lysophosphatidic acid-producing enzyme, as autotaxin, a multifunctional phosphodiesterase. *J Biol Chem* 277, 39436-39442.
- Toschi, A., Edelstein, J., Rockwell, P., Ohh, M., and Foster, D. A. (2008). HIF alpha expression in VHL-deficient renal cancer cells is dependent on phospholipase D. *Oncogene* 27, 2746-2753.
- Toschi, A., Lee, E., Xu, L., Garcia, A., Gadir, N., and Foster, D. A. (2009). Regulation of mTORC1 and mTORC2 complex assembly by phosphatidic acid: competition with rapamycin. *Mol Cell Biol* 29, 1411-1420.
- Tou, J., and Urbizo, C. (2001). Resveratrol inhibits the formation of phosphatidic acid and diglyceride in chemotactic peptide- or phorbol ester-stimulated human neutrophils. *Cell Signal* 13, 191-197.
- Tou, J. S., and Urbizo, C. (2008). Diethylstilbestrol inhibits phospholipase D activity and degranulation by stimulated human neutrophils. *Steroids* 73, 216-221.

Tsuda, S., Okudaira, S., Moriya-Ito, K., Shimamoto, C., Tanaka, M., Aoki, J., Arai, H., Murakami-Murofushi, K., and Kobayashi, T. (2006). Cyclic phosphatidic acid is produced by autotaxin in blood. *J Biol Chem* *281*, 26081-26088.

Uchida, N., Okamura, S., Nagamachi, Y., and Yamashita, S. (1997). Increased phospholipase D activity in human breast cancer. *J Cancer Res Clin Oncol* *123*, 280-285.

Uesugi, Y., and Hatanaka, T. (2009). Phospholipase D mechanism using *Streptomyces* PLD. *Biochim Biophys Acta* *1791*, 962-969.

Umez-Goto, M., Kishi, Y., Taira, A., Hama, K., Dohmae, N., Takio, K., Yamori, T., Mills, G. B., Inoue, K., Aoki, J., and Arai, H. (2002). Autotaxin has lysophospholipase D activity leading to tumor cell growth and motility by lysophosphatidic acid production. *J Cell Biol* *158*, 227-233.

van Meeteren, L. A., Frederiks, F., Giepmans, B. N., Pedrosa, M. F., Billington, S. J., Jost, B. H., Tambourgi, D. V., and Moolenaar, W. H. (2004). Spider and bacterial sphingomyelinases D target cellular lysophosphatidic acid receptors by hydrolyzing lysophosphatidylcholine. *J Biol Chem* *279*, 10833-10836.

van Meeteren, L. A., Ruurs, P., Christodoulou, E., Goding, J. W., Takakusa, H., Kikuchi, K., Perrakis, A., Nagano, T., and Moolenaar, W. H. (2005). Inhibition of autotaxin by lysophosphatidic acid and sphingosine 1-phosphate. *J Biol Chem* *280*, 21155-21161.

van Rooij, H. H., Waterman, R. L., and Kraak, J. C. (1979). Dynamic cation-exchange systems for the separation of drugs derived from butyrophenone and diphenylpiperidine by high-performance liquid chromatography and applied in the determination of halopemide in plasma. *J Chromatogr* *164*, 177-185.

Vance, D. E., and Vance, J. E. (2002). *Biochemistry of lipids, lipoproteins and membranes*, 4th edn (Amsterdam ; Boston: Elsevier).

Veverka, V., Crabbe, T., Bird, I., Lennie, G., Muskett, F. W., Taylor, R. J., and Carr, M. D. (2008). Structural characterization of the interaction of mTOR with phosphatidic acid and a novel class of inhibitor: compelling evidence for a central role of the FRB domain in small molecule-mediated regulation of mTOR. *Oncogene* *27*, 585-595.

Viparelli, F., Cassese, A., Doti, N., Paturzo, F., Marasco, D., Dathan, N. A., Monti, S. M., Basile, G., Ungaro, P., Sabatella, M., *et al.* (2008). Targeting of PED/PEA-15 molecular interaction with phospholipase D1 enhances insulin sensitivity in skeletal muscle cells. *J Biol Chem* *283*, 21769-21778.

Vivanco, I., and Sawyers, C. L. (2002). The phosphatidylinositol 3-Kinase AKT pathway in human cancer. *Nature Reviews Cancer* *2*, 489-501.

Vorland, M., and Holmsen, H. (2008). Phospholipase D activity in human platelets is inhibited by protein kinase A, involving inhibition of phospholipase D1 translocation. *Platelets* *19*, 300-307.

- Voss, M., Weernink, P. A., Hauptenthal, S., Moller, U., Cool, R. H., Bauer, B., Camonis, J. H., Jakobs, K. H., and Schmidt, M. (1999). Phospholipase D stimulation by receptor tyrosine kinases mediated by protein kinase C and a Ras/Ral signaling cascade. *J Biol Chem* *274*, 34691-34698.
- Walker, S. J., and Brown, H. A. (2002). Specificity of Rho insert-mediated activation of phospholipase D1. *J Biol Chem* *277*, 26260-26267.
- Wang, J., Okamoto, Y., Morishita, J., Tsuboi, K., Miyatake, A., and Ueda, N. (2006). Functional analysis of the purified anandamide-generating phospholipase D as a member of the metallo-beta-lactamase family. *J Biol Chem* *281*, 12325-12335.
- Wang, J., and Ueda, N. (2009). Biology of endocannabinoid synthesis system. *Prostaglandins Other Lipid Mediat* *89*, 112-119.
- Wang, X. (1999). The role of phospholipase D in signaling cascades. *Plant Physiol* *120*, 645-652.
- Wang, X. (2000). Multiple forms of phospholipase D in plants: the gene family, catalytic and regulatory properties, and cellular functions. *Prog Lipid Res* *39*, 109-149.
- Wang, X., Xu, L., and Zheng, L. (1994). Cloning and expression of phosphatidylcholine-hydrolyzing phospholipase D from *Ricinus communis* L. *J Biol Chem* *269*, 20312-20317.
- Westerheide, S. D., Kawahara, T. L., Orton, K., and Morimoto, R. I. (2006). Triptolide, an inhibitor of the human heat shock response that enhances stress-induced cell death. *J Biol Chem* *281*, 9616-9622.
- Williger, B. T., Ho, W. T., and Exton, J. H. (1999). Phospholipase D mediates matrix metalloproteinase-9 secretion in phorbol ester-stimulated human fibrosarcoma cells. *J Biol Chem* *274*, 735-738.
- Wojnowski, L., Stancato, L. F., Zimmer, A. M., Hahn, H., Beck, T. W., Larner, A. C., Rapp, U. R., and Zimmer, A. (1998). Craf-1 protein kinase is essential for mouse development. *Mech Dev* *76*, 141-149.
- Wojnowski, L., Zimmer, A. M., Beck, T. W., Hahn, H., Bernal, R., Rapp, U. R., and Zimmer, A. (1997). Endothelial apoptosis in Braf-deficient mice. *Nature Genetics* *16*, 293-297.
- Xie, M. S., Jacobs, L. S., and Dubyak, G. R. (1991). Regulation of phospholipase D and primary granule secretion by P2-purinergic- and chemotactic peptide-receptor agonists is induced during granulocytic differentiation of HL-60 cells. *Journal of Clinical Investigation* *88*, 45-54.
- Xie, Z., Ho, W.-T., Spellman, R., Cai, S., and Exton, J. H. (2002a). Mechanisms of Regulation of Phospholipase D1 and D2 by the Heterotrimeric G Proteins G13 and Gq. *J Biol Chem* *277*, 11979-11986.

- Xie, Z., Ho, W. T., and Exton, J. H. (2002b). Functional implications of post-translational modifications of phospholipases D1 and D2. *Biochim Biophys Acta* 1580, 9-21.
- Xu, L., Salloum, D., Medlin, P. S., Saqena, M., Yellen, P., Perrella, B., and Foster, D. A. (2011). Phospholipase D Mediates Nutrient Input to Mammalian Target of Rapamycin Complex 1 (mTORC1). *J Biol Chem* 286, 25477-25486.
- Yabu, T., Imamura, S., Yamashita, M., and Okazaki, T. (2008). Identification of Mg²⁺ -dependent neutral sphingomyelinase 1 as a mediator of heat stress-induced ceramide generation and apoptosis. *J Biol Chem* 283, 29971-29982.
- Yamada, Y., Hamajima, N., Kato, T., Iwata, H., Yamamura, Y., Shinoda, M., Suyama, M., Mitsudomi, T., Tajima, K., Kusakabe, S., *et al.* (2003). Association of a polymorphism of the phospholipase D2 gene with the prevalence of colorectal cancer. *J Mol Med* 81, 126-131.
- Yamamoto, H., Hanada, K., Kawasaki, K., and Nishijima, M. (1997). Inhibitory effect on curcumin on mammalian phospholipase D activity. *FEBS Lett* 417, 196-198.
- Yang, H., and Roberts, M. F. (2003). Phosphohydrolase and transphosphatidylase reactions of two *Streptomyces* phospholipase D enzymes: covalent versus noncovalent catalysis. *Protein Sci* 12, 2087-2098.
- Yang, S. F., Freer, S., and Benson, A. A. (1967). Transphosphatidylase by phospholipase D. *J Biol Chem* 242, 477-484.
- Yin, H., Gui, Y., Du, G., Frohman, M. A., and Zheng, X. L. (2010). Dependence of phospholipase D1 multi-monoubiquitination on its enzymatic activity and palmitoylation. *J Biol Chem* 285, 13580-13588.
- Yoshioka, K., Mizoguchi, M., Takahara, M., Iwanamura, S., Beppu, T., Horinouchi, S. (1991). DNA encoding PLD and its application. In, (Japanese Patent).
- Zajicek, J., Fox, P., Sanders, H., Wright, D., Vickery, J., Nunn, A., and Thompson, A. (2003). Cannabinoids for treatment of spasticity and other symptoms related to multiple sclerosis (CAMS study): multicentre randomised placebo-controlled trial. *Lancet* 362, 1517-1526.
- Zambonelli, C., Casali, M., and Roberts, M. F. (2003). Mutagenesis of putative catalytic and regulatory residues of *Streptomyces chromofuscus* phospholipase D differentially modifies phosphatase and phosphodiesterase activities. *J Biol Chem* 278, 52282-52289.
- Zeng, X. X., Zheng, X., Xiang, Y., Cho, H. P., Jessen, J. R., Zhong, T. P., Solnica-Krezel, L., and Brown, H. A. (2009). Phospholipase D1 is required for angiogenesis of intersegmental blood vessels in zebrafish. *Dev Biol* 328, 363-376.

Zhang, H., Hilton, D. A., Hanemann, C. O., and Zajicek, J. (2011). Cannabinoid receptor and N-acyl phosphatidylethanolamine phospholipase D - evidence for altered expression in multiple sclerosis. *Brain Pathol.*

Zhang, Y. (2003). Rheb is a direct target of the tuberous sclerosis tumour suppressor proteins. *Nature Cell Biol* 5, 578-581.

Zhang, Y., Huang, P., Du, G., Kanaho, Y., Frohman, M. A., and Tsirka, S. E. (2004). Increased expression of two phospholipase D isoforms during experimentally induced hippocampal mossy fiber outgrowth. *Glia* 46, 74-83.

Zhao, C. (2007). Phospholipase D2-generated phosphatidic acid couples EGFR stimulation to Ras activation by Sos. *Nat Cell Biol* 9, 706-712.

Zhao, Y., Ehara, H., Akao, Y., Shamoto, M., Nakagawa, Y., Banno, Y., Deguchi, T., Ohishi, N., Yagi, K., and Nozawa, Y. (2000). Increased activity and intranuclear expression of phospholipase D2 in human renal cancer. *Biochem Biophys Res Commun* 278, 140-143.

Zheng, Y., Rodrik, V., Toschi, A., Shi, M., Hui, L., Shen, Y., and Foster, D. A. (2006). Phospholipase D couples survival and migration signals in stress response of human cancer cells. *J Biol Chem* 281, 15862-15868.

Zhong, M., Shen, Y., Zheng, Y., Joseph, T., Jackson, D., and Foster, D. A. (2003). Phospholipase D prevents apoptosis in v-Src-transformed rat fibroblasts and MDA-MB-231 breast cancer cells. *Biochem Biophys Res Commun* 302, 615-619.